Università
Ca'Foscari
Venezia

PhD degree

in Environmental Science

Cycle 33

Research thesis

Variability of Inorganic nutrients in the Western Mediterranean Sea

Supervisor
Prof. Bruno Pavoni

Co-Supervisors
Dr. Katrin Schroeder
Dr. Jacopo Chiggiato

PhD student
Malek Belgacem
Matricola 956390

2020

ABSTRACT

Ocean life relies on the loads of marine nutrients within the euphotic layer. Dissolved inorganic nutrients play a crucial role in marine ecosystem functioning. They serve as regulators of ocean biological productivity, and are trace elements for biogeochemical cycling as well as for natural and anthropogenic sources and transport processes (Bethoux, 1989; Bethoux et al., 1992). They are also non-conservative tracers, since their distribution varies according to both biological (such as primary production and respiration) and physical (such as convection, advection, mixing and diffusion) processes.

Nutrients control primary productivity and therefore carbon sequestration which have an impact on climate and global warming. In this context, changes in biogeochemical properties of the oceans are to be expected (Moore et al., 2013).

Very schematically, inorganic nutrients fuel phytoplankton growth (due to primary production) in the sea surface and regenerate in the mesopelagic layer by bacteria and animals (due to respiration). These nutrients may reach deeper levels through vertical mixing/upwelling, and remineralization of sinking organic matter and its decomposition increases nutrients in the intermediate and deep-water masses over time.

Ocean circulation and physical processes continually drive the large-scale distribution of chemicals (Williams and Follows, 2003) toward a homogeneous distribution. Therefore, nutrient dynamics is important to understand the overall ecosystem productivity and carbon cycles.

In general, the surface layer is depleted in nutrients in regions of low latitude (Sarmiento and Toggweiler, 1984), but in some ocean regions, called high nutrient low chlorophyll (HNLC) regions, nutrient concentrations tend to be anomalously high, particularly in areas of the North Atlantic and Southern Ocean, as well as in the eastern equatorial Pacific, and the in the North Pacific; see e.g. Garcia et al., 2010). The Mediterranean Sea is considered as a complex marine ecosystem because of its changes and the variety of the regional physical processes occurring in the area. Its surface layer is usually nutrient-depleted.

Most studies show that nitrate is the most common limiting factor for primary production in the global ocean (Moore et al., 2013), while others evidence that phosphate may be a limiting factor in some specific areas, as is the case of the Mediterranean Sea (Diaz et al., 2001; Krom et al., 2004). Being an enclosed marginal sea, the Mediterranean Sea exhibits an anti-estuarine

circulation, responsible for its oligotrophic character and acting like a subtropical anticyclonic gyre.

The focus of this thesis is the distribution of dissolved inorganic nutrients and its variability in the Western Mediterranean Sea. The spatial and temporal variability in biogeochemical properties of the WMED water masses throughout the past decade have been investigated.

After a general introduction of biogeochemical processes and the study area (the western Mediterranean Sea), the thesis describes in detail the careful primary and secondary quality control procedures applied to long term measurements of nitrate, phosphate and silicate, that lead to generation of a new product (CNR_DIN_WMED, Belgacem et al., 2019) containing unpublished biogeochemical data in the western Mediterranean Sea collected between 2004 and 2017. Making use of this data product, the thesis is then devoted to assessing the peculiar biogeochemical footprint of the typical water masses found in the study area, both in terms of average concentrations (in different regions and layers), and stoichiometric ratios.

In the final part, a climatological analysis (1981-2017) of the dissolved inorganic nutrient distribution in the WMED was performed, using all available biogeochemical datasets (including the CNR_DIN_WMED, Belgacem et al., 2019), to quantify and describe the spatial and temporal variability of nutrients at different depth levels using a new climatological biogeochemical product (BGC-WMED, Belgacem et al., in preparation). Discussions of the main outcomes and conclusions are drawn at the end.

ACKNOWLEDGEMENTS

I would first like to thank my supervisors Katrin Schroeder, Jacopo Chiggiato and Bruno Pavoni for their guidance, support and help through the thesis. I would especially like to thank them for the generous amount of time they all have taken to discuss ideas and their scrupulous comments on my work to help me improve my academic writing and for sharing their scientific experience and knowledge with me. Thank you for providing opportunities, you have fostered enormous growth in me as an early career academic. I have learnt from you and I am extremely grateful for having worked with you during these years.

I Wish to thank Marta Alvarez, Siv K. Lauvset and Sarah Jutterström for the invaluable help in Quality Control discussions.

I wish to thank Alexander Barth, Charles Troupin and Jean-Marie Beckers for their assistance with the technical and theoretical aspects of climatological analysis and for the help with 'Julia' coding.

I would like to thank also the INOCEN laboratory team at the Spanish national institute of oceanography (IEO) and the GHER at the University of Liége for their help and collaboration during my stay there.

I wish to thank Mireno Borghini for the help with cruise data archiving. I would like also to thank the research team and ship crew of the cruises ICHNUSSA17, ICHNUSSA-JERICO 2018 and JERICO 2019 held on board of the R/V Minerva Uno and R/V DallaPorta, during which I collected measurements.

I am indebted to all investigators and analysts from different observing systems who contributed to data collection at Sea during so many years, as well as to the PIs of the cruises (S. Aliani, M. Astraldi, M. Azzaro, M. Dibitetto, G. P. Gasparini, A. Griffa, J. Haun, L. Jullion, G. La Spada, E. Manini, A. Perilli, C. Santinelli, S. Sparnocchia and PIs of the MOOSE programs), the captains and the crews for allowing the collection of this enormous dataset; without them, this work would not have been possible.

I also want to thank the Department of environmental science and ISMAR who provided the funding. I thank my office mates at ISMAR and DAIS-Ca'Foscari for their friendship and encouragement.

I thank my friends in Venice and Bizerte for giving me many things to enjoy outside of the PhD.

Finally, I must express my very profound gratitude to my family for providing me with unfailing support and continuous encouragement throughout my years of study and through the process of researching and writing this thesis. This accomplishment would not have been possible without them. Rahma, you are the best sister, Jawher and Dhia, the best brothers, thank you for the long phone conversations and for always making me smile. Thank you, mum, and dad, Raoudha and Mostari for the continuous support and encouragement and for always being there for me no matter where I am. Thank you, Ali, my grandfather.

CONTENTS

LIST OF FIGURES

LISTE OF TABLES

Chapter 1. GENERAL INTRODUCTION TO THE BIOGEOCHEMICAL PROCESSES AND THE STUDY AREA (MEDITERRANEAN SEA)

In marine environments, the distribution of nutrients is dependent on both biological and physical processes. In the euphotic layer, near the surface, nutrients are consumed by phytoplankton, while in the deep ocean they are released by remineralizing bacteria in the so-called microbial loop. This is why surface layers are generally depleted in nutrients and concentrations increase with depth. Nonetheless, there are different physical and biological processes responsible for the enrichments of the surface waters. These processes vary in time and space.

The aim of this introductory chapter is to present a general overview of the biogeochemical processes (section 1.1) and drivers of nutrient variability (section 1.2). Then, the focus is on the peculiarity of the Mediterranean Sea particularly the Western basin (section 1.3), the study area of the thesis, a complex ecosystem and one of the oligotrophic oceanic regions.

1.1 Nutrients and biological processes

1.1.1 Biological activity and nutrient vertical distribution

Seawater is composed of minerals and organic matter. Among the most important components are the dissolved nutrients, that constitute one of fundamental resources needed for life, together with light, energy, and space.

The majority of seawater elements are conservative, their concentration is relatively constant and only affected by physical processes (vertical mixing and ocean convection). This category includes sodium for example. Other elements are non-conservative, their distribution is altered by both biological processes (primary production and respiration) and physical processes. These elements include micronutrients which include the bioactive metals e.g. iron and zinc, and macro-nutrients such as nitrate, phosphate, and silicate. The latter fuel phytoplankton growth and maintain the equilibrium of the food web. Phytoplankton forms the base of the oceanic food web and consumes part of these macronutrients during the primary productivity, and therefore control part of the carbon sequestration.

Nitrogen and phosphorus are both found in their inorganic and organic form. The inorganic forms do not contain carbon in their structure. During the photosynthetic activity, primary producers assimilate dissolved nutrients from the surface euphotic layer and transform dissolved CO_2 into organic carbon, releasing oxygen. For 106 atoms of carbon used in the organism, 16 atoms of nitrate and 1 phosphate are used (Redfield et al., 1963). This synthesis of organic matter can be represented by the reaction shown below (Anderson, 1995):

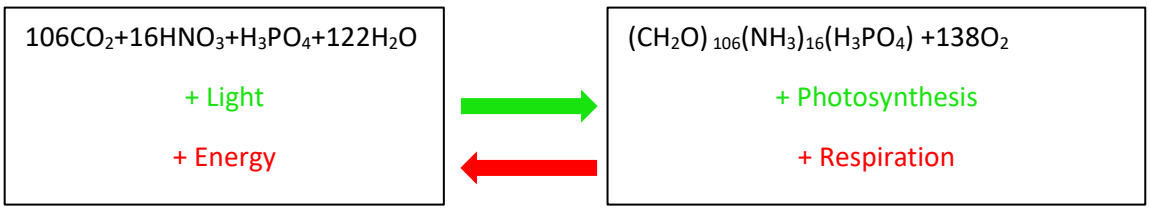

Some of the particulates are transported below the euphotic layer, where there is insufficient light to sustain primary productivity and photosynthesis.

Dissolved inorganic nutrients are an important tracer of biological processes and anthropogenic perturbations (Bethoux et al., 1992). The knowledge of nutrient cycling helps to understand ocean productivity and how it is controlled.

As mentioned previously, nutrient distribution is modulated by an interaction between the biological process and the physical transport of materials.

The reverse reaction of the conversion of organic matter is the remineralization. Part of the organic matter is remineralized by heterotrophic organisms, zooplankton grazing and microbial hydrolysis in the photic zone (Fig.1.1), i.e. the biological uptake, where there is consumption of O_2 and an increase of CO_2.Some fractions are transported by sinking to the deep layer and sediment (Williams and Follows, 2003).

In ideal cases, the biological uptake removes CO_2 from the atmosphere and releases O_2. Nonetheless, there are many situations where vertical mixing and the upward movement of the thermocline to the shallower depths leading to CO_2 release and the uptake of O_2 from the atmosphere.

Part of the organic matter sank into the deep layer and reached the sediment in the form of suspended particulates through vertical mixing/upwelling, and remineralization of sinking organic matter considered as a source of inorganic materials to deep layers. At this level, nutrients are recycled and regenerated within the water column through the biological pump. This process is responsible for the lateral and vertical gradient of nutrients (Williams and Follows, 2003).

Below the euphotic layer, nutrient concentration accumulates since they are consumed by phytoplankton in low light conditions. This nutrient rich interface lays between the surface and deep layer at intermediate depths, the so-called nutricline.

This maximum vertical gradient in nutrient concentration results from the biological pump. Consequently, the typical vertical distribution of nutrient profile shows lower concentrations in the surface and higher concentrations at greater depths (Williams and Follows, 2003) for most nutrients (Fig.1.2). This implies that nutrients are removed by biological uptake and assimilation into particles that are responsible for the enrichment at deep layers.

Nutrients stimulate and maintain ocean productivity and can be a limiting factor of phytoplanktonic growth, hence limiting the capacity of the food chain. Their availability influences the difference in cellular elemental composition (Geider and La Roche, 2002) and features of the plankton community.

Besides to the biological processes, ocean circulation and physical processes continually drive (see section 1.2) the large-scale distribution of chemicals (Williams and Follows, 2003) toward a homogeneous distribution. The increase of nutrients with depth means that physical processes and ocean circulation will be supplying the ocean surface.

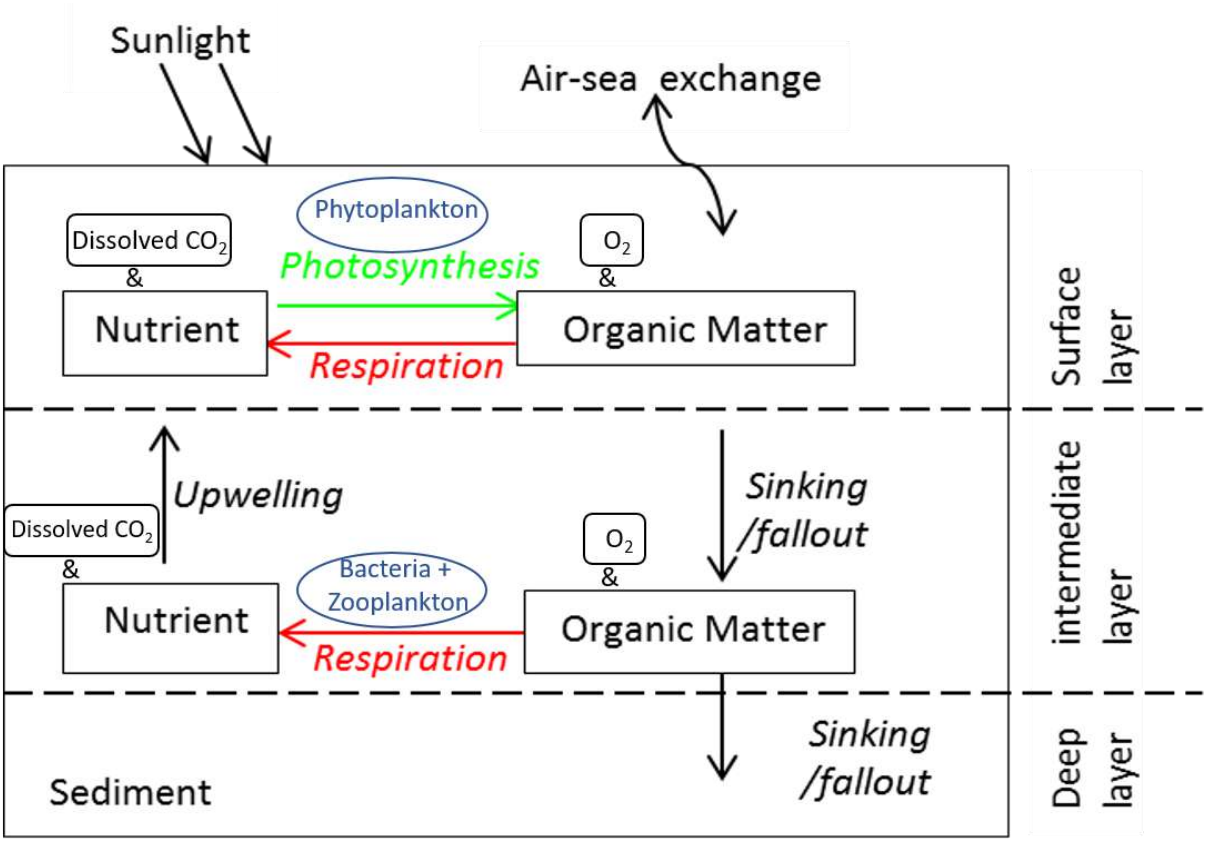

Figure 1.1: A schematic illustration of biological pump (adapted from (De La Rocha and Passow, 2013)) and its role in the oceans.

1.1.2 Nitrogen, phosphorus, and silica cycles

There is a difference between individual nutrient assimilation by primary producers, thus their vertical distribution might also differ.

- *Nitrogen*

Nitrogen is presented in four forms in sea water: nitrate (NO_3^-), nitrite (NO_2^-), ammonium (NO_4^+) and nitrous oxide (N_2O). Nitrate is one of the most important inorganic nutrients, it is the most oxidized and abundant form which makes it the most accessible form for phytoplankton. To maintain the 'equilibrium' of the ecosystem, several chemical reactions occur to compensate for the shortage of nitrate due to consumption.

The nitrogen cycle is mediated by bacterial transformations that include nitrogen fixation, denitrification, anammox, nitrification and assimilation.

Only the diazotrophic bacteria can assimilate N_2 from the atmosphere through nitrogen fixation to be consumed by phytoplankton. These processes are sensitive to dissolved oxygen levels and ocean acidification (Gruber, 2011).

In case of nitrate excess, nitrate is removed by denitrification in anaerobic conditions (Powley et al., 2017; Sarmiento and Gruber, 2006): this process reduces nitrate to gaseous N_2. Its role is to ensure the regulation of the biological process. Another process that removes nitrogen is the anammox (anaerobic ammonium oxidation)

Nitrification or nitrate gain refers to the oxidation of NH_4^+ ,ammonium to nitrate by nitrifying bacteria, it occurss mainly in the deep ocean and plays a crucial role in nutrient recycling since it is a source of nitrate which will eventually be upwelled into the surface euphotic layers supplying primary productivity. Nitrification requires oxygen and is constrained by light (Sarmiento and Gruber, 2006).

Sources of nitrate are loads from deep layers (vertical mixing and upwelling), nitrogen fixation during which the gaseous N_2 is used for the synthesis of organic matter, atmospheric deposition, and riverine input. The sinks for nitrate are denitrification (nitrate loss), especially in conditions of very low oxygen concentrations where nitrate is used as an alternative to oxygen during the process of the oxidation of organic matter (Ward, 2013; Ward et al., 2009; Sarmiento and Gruber, 2006), and consumption by primary producers.

Nitrogen cycling is closely connected with carbon and phosphorus cycles and other elements. This connection implies that any change in nitrogen cycling can impact the biogeochemical process and the ecosystem functioning.

- *Phosphorus*

Inorganic phosphorus is orthophosphate (PO_4^{3-}), found in seawater in particulate and dissolved forms. There is the tendency to consider mainly phosphorus, and there is also H_2PO_4. The organic forms are absorbed by phytoplankton.

The major supply in phosphorus is delivered by external sources mainly continental, through river runoff, wastewater discharges and other sources, such as atmospheric precipitation, volcanism and coastal abrasion (Baturin 2003).

It has been largely introduced to soil as fertilizer and is then transported to oceans through rivers (Baturin, 2003). The principle form of inorganic phosphorus present in seawater is phosphate (Moutin, 2000).

Baturin (2003) suggested that phosphorus cycling is tightly connected to carbon dioxide in the atmosphere. An increase in carbon dioxide leads to warming and the rise of the phosphorus input into the sea, an accelerated rate of sinking of organic matter and phosphorus. Phosphate is important in balancing the functioning of microbial communities in a phosphate depleted surface (Lomas et al., 2014).

The organic forms are used by heterotrophic bacteria and diazotrophs in extreme conditions of oligotrophy. These processes are still not well documented (Dyhrman et al., 2009).

The particularity of phosphorus is that its cycle contains sinks meaning that biological processes cannot generate phosphorus (De la Rocha, 2007).

- *Silica*

Silicon or Silicic acid ($Si(OH)_4$) releases ions of orthosilicate SiO_4^{4-}. It is the principal component of diatoms and radiolarian skeletons. When these organisms are blooming (in cold conditions), there is a significant consumption of silicate (Levitus et al., 1993). It is considered as an important nutrient in the ocean.

Silica enters the ocean through river discharge as solution and suspensions, dissolve through the water column, to reach the sediment. The remineralization of silicate from the sinking particles is slow and requires a higher amount of energy from the organisms, compared to nitrate and phosphate (Williams and Follows, 2003). Although silicate is not very reactive and has a very low solubility, it plays an important role in marine life (Bogoyavlenskiy, 1967).

Silicate accumulation in the sediments is closely related to dissolution of silicate in the overlying layer. The increase in silicate dissolution is enhanced by the warming of the water masses. there is decoupling between silicate cycle and other nutrients (nitrate and silicate) since silicate is not used by all phytoplankton (De la Rocha, 2007).

1.1.3 Remineralization ratios

In the past decades, global nutrients cycles have been altered by human activities and anthropogenic perturbation (Galloway et al., 2004).

The remineralization or stoichiometric ratios are the ratios at which phytoplankton uses inorganic chemicals to produce biomass. In other words, it is the conversion of organic matter that is exported from the surface back into its inorganic form, this is the remineralization process.

Termed also after Alfred Redfield (Redfield et al., 1963), according to him the elemental ratio N:P (i.e. the ratio of inorganic nitrate to phosphate) in deep water is on average $C:N:P:O_2$ = 106:16:1:-138 in the majority of the oceans. He deduced that this ratio could give indications about the state of the biological control of the phytoplankton composition, as well as about which nutrient is limiting phytoplankton growth (Redfield et al., 1963).

The Redfield ratio is a result of biogeochemical processes in spatial and temporal scale. This elemental ratio is considered to be highly conserved (Falkowski et al., 1998), and can give information about the element that is found in low proportions and in short supply (Gibson, 1971) preventing phytoplankton growth. Geider and La Roche (2002) showed that the phytoplankton internal physiology tends to attain a ratio to 16 which indeed influences the uptake of nutrients.

The variation of the N:P ratios of the surface layer can alter the structure, composition, and physiology of phytoplankton communities (Deutsch and Weber, 2012). Redfield ratio includes also other elements like silicate, the ratio C:Si:N:P=106:15:16:1 is used to understand nutrient limitation with respect to silicate, nitrate, and phosphate (Choudhury and Bhadury, 2015)

Hence, concentrations of nutrients are compared to the fixed Redfield ratio to find the nutrient that is constraining primary production; if N:P > 16, phosphate is considered to be the limiting nutrient, and conversely, when N:P < 16, nitrate is limiting the production.

In most oceans, the stoichiometry of inorganic nutrients is identical or close to the Redfield ratio. The ratio variability is not fully understood, though nutrient availability especially of phosphate is seen as a driver (Matsumoto et al., 2020). There is evidence that this ratio vary regionally (Geider and La Roche, 2002).

Generally, in most regions, nitrate is considered a limiting factor, yet phosphate plays a crucial role in determining the Atlantic Ocean (Howarth and Marino, 2006) and the Mediterranean Sea productivity (Krom et al., 1991). These regions where N:P ratio exceeds the 16, are characterized by unbalanced loads from external inputs and nutrient depletion.

1.1.4 Distribution of inorganic nutrient in the World ocean

The global distribution of nutrients and patterns of biological production are controlled by the interplay of various local drivers: the physical and biogeochemical mechanisms and external inputs. Along with the biogeochemical processes, the global ocean circulation patterns play a fundamental role in nutrient distribution and transport (Williams and Follows, 2003).

Largely, nutrient concentrations at the surface are very low and below detection limit for nitrate, phosphate, and silicate. Generally, nitrate becomes depleted before phosphate in most oceans. Referring to Sarmiento and Gruber (2006), adding nitrate to a laboratory culture of phytoplankton in nitrate depleted condition, increases growth, while adding phosphorus does not. It is thus in most world oceans except for the Atlantic, nitrate tends to be a limiting nutrient that is depleted before phosphate (Sarmiento and Gruber, 2006).

The primary production of a region is evaluated by the phytoplankton abundance based on the chlorophyll distribution. The nutrient-rich waters are characterized by high biological productivity referred to as eutrophic region, the example of the tropical and subpolar regions, surface waters.

Inorganic nutrients are introduced into the euphotic layer by upwelling which sustains the increase in chlorophyll concentration and phytoplankton growth near the surface depending on seasons. The high chlorophyll concentrations through the increased light absorption, constrain the production at deep layers. These nutrient-rich zones accounts for 20% of the global ocean, the example of the Southern Ocean (Edwards et al., 2004).

The subtropical regions surface layer is depleted in nutrients with low biological productivity, these zones are oligotrophic (Sarmiento and Gruber, 2006; Sarmiento and Toggweiler, 1984) and characterized by an increase of nutrient with depth where generally the nutricline coincide with the base of the euphotic layer. In the case where the biological pump is limited, the deficiency of the subtropical gyres in nutrient is balanced by lateral transport of nutrient from upwelling and deep convection regions like the nutrient-depleted North Atlantic subtropical gyre.

Some ocean regions show anomalous patterns, they are called high nutrient low chlorophyll (HNLC) regions, where nutrient concentrations tend to be anomalously high and the biological pump is low, particularly in areas of the North Atlantic, equatorial Pacific, North Pacific and Southern Ocean (see e.g. Garcia et al., 2010). At greater depths below 1000 m, nutrient variability is mainly horizontal and reflects the distribution of water masses (Levitus et al., 1993). Low concentrations characterize recently formed deep waters, such as the north Atlantic deep water, which accumulate nutrients with age through remineralization (Reinthaler et al., 2013).

It is necessary to understand the biogeochemical processes and mechanisms deriving nutrient loads and losses and controlling the availability of nutrients, since without them, in the oligotrophic zones surface waters would be in a continuous state of nutrient depletion and could not maintain biologic activity.

1.2 Physical drivers of nutrient variability

Organic materials produced in the surface layer are transported and redistributed within the water column. The surface deficit of nutrients due to the export of organic matter, and its remineralization at depths, is partly compensated by the physical transfer of nutrients through advection, diffusion, mixed layer, upwelling/downwelling (Fig. 1.2) and to the contribution of external inputs.

A fraction of the organic materials is exported to deep layers by gravitational sinking as earlier introduced in section 1.1.1. The organic materials are eventually remineralized leading to the accumulation of nutrients in deep layers and in old water masses. Another fraction is regenerated within the surface layer itself.

The biological processes change the nutrients' form, while the physical processes are responsible for their redistribution within the water column.

- Upwelling

With the action of wind, blowing from a certain direction with respect to the coast, the surface water is pushed away, and water rises from below to replace the displaced surface water (continuity), inducing what is generally called upwelling.

Upwellings bring nutrients from deep layers to the surface where they act as fertilizers of the surface water. The reverse process is downwelling and occurs under the action of wind blowing in the opposite direction with respect to the coast, and in this case the surface water sinks to greater depths (Nieblas et al., 2009).

- Mixed layer deepening

The mixed layer depth (MLD) is the surface layer in which physical and biological characteristics are uniform (Chu and Fan, 2011), it is where an active turbulence is observed, a layer of intense air-sea interactions. Hence, it shows seasonal variations. For example, in the Mediterranean Sea, the deepening of the mixed layer, after summer, leads to an autumnal bloom (Mignot et al., 2014; Ortenzio et al., 2014). Thus, the MLD affects phytoplankton dynamics by controlling nutrient availability, and therefore biological productivity (Jang et al., 2011).

- Mesoscale structures and diapycnal supply

Nutrient supply to the euphotic layer is not only based on large scale terms, mesoscale eddies and fine scale structures can reveal additional nutrient signatures and patterns (Williams and Follows, 2003).

Eddies are formed through baroclinic instability of currents but also through density fronts, interaction with bathymetry or winds. The water mass inside the eddies is isolated and can be identified by its properties.

Schematically, cold nutrient-rich water rises toward the surface in cold-core eddies (McGillicuddy et al., 2007). Likewise, nutrient-depleted surface water is downwelled in the centre of warm-core eddies (Benitez-Nelson et al., 2007). These structures transport water and heat and promote ocean large scale mixing. In the process, they also transport nutrients and contribute to the recharging of nutrient-depleted waters (Oschlies, 2008), thus, impacting the upper-ocean biology (Falkowski et al., 1991).

The diapycnal supply of nutrient to the surface layers is an upward flux of nutrient which is the product of diapycnal diffusivity and the vertical nutrient concentration (Zhang et al., 2017).

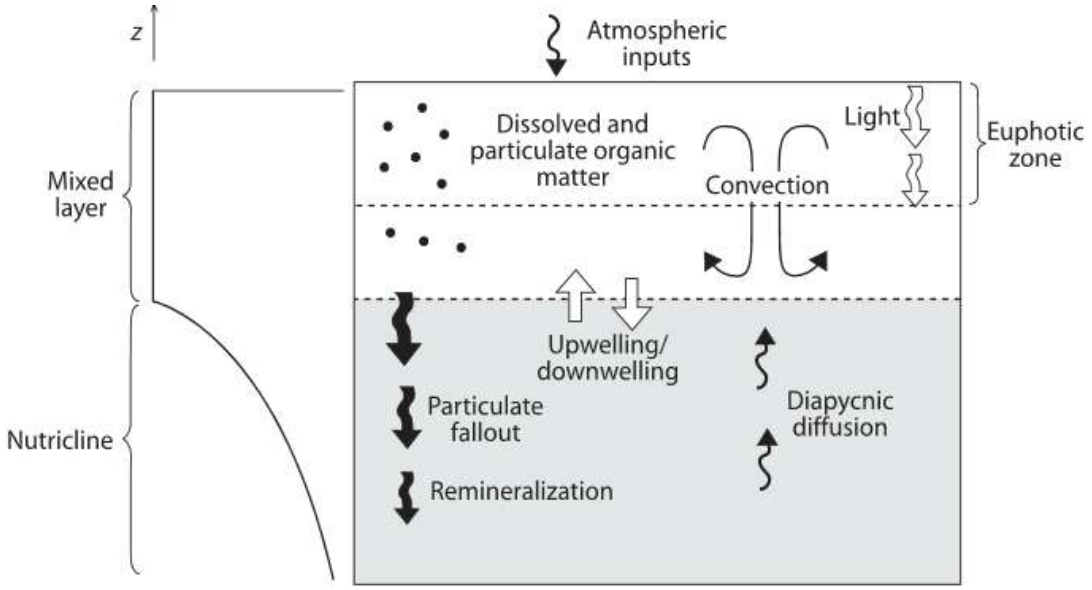

Figure 1.2: Schematic representation of physical processes affecting biological processes within the water column (Williams and Follows, 2003).

- External input

The external sources or land-based emission inputs of nutrients emit significant loads to the sea. Indeed, the atmospheric deposition through wind transport of particles is believed to be an important

and terrestrial inputs: river discharge, influence the biogeochemical cycles. These external inputs bring a significant amount of terrestrial nutrients to the ocean surface and influence patterns of limitations (Moore et al., 2013).

In general, anthropogenic perturbations have increased the external input of nutrient to the ocean, major change are expected at local scale and a modest change is noted in the whole ocean biogeochemistry (Moore et al., 2013) because the transported elements sink quickly to the sediment in coastal areas and barely reach open ocean.

The fluvial fluxes of nitrogen and phosphorus to the ocean were increased over the preindustrial period (after 1860). Atmospheric inputs, on the other hand, are predicted to bring more nitrogen relative to phosphate (Moore et al., 2013). For silicate and phosphate, the external input is limited to atmospheric deposition and river input, their main sink in the sedimentation of particulate matter

Nitrogen, however, has additional biological sources, N_2 gas fixation, and sinks, through denitrification and anammox processes (Bristow et al., 2017).The mechanisms described above vary in time and space and are found in most oceans.

Regardless of the vital role of physical processes, there is a significant disparity between individual nutrient distributions. Silicate for example has a slow remineralization rate from

sinking particles compared to nitrate and phosphate (Gnanadesikan, 1999). Also nitrate distribution could be different from phosphate through fixation of N_2 gas at the surface layer.

Therefore, nutrients have different distributions and each one can be a limiting factor over different regions and at different times in the surface ocean (Moore et al., 2001).

1.3 The area of study

1.3.1 Mediterranean Sea, a peculiar environment

The Mediterranean is one of the richest areas in marine biodiversity, it presents 4 to 18% of the world's marine species (Bianchi and Morri, 2000). The region displays different environmental and climatic conditions. It is considered as a miniature ocean, presenting a wide variety of physical and biological processes, including deep water formation ,that is only found in the polar regions, and the thermohaline circulation (Volpe et al., 2012), a peculiar oligotrophy, that can be found in other ocean systems of the globe (like a subtropical gyre). The Mediterranean Sea can be considered as a 'scale model', a 'laboratory basin' of the world's ocean since its thermohaline circulation reproduces the global circulation on a small scale. Thus, understanding its functioning allows insights about phenomena that go beyond its own borders of larger marine ecosystems that are more complex to study.

The Mediterranean Sea is the largest land-locked sea in the world. Excluding the Black Sea, its area extent is 3700 km in longitude and 1600 km in latitude, covering an area of about 2.5 million square kilometers, with a volume of 3.7 million cubic kilometers.

It is located in a transitional band between the mid-latitude and subtropical regimes, which is the origin of its high climatic variability. It is under the influence of both the ocean and desert. Its seasonal cycle is characterized by hot, dry summers and windy, wet winters. The climate is under the effect of regional strong winds such as Scirocco from the south, Bora, and Mistral from the north.

The average depth of the sea is about 1500 m, and its deepest trench is at 5121 m in the Ionian Sea (Matapan Pit). The coastline is 46.000 km long and it is fed by the four major rivers ,the Nile (Egypt), the Po (Italy), the Rhone (France) and the Ebro (Spain). The Mediterranean Sea is separated by straits and channels dividing it into several basins.

It communicates with the Atlantic Ocean through the Strait of Gibraltar, which is only 14 km wide and 300 m depth, and with the Black Sea through the Dardanelles strait, which is 1.2 to 6 km wide and 55 m depth.

The Mediterranean Sea is divided into two large basins, the Western Mediterranean (WMED) and the Eastern Mediterranean (EMED), separated by Sicily Channel (400 m depth). The two basins are also divided into several sub basins (Fig. 1.3).

Although it represents only 0.7% of the world ocean surface, the Mediterranean Sea is an important marginal sea, economically and ecologically. It is undergoing an increasing anthropogenic perturbation (i.e. overfishing, pollution …) that is heavily impacting the marine ecosystem (i.e. ocean acidification, warming, bioinvasion, habitat loss). The coastline, about 46 000 km, is heavily populated, about one-third of the population live along the shore.

A clear demonstration of man-made change is the opening of the Suez Canal that caused the Lessepsian migration (Zakaria, 2015), causing invasion of the marine endemic fauna and a drastic change in the marine ecosystem. Some endemic benthic and pelagic marine biota have been lost, due to the increase in sea temperature as well, adding to that overfishing and habitat loss that impacted highly the Mediterranean marine ecosystem (Lejeusne et al., 2010).

Touratier and Goyet (2011) showed that the Mediterranean water mass pH decreased due to increasing anthropogenic perturbations. These significant changes urged the International Panel on Climate Change (IPCC) to classify Mediterranean Sea as one of the most perturbed marine ecosystems of the global ocean.

Hermann et al. (2008) studied the impact of climate variability on the Mediterranean marine ecosystem and found that the increase in temperature increased the stratification of the water column, causing a reduction in the rate of deep convection, hence limiting the transport of nutrients near the surface and inducing a decline in phytoplankton bloom.

The decrease rate in Phytoplankton bloom cause disorder in the ecosystem i.e. Trophic chain. Various factors can act on transforming, retaining and removing nutrients like inputs from land through rivers discharge that contribute considerably to the nutrient balance. Yet, human activities have changed the freshwater discharge through time and consequently put the marine ecosystem under pressure (Grizzetti et al., 2017).

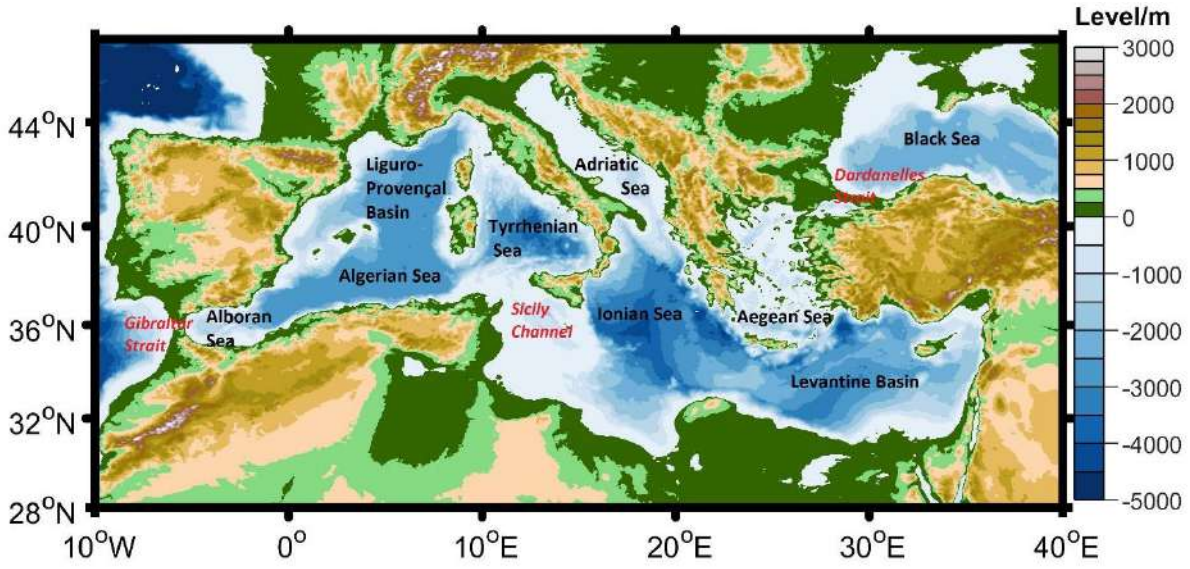

Figure 1.3: Elevation Map of the Mediterranean Sea and the main sub-basins.

According to Malanotte-Rizzoli et al. (2014), the Mediterranean Sea had undergone an impressive change in physical and biogeochemical properties. An increase in temperature and salinity, with a high inorganic and anthropogenic carbon levels. Models have predicted that with increasing atmospheric CO_2 concentrations, there will be a decline in the dissolved oxygen in the ocean interior.
In deep layers, the changes are a result of a low ventilation rate and a continuous consumption of dissolved oxygen through remineralization sinking organic matter (Matear and Hirst, 2003).

1.3.2 Mediterranean Sea circulation and water masses

To understand the biogeochemical properties of the Mediterranean Sea, it is necessary to start with a description of the general circulation. The Mediterranean thermohaline circulation exhibits an interannual and seasonal variability. It consists of circulation of several water masses, eddies, and currents. Different forces induce the changes in the Mediterranean hydrology.

The high evaporation rate (Tanhua et al., 2013), the low precipitations and rivers runoff characterize the Mediterranean Sea with high salinity and force an anti-estuarine circulation (Brenner, 2012). The deep water of the EMED are formed within semi-enclosed subbasin (i.e. Adriatic Sea and Aegean Sea), while deep water formation (DWF) area in the WMED is located in the Gulf of Lion.

1.3.2.1 Surface circulation

Because of the negative heat and freshwater budget, the Mediterranean Sea is receiving heat and water from the Atlantic Ocean to compensate for the deficit. The Atlantic Water (AW), characterized by low-salinity and low-nutrient content, enters the Western Mediterranean Sea (WMED) at the surface, through the Strait of Gibraltar, and moves toward the Eastern Mediterranean Sea (EMED).

This surface water flow (Fig. 1.4a) at the upper 150-200 m and as it progresses, its physical properties are modified by mixing processes with the resident waters gaining salt and heat. The AW is identified by its salinity minimum that spans from 36.5 in the Alboran Sea, 37.5 in the Sicily Channel and 38.9 in the Levantine basin.

Crossing the Sicily Channel, the flow splits, and partly progresses to the EMED through the Sicily Channel, while another vein of AW flows into the Tyrrhenian Sea, where it gains salinity (up to 38) after mixing with the Intermediate water (IW). From there, AW crosses the Corsica Channel to reach the Ligurian Sea and the Gulf of Lion (salinity up to 38-38.4). When it reaches the Balearic Sea, salinity of the AW is somewhat decreased, as a result of intrusion of mesoscale structures and eddies formed in the Algerian basin (Millot, 1999).

In the Levantine basin Cretan Sea, the AW becomes saltier, warmer, and denser, then it sinks to intermediate levels and forms the IW (200-500m).

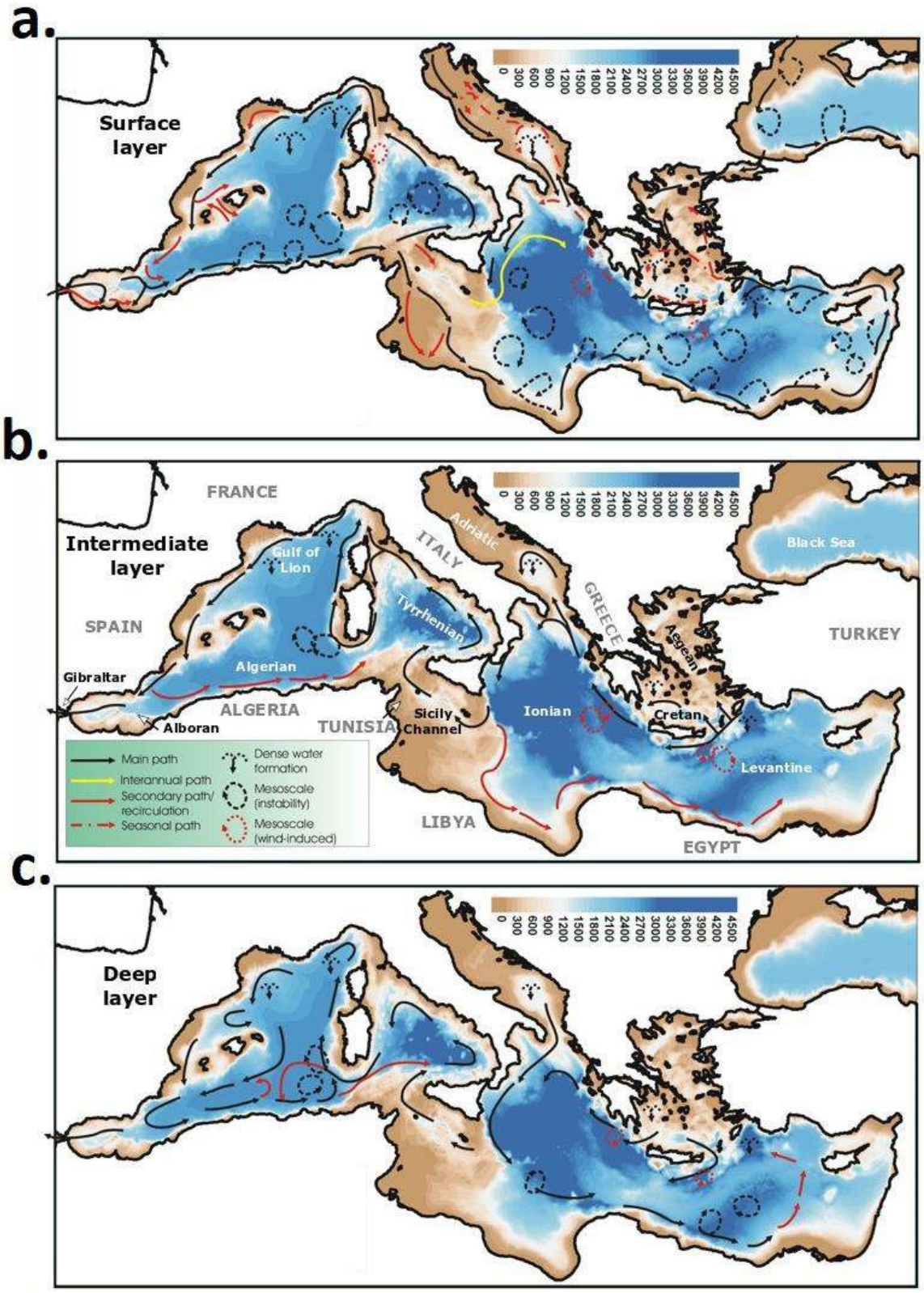

Figure 1.4: Circulation schemes of the surface layer (**a.**, AW), the intermediate layer (**b.**,IW) , and the deep layer (**c.**,WMDW, EMDW). Here some geographical names of sub-basins, channels and bordering countries are included for clarity) (Schroeder, 2019).

1.3.2.2 Intermediate and Deep circulation

This intermediate water flows westward across the entire Mediterranean Sea to the Atlantic Ocean. Coming from the Levantine basin or Cretan Sea, it is named depending on its formation area, Levantine intermediate water (LIW) if it originates from Levantine Basin or Cretan Intermediate Water (CIW), if it flows from the Cretan Sea (Schroeder et al., 2017). To avoid any confusion, it is considered as the intermediate water (IW); this water mass is recognized by a salinity maximum in the whole basin.

The IW enters the Sicily channel after a long journey of 16-18 yr (Gačić et al., 2013), its content in nutrients increase (relatively to the conditions in the EMED) with age (Schroeder et al., 2010), it arrives to the Tyrrhenian Sea and diffuse along the intermediate layer.

It is a key water mass, because it is involved in the formation and transformation of the deep waters of the EMED and the WMED.

The IW travels through the Sicily Channel with a salinity of 38.75 to reach the Tyrrhenian Sea where it gradually becomes less saline (38.6). In the Tyrrhenian Sea, IW contributes to the Tyrrhenian Deep Water (TDW) formation (Menna et Poulain, 2010).

As for the deep layer, the Western Mediterranean Deep Water (WMDW) is formed in the Gulf of Lion through deep convection (Testor et al., 2018) while the Eastern Mediterranean Deep Water (EMDW) is formed in the Adriatic Sea and occasionally in the Aegean Sea (Lascaratos et al., 1999; Roether et al., 1996, 2007).

The WMDW moves cyclonically and is responsible for the overturning of the water column over 2000 m.

As highlighted above, the Mediterranean region is very sensitive and vulnerable to climate change (Giorgi, 2006) since it responds quickly to atmospheric perturbations. Temperature and salinity of the Mediterranean Sea waters have increased with an accelerated trend during the past decades (Vargas-Yáñez et al., 2012).

Previous studies (Bethoux et al., 1999; Borghini et al., 2014; Schroeder et al., 2006; Schroeder et al., 2016; Skliris et al., 2014; Smith et al., 2008; Vargas-yáñez et al., 2009; Zunino et al., 2009) about the Mediterranean Sea temperature and salinity showed a tendency toward the warming and salting of the deep and intermediate layer in the WMED and EMED since the 1980s, and reported the existence of a possible long-term trend in the intermediate and surface waters. Millot et al. (2006) observed an increased salinity in the Mediterranean outflows in Gibraltar strait. Other studies divulgated changes in the thermohaline properties (Béthoux et al., 1998; Maillard et al., 2005; Rohling and Bryden, 1992).

In recent years, there was an abrupt shift detected in the Mediterranean Sea, a change in the source of deep water in the EMED that occurred between 1992 and 1995 (Roether et al., 2007). The deep-water formation in EMED changes from the Adriatic Sea to Aegean, this change is known as the Eastern Mediterranean Transient (EMT, (Roether et al., 1996). The

major changes resulted in a new dense water EMDW and an enhanced salinity of the intermediate water. The IW with its increased salinity entering the WMED (Gasparini et al., 2005) contributed to the formation of the WMDW during 2004-2006 cold winters (Schroeder et al., 2006, 2009). Climatological events known as the Western Mediterranean Transition (WMT, (Schroeder et al., 2009, 2016)).

The WMT started in 2004/05 induced by a progressive increase in temperature and salinity of the intermediate water inflow from the EMED, that led to the occurrence of an important deep convection and increasing abnormally the rate of deep-water formation between 2004 and 2005 (Schroeder et al., 2016).

The result of this climatological event was a newly generated deep water that is denser, saltier, and warmer than the resident old WMDW. The new WMDW propagates eastward toward Tyrrhenian sea and westward toward the Alboran Sea.

Studies have described an overall increase in temperature salinity and density of intermediate and deep layers after this event (Schroeder et al., 2016; Vargas-yáñez, 2017) and a recent study of Li and Tanhua (2020) demonstrated an enhanced ventilation in deep layer over time in the WMED.

This ventilation process and its variability has an impact on the distribution of inorganic nutrients and thus influence changes of biogeochemical cycles (Shepherd et al., 2017). An increased ventilation means an increase in dissolved oxygen in the sea interior, implying an increase in mineralization rate and thus in dissolved nutrients.

However, oxygen is consumed over time by biological activity leading to the decline of the oxygen content, which in turns accelerates the denitrification, a nitrate sinking, and promotes the release of phosphate in the case of an increase in temperature (Watson et al., 2017). The impact of the WMT on nutrient distribution is investigated in Chapter 4.

It is not yet clear how these events will impact the long-term change of biogeochemical properties. We might however expect that stratification will increase, and this will have an impact on biogeochemical cycles, with a further reduction in the surface layers nutrient supply, and a reduction of the ventilation rate.

The Mediterranean Sea is a well-ventilated basin especially the WMED indicating a longer residence time of the deep waters while the Eastern Basin is characterized by a slow ventilation (Schroeder et al., 2015). We will focus on patterns within the WMED.

1.3.3 Mediterranean Sea Biogeochemistry: Inorganic nutrients

Being an enclosed marginal sea, the Mediterranean Sea exhibits an anti-estuarine circulation, responsible for its oligotrophic character (Bethoux et al., 1992; Krom et al., 2010), it is considered as the least productive marine ecosystem, acting like a subtropical anticyclonic

gyre, also known as a Low-Nutrient Low-Chlorophyll (LNLC) region contrary to the HNLC ocean region (Migon et al., 2020).

The Mediterranean Sea has been identified as a sensitive region significantly affected by ongoing climatic changes, like warming and decreasing precipitation rate (Giorgi, 2006). In addition, it is a region particularly valuable for climate change research because it behaves like a miniature ocean (Bethoux et al., 1999) with a well-defined overturning circulation characterized by spatial and temporal scales much shorter than for the global ocean, with a turnover of only several decades.

Being an intercontinental sea, and subjected to more terrestrial nutrient inputs (river runoff, submarine groundwater discharge) and atmospheric deposition, the Mediterranean Sea has a nitrate to phosphate N:P ratio that is anomalously high compared to the “classical” world's oceans Redfield ratio, indicating a general P-limitation regime, which becomes stronger along a west-to-east gradient.

The Mediterranean Sea is therefore a potential model to study global patterns that will be experienced in the next decades worldwide, not only regarding ocean circulation, but also the marine biota (Lejeusne et al., 2010). Several environmental variables can act as stressors for marine ecosystems, by which climatically driven ecosystem disturbances are generated (Boyd, 2011). These changes affect, among others, the distribution of biogeochemical elements (including inorganic nutrients), the functioning of the biological pump and CO_2 regulation.

In spite of being one of the most studied regions, the Mediterranean Sea nutrient variability remains relatively not well defined. Various international research programs are set to monitor and collect measurements of inorganic nutrients over the last decades in the WMED (Schroeder et al., 2013): the Medar/Medatlas (Fichaut et al., 2003), SESAME, MATER databases and the MOOSE program (http://www.moose-network.fr/).

From a biogeochemical point of view, the Mediterranean Sea oligotrophy is marked (Siokou-Frangou et al., 2010) by a low biological productivity due to low concentration of inorganic nutrients essential for phytoplankton growth. This oligotrophic regime is due to the low supply from deep layers and to the lateral supply from adjacent high nutrient regions that is used up before being horizontally transported. The particularity of the Mediterranean Sea biogeochemistry is the importance of the new production of nutrient (regeneration and recycling processes), and the episodic supply of nutrient by mixing processes and nitrogen fixation (Sarmiento and Gruber, 2006).

De Fommervault et al. (2015) has shown the seasonal cycling of nutrients within the northwest most area, indicating the low concentration of nutrients in the surface layer all year, except in winter and spring explained by the important mixing in these periods.

Indeed, the vertical mixing in the convection areas of both basins, the WMED and the EMED, ventilates the deep layers and brings nutrient rich waters to the surface layer favoring phytoplankton growth.

Figure 1.5 shows the variation of nutrients along a longitudinal section crossing the WMED and EMED (see map in figure 1.5c). We can clearly identify the Mediterranean Sea biology, through a vertical gradient which separates the surface depleted layer and the intermediate and deep enriched layers in nitrate, phosphate, and silicate. The vertical distribution of nutrients is explained by the biological processes within the water column that is dependent also on local events.

The surface layer is almost always depleted in nitrate and phosphate. Silicate is also low because of the presence of diatoms that consume silicate. The Atlantic surface water enters the WMED via Gibraltar with a low amount of inorganic nutrients which are consumed along its path toward east. The decreased oligotrophy from east to west is explained by the outflow of the intermediate water which exports nutrients out of the WMED, this is considered as a loss of nutrient pool resources.

The Mediterranean Sea is deficient in phosphate relative to nitrate (Béthoux et al., 1998). It has low nutrient resources that condition the low phytoplankton biomass communities and primary production.

As shown in Figure 1.5, the thickness of the nutrient-depleted layer is variable and increases from West to East, to more than 100 m in the Levantine basin (Pujo-Pay et al., 2011). The intermediate and deep waters on the other hand are rich in nutrients, due to the remineralization of organic matter by bacteria.

According to Ribera d'Alcalà (2003), in the IW of the WMED, nitrate concentrations vary between 4 and 10 μM, phosphate concentrations between 0.18 and 0.47 μM and silicate concentrations between 6.46 and 8.4 μM. The lowest concentrations are observed in the EMED, where nitrate concentrations vary between 3 and 5 μM, phosphate concentrations between 0.04 and 0.18 μM and silicate concentrations between 3.96 and 7 μM.

As can be noted also from Figure 1.5c, silicate does not show a clear west-east gradient, like nitrate (Fig.1.5a) and phosphate (Fig.1.5b).

Higher values were noted in the deep layer by Ribera d'Alcalà (2003), with the same difference between basins notably for nitrate and phosphate (Fig. 1.5). The maximum concentration of nutrients is found between 800 and 1200 m (Ribera d'Alcalà, 2003; Schlitzer et al., 1991). This is also why the two basins have different primary production rates (D'Ortenzio and Ribera d'Alcalà, 2009; Krom et al., 1991; Moutin and Raimbault, 2002; Pulido-Villena et al., 2010).

Nutrient budget in the Mediterranean Sea, according to Ribera d'Alcalà et al. (2003) is based on nitrogen loss that is compensated by the external sources (atmospheric and terrestrial deposition). Phosphate and silicate budget are in permanent deficiency. de Fommervault et

al. (2015a), evaluated the atmospheric inputs on the nutrient budget of the Northern WMED for being the second most important nutrient loads for the surface layer after the deep convection.

It seems that the Mediterranean Sea nutrient budget is difficult to balance even with the external inputs.

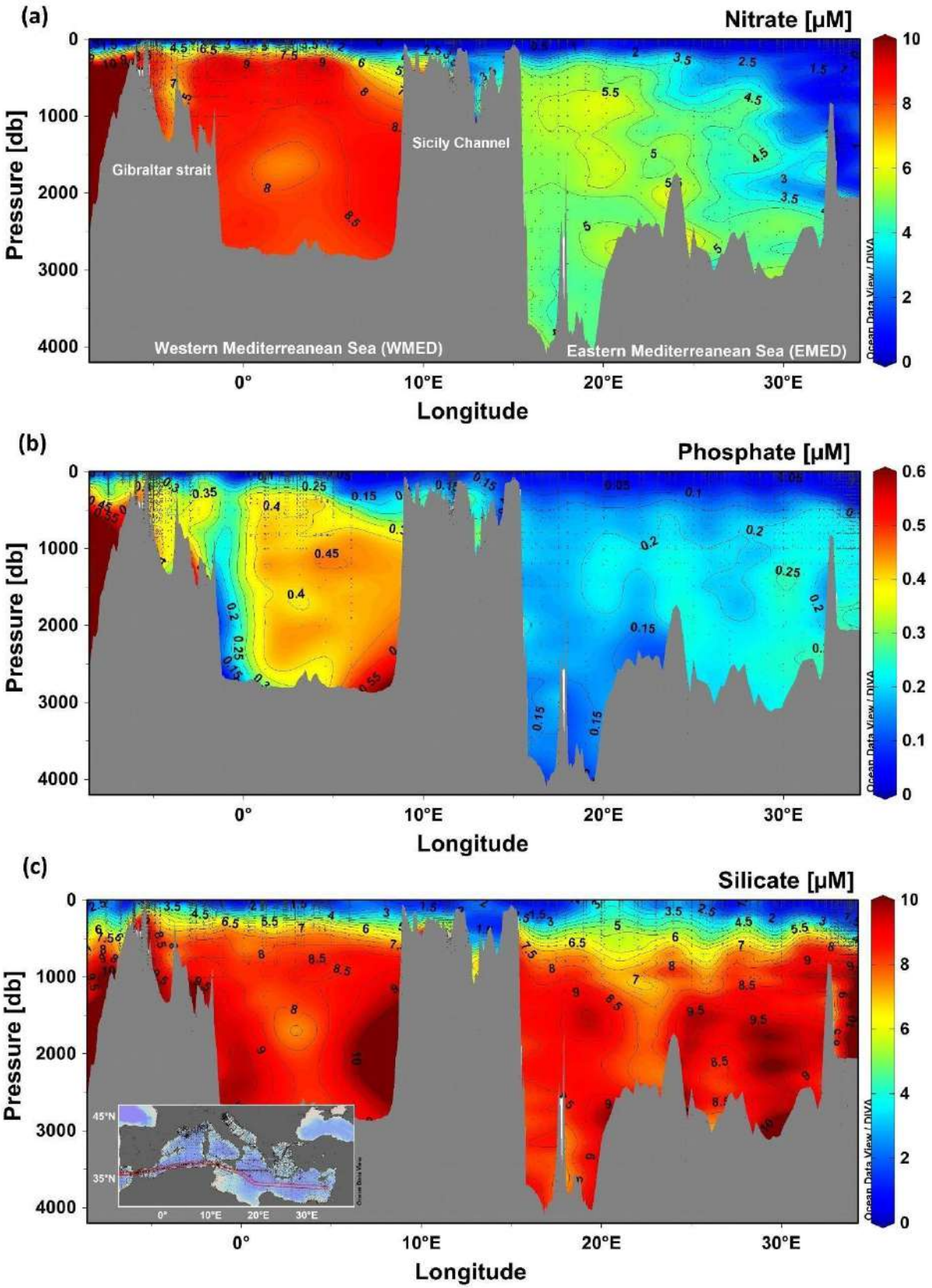

Figure 1.5: West-East section (red line on the map) of concentrations of (a) nitrate, (b) phosphate and (c) silicate (color shading in μM) in the Mediterranean Sea on average for the 1950-1999 period (MEDATLASII dataset, 2002) (Transect along the red line on the map). Note that the pressure scales are identical, and the color scales are different.

1.3.4 Remineralization ratio

The stoichiometry of remineralization in the Mediterranean Sea shows a nitrate to phosphate ratio that deviates from the global ocean Redfield ratio. This divergence is related to various processes and mechanisms. Early studies associated the unusual ratio to the important nitrogen fixation (Ribera d'Alcalà, 2003), the ecosystem behavior, and the composition of the phytoplankton community. Others (Huertas et al., 2012; Krom et al., 2010) related it to external loads from river discharge or atmospheric deposition.

The average Redfield ratio in the deep ocean is N:P=16:1 (Redfield et al., 1963), in the Mediterranean Sea values vary from 21 to 24 for N:P, while Si:N is less than 1 in the WMED (Ribera d'Alcalà et al., 2003) and can reach 100 in the surface layer (Moutin and Raimbault, 2002) at the deep chlorophyll maximum (Diaz et al., 2001; Moutin and Raimbault, 2002). In the EMED N:P=28:1 and Si:N > 1.3 in the deep water. Both N:P and Si:N ratios increase from west to east.

One of the reasons for this peculiarity in both basins is the influence of atmospheric deposition (Bartoli et al., 2005; Béthoux et al., 2002; Huertas et al., 2012; Krom et al., 2004, 2010; Markaki et al., 2010) and rivers discharges that are rich in nitrate and poor deficient in phosphate. These influences increase from west to east as well (Herut et al., 1999; Ludwig et al., 2009a).

The EMED has a skewed remineralization N:P ratio that could be due to the increased rate of nitrogen fixation in some areas (Rahav et al., 2013). Some studies suggest that nitrogen fixation is stimulated by the dust input (Ridame et al., 2013) that can impact not only the photic layer (Halm et al., 2011) , although recent works found low rate N-fixation (Krom et al., 2010; Powley, 2017).

Krom et al. (2004) related the increase in the Redfield ratio to reduced vertical fluxes of organic matter and a very low rate of denitrification (microbial reduction of nitrate to N_2 in anoxic conditions where oxygen consumption exceeds oxygen supply), as most likely symptoms of an oligotrophic basin. Another hypothesis explaining the high nitrate and phosphate concentration in the Western basin is that the azote fixation is enhanced by the Saharan dust.

The N:P ratio identifies the nutrient responsible for limiting primary production. In the case of the Mediterranean Sea, the high N:P ratio indicates that phosphorus is constraining primary production, rather than nitrogen (Krom et al., 2010; Macias et al., 2019). These conditions are able to induce physiological adaptations of phytoplankton communities, being the causes for instance of the dominance of small sized phytoplankton in the community (Siokou-Frangou et al., 2010).

Findings of Barale et al. (2008) highlighted an increase in nutrient-limiting symptoms, caused by the increased episodes of stratification and the reduction of the vertical mixing, a direct response of the warming trend of the Mediterranean Sea.

It has been shown that the molar ratio exhibits a seasonal variability, notably it increases in stratification periods (Kress and Herut, 2001; Pujo-Pay et al., 2011). It has been revealed also an increased trend in nutrient in deep layers of the WMED due the deep-water uplift (Fommervault et al., 2015). It seems that the use of the reference Redfield does not fit the Mediterranean Sea conditions. In section a detailed study (see section 3.4) about the remineralization ratio in the Western part of the basin.

1.3.5 Water mass circulation and its effect on nutrient concentrations

The Mediterranean Sea did experience various changes that influenced the composition and the equilibrium of its ecosystem. Nutrient availability in the Mediterranean Sea is influenced by a range of factors. As detailed in section 1.2, nutrient availability is maintained through physical drivers (general circulation patterns, upwelling, mixing…).

Since the Mediterranean Sea exhibits an anti-estuarine circulation and an unbalanced river input, it is characterized by a nutrient-depleted surface layer (Redfield et al., 1963) and a west-to-east increasing oligotrophy (Crispi et al., 2001).

Salinity of the water masses increases along the anti-estuarine circulation while nutrients decrease. These Atlantic nutrients are quickly consumed before reaching the Sicily channel (Crispi et al., 2001).

The Atlantic surface water is poor in nutrients, and along its path through the Mediterranean the external inputs (atmospheric and terrestrial inputs) are not enough to enrich the surface layer. In addition, the short residence time of Mediterranean water masses (Van Cappellen et al., 2014) in the surface layer constrain the accumulation of nutrients within the water column, explaining the permanent oligotrophy of the surface waters (Lazzari et al., 2016). At the Gibraltar Strait, there is an upward displacement of isopycnals, that help to inject nitrate and phosphate into the surface layer (Huertas et al., 2012).

The surface water (AW) and the intermediate water (IW) outflow in the opposite direction. The IW accumulates nutrients as it ages and along its path to the west (Schroeder et al., 2020), and then exports them to the Atlantic.

Average phosphate and nitrate concentrations found in the Atlantic deep layer is 1.5 μM (phosphate) and >15 μM to 20 μM (nitrate) (Emeis et al., 2010) , while in the WMED deep layer concentrations are much lower: 0.3-0.6 μM phosphate, 6-10 μM nitrate in the WMDW, and 0.1-0.3 μM phosphate , 3-6 μM nitrate in the EMDW (Fig.1.4, MEDAR/MEDATLAS).Very low values are found in the WMED and EMED;

The Mediterranean Sea is losing 10% of its nitrogen and phosphorus budget and 50% from its silicate budget (Coste et al., 1988) through the Strait of Gibraltar. According to recent modelling studies (Powley et al., 2018), the Atlantic water coming from the Strait of Gibraltar

is the main source of phosphate and nitrate, but the anti-estuarine circulation is removing about 45% of nutrients.

During the mixing period, from late autumn to winter, surface nutrient concentrations increase, photosynthesis is at its maximum.

According to García-Martínez et al. (2019) nutrient maxima at the depth of IW depth coincides with a minimum in dissolved oxygen. The latter increase with depth since deep waters are well ventilated in the WMED thanks to the winter deep convection. This process is an important fertilizing event occurring in the Gulf of Lion, during which the entire water column becomes homogeneous. The upper layer productivity is increased during this season, and the surface chlorophyll is at its maximum. This is related to the enrichment of the surface waters with deep nutrient rich water, adding to that the external inputs, river discharge from the Ebro and Rhône (Falco et al., 2010; Salat et al., 2002).

In the WMED, the limiting factor for phytoplankton bloom is variable from region to another. During spring bloom, it has been reported that both nitrate and phosphate are limiting in the Gulf of Lion (Fommervault et al., 2015). Phytoplankton spring bloom is limited by phosphate during stratification episodes, and nitrate limited during winter (Marty et al., 2002). During the rest of the year, in stratified conditions, primary production is maximum at the deep chlorophyll maximum, a structure characterizing oligotrophic regimes (Segura-Noguera et al., 2016).

The EMED on the other hand is highly oligotrophic and is considered as the largest P-limited ecosystem worldwide (Howarth and Marino, 2006). The EMED primary productivity is much lower than in the WMED (Turley et al., 2000). The P-limiting character and the higher nitrate to phosphate ratio (Krom et al., 2005) of the EMED has been attributed to the biogeochemical processes related to the decreased nitrification rate in the surface waters (Emeis et al., 2010), as explained above.

As a result, during winter, phytoplankton proliferation is limited by phosphate, and some excess of nutrients remain in the surface (D'Ortenzio and Ribera d'Alcalà, 2009; Mayot et al., 2016). After the seasonal thermocline, nitrate and phosphate become limiting factors. The reason is that phosphate is entirely assimilated while part of the nitrate enters the dissolved organic nitrogen pool (Emeis et al., 2010).

Despite the general oligotrophy, the Mediterranean Sea is able to maintain primary production. The reason behind this sustainability is the recycling of nutrients and the existence of physical mechanisms that act as fertilizer in some sub-basins. These mechanisms are mesoscale structures and upwellings responsible for the vertical transfers of nutrients, and the winter convection, which is considered the main process, though it is only locally effective (Astraldi et al., 2002).

The Alboran sea is a permanent upwelling area where a continuous uplift of nutrients occurs to the surface water (Reul et al., 2005). The recurrent meandering of the Provencal-Catalan

along-shelf current enhances the transport of nutrients from coastal areas to the open sea. Also, the Balearic Sea is characterized by shelf-slope exchange due to mesoscale eddies (Bouffard et al., 2010). These fertilization mechanisms enhance biological activity locally, impacting the overall productivity levels of the basin.

The biological processes have an important role to maintain and recycle nutrients. In the Mediterranean waters, different factors could be related to the depleted surface, among them the deepening of the nutricline from west to east (Ribera d'Alcalà, 2003). Nitrate and phosphate show similar gradients, while silicate has a different behavior: according to Ribera d'Alcalà (2003) silicate is consumed after nitrate and phosphate in surface layers, while others (e.g. Krom et al., 2014) suggest the existence of an external silicate source in the EMED.

It has been suggested that with the continuous temperature increase, the stratified period would increase as well reducing the nutrient supply to the euphotic layer (Calvo et al., 2011). A reduction of the intensity and frequency of deep-water convection would have the same effect. The deep-water convection is responsible for the ventilation of the deep layers and the enrichment of the upper layer in nutrients. It has been proven that the decline in dissolved oxygen is associated with the reduced ventilation rate in the deep ocean and by the warming decreasing the solubility and biological consumption (Schmidtko et al., 2017).

1.4 Thesis objectives and outline

The objectives of this work are to improve our knowledge about the biogeochemistry of the Western Mediterranean Sea through inorganic nutrients (nitrate, phosphate, and silicate) and understand the processes that regulate the mean nutrient concentrations spatial and temporal variation. Few studies have investigated the multi-annual, in this case 14 years of measurements, distribution of dissolved inorganic nutrients over the entire WMED, with particular regards to the most recent years.

The area of study is characterized by a complex hydrodynamics and significant influence of mesoscale structures on the biogeochemical properties: changes in the thermohaline circulation have consequences on the functioning of the entire basin. The Mediterranean is a well oxygenated, oligotrophic to ultra-oligotrophic sea, adding complexity to the analysis.

1.4.1 Research Questions

This thesis addresses the following questions:

- Are the CNR-WMED biogeochemical observations consistent with previous measurements in the region?
- Is there a regional difference in remineralization ratios in the WMED and is nutrient variability dependent on physical properties of subregions and local events?
- What could cause the vertical gradient in nutrients?

- Is climate change impacting nutrient availability in the WMED and what could be the consequences of such change if existing?

1.4.2 Thesis Organization

In the first part of the project, I started with the compilation and production of reliable accurate biogeochemical measurements from different years; this was a fundamental prerequisite to the analysis of the spatio-temporal distribution of biogeochemical properties.

I focused then on carrying out a consistency analysis of in-situ observations. This task was challenging since I needed to merge different cruises, different operating standards, periods, regions.

In Chapter 2, I reconstructed a dataset for the WMED to have an internally consistent data product. This exercise was fundamental since systematic errors in measurements can lead to inaccurate, misguided conclusions when it comes to long-term trends and interannual variability. Primary and secondary quality control of nitrate, phosphate and silicate measurements on the CNR-DIN-WMED (2004-2017) dataset were implemented; this work was published in Earth System Science Data journal (ESSD) and the chapter is organized according to the published version.

Results from the 14 years regional analysis of biogeochemical properties are discussed in Chapter 3, enabling to disentangle the variability in recent years (2004-2017) of nitrate, phosphate and silicate between subregions giving the circulation features in each subregion. I investigate nitrate, phosphate, silicate and AOU distribution and stoichiometry in the water column as well as their relationships with salinity. Chapter 3is structured as an introduction, method, and results, discussion, and conclusions.

The last part of the project, in Chapter 4, results from a long-term (36 years) climatological analysis are presented and discussed. Together with the data product issued from Chapter 2, other data sources are included and merged to thoroughly investigate the spatial and temporal distribution of nutrients through the climatological analysis of two time periods (1981-2004, 2005-2017) and make available a regional climatological product.

Finally, in Chapter 5, concluding remarks, outlook and perspective will be presented. The bibliography of draft articles will be gathered at the end of the document as well. Lastly, Chapter 2, Chapter 4 consist of draft articles.

Chapter 2. DISSOLVED INORGANIC NUTRIENTS IN THE WESTERN MEDITERRANEAN SEA (2004-2017)

2.1 Introduction

Dissolved inorganic nutrients may be used as tracers of water masses like salinity and temperature, to assess mixing processes, and to understand the biogeochemical circumstances of their formation regions. Understanding the complex interplay of changing ocean variables and the biological implication for marine ecosystems is a difficult task and requires not only modelling, but also extensive data collection for monitoring, hypothesis testing and validation. Monitoring gaps still remain both in time and in space, especially for marginal seas such as the Mediterranean Sea.

The aim of this chapter is to compile an extensive dataset of dissolved inorganic nutrient observations (nitrate, NO_3; phosphate, PO_4^{3-}; and silicate, SiO_2) collected between 2004 and 2017 in the Western Mediterranean Sea (WMED), to describe the quality control techniques and to provide the scientific community with a publicly available, long-term, quality controlled, and internally consistent biogeochemical data product, contributing to previously published Mediterranean Sea datasets like the MEDAR/Medatlas (time period:1908–1999), (Fichaut et al., 2003) and the Mediterranean Sea – Eutrophication and Ocean Acidification aggregated datasets v2018 (time period: 1911-2017) provided by EMODnet Chemistry (Giorgetti al.,2018) available at https://www.seadatanet.org/Products/Aggregated-datasets.

The contents of this chapter have been published in the scientific journal Earth System Science Data (ESSD, Impact Factor 9.197):

Belgacem, M., Chiggiato, J., Borghini, M., Pavoni, B., Cerrati, G., Acri, F., Cozzi, S., Ribotti, A., Álvarez, M., Lauvset, S. K., and Schroeder, K.: Dissolved inorganic nutrients in the western Mediterranean Sea (2004–2017), Earth Syst. Sci. Data, 12, 1985–2011, https://doi.org/10.5194/essd-12-1985-2020, 2020.

Data coverage

Coverage: 44°N-35°S; -6°W-14°E
Location Name: Western Mediterranean Sea
Date start: May 2004
Date end: November 2017
Both original and quality-controlled data are available in PANGAEA:
https://doi.pangaea.de/10.1594/PANGAEA.904172

2.2 Dissolved inorganic nutrient data collection

2.2.1 The CNR dissolved inorganic nutrient data in the WMED

Long-term time-series, such as the OceanSites global time series (www.oceansites.org), are a fundamental prerequisite to understand and detect climate shifts and trends. However, biogeochemical time-series are still limited to the northern western Mediterranean Sea (MOOSE network, Coppola et al., 2019) Yet, inorganic nutrients in the Mediterranean Sea has received more attention in recent years, and various datasets have been compiled to understand its unique characteristics such as the one build by the PERSEUS project Consortium ("Policy-oriented marine environmental research in the southern European seas" - EU FP7 project GA #287600), that included 100 cruises collected during the project's lifetime, in addition to those from other projects like SESAME, EU FP7 project GA #GOCE-036949), and data products such as the MEDAR/Medatlas. In addition to that, the data assembly system EMODnet Chemistry, a leading infrastructure supported by pan-European directorate General MARE set up (Martin Miguez et al., 2019, Tintoré et al.,2019).

The dataset presented here consists of 24 oceanographic cruises (Fig. 2.1 and Table 2.1) conducted in the WMED on board of research vessels run by the Italian National Research Council (CNR) and the Science and Technology Organisation Centre for Maritime Research and Experimentation (NATO-STO CMRE). All cruises were merged into a unified dataset with 870 nutrient stations and ~ 9666 data points over a period of 14 years (2004-2017). The overall spatial distribution of the stations covers the whole WMED, but the actual distribution strongly varies depending on the specific cruise and most of the data are collected along sections. At all stations, pressure, salinity, and temperature were measured with a CTD-rosette system consisting of a CTD SBE 911 plus and a General Oceanics rosette with 24 12L Niskin Bottles. Temperature measurements were performed with the SBE-3/F thermometer with a resolution of 10^{-3} °C; conductivity measurements were performed with the SBE-4 sensor with a resolution of $3 \cdot 10^{-4}$ S/m. The probes were calibrated before and after each cruise. During all CNR cruises, redundant sensors were used for both temperature and salinity measurements.

Seawater samples for dissolved inorganic nutrient measurements were collected during the CTD up-cast at standard depths (with slight modifications according to the depth at which the deep chlorophyll maximum was detected). The standard depths are usually 5, 25, 50, 75, 100, 200, 300, 400, 500, 750, 1000, 1250, 1500, 1750, 2000, 2250, 2500, 2750, 3000 m. No filtration was employed, nutrient samples were immediately stored at −20 °C. Note that sample storage

and freezing duration varied greatly from one cruise to another (Table 2.4 shows the cruises where this exceeded 1 year).

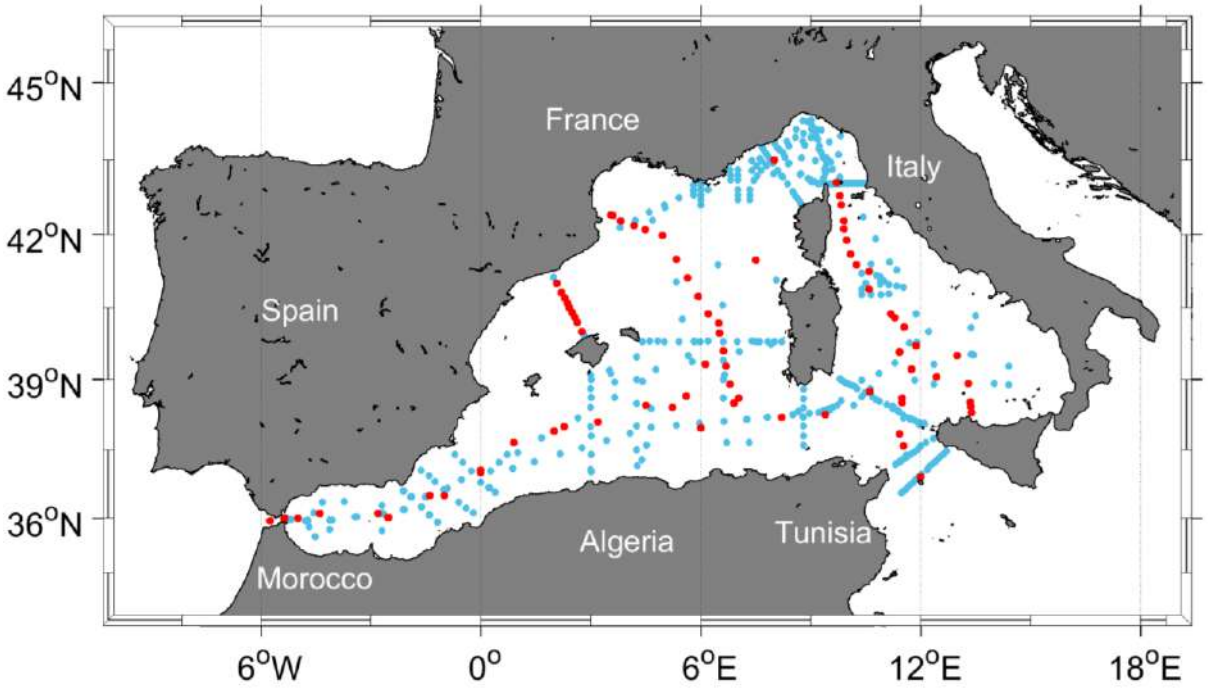

Figure 2.1: Map of the Western Mediterranean Sea showing the biogeochemical stations (in blue) and the five reference cruise stations (in red).

Table 2.1: Cruise summary table and parameters listed with number of stations and samples. Cruises were identified with an ID number and expedition code ('EXPOCODE' of format AABBYYYYMMDD with AA: country code, BB: ship code, YYYY: year, MM: month, DD: day indicative of cruise starting day)

Cruise ID (#)	Common Name	EXPOCODE	Research vessel (RV)	Date Start/End	Stations	Samples NO_3	Samples PO_4	Samples SiO_2	Maximum bottom depth (m)	Chief scientist
1	TRENDS2004/MEDGOOS8leg2	48UR20040526	Urania	26 MAY - 14 JUN 2004	36	255	253	255	3499	M. Borghini
2	MEDGOOS9	48UR20041006	Urania	6 - 25 OCT 2004	68	627	626	627	3610	M. Borghini
3	MEDOCC05/MFSTEP2	48UR20050412	Urania	12 APR - 16 MAY 2005	68	828	828	828	3598	M. Borghini
4	MEDGOOS10	48UR20050529	Urania	29 MAY - 10 JUN 2005	36	577	577	577	3505	A. Perilli
5	MEDGOOS11	48UR20051116	Urania	16 NOV - 3 DEC 2005	14	143	143	143	2810	A. Perilli, M. Borghini, M. Dibitetto
6	MEDOCC06	48UR20060608	Urania	8 JUN - 3 JUL 2006	66	787	785	787	2881	M. Borghini
7	SIRENA06	06A420060720	NRV Alliance	20 JUL - 6 AUG 2006	35	208	208	209	1854	J. Haun
8	MEDGOOS13/MEDBIO06	48UR20060928	Urania	28 SEP - 8 NOV 2006	37	519	520	520	2862	A. Ribotti
9	MEDOCC07	48UR20071005	Urania	5 - 29 OCT 2007	71	977	977	979	3497	A. Perilli
10	SESAMEIt4	48UR20080318	Urania	18 MAR - 7 APR 2008	11	164	164	164	2882	C. Santinelli
11	SESAMEIT5	48UR20080905	Urania	5 - 16 SEP 2008	12	74	74	74	536	S. Sparnocchia, G.P. Gasparini, M. Borghini
12	MEDCO08	48UR20081103	Urania	3 - 24 NOV 2008	24	342	350	348	2880	A. Ribotti
13	TYRRMOUNTS	48UR20090508	Urania	8 MAY - 3 JUN 2009	41	430	441	440	2559	G.P. Gasparini
14	BIOFUN010	48UR20100430	Urania	30 APR - 17 MAY 2010	26	405	405	405	3540	E. Manini, S. Aliani
15	VENUS1	48UR20100731	Urania	31 JUL - 25 AUG 2010	32	431	432	428	3544	G.P. Gasparini, M. Borghini
16	BONSIC2010	48UR20101123	Urania	23 NOV - 9 DEC 2010	18	144	143	143	3540	A. Ribotti
17	EUROFLEET11	48UR20110421	Urania	21 APR - 8 MAY 2011	28	277	275	277	3540	G.P. Gasparini, M. Borghini
18	BONIFACIO2011	48UR20111109	Urania	9 - 23 NOV 2011	13	180	180	181	3541	A. Ribotti, G. La Spada, M. Borghini
19	TOSCA2011	48MG20111210	Maria Grazia	10 - 20 DEC 2011	21	310	310	309	2728	M. Borghini
20	ICHNUSSA12	48UR20120111	Urania	11 - 27 JAN 2012	21	353	352	323	3551	A. Ribotti
21	EUROFLEET2012	48UR20121108	Urania	8 - 26 NOV 2012	53	429	434	434	2633	M. Borghini
22	ICHNUSSA13	48UR20131015	Urania	15 - 29 OCT 2013	37	405	404	405	3540	A. Ribotti
23	OCEANCERTAIN15	48QL20150804	Minerva Uno	4 - 29 AUG 2015	71	531	531	531	3513	J. Chiggiato
24	ICHNUSSA17/INFRAOCE17	48QL20171023	Minerva Uno	23 OCT- 28 NOV 2017	31	251	254	254	3536	A. Ribotti, S. Sparnocchia, M. Borghini

2.2.2 Analytical methods for inorganic nutrients

For all cruises, nutrient determination (nitrate, orthosilicate and orthophosphate) was carried out following standard colorimetric methods of seawater analysis, defined by Grasshoff et al. (1999) and Hansen and Koroleff (1999). For inorganic phosphate, the method is based on the reaction of the ions with an acidified molybdate reagent to yield a phosphomolybdate heteropoly acid, which is then reduced to a blue-colored compound (absorbance measured at 880 nm). Inorganic nitrate is reduced (with cadmium granules) to nitrite that reacts with an aromatic amine leading to the final formation of the azo dye (measured at 550 nm). Then, the nitrite separately determined must be subtracted from the total amount measured to get the nitrate concentration only. The determination of dissolved silicon is based on the formation of a yellow silicomolybdic acid reduced with ascorbic acid to blue-colored complex (measured at 820 nm).

Nutrient analysis was performed in three laboratories. From 2004 to 2013, all cruises nutrients were analysed by ENEA, while for those of 2015 (cruise #23) and 2017 (cruise #24), nutrient concentrations were analysed by CNR-ISMAR. Referring to Table 2.2, four different models of autoanalyzer were used. Measurements from the autoanalyzer were reported in μmol L^{-1}. Inorganic nutrient concentrations were converted to the standard unit μmol kg^{-1}, using sample salinity from CTD and a mean laboratory analytical temperature of 20°C. Data from nutrient analysis were then merged to ancillary CTD bottle data.

Table 2.2: Summary table of laboratories and instruments used for nutrient analysis.

Laboratory	Autoanalyzer	Detection limit
ENEA	continuous-flow system multichannel (Auto Analyzer Bran+Luebbe III Generation	limit of 0.01 μM for nitrate+nitrite, 0.01 μM for phosphate and 0.05 for silicate
CNR-ISMAR Trieste	OI-Analytical (Flow Solution III) flow-segmented	limit of 0.01 μM for nitrate+nitrite, 0.01μM for phosphate and 0.05 for silicate
CNR-ISMAR Venezia	Systea discrete analyzer EasyChem Plus	limit of 0.1 μM for nitrate, 0.01 μM for phosphate and 0.02 μM for silicate

2.2.3 Reference inorganic nutrient data

In addition to the data collected during the above-mentioned cruises, and in order to perform the secondary quality control (described below), we identified five reference cruises (Table 2.3), based on their spatial and temporal distribution of the data and the reliability of the measurements (see Fig. 2.2, Fig. 2.3 –Table 2.4). Cruises 06MT20110405 and 06MT20011018 are the only two Mediterranean cruises included in the publicly available Global Ocean Data Analysis Project version 2 (GLODAPv2, Olsen et al. 2016). These cruises, conducted on board

the R/V Meteor, provide a reliable reference because nutrient analysis strictly followed the recommendation of the World Ocean circulation experiment (WOCE) and the GO-SHIP protocols (Hydes et al., 2010; ,Tanhua et al., 2013). Cruises 29AH20140426 and 48UR20070528 are to be included in the CARIMED data product (personal communication by M. Álvarez, in preparation but not yet available) and have undergone rigorous quality control following GLODAP routines. Finally, 29AJ20160818 was carried out in the framework of the MedSHIP programme (Schroeder et al., 2015) and its data are available at https://doi.org/10.1594/PANGAEA.902293 (Tanhua, 2019).

Table 2.3: Cruise summary table of the reference cruises collection used in the secondary quality control, collected from 2001 to 2016.

Common name	EXPOCODE	Date Start/End	Stations	NO^3 Sample	PO_4 Sample	SiO_2 Sample	Source	Nutrient PI	Chief scientist
M51/2	06MT20011018	18 OCT - 11 NOV 2001	6	79	79	82	GLODAPv2	B. Schneider	W. Roether
TRANSMED_LEGII	48UR20070528	28 MAY- 12 JUN 2007	4	78	77	78	CARIMED (not yet available)	S. Cozzi, V. Ibello	M. Azzaro
M84/3	06MT20110405	5 - 28 APR 2011	20	339	343	-	GLODAPv2	G. Civitarese	T. Tanhua
HOTMIX	29AH20140426	26 APR- 31 MAY 2014	18	144	140	144	CARIMED (not yet available)	XA Álvarez-Salgado	J. Aristegui
TALPro-2016	29AJ20160818	18 - 28 AUG 2016	42	293	293	293	MedSHIP programme	L. Coppola	L. Jullion, K. Schroeder

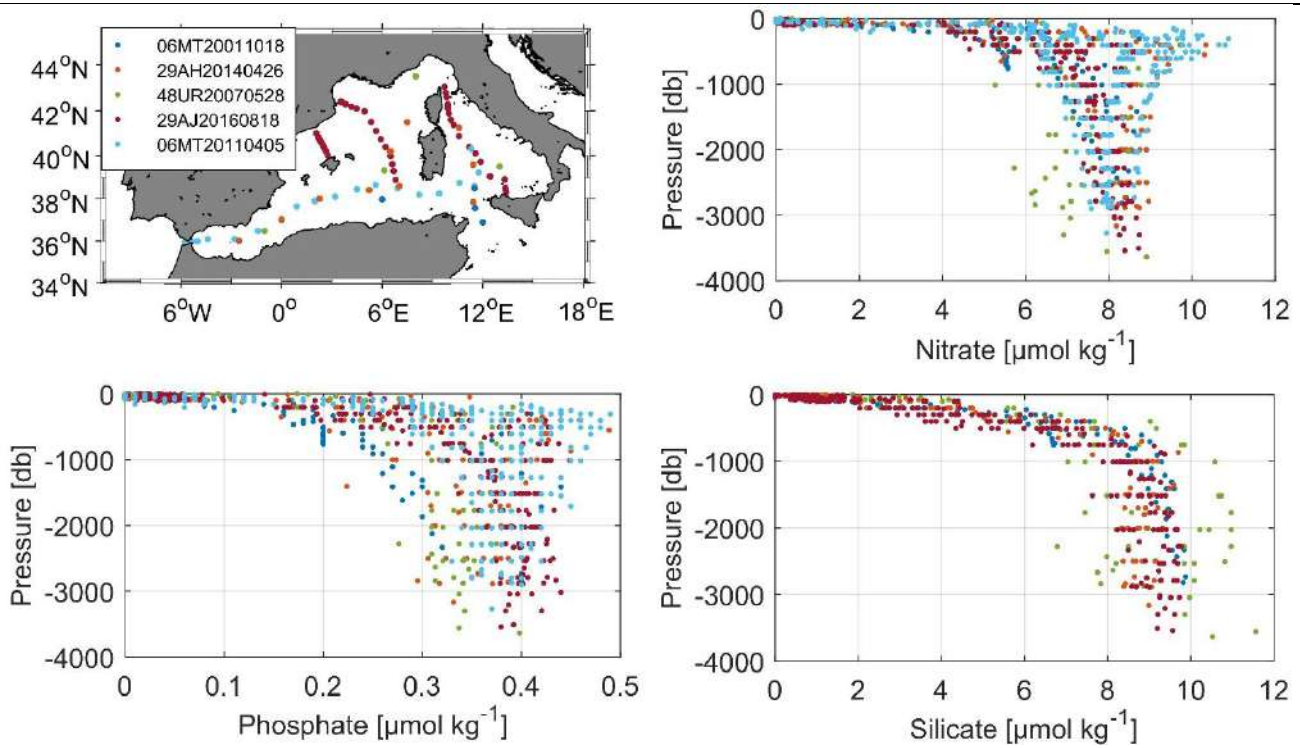

Figure 2.2: Overview of the reference cruise spatial coverage and vertical distributions of the inorganic nutrients. Top left: geographical distribution map, top right: vertical profiles of nitrate in μmol kg^{-1}, bottom left: vertical profiles of phosphate in μmol kg^{-1}, bottom right: vertical profiles of silicate in μmol kg^{-1}.

Table 2.4: Reference cruises and coefficient of variation of nitrate, phosphate and silicate below 1000db.

Reference cruise ID	EXPOCODE	std NO_3	std PO_4	std SiO_2	# samples
6	06MT20011018	0.064	0.179	0.035	26
22	48UR20070528	0.121	0.074	0.144	34
27	29AJ20160818	0.052	0.062	0.054	116
64	06MT20110405	0.073	0.071	-	42
17	29AH20140426	0.045	0.112	0.036	91

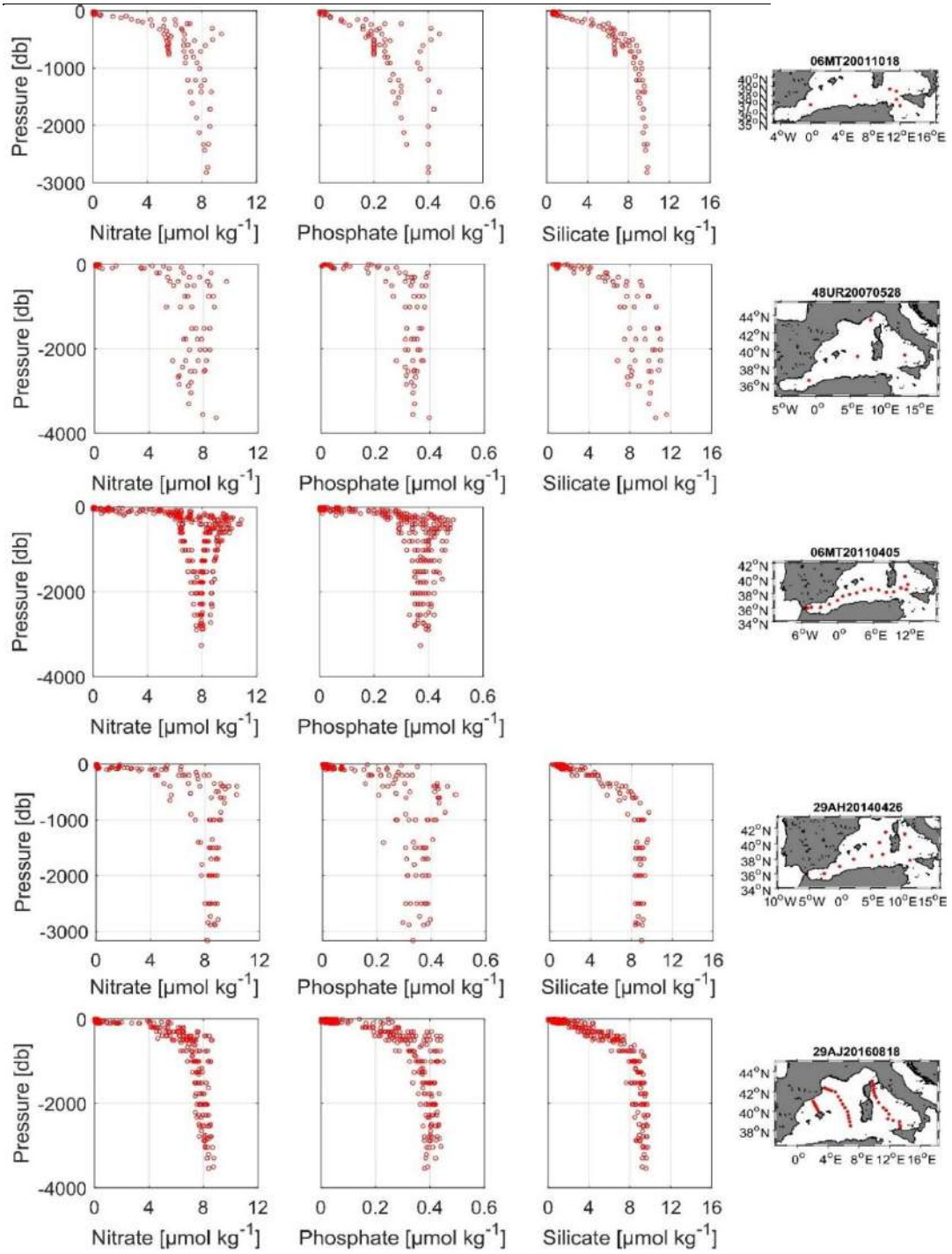

Figure 2.3: Overview of vertical inorganic nutrient profiles and spatial coverage of reference cruises

2.3 Quality Assurance and quality control methods

Combining inorganic nutrient data from different sources, collected by different operators, stored for different amounts of time, and analyzed by multiple laboratories, is not a straightforward task. This is widely recognized in the biogeochemical oceanographic community. Since the 1990s, several studies and programmes (e.g. World Ocean Database, World Ocean Atlas, WOCE) have been devoted to facilitate the exchange of oceanographic data and develop quality control procedures to compile databases by the estimation of systematic errors (Gouretski and Jancke, 2001) to increase the inter-comparability, generate consistent data sets and accurately observe the long-term change.

An example of a first quality control procedure is the use of reference materials that are available for salinity (IAPSO, salinity standard by OSIL) and temperature (SPRT, Standard Platinum Resistance Thermometer). As for the inorganic carbon, total alkalinity (Dickson et al., 2003) and inorganic nutrients (Aoyama et al., 2016), certified reference materials (CRM) have been recently made applicable for oceanographic cruises. However, since CRM are not always available or used for biogeochemical oceanographic data, Lauvset and Tanhua (2015) developed a secondary quality control tool to identify biases in deep data. The method suggests adjustments that reduce cruise to cruise biases, increase accuracy and allow for the inter-comparison between data from various sources. This approach, based on a crossover and inversion method (Gouretski and Jancke, 2001; Johnson et al., 2001), was used to generate the CARbon IN Atlantic ocean (CARINA, see Hoppema et al., 2009), GLODAPv2.2019 (Olsen et al., 2019) and PACIFICA (Suzuki al al.,2013) databases.

2.3.1 Primary Quality control

Each individual cruise was first subjected to a primary quality control (1st QC) that included a check of apparent and extreme outliers in CTD salinity, nitrate, phosphate, and silicate. Each parameter included a quality control flag, following standard WOCE flags (Table 2.5). Surface, intermediate, and deep layers were evaluated separately because nutrient observations evolve differently in each layer. The coefficient of variation (CV, defined as standard deviation over mean) was computed for each depth layer. Coefficients of variation in the surface (0-250 db) layer were high (nitrate CV=1.16, phosphate CV=1.005, silicate CV=0.75) due to air-sea interaction (Muniz et al., 2001) occurring in this layer rendering it difficult to flag. These influences are of reduced importance in the intermediate (250-1000 db) layer (nitrate CV=0.23, phosphate CV=0.31, silicate CV=0.24) and the deep (>1000 db) layer (nitrate CV=0.15, phosphate CV=0.22, silicate CV=0.14), decreasing the total variance. Flags in the upper and intermediate layer were thus set based on outliers within pressure ranges defined

according to standard pressures (0-10, 10-30, 30-60, 60-80, 80-160, 160-260, 260-360, 360-460, 460-560, 560-1000 db).

Table 2.5: WOCE flags used in the original data product and in the adjusted product.

WOCE flag value	Interpretation in original dataset	Interpretation in adjusted product
2	Acceptable/ measured	Adjusted and acceptable
3	Questionable/not used	Adjusted and recommended questionable
9	not measured/no data	-

Below 1000 db, flagging included an inspection of nitrate to phosphate (N:P) and nitrate to silicate (N: Si) ratios. The Median and Median Absolute Deviation (MAD) were computed by pressure classes: any atypical observation and any value that departs from the median by more than three MADs in the different pressure ranges for each cruise has been classified as outlier.

An overview of the nutrient distribution is provided with scatter plots, also showing the flagged measurements (Fig. 2.4). Each measurement was flagged 2 ("Acceptable/ measured") or flagged 3 ("Questionable"): 4.1% of nitrate data, 3.37% of phosphate data, 3.16% of silicate data, and 0.07% of CTD salinity data were considered outliers and flagged 3. As highlighted by Tanhua et al. (2010), the primary QC can be subjective depending on the expertise of the person flagging the data, thus flagging could bring in some uncertainties.

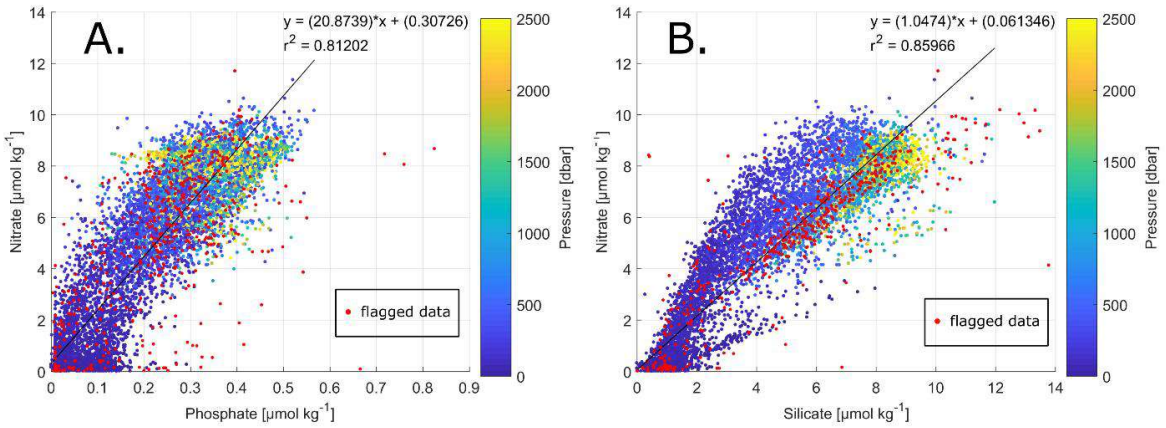

Figure 2.4: Scatter plots of (A.) phosphate vs. nitrate (in μmol kg^{-1}) and (B.) silicate vs. nitrate (in μmol kg^{-1}). Data that have been flagged as "questionable" (flag=3) are in red, the colour bar indicates the pressure (in dbar). The black lines represent the best linear fit between the two parameters, and the corresponding equations and r^2 values are shown on each plot. Average resulting N:P ratio is 20.87, average resulting N:Si ratio is 1.05 (whole depth).

In order to have a first assessment of the precision of each cruise measurements, the standard deviation of observations deeper than 1000 db was calculated along with averages and standard deviations for each cruise and by subregions to have an overview about nutrient content variability in the deep layer and about the observations spatial spread of individual

cruises (Table 2.7). Following the subdivision of Manca et al. (2004), the WMED has been divided into subregions (Fig. 2.5, Table 2.6) according to the general circulation patterns (details in Manca et al.,2004).

Table 2.6: Geographical limits of subregion referring to Manca et al. (2004).

Code	Region	Lat °N (min)	Lat °N (max)	Lon °E (min)	Lon °E (max)	Maximum pressure(db)
DF2	Gulf of Lions	42	43.36	1	6.18	2517
DF3	Liguro-Provençal	41	45	6.18	9.18	2728
DF4	Ligurian East	42.48	45	9.18	11	1299
DS2	Balearic Sea	38.30	42	-1	4.3	2741
DF1	Algero-Provençal	39.18	41	4.3	9.18	2891
DS1	Alboran Sea	35.0	37.3	-6	-1	2683
DS3	Algerian West	35.36	38.3	-1	4.3	2837
DS4	Algerian East	36.30	39.18	4.3	8.24	2890
DT1	Tyrrhenian North	39.18	42.48	9.18	16.16	3610
DT3	Tyrrhenian South	38	39.18	10	16.16	3551
DI1	Sardinia Channel	36.0	39.18	8.24	10	2455
DI3	Sicily Channel	35	38	10	15	664

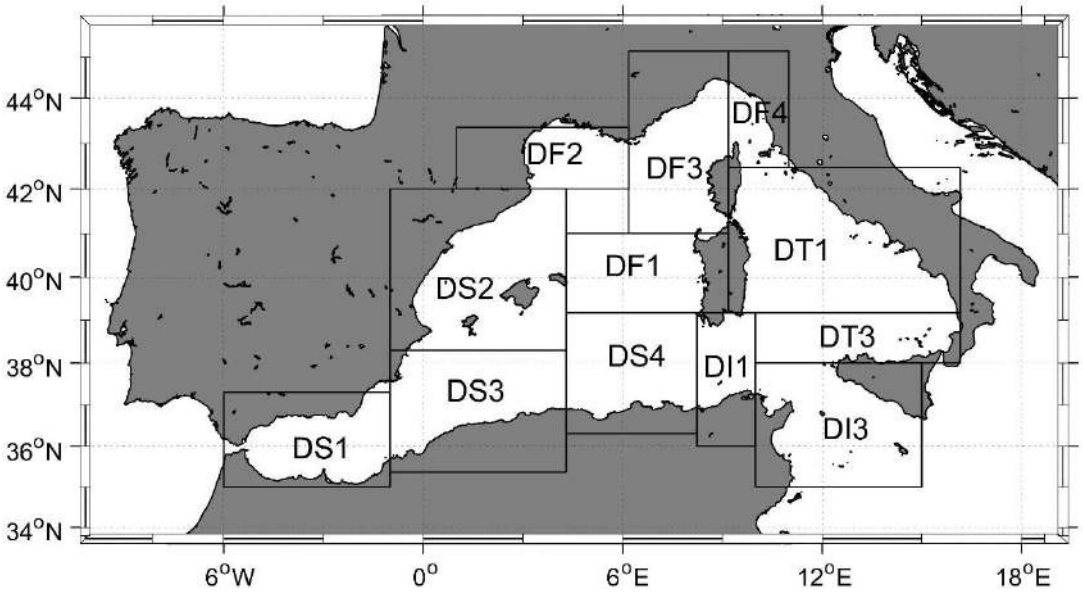

Figure 2.5: Map of the WMED showing the geographical limits of the MEDAR/Medatlas subregions defined in Table.2.6 according to Manca et al. (2004).

Table 2.7 displays the comparison of standard deviation of deep measurements for each cruise and within subregions. The overall standard deviation between cruises in the deep layer varied between 0.51 and 1.41 μmol kg^{-1} for nitrate, between 0.1 and 1.64 μmol kg^{-1} for silicate and between 0.025 and 0.078 μmol kg^{-1} for phosphate. Regional standard deviation of nitrate measurements below 1000 db varied between 0.08 μmol kg^{-1} in the Gulf of Lion (DF2) with cruise #9 and 1.6 μmol kg^{-1} in the Balearic Sea (DS2) observations of cruise #14. Phosphate lowest regional standard deviation was 0.01 μmol kg^{-1} found in the observations of cruise #9

in Gulf of Lion (DF2), cruise #10 in Balearic Sea (DS2) and Algerian West (DS3), cruise #14 and cruise # 15 in Tyrrhenian South (DT3), cruise #18 in Algero-Provençal (DF1) and Sardinia Channel (DI1) while the highest standard deviation was 0.1 μmol kg^{-1} in the observations of cruise #12 in Algerian West (DS3). As for silicate, the lowest standard deviation was 0.02 μmol kg^{-1} observed in cruise #9 measurements of Gulf of Lion subregion (DF2) and the highest deep standard deviation was observed in cruise #6 in its all subregions together with cruise #5 measurement in Tyrrhenian North (DT1) with 1.83 μmol kg^{-1} standard deviation.

Cruises #3, #6 and #9 had the largest spatial extension (see right side of Fig. 2.11) with a high number of samples over more than seven subregions (Table 2.7) and the geographical variability of the distribution in dissolved inorganic nutrients results thus in the largest standard deviations. Conversely, cruises with smaller spatial coverages have lower standard deviations. Therefore, a relatively small spatial coverage and high standard deviation is considered as indicative of data with low precision (Olsen et al., 2016). This applies to cruises #1, #5, and #16. Despite the small spatial coverage, samples of nitrate and phosphate of cruise #5 have an overall standard deviation of 1.35 μmol kg^{-1} and 0.07 μmol kg^{-1}, respectively, a high standard deviation pointed out in also in the regional standard deviation of deep measurements in Tyrrhenian North (DT1) and South (DT3) . Cruise #1, with few stations in Tyrrhenian North (DT1) and South (DT3) subregions and 21 samples below 1000 db, has an overall standard deviation of 1.25 μmol kg^{-1} for nitrate, 0.06 μmol kg^{-1} for phosphate and 1.64 μmol kg^{-1} for silicate. The regional standard deviation was relatively high for nitrate (0.51-1.32 μmol kg^{-1}) phosphate (0.02-0.065 μmol kg-1) and silicate (0.53-1.83 μmol kg^{-1}). A comparison with the deviations from e.g. cruise # 2, carried out in the same year and e.g. cruise #17 (with a similar cruise track), confirms the lower precision of the data of cruise#1. Similar considerations apply to the quality of nitrate samples (0.87-1.02 μmol kg^{-1}) and silicate (0.87-0.9 μmol kg^{-1}) from cruise #16, covering a small area in Tyrrhenian North (DT1) and South (DT3), compared to cruise #17, carried out in the same regions (right side of Fig. 2.11 and Table 2.7).

Deep silicate measurements of cruise #6 have twice the overall standard deviation of silicate data of cruise #8 from the same year. Adding to that, in the seven subregions, the regional standard deviation of deep silicate observations was the highest, between 1.04-2 μmol kg^{-1} which was relatively high compared to the surrounding cruises that have observations in the same subregions. This is again suggestive of the limited precision. On the other hand, trying to explain the source of relatively high standard deviations in specific cruises is not always straightforward, as they could stem from a variety of sources, sampling, conservation, and analysis. The bottom water in the WMED exhibits a high nutrient content below 1000 db (Table 2.7), due to the longer residence time. Dividing the WMED into subregions, has effectively removed the natural spatial change in nutrients, making the interpretation of the standard deviation a matter of the precision of the measurements only.

In Table 2.7, deep averages by subregions showed that overall nutrient fluctuated around 7.4 ±0.9 μmol kg^{-1} for nitrate, 0.3 ±0.06 μmol kg^{-1} for phosphate and 7.7 ±0.8 μmol kg^{-1} for silicate,

similar findings were reported by Manca et al. (2004). Comparing cruise averages in each region enabled the identification of "suspect" cruises. Cruise #24 has the lowest deep average in nitrate in Algéro-Provençal (DF1), Tyrrhenian North (DT1) subregions and Sardinia Channel (DI1). As for silicate of cruises #24 and #16 was very low compared to the overall regional average in Liguro-Provençal (DF3) and Tyrrhenian South (DT3) subregions. Deep average of phosphate did not show any outlier cruises in all subregions. Different reasons could explain the low precision in the samples, freezing is one. Although it is a valid preservation method (Dore at al.,1995), the error is higher when samples were not analysed immediately (Segura-Noguera et al., 2011), so the storage time could have an influence.

Table 2.7: Average and Standard deviations of nitrate, phosphate and silicate measurements by cruise and for each region with number of samples deeper than 1000db included in the 2nd QC. Average storage time: the minimum storage time defined as time difference between the cruise ending day and the 1st day of the laboratory analysis.

Cruise ID	EXPOCODE/ Region	Regional Avg NO_3	std NO_3	Regional Avg PO_4	std PO_4	Regional Avg SiO_2	std SiO_2	# samples	Avg storage (in days)
1	48UR20040526/		**1.25**		**0.062**		**1.64**	21	131
	DT1-Tyrrhenian North	6.07	1.32	0.26	0.065	6.92	1.83	16	
	DT3-Tyrrhenian South	7.03	0.51	0.31	0.02	7.66	0.53	5	
2	48UR20041006/		**0.59**		**0.029**		**0.81**	21	251
	DT1-Tyrrhenian North	7.68	0.53	0.41	0.031	8.74	0.75	15	
	DT3-Tyrrhenian South	8.17	0.60	0.41	0.025	9.31	0.87	6	
3	48UR20050412/		**1.15**		**0.050**		**1.41**	233	135
	DF2-Gulf of Lion	7.89	0.98	0.40	0.044	8.17	1.06	24	
	DF3-Liguro-Provençal	7.45	1.08	0.41	0.05	7.72	1.10	66	
	DS2-Balearic Sea	7.44	1.14	0.40	0.039	7.68	1.47	21	
	DF1-Algero-Provençal	7.87	1.16	0.41	0.043	8.88	1.96	42	
	DS3-Algerian West	7.7	0.816	0.39	0.048	8.14	0.94	23	
	DT1-Tyrrhenian North	6.57	1.065	0.36	0.047	7.41	1.15	21	
	DT3-Tyrrhenian South	6.52	1.12	0.36	0.05	7.56	1.42	22	
	DI1-Sardinia Channel	7.22	1.065	0.40	0.04	8.08	1.11	14	
4	48UR20050529/		**1.13**		**0.057**		**1.08**	205	314
	DS1-Alboran Sea	6.4	1.15	0.38	0.041	6.26	1.02	32	
	DS3-Algerian West	7.6	1.13	0.41	0.06	7.33	0.99	73	
	DS4-Algerian East	7.48	1.13	0.41	0.06	7.50	1.23	47	
	DT1-Tyrrhenian North	7.24	0.44	0.42	0.03	7.91	0.56	16	
	DT3-Tyrrhenian South	7.70	0.38	0.41	0.03	7.55	0.36	14	
	DI1-Sardinia Channel	7.58	1.08	0.43	0.049	7.42	0.82	23	
5	48UR20051116/		**1.35**		**0.078**		**0.98**	16	738
	DT1-Tyrrhenian North	5.68	1.26	0.19	0.08	6.30	0.92	10	
	DT3-Tyrrhenian South	6.71	1.51	0.20	0.06	6.86	1.06	5	
	DI1-Sardinia Channel	6.29	0	0.26	0	7.53	0	1	
6	48UR20060608/		**1.16**		**0.054**		**1.47**	221	27
	DF2-Gulf of Lion	7.69	1.02	0.42	0.04	7.089	1.04	27	
	DF3-Liguro-Provençal	8.08	0.78	0.43	0.04	7.41	1.21	35	
	DS2-Balearic Sea	8.06	0.9	0.43	0.03	7.07	1.18	30	
	DF1-Algero-Provençal	7.97	1.16	0.44	0.05	7.34	1.32	61	
	DS3-Algerian West	8.39	0.9	0.42	0.03	8.5	2	28	
	DT3-Tyrrhenian South	6.39	1.28	0.36	0.06	6.86	1.7	26	
	DI1-Sardinia Channel	8.04	0.85	0.43	0.04	7.77	1.25	14	
7*	06A420060720		-		-		-	-	1367
8	48UR20060928/		**0.71**		**0.036**		**0.76**	179	606
	DS2-Balearic Sea	7.97	0.17	0.33	0.017	7.84	0.27	4	
	DF1-Algero-Provençal	8.17	0.22	0.33	0.026	8.11	0.3	22	
	DS1-Alboran Sea	8.2	0.14	0.35	0.02	8.59	0.35	47	
	DS3-Algerian West	7.93	0.89	0.33	0.03	8.09	0.91	70	

	DS4-Algerian East	7.98	0.68	0.34	0.04	8.01	0.7	28	
	DT3-Tyrrhenian South	6.2	1.51	0.28	0.04	6.71	1.45	3	
	DI1-Sardinia Channel	7.66	0.6	0.28	0.02	8.00	0.49	5	
9	48UR20071005/		**0.89**		**0.040**		**0.86**	302	751
	DF2-Gulf of Lion	8.41	0.08	0.31	0.01	7.43	0.02	4	
	DF3-Liguro-Provençal	8.17	1.08	0.31	0.03	7.64	1.08	81	
	DS2-Balearic Sea	8.17	0.43	0.31	0.02	7.58	0.39	29	
	DF1-Algero-Provençal	8.33	0.6	0.32	0.03	7.79	0.69	82	
	DS4-Algerian East	8.41	0.2	0.33	0.018	7.90	0.26	19	
	DT1-Tyrrhenian North	7.83	0.41	0.28	0.03	8.26	0.55	26	
	DT3-Tyrrhenian South	7.49	1.22	0.28	0.05	7.71	1.26	38	
	DI1-Sardinia Channel	7.92	1.05	0.33	0.02	8.26	0.41	23	
10	48UR20080318/		**0.51**		**0.026**		**0.34**	66	31
	DF2-Gulf of Lion	8.54	0.6	0.35	0.03	8.62	0.43	5	
	DS2-Balearic Sea	9.12	0.18	0.38	0.01	8.40	0.21	9	
	DF1-Algero-Provençal	9.02	0.36	0.38	0.03	8.65	0.25	15	
	DS3-Algerian West	8.93	0.46	0.36	0.01	8.69	0.35	20	
	DS4-Algerian East	8.43	0.25	0.38	0.02	8.32	0.22	10	
	DI1-Sardinia Channel	7.62	0.6	0.34	0.03	8.49	0.36	3	
11*	48UR20080905		-		-		-	-	211
12	48UR20081103/		**1.11**		**0.077**		**0.10**	110	536
	DS1-Alboran Sea	6.4	1.21	0.21	0.06	7.20	1.43	26	
	DS3-Algerian West	7.58	0.9	0.27	0.1	7.89	0.9	30	
	DS4-Algerian East	7.15	1.04	0.23	0.04	7.38	0.9	35	
	DT3-Tyrrhenian South	7.44	0.5	0.22	0.05	8.28	0.4	10	
	DI1-Sardinia Channel	7.40	1.23	0.17	0.04	8.09	0.45	9	
13	48UR20090508/		**1.41**		**0.051**		**1.42**	88	164
	DT1-Tyrrhenian North	5.95	1.55	0.24	0.05	6.28	1.58	46	
	DT3-Tyrrhenian South	6.76	0.77	0.24	0.03	7.37	0.77	29	
	DI1-Sardinia Channel	7.62	1.1	0.28	0.05	7.76	0.9	13	
14	48UR20100430/		**1.06**		**0.036**		**1.03**	159	213
	DS2-Balearic Sea	7.66	1.6	0.25	0.03	7.38	1.75	33	
	DF1-Algero-Provençal	8.43	0.29	0.26	0.03	8.06	0.31	61	
	DS3-Algerian West	8.5	0.14	0.26	0.03	8.25	0.3	26	
	DT1-Tyrrhenian North	6.88	0.8	0.23	0.022	7.17	0.77	11	
	DT3-Tyrrhenian South	6.38	1.35	0.22	0.01	6.76	1.56	7	
	DI1-Sardinia Channel	7.71	0.87	0.23	0.02	7.80	0.74	21	
15	48UR20100731/		**1.34**		**0.053**		**0.14**	149	213
	DS1-Alboran Sea	7.30	1.18	0.29	0.05	7.21	1.11	25	
	DS3-Algerian West	7.67	1.15	0.28	0.045	7.24	1.16	54	
	DS4-Algerian East	7.38	0.89	0.29	0.03	7.00	0.78	29	
	DT1-Tyrrhenian North	7.66	0.96	0.29	0.05	7.89	1.07	10	
	DT3-Tyrrhenian South	5.4	0.67	0.22	0.01	5.52	1.56	30	
	DI1-Sardinia Channel	4.92	0	0.20	0	5.55	0	1	
16	48UR20101123/		**1.02**		**0.045**		**1.02**	14	170
	DT1-Tyrrhenian North	6.34	0.87	0.27	0.02	6.12	0.87	8	
	DT3-Tyrrhenian South	5.43	1.02	0.22	0.04	5.08	0.9	6	
17	48UR20110421/		**0.62**		**0.029**		**0.52**	56	160
	DT1-Tyrrhenian North	7.77	0.45	0.28	0.02	8.11	0.35	21	
	DT3-Tyrrhenian South	7.76	0.7	0.28	0.03	8.017	0.6	35	
18	48UR20111109/		**0.68**		**0.025**		**0.70**	77	74
	DF3-Liguro-Provençal	6.68	0	0.33	0	6.26	0	1	
	DF1-Algero-Provençal	8.17	0.5	0.32	0.01	8.16	0.66	43	
	DT1-Tyrrhenian North	7.26	0.93	0.29	0.02	8.15	1.03	12	
	DT3-Tyrrhenian South	7.61	0.37	0.30	0.02	8.18	0.35	11	
	DI1-Sardinia Channel	7.64	0.45	0.29	0.01	8.08	0.41	10	
19*	48MG20111210		-		-		-	-	38
20	48UR20120111/		**0.97**		**0.051**		**0.26**	152	317
	DF1-Algero-Provençal	8.45	0.49	0.31	0.039	7.91	0.53	23	
	DT1-Tyrrhenian North	7.67	0.83	0.27	0.02	8.29	0.8	30	
	DT3-Tyrrhenian South	7.65	1.06	0.31	0.06	8.03	1.26	69	
	DI1-Sardinia Channel	7.65	0.96	0.31	0.03	7.86	0.78	30	
21*	48UR20121108		-		-		-	-	72

22	48UR20131015/		**1.03**		**0.043**		**0.79**	98	76
	DF1-Algero-Provençal	8.54	0.64	0.33	0.02	7.96	0.38	36	
	DS4-Algerian East	7.67	1.28	0.27	0.04	6.82	1.07	8	
	DT1-Tyrrhenian North	6.47	0.83	0.24	0.025	7.12	0.84	10	
	DT3-Tyrrhenian South	7.81	0.71	0.30	0.03	8.09	0.65	28	
	DI1-Sardinia Channel	7.32	0.99	0.27	0.02	7.47	0.89	16	
23	48QL20150804/		**0.84**		**0.038**		**0.85**	94	30
	DF3-Liguro-Provençal	8.51	0.96	0.39	0.03	8.06	0.85	23	
	DS2-Balearic Sea	7.75	0.66	0.36	0.02	7.86	0.81	20	
	DF1-Algero-Provençal	7.9	0.59	0.37	0.03	8.34	0.68	23	
	DS3-Algerian West	7.84	0.67	0.36	0.02	7.75	0.68	6	
	DT1-Tyrrhenian North	7.92	0.61	0.37	0.02	8.75	0.4	8	
	DT3-Tyrrhenian South	7.23	0.75	0.34	0.025	8.2	0.94	13	
	DI1-Sardinia Channel	6.30	0	0.25	0	5.36	0	1	
24	48QL20171023/		**0.68**		**0.055**		**1.24**	55	30
	DF3-Liguro-Provençal	6.63	0.41	0.40	0.05	10.76	1.07	3	
	DF1-Algero-Provençal	5.14	0.7	0.43	0.02	7.94	1.19	6	
	DT1-Tyrrhenian North	4.98	0.58	0.36	0.02	8.10	0.87	9	
	DT3-Tyrrhenian South	5.43	0.5	0.36	0.04	9.03	0.87	26	
	DI1-Sardinia Channel	5.16	0.76	0.41	0.07	7.58	1.17	11	

2.3.2 Multi-linear regression analysis

Trying different approaches for the secondary quality control, a trial with a regional multi-linear regression (MLR) was carried out following Jutterström et al. (2010). Bias in the measurements was identified by comparing the MLR using the measured values. The analysis was conducted on observations below 1000db to minimize the surface water variation. Different combinations of independent predictor variables were set to get the best fit. Each MLR was checked for the best fitting equation by the evaluation of the adjusted-R^2 and the Mean Squared Error (MSE).

The following linear combinations were used:

$NO_3 = a_1$ CTD Salinity + a_2 Theta + a_3 SiO_2

$PO_4 = b_1$ CTD Salinity + b_2 Theta + b_3 SiO_2 + b_4 NO_3

$SiO_2 = c_1$ CTD Salinity + c_2 Theta + c_3 PO_4 + c_4 NO_3

Where Theta has units of °C and NO_3, PO_4 and SiO_2 have units of μmol kg^{-1} , *a, b, c,* and *d* are the coefficients/constants for each MLR.

For the MLR, the different regional subdivision explained below was adopted.

Region 1: the central Mediterranean a region in direct contact with and under the influence of the Eastern Mediterranean (EMED).

Region 2: the Tyrrhenian Sea, the most isolated sub basin of the WMED.

Region 3: the northern WMED, where deep water formation occurs.

Region 4: the southern WMED, under the direct influence of the AW.

Regional deep averages of each parameter were also calculated below 1000 m for each cruise according to samples in each region.

The results showed that there are significant differences between some cruises within the same region. But they also showed cruises that are within the range of the parameter deep regional average.

The 1st regression analysis used all cruises in the specified region. The 2nd regression analysis excluded the outlier cruises highlighted in the 1st regression and agreed with the deep regional average. The 3rd regression analysis used only the coefficients of the 'good quality cruises' to calculate the estimated parameters of all the remaining cruises. The average difference between the predicted (or estimated) and the measured values of the three nutrients is defined as the "offset". A comparison between the three regressions is made to choose the best based on its adjusted regional average.

To apply an adjustment, MLRs and deep layer average comparison need to agree and the offset need to be greater than 0.02 μmol kg^{-1} for all nutrients (Jutterström et al., 2010).

Unfortunately, it was difficult to find a reliable correction factor for all measurements at all depth levels. The result from the MLR approach suggested very large adjustments in deep observations reaching 46 % increase , and different correction factors in each region for one cruise, it was difficult to make an objective decision about the proposed adjustments.

Due to this, the MLR results will not be discussed. It is noteworthy that the MLR results did not contradict the regional average results besides it revealed suspect measurements that had bias compared to data within same regions.

2.3.3 Secondary Quality control: the crossover analysis

The method used to perform the secondary QC on the dissolved inorganic nutrient dataset in the WMED makes use of the quality-controlled reference data, and the crossover analysis toolbox developed by Tanhua (2010) and Lauvset and Tanhua (2015). The computational approach is based on comparing the cruise data set to a high-quality reference data set to quantify biases, described in detail in Tanhua et al. (2010).

Here, we summarize the technique with emphasis on inorganic nutrients. The first step consisted of selecting reference data, as described in section 2.3. The second step is the crossover analysis that was carried out using a MATLAB Toolbox (available online: https://cdiac.ess-dive.lbl.gov/ftp/oceans/2nd_QC_Tool_V2/) where crossovers are generated as difference between two cruises using the "running cluster" crossover routine. Each cruise is thus compared to the chosen set of reference cruises. For each crossover, samples deeper than 1000 db are selected within a predefined maximum distance set to 2°arc distance, defined as a crossing region, to ensure the quality of the offset with a minimum number of crossovers and to minimize the effect of the spatial change.

The reason to select measurements deeper than 1000 db, is to remove the high frequency variability associated with mesoscale features, biological activity and the atmospheric forcing acting in the upper layers, that might induce changes in biogeochemical properties of water masses. On the other hand, also the deep Mediterranean cannot be considered truly "unaffected" by changes, as it is intermittently subjected to ventilation (Schroeder et al., 2016; Testor et al., 2018) and the real variability can be altered in adjusting data.

The computational approach takes this into account, since weights are given to the less variant profile in the crossing region, according to the "confidence" in the determined offset of the compared profiles (i.e. the weighted mean offset of a given crossover-pair is weighted to the depth where the offsets of all compared profiles have the smallest variation (which indeed is strongly interlinked with the degree of variance of each profile) (for further details see Lauvset and Tanhua, 2015).

Before identifying crossovers, each profile was interpolated using the piecewise cubic Hermite method and the distance criteria outlined in Lauvset and Tanhua (2015), their Table 1, and detailed in Key et al. (2004). The crossover is a comparison between each interpolated profile of the cruise being evaluated and the interpolated profile of the reference cruise. The result is a weighted offset (defined as difference cruise/reference) and a standard deviation of the offset. The standard deviation is indicative of the precision; however, it is important to note that this assumption only works because it is a comparison to a reference, and the absolute offset is indicative of accuracy.

The third step consists in evaluating and selecting the suggested correction factor that was applied to the whole water column. The correction factor was calculated from the weighted mean offset of all crossovers found between the cruise and the reference data set, involving a somewhat subjective process.

For inorganic nutrients, offsets are multiplicative so that a weighted mean offset > 1 means that the measurements of the corresponding cruise are higher than the measurements of the reference cruise in the crossing region and applying the adjustment would decrease the measured values. The magnitude of an increase or a decrease is the difference of the weighted offset from 1.

In general, no adjustment smaller than 2% (accuracy limit for nutrient measurements) is applied (detailed description is found in Hoppema et al., 2009; Lauvset and Tanhua, 2015; Olsen et al., 2016; Sabine et al., 2010; Tanhua et al., 2010).

The last step is the computation of the weighted mean (WM) to determine the internal consistency and quantify the overall accuracy of the adjusted product (Hoppema et al., 2009; Sabine et al., 2010; Tanhua et al., 2009), with the difference that our assessment is based on the offsets with respect to a set of reference cruises.

This WM reflects the absolute weighted mean offset of the data set compared to the reference data set, hence the smaller the WM the higher the internal consistency. The accuracy was computed from the individual absolute weighted offsets. The WM, which will be discussed in section 2.4.4., was computed using the individual weighted absolute offset (D) of number of crossovers (L) and the standard deviation (σ):

$$\mathrm{WM}=\frac{\sum_{i=1}^{L} D(i)/(\sigma(i))^2}{\sum_{i=1}^{L} 1/(\sigma(i))^2}$$

2.4 Results of the secondary QC

The results of the secondary QC revealed the necessary corrections for nitrate, phosphate, and silicate. Four cruises were not considered in the crossover analysis: cruises #7 and #11 do not have enough stations > 1000 db (at least 3 to get valid statistics), while cruises#19 and #21 were outside the spatial coverage of the reference cruises. Cruises that were not used for the crossover analysis are made available in the original dataset but were not included in the final data product (see Appendix A).

Overall, we found a total number of 73 individual crossovers for nitrate, 72 for phosphate and 54 for silicate. An example of the running cluster crossover output is shown in Fig.2.6

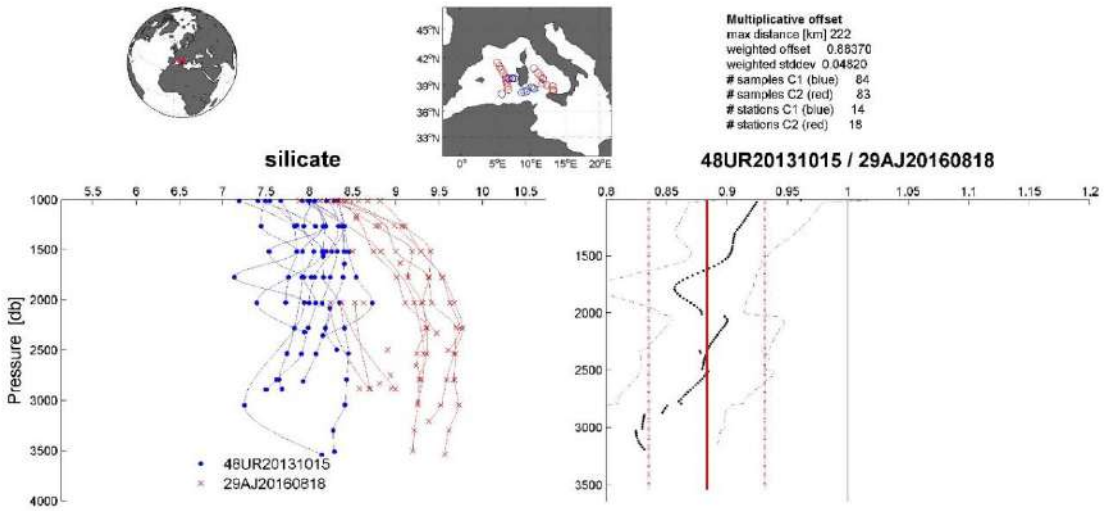

Figure 2.6: An example of the calculated offset for silicate between cruise 48UR20131015 and cruise 29AJ2016818 (reference cruise). Above: location of the stations being part of the crossover and statistics. Bottom left: vertical profiles of silicate data in (μmol kg^{-1}) of the two cruises that fall within the minimum distance criteria (the crossing region), below 1000 dbar. Bottom right: vertical plot of the difference between both cruises (dotted black line) with standard deviations (dashed black lines) and the weighted average of the offset (solid red line) with the weighted standard deviations (dotted red line).

The results of the crossover analysis are adjustment factors for each cruise and each nutrient, that are shown in Table 2.8 and Fig. 2.7-2.8-2.9. Each adjustment factor was calculated from

the weighted mean of absolute offset summarized in Table 2.9 and Fig. S1-S2-S3 (Appendix B). Table 6 details the improvement of the weighted mean of absolute offset by cruise prior to and after adjustments, the information is also displayed graphically in Fig. S1-S2-S3. Cruises are in chronological order in all figures and tables.

Table 2.8: Summary of the suggested adjustment for nitrate, phosphate and silicate resulting from the crossover analysis. Adjustments for inorganic nutrients are multiplicative. NA: denotes not adjusted, i.e. data of cruises that could not be used in the crossover analysis, because of the lack of stations or data are outside the spatial coverage of reference cruises.

Cruise ID	EXPOCODE	NO_3 (x)	PO_4 (x)	SiO_2 (x)
1	48UR20040526	1.14	1.23	1.21
2	48UR20041006	0.98	0.9	1.06
3	48UR20050412	1.08	0.93	1.15
4	48UR20050529	1.04	0.85	1.183
5	48UR20051116	1.19	1.34	1.232
6	48UR20060608	1.05	0.86	1.261
7	06A420060720*	-	-	-
8	48UR20060928	1.03	1.14	1.1
9	48UR20071005	0.97	1.14	1.115
10	48UR20080318	0.94	1.09	1.02
11	48UR20080905*	-	-	-
12	48UR20081103	1.08	1.38	1.12
13	48UR20090508	1.05	1.33	1.15
14	48UR20100430	NA	1.34	1.123
15	48UR20100731	1.13	1.25	1.262
16	48UR20101123	1.15	1.29	1.28
17	48UR20110421	NA	1.25	1.12
18	48UR20111109	NA	1.14	1.09
19	48MG20111210*	-	-	-
20	48UR20120111	NA	1.17	1.08
21	48UR20121108*	-	-	-
22	48UR20131015	NA	1.17	1.11
23	48QL20150804	1.02	1.02	1.08
24	48QL20171023	1.34	0.98	1.06

2.4.1 Nitrate

The crossover analysis suggests a significant adjustment for nitrate concentrations on 15 cruises, between 0.94 and 0.98 (for adjustments <1) and between 1.02 and 1.34 (for adjustments >1) (Table 2.8 and Fig.2.7). Offsets suggest that the deep measurements of cruises #1, #3, #4, #5, #6, #8, #12, #13, #15, #16, #23 and #24 need to be adjusted towards higher concentrations, when compared to the respective reference (Fig.S1, see appendix B).

Nitrate observations of cruises #2, #9 and #10 on the other hand were higher than the reference cruises and exhibit variation outside the accepted accuracy limit, thus requiring a downward adjustment.

Finally, five cruises (#14, #17, #18, #20, and #22) were consistent with the reference data and no adjustment was necessary. Considering the weighted mean of absolute offset after adjustments shown in Table 2.9, two cruises (#5 and #24) required large correction factors but still remain outside the accuracy threshold (Fig. 2.7). These cruises are considered in detail later (section 2.4.4).

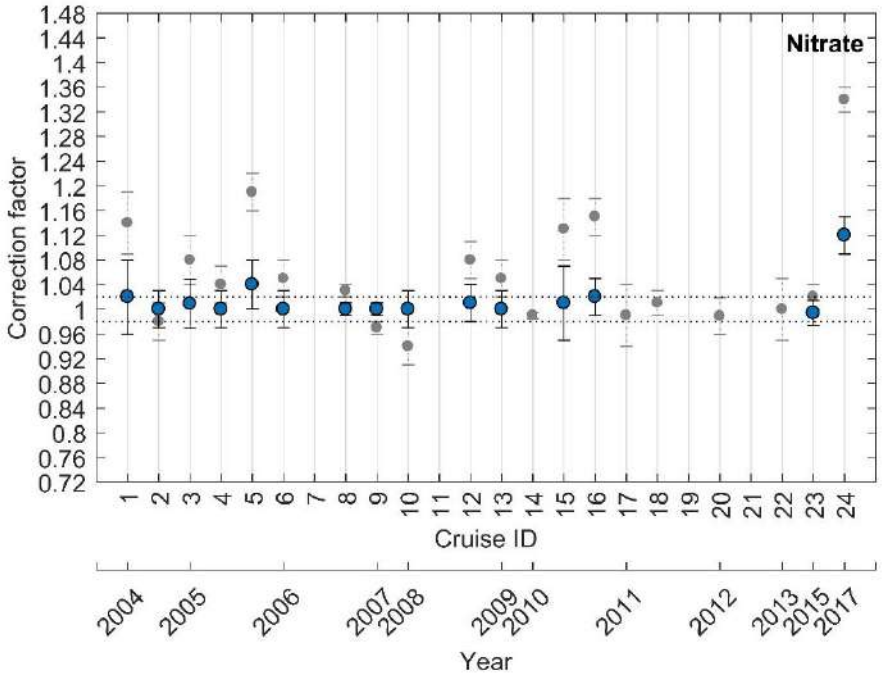

Figure 2.7: Results of the crossover analysis for nitrate, before (grey) and after adjustment (blue). Error bars indicate the standard deviation of the absolute weighted offset. The dashed lines indicate the accuracy limit 2% for an adjustment to be recommended.

2.4.2 Phosphate

For phosphate the crossover analysis suggests adjustments for 20 cruises, as shown in Fig. 2.8. Deep phosphate measurements of 15 cruises (Table 2.9) appear to be lower than the respective reference measurements (i.e. phosphate data of these cruises require an upward adjustment), while the data of five cruises (#2, #3, #4, #6, #24) are higher (i.e. they need a downward adjustment) (Fig.S2, see appendix B). Applying all the indicated adjustments, the large offsets of cruises #2, #3, #4, #6, #8, #9, #10, #18, #20, #23 and #24 are reduced and become consistent with the reference. Cruises #1, #5, #12, #13, #14, #15, #16, #17, and #22 retain an offset even after applying the indicated adjustment. These cruises are considered in detail later. According to Olsen et al. (2016), if a temporal trend is detected in the offsets, no adjustments should be applied. There is indeed a decreasing trend between 2008 and

2017 in the phosphate correction factor (Fig. 2.8), and thus an increasing one in the weighted mean offset (Fig.S2, see appendix B), implying a temporal increase of phosphate. Therefore, phosphate data of the cruises being part of the trend were not flagged as questionable, except some cruises that are discussed further in section 2.4.4.
Comparing phosphate before and after adjustments, the corrections did minimize the difference with the reference, while the actual variation with time was preserved (Fig.2.8). The temporal trend towards higher phosphate concentrations in the Mediterranean Sea is considered to be real, even though studies concerning the biogeochemical trends in the deep layers of the WMED are scarce (de Fommervault et al., 2015b). However, this variation could be consistent with the findings of Béthoux et al.(1998, 2002) and the modelling studies by Moon et al. (2016) and Powley et al. (2018) who indeed found an increasing trend in phosphate concentrations over time, due to the increase in the atmospheric and terrestrial inputs.

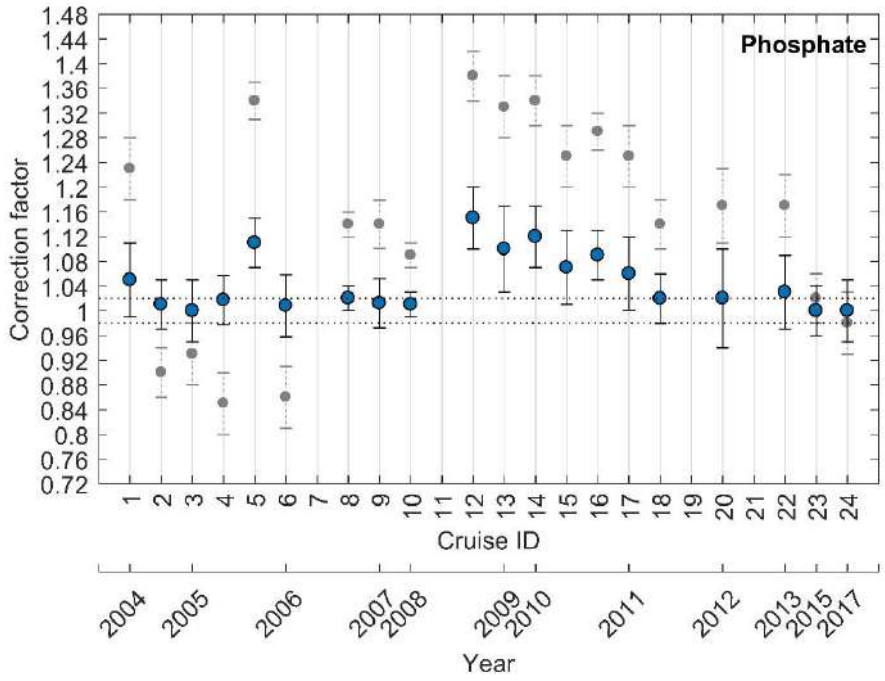

Figure 2.8: The same as Fig. 2.7 but for phosphate.

2.4.3 Silicate

The results of the crossover analysis for silicate suggests corrections for all cruises (Fig. 2.9). The crossovers indicate that deep silicate measurements are lower in the evaluated cruises than in the corresponding reference cruises (i.e. they need to be adjusted upward) (Fig.S3,appendix B). This is likely to be a direct result of freezing the samples before analysis, since the reactive silica polymerizes when frozen (Becker et al., 2019). After applying the adjustment (Table 2.8), as expected, the offsets are reduced (Table 2.9), but five cruises (#1, #5, #6, #15, and #16) remain outside the accuracy envelope. Due to the large offsets, these cruises will be discussed further in section 2.4.4.

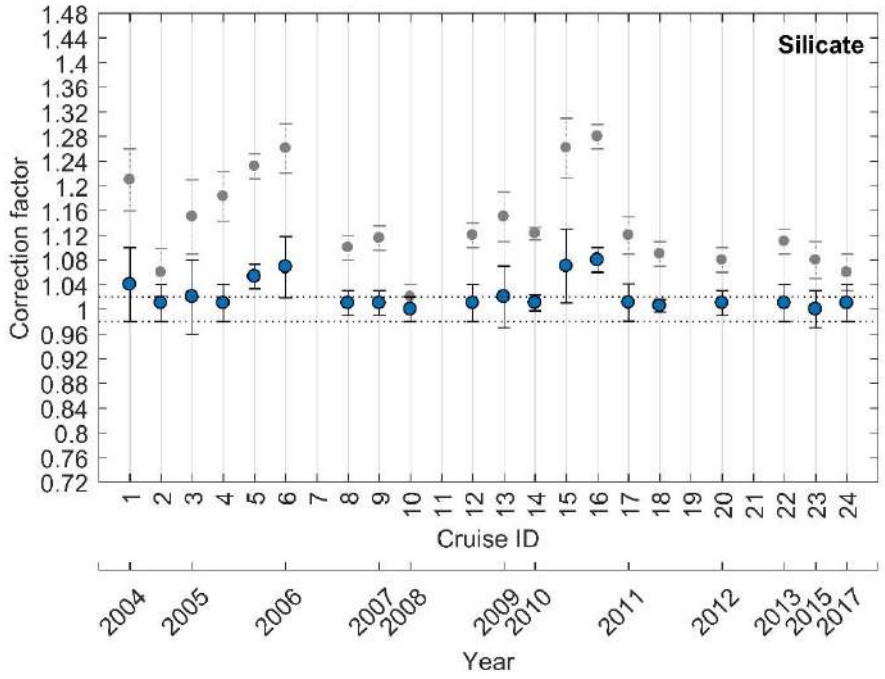

Figure 2.9: The same as Fig. 2.7 but for silicate.

Table 2.9: Secondary QC toolbox results: improvements of the weighted mean of absolute offset per cruise of unadjusted and adjusted data; (n) is the number of crossovers per cruise. The numbers in red (less than 1) indicate that the cruise data are lower than the reference cruises. NA: not adjusted.

Cruise ID	EXPOCODE	NO_3 [%]			PO_4[%]			SiO_2[%]		
		n	*unadjusted*	*adjusted*	*n*	*unadjusted*	*adjusted*	*n*	*unadjusted*	*adjusted*
1	48UR20040526	2	0.86	0.98	2	0.77	0.95	1	0.79	0.96
2	48UR20041006	2	1.02	1.00	2	1.10	0.99	1	0.94	0.99
3	48UR20050412	5	0.92	0.99	5	1.07	1.00	4	0.85	0.98
4	48UR20050529	5	0.96	1.00	5	1.15	0.98	4	0.82	0.99
5	48UR20051116	2	0.81	0.96	1	0.66	0.89	1	0.77	0.95
6	48UR20060608	5	0.95	1.00	5	1.14	0.99	4	0.74	0.93
7	06A420060720	0	-	-	0	-	-	0	-	-
8	48UR20060928	4	0.97	1.00	4	0.86	0.98	3	0.90	0.99
9	48UR20071005	5	1.03	1.00	5	0.86	0.98	4	0.88	0.99
10	48UR20080318	3	1.06	1.00	3	0.91	0.99	2	0.98	1.00
11	48UR20080905	0	-	-	0	-	-	0	-	-
12	48UR20081103	5	0.92	0.99	5	0.62	0.85	4	0.88	0.99
13	48UR20090508	3	0.95	1.00	3	0.67	0.90	2	0.85	0.98
14	48UR20100430	4	1.01	NA	4	0.66	0.88	3	0.88	0.99
15	48UR20100731	5	0.87	0.99	5	0.75	0.93	4	0.74	0.93
16	48UR20101123	1	0.85	0.98	1	0.71	0.91	1	0.72	0.92
17	48UR20110421	2	1.01	NA	2	0.75	0.94	1	0.88	0.99
18	48UR20111109	4	0.99	NA	4	0.86	0.98	3	0.91	0.99
19	48MG20111210	0	-	-	0	-	-	0	-	-
20	48UR20120111	4	1.01	NA	4	0.83	0.98	3	0.92	0.99
21	48UR20121108	0	-	-	0	-	-	0	-	-
22	48UR20131015	4	1.00	NA	4	0.83	0.97	3	0.89	0.99
23	48QL20150804	5	0.98	1.00	5	0.98	1.00	4	0.92	1.00
24	48QL20171023	3	0.66	0.88	3	1.02	1.00	2	0.94	0.99

red: data lower than reference.

2.4.4 Discussion and recommendation

Adjustments were evaluated for each cruise separately. As a general rule no correction was applied when the suggested adjustment is strictly within the 2% limit (indicated with NA in Table 2.8). The average correction factors were 1.06 for nitrate, 1.14 for phosphate and 1.14 for silicate, respectively. To verify the results, we re-ran the crossover analysis and re-computed offsets and adjustment factors using the adjusted data (as shown in blue in Fig. S1-S2-S3, in Appendix B and Fig. 2.7-2.8-2.9). Most of the new adjustments are within the accuracy envelope and few are outside the limit, except for the cruises belonging to the above mentioned "phosphate-trend" and the other outlying cruises which are detailed hereafter. By the application of adjustments, the deep-water offsets were reduced. This can be seen in the decrease of the weighted mean offset between the data before adjustments (after 1st QC, Fig. S1-S2-S3, in grey) and the adjusted data (after 2nd QC, Fig. S1-S2-S3, in blue).

Referring to the analysis detailed in section 2.3.3, the internal consistency of the nutrient data set has improved and increased significantly after the adjustment, from 4% for nitrate, 19% for phosphate and 13% for silicate, to a more unified dataset with 3 % for nitrate, 6 % for phosphate and 3% for silicate.

A comparison between the original and the adjusted nutrient observations is shown in Fig. 2.10A-B-C, indicating an improvement in the accuracy based on the reference measurement and a relatively reduced range particularly for phosphate (Fig. 2.10B). Figure 2.10. D-E scatterplots show that after the quality control, nutrient stoichiometry slopes obtained from regressions, between tracers along the water column show a strong coupling and provide a nitrate to phosphate ratio of ~22.09 and a nitrate to silicate ratio of ~0.94. These values are consistent with nutrient ratios range found in the WMED as reported in Lazzari et al. (2016); Pujo-Pay et al., (2011) and Segura-Noguera et al. (2016).

The regression model is more accurate after adjustments with an improved r^2 for N:P (from 0.81 to 0.90) and for N: Si (from 0.85 to 0.87). One of the main reasons for an upward/ downward bias would be the lack of use of CRM for nutrients in all cruises as also noted in CARINA (Tanhua et al., 2009) or in the most recent global comparability study by Aoyama (2020).

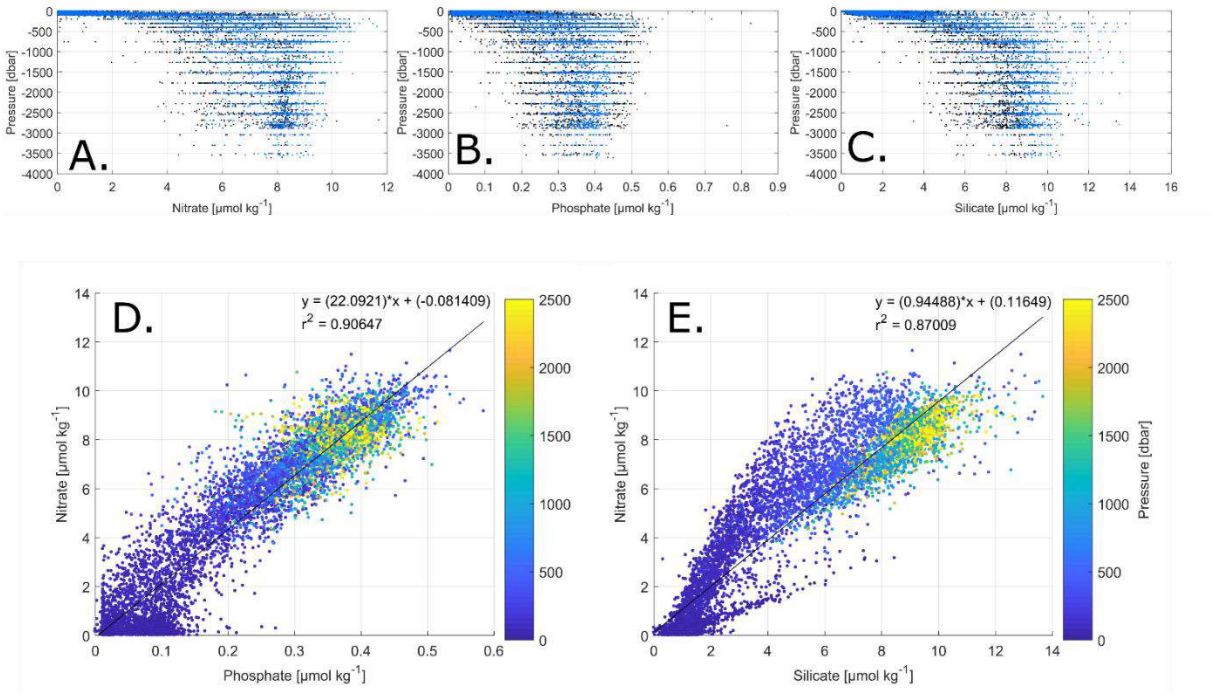

Figure 2.10: Dataset comparison before (black) and after (blue) adjustment, showing vertical profiles of (A.) nitrate (in μmol kg^{-1}), (B.) phosphate (in μmol kg^{-1}) and (C.) silicate (in μmol kg^{-1}). Scatter plots of the adjusted data from all depths after 1st and 2nd quality control for (D.) nitrate vs. phosphate (in μmol kg^{-1}) and (E.) nitrate vs. silicate (in μmol kg^{-1}). The black lines represent the best linear fit between the two parameters, and the corresponding equations and r^2 values are shown on each plot. Average resulting N:P ratio is 22.09, average resulting N:Si ratio is 0.94 (whole depth).

In the following some details on the adjustment of specific cruises are given:

Cruise #2 [48UR20041006] needed an adjustment of 0.98 for nitrate, 0.9 for phosphate and 1.06 for silicate. Most of the crossover profiles occur in the Tyrrhenian sea (Tyrrhenian North and Tyrrhenian South subregions). After adjustment, the cruise is inside the 2% envelope.

Cruise #3 [48UR20050412] appeared to be outside the 2% envelope before adjustments. Its offsets with five reference cruises, crossing the Tyrrhenian sea, Sardinia Channel, Gulf of Lion and Algero-Provençal subregions, showed that nitrate and silicate values to be relatively low, and thus an adjustment of 1.08 and 1.15 was applied respectively. On the other hand, phosphate values were relatively high, and a 0.93 adjustment was applied.

Cruise #4 [48UR20050529] correction factor estimate was based on five crossovers that covered five subregions: Tyrrhenian South, Sardinian Channel, Algerian East and West and the Alboran sea. Table 2.6 show that there are no large differences between regional averages within the cruise which justify an adjustment of 1.04 for nitrate, 0.85 for phosphate and 1.183 for silicate.

Cruise #8 [48UR20060928] was adjusted by 1.03 for nitrate, 1.14 for phosphate and 1.1 for silicate, because it showed values to be low compared to four references. After adjustment, the data were inside the acceptable range.

Cruise #9 [48UR20071005] values of nitrate were slightly outside the 2% envelope before adjustments, similar to phosphate and silicate that were lower compared to the reference. The adjustments of 0.97 for nitrate, 1.14 for phosphate and 1.115 for silicate suggested by the mean offset against the reference cruises were recommended.

Cruise #10 [48UR20080318] has only three crossovers in the Algero-Provençal subregion, showing that nitrate is too high compared to the reference while phosphate and silicate are slightly lower. We therefore applied the adjustments of Table 2.8, since the deep averages for each region (Table 2.6) did not show large regional differences.

Cruise #13 [48UR20090508] has three crossovers in the common crossing zone that included Tyrrhenian North, Tyrrhenian South, and Sardinia Channel subregions. The crossover suggests that this cruise has too low values and needs an adjustment of 1.05 for nitrate, 1.33 for phosphate and 1.15 for silicate.

Cruise #14 [48UR20100430] has a mean offset with four reference cruises that suggests an adjustment for phosphate of 1.34 and silicate of 1.123. Nitrate did fall within the accuracy envelope.

Cruise #17 [48UR20110421] crossover analysis did not suggest any correction for nitrate, However, for phosphate and silicate with an offset based on two crossovers in the Tyrrhenian North and South subregions, adjustments were recommended for phosphate (1.25) and silicate (1.12), for being lower than the reference cruises.

Cruise #18 [48UR20111109] is similar to cruise #17, since it was suggested to correct phosphate by 1.14 and silicate by 1.09, based on four crossovers in the Tyrrhenian North and South, Sardinia Channel and Algero-Provençal subregions.

Cruise #20 [48UR20120111] has four crossovers over the Tyrrhenian North and South and Algero-Provençal subregions. Its measurements were slightly lower than the reference cruises suggesting a correction factor of 1.17 for phosphate and 1.08 for silicate.

Cruise #22 [48UR20131015] has similar correction factors as cruise#20, based on three crossovers in the Sardinia Channel and Tyrrhenian North and South subregion, with measurements being lower than the reference.

Cruise #23 [48QL20150804] showed nutrient values slightly lower than the reference cruises as well, suggesting small correction factors of 1.02 for both nitrate and phosphate and 1.08 for silicate that were based on offsets with five cruises.

Below, we discuss the recommended flags in the final product (Table 2.6) assigned for some cruises that needed further consideration, since they required larger adjustment factors:

Cruise #1 [48UR20040526]: The adjusted values are still lower than the reference (Fig.2.7-2.8-2.9-Fig.S1-S2-S3 (see appendix B)) and are still outside the 2% accuracy range. This cruise had stations in the Sicily Channel, Tyrrhenian North, and South and Ligurian East subregions. (Fig. 2.11, right side) and only 4 stations were deeper than 1000 db (those within the Tyrrhenian Sea). The low precision of this cruise has already been evidenced during the primary QC (section 2.3.1). We recommend flagging this cruise as questionable (flag 3).

Cruise #5 [48UR20051116]: This cruise took place between the Sicily Channel and the Tyrrhenian North and South (Fig. 2.11, right side). Nitrate, phosphate, and silicate data were lower than those from other cruises (#3 and #4) run the same year (Fig.2.7-2.8-2.9-Fig.S1-S2-S3 (see appendix B))) and are still biased after adjustments. Considering the limited precision and the low number of crossovers, it is recommended to flag the cruise as questionable (flag 3).

Cruise #6 [48UR20060608]: This cruise had an offset with five cruises giving evidence that adjustments of 1.05 for nitrate, 0.86 for phosphate and 1.26 for silicate are needed. The silicate bias was reduced after adjustment but remains large with respect to the accuracy limit (Fig. 2.9-Fig. S3). This cruise has a wide geographic coverage, with stations along 9 sections (Fig. 2.11, right side). Considering also the high standard deviation (Table 2.6), which is partially attributed to the spatial coverage of the cruise, there is still uncertainty about the quality of the samples. It is recommended to flag silicate data of cruise #6 as questionable (flag 3).

Cruise #12 [48UR20081103]: Phosphate data have low accuracy with respect to the reference cruises (Fig. 2.8-Fig. S2). This cruise has stations along a longitudinal section from the Sicily Channel to the Alboran Sea, which might explain the large standard deviation of deep phosphate samples (Table 2.6). Cruise #12 was given a correction of 1.08 for nitrate, 1.12 for silicate and 1.38 for phosphate. The mean offset from five crossovers computed within the Tyrrhenian South, Sardinia Channel, Algerian East, Algerian West, and Alboran Sea subregions suggests that this cruise has lower nutrient values than the reference cruise. After adjustment, cruise #12 is within the acceptable range for nitrate and silicate but not for phosphate as highlighted in section 2.3.3. In addition, considering the relatively high number of stations >1000 db and a plausible trend in phosphate, it is recommended to flag the phosphate data as good/acceptable.

Cruise #15 [48UR20100731]: This cruise had 149 station along a similar track as cruise #12 but shows larger offsets for phosphate and silicate (Fig. 2.8-2.9-Fig. S2-S3), compared to cruise #12. Considering that deep silicate data was not of low quality (small standard deviation, see Table 2.6), and that deep phosphate falls within the “phosphate-trend” discussed above, these data are flagged good/acceptable.

Cruise #16 [48UR20101123]: The cruise shows large offsets for phosphate and silicate (Fig. 2.8-2.9- Fig. S2-S3), similar to cruise #15. Considering that the overall cruise standard deviation of silicate samples below 1000 db was relatively high (1.02 over 14 samples, see Table 2.6),

and that it has only one crossover between the Tyrrhenian North and South subregions (Table 2.9), and that when comparing deep regional averages, this cruise had the lowest average silicate value, it is recommended to flag silicate data of cruise #16 as questionable (flag 3). As for phosphate, the cruise is part of the "phosphate-trend" and is therefore flagged good/acceptable.

Cruise #24 [48QL20171023]: This cruise has the largest offset for nitrate even after adjustment. It is very likely due to a difference between laboratories (calibration standards) concerning nitrate, which needs to be flagged as questionable in the final product.

The cruises discussed in this section were not removed from the final product but are retained along with their recommended quality flag (Table 2.6) detailed above and in the Appendix A. We have done the evaluation of their overall quality but leave it up to the users how to appropriately use these data.

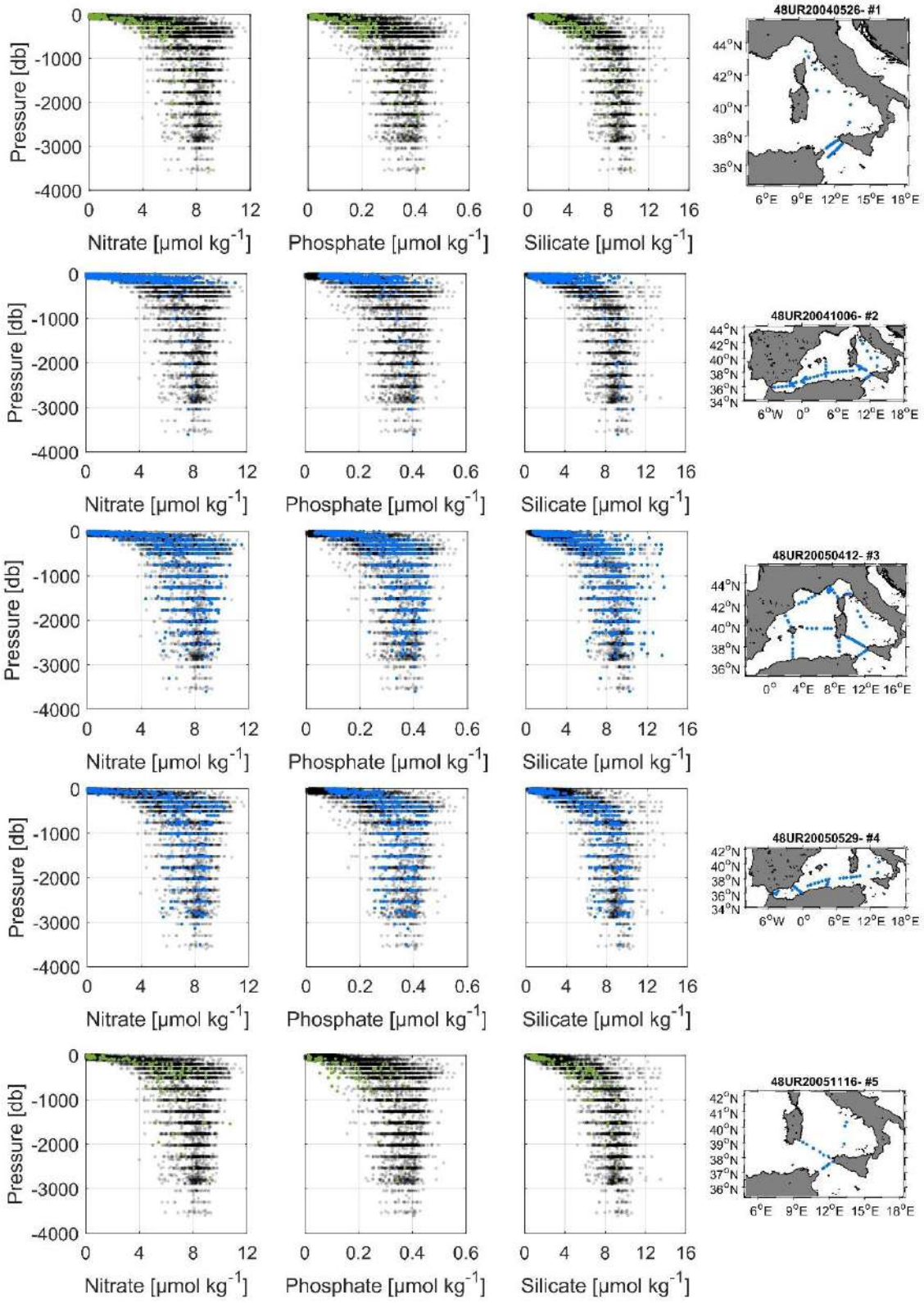
Pressure [db]
0
-1000
-2000
-3000
-4000
Nitrate [µmol kg-1]
Phosphate [µmol kg-1]
Silicate [µmol kg-1]
48UR20040526- #1
48UR20041006- #2
48UR20050412- #3
48UR20050529- #4
48UR20051116- #5

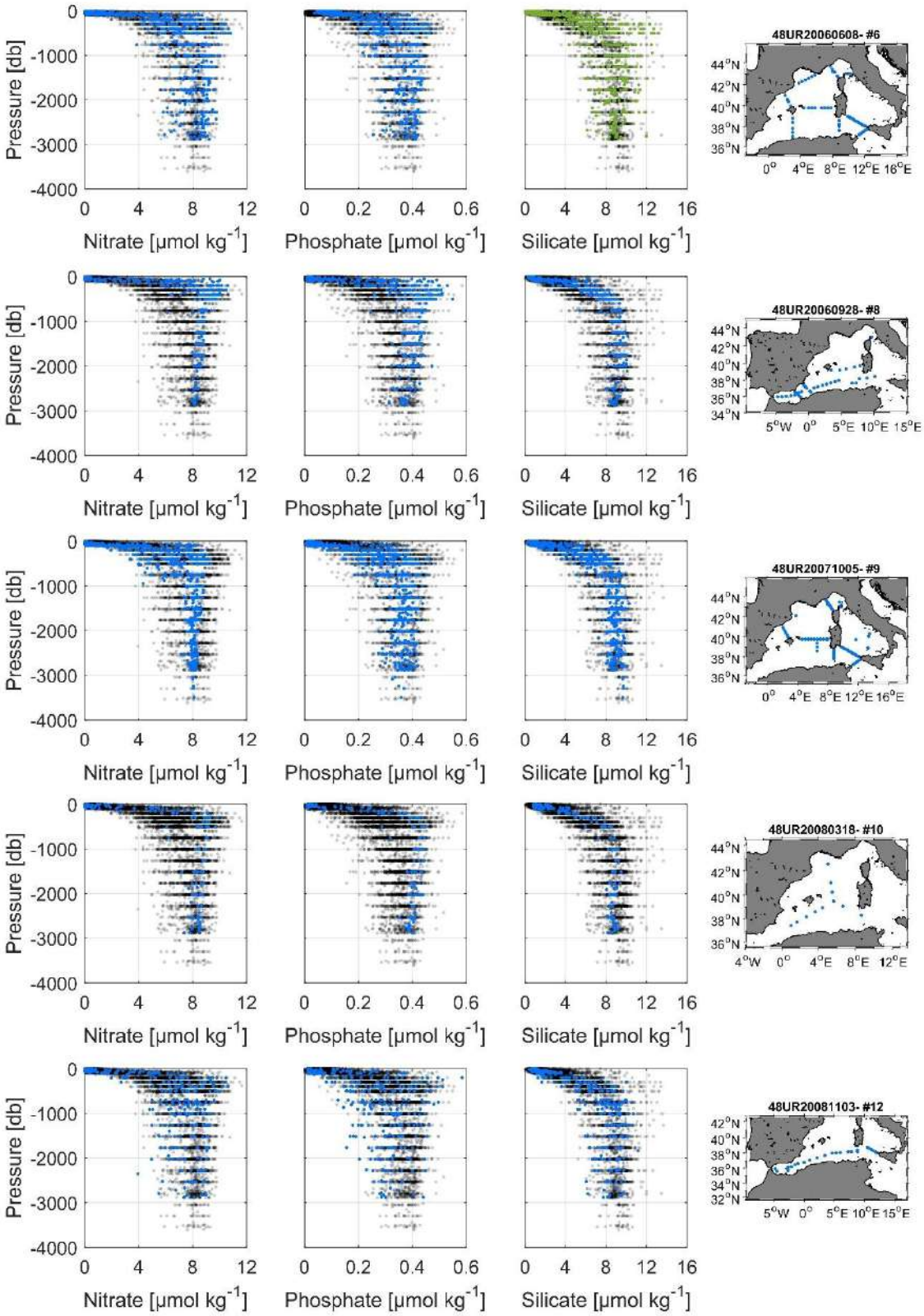
Pressure [db]
Nitrate [µmol kg-1]
Phosphate [µmol kg-1]
Silicate [µmol kg-1]
48UR20060608- #6
48UR20060928- #8
48UR20071005- #9
48UR20080318- #10
48UR20081103- #12

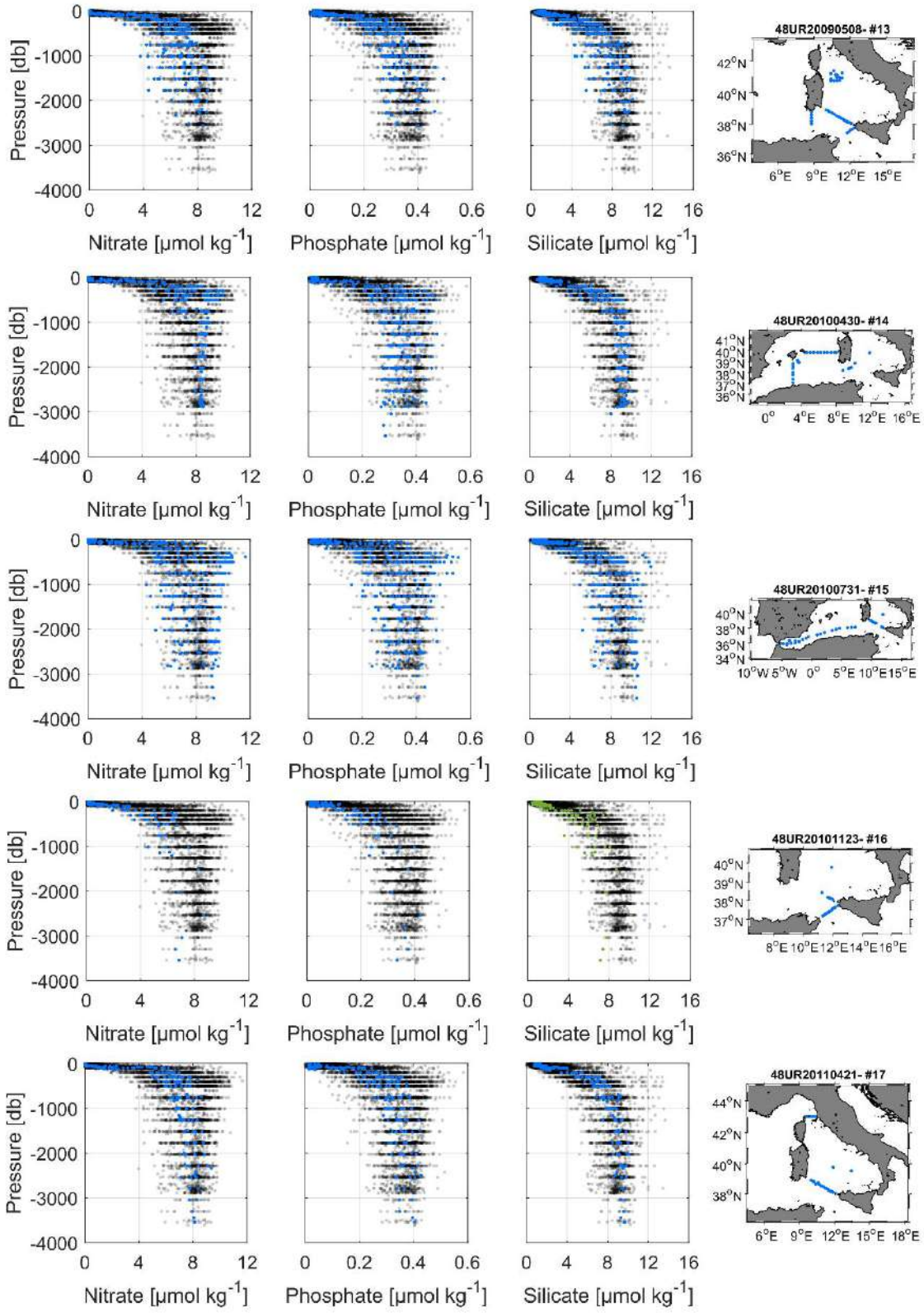
Pressure [db]
Nitrate [µmol kg-1]
Phosphate [µmol kg-1]
Silicate [µmol kg-1]
48UR20090508- #13
48UR20100430- #14
48UR20100731- #15
48UR20101123- #16
48UR20110421- #17

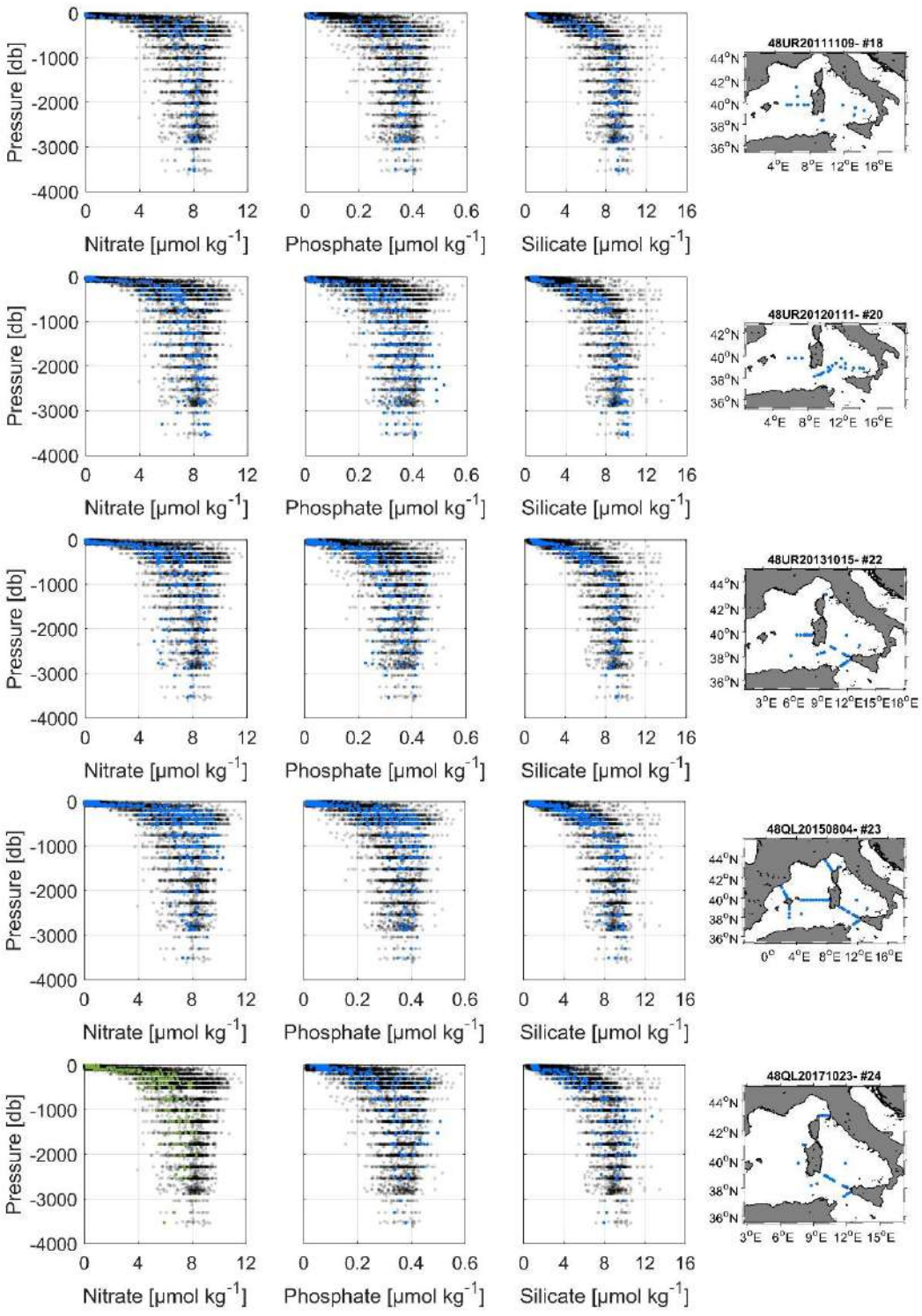

Figure 2.11: Vertical profiles of the inorganic nutrients in the dataset after adjustments and spatial coverage of each cruise (reference to cruise ID is above each map). The whole WMED adjusted product is shown in black while the data of each individual cruise are shown in blue (flag=2) and green (flag=3).

2.4.5 Product assessment: Comparison with MEDATLAS

Averages water mass properties have been computed from the adjusted product (Table 2.10), and compared to the MEDAR/Medatlas annual climatological profiles, downloaded from the Italian NODC website (http://doga.ogs.trieste.it/medar/) given by Manca et al. (2004), in order to evaluate and asses the new product. Since nutrient properties exhibit differences with depths, we compared average nutrient concentrations of the three main water masses in twelve subregions of the WMED (Table 2.10).

The results of Table 2.10 compare water mass biogeochemical properties with the reference climatology. The new product agrees well with the Medatlas climatology. However, there are some distinctions. The surface layer (0-150db) is characterized by a low nutrient content. The surface nitrate varies between 0.69 and 2.75 μmol kg^{-1} with a maximum found in the Ligurian East (DF4) and the minimum in the Alboran Sea (DS1) subregions, similar values were recorded in the climatology (0.61- 3.00 μmol kg^{-1}). The differences in nitrate averages in the surface layer are observed in the Gulf of Lion (DF2) where the new product is higher than the climatology and slightly lower in the Liguro-Provençal (DF3). As for, the surface content in phosphate, it varied between 0.04 and 0.16 μmol kg^{-1} with a maximum found in the Ligurian East (DF1) and a minimum in the Alboran Sea (DS1), alike the Medatlas climatology, where phosphate averages fluctuate between 0.05 and 0.19 μmol kg^{-1} .

The new product is slightly lower compared to the climatology. As to the average surface in silicate, it varies between 1.36 and 2.91 μmol kg^{-1} with a minimum found in the Ligurian East (DF4), the maximum in the Gulf of Lion (DF2)) while in the climatology it varied between 1.27 and 2.31 μmol kg^{-1} (the minimum in the Ligurian East (DF4) and the maximum in the Alboran Sea (DS1)). The new product is slightly higher in silicate.

Table 2.10: Water mass properties and regional average concentrations of inorganic nutrients: comparison between the new adjusted product and the MEDAR/Medatlas climatology (with standard deviations and number of observations in brackets).

Region/ Water mass	NO3 (μmol kg^{-1})		PO4 (μmol kg^{-1})		SiO2 (μmol kg^{-1})	
	Avg new Product	Avg Medar	Avg new Product	Avg Medar	Avg new Product	Avg Medar
DF2- Gulf of Lion						
surface water (0-150db)	2.68±2.53(68)**	1.7±1.1	0.15±0.06(68)	0.13±0.04	2.91±1.33(68)	1.72±0.64
IW core (S_{max} depth range: 300-500db)	8.49±0.18(17)	6.13±0.32	0.38±0.02(17)	0.34±0.01	8.67±0.69(17)	6.12±0.61
Deep water (>1500db)	8.03±0.43(33)	7.64±0.31	0.37±0.01(33)	0.37±0.015	8.7±0.67(33)	7.95±0.06
DF3- Liguro-Provençal						
surface water (0-150db)	2.31±2.4(205)	3.0±2.6	0.12±0.07(205)	0.19±0.05	2.45±1.05(205)	2.16±1.05
IW core (S_{max} depth range: 300-500db)	8.05±0.18(76)	7.74±0.13	0.36±0.01(76)	0.35±0.01	7.49±0.55(76)	6.26±0.60
Deep water (>1500db)	8.18±0.25(142)	7.79±0.04	0.37±0.02(142)	1.03±1.29	8.98±0.39(142)	7.60±0.21
DF4- Ligurian East						
surface water (0-150db)	0.7±0.69(228)	0.61±1.03	0.05±0.02(228)	0.18±0.02	1.37±0.45(228)	1.27±1.86
IW core (S_{max} depth range: 300-500db)	6.8±0.4(23)	5.54±0	0.3±0.02(21)	0.36±0.06	5.86±0.9(24)	4.86±0
Deep water (>1500db)	-	-	-	-	-	-
DS2- Balearic Sea						
surface water (0-150db)	1.32±1.46(196)	1.19±1.5	0.08±0.04(196)	0.11±0.04	1.61±0.64(196)	1.54±0.78
IW core (S_{max} depth range: 300-500db)	8.32±0.32(58)	6.92±0.12	0.37±0.02(60)	0.39±0.003	7.31±0.9(60)	7.55±0.62
Deep water (>1500db)	8.2±0.35(88)	-	0.37±0.01(88)	-	8.71±0.51(88)	8.45±0.8
DF1- Algero-Provençal						
surface water (0-150db)	0.87±0.85(372)	1.08±1.7	0.05±0.02(372)	0.07±0.05	1.42±0.3(372)	1.28±0.73
IW core (S_{max} depth range: 300-500db)	8.07±0.34(126)	7.51±0.18	0.36±0.02(126)	0.34±0.008	6.84±0.95(126)	5.96±0.77
Deep water (>1500db)	8.36±0.27(300)	7.87±0.13	0.38±0.02(300)	0.38±0.001	9.01±0.33(300)	8.18±0.10
DS1- Alboran Sea						
surface water (0-150db)	2.75±2.87(299)	2.51±2.23	0.17±0.11(299)	0.16±0.07	2.07±1.38(299)	2.31±1.14
IW core (S_{max} depth range: 400-600db)	8.89±0.4(77)	8.14±0.11	0.42±0.02(77)	0.37±0.008	8.77±1.66(76)	7.95±0.34
Deep water (>1500db)	7.72±0.81(65)	-	0.36±0.04(65)	-	8.98±0.63(65)	8.16±0
DS3- Algerian West						
surface water (0-150db)	1.8±1.88(254)	1.82±2.01	0.11±0.05(354)	0.11±0.06	1.71±0.68(354)	2.10±0.91
IW core (S_{max} depth range: 400-600db)	9.33±0.08(70)	8.28±0.15	0.41±0(73)	0.38±0.012	8.1±0.53(72)	6.68±0.80
Deep water (>1500db)	8.37±0.27(246)	8.047±0.013	0.37±0.02(246)	0.36±0.006	9.22±0.35(246)	8.87±0.23
DS4- Algerian East						
surface water (0-150db)	0.94±0.77(170)	0.75±1.26	0.07±0.02(170)	0.05±0.03	1.53±0.12(170)	1.35±0.52
IW core (S_{max} depth range: 400-600db)	8.5±0.25(43)	8.60±0.06	0.38±0.03(43)	0.38±0.008	7.27±0.67(42)	7.092±0.55
Deep water (>1500db)	7.94±0.24(132)	8.06±0.06	0.36±0.02(132)	0.38±0.006	8.73±0.38(132)	9.04±0.24
DT1- Tyrrhenian North						
surface water (0-150db)	1.03±1.14(231)	0.88±1.2	0.06±0.02(231)	0.09±0.03	1.64±0.52(231)	2.19±0.59
IW core (S_{max} depth range: 400-600db)	5.95±0.49(43)	5.86±0.36	0.27±0.03(44)	0.308±0.02	7.06±0.08(44)	6.76±0.59
Deep water (>1500db)	7.75±0.37(194)	7.12±0.47	0.36±0.03(194)	0.40±0.02	9.19±0.47(194)	7.51±0.49
DT3- Tyrrhenian South						
surface water (0-150db)	1.21±1.38(711)	1.23±1.80	0.06±0.03(711)	0.061±0.04	1.58±0.61(711)	1.55±1.05
IW core (S_{max} depth range: 300-500db)	6.2±0.28(225)	6.42±0.01	0.26±0.02(225)	0.254±0.005	6.28±0.65(224)	6.68±0.44
Deep water (>1500db)	7.88±0.4(227)	7.12±0.26	0.37±0.02(227)	0.31±0.007	9.04±0.52(227)	8.02±0.07
DI1- Sardinia Channel						
surface water (0-150db)	1.22±1.39(271)	1.42±1.95	0.07±0.03(271)	0.064±0.03	1.57±0.68(271)	1.39±1.01
IW core (S_{max} depth range: 300-500db)	6.52±0.17(89)	6.45±0.22	0.27±0.02(89)	0.250±0.01	6.36±0.67(89)	6.27±0.70
Deep water (>1500db)	7.91±0.62(107)	-	0.37±0.03(107)	0.32±0	8.64±0.91(107)	-
DI3- Sicily Channel						
surface water (0-150db)	0.87±0.68(583)	0.77±0.81	0.06±0.02(583)	0.063±0.02	1.53±0.29(583)	1.44±0.58
IW core (S_{max} depth range: 200-400db)	4.95±0.47(80)	5.14±0.14	0.21±0.02(78)	0.194±0.004	5.26±0.79(81)	6.744±0.41
Deep water (>1500db)	-	-	-	-	-	-

Overall, the differences in the surface layer are observed in Gulf of Lion (DF2), Liguro-Provençal (DF3), Ligurian East (DF4), which is due to the intense variability of the vertical mixing occurring in the northern WMED compared to the other regions.

In the intermediate layer, averages were computed from the depth of the salinity maximum (S_{max}) ±100m from a regional average profile, indicative of the Levantine Intermediate Water (IW) core. Nitrate average varies between 4.94 and 9.32 μmol kg^{-1} where the minimum content is recorded in Sicily Channel (DI3) and the maximum in the Algerian West (DS3) while in the in the Medatlas climatology nitrate was between 5.14 and 8.60 μmol kg^{-1} . In average, the lowest content in nitrate was in Tyrrhenian North (DT1), South (DT3), Sardinia Channel (DI1) and Sicily Channel (DI3) while IW of Gulf of Lion (DF2), Liguro-Provençal (DF3), Ligurian East (DF4), Balearic Sea (DS2), Algero-Provençal (DF1), Alboran Sea (DS1), Algerian West (DS3) and East (DS4) subregions is relatively rich in nitrate. Compared to the Medatlas product, though the new product is slightly higher mainly in the Gulf of Lion (DF2), Ligurian East (DF4) and Balearic Sea (DS2). As for phosphate, intermediate water (IW) averages show similar behavior as nitrate, the lowest phosphate content (0.21- 0.27 μmol kg^{-1}) is observed in the Eastern subregions of WMED (Sicily Channel (DI3),Sardinia Channel (DI1), Tyrrhenian South (DT3) and North (DT1), when the maximum concentrations (0.4-0.37 μmol kg^{-1}) were reported in the Western subregions of the WMED (the Alboran Sea (DS1), Algerian West (DS3) and East (DS4), Balearic Sea (DS2) and Gulf of Lion (DF2)). The large differences between the two products were in Ligurian East (DF4) and the Alboran Sea (DS1), subregions of few numbers of observations.

Concerning silicate, the lowest average concentration (5.25 μmol kg^{-1}) is observed in IW core of the Sicily Channel (DI3,) and the maximum concentrations (8.66 - 8.77 μmol kg^{-1}) are in Alboran Sea (DS1) and Gulf of Lion (DF2), similar values were recorded in the Medatlas climatology (4.86-7.95 μmol kg^{-1}). There are some discrepancies, where the new product is higher particularly in the Gulf of Lion (DF2), Liguro-Provençal (DF3) and Algerian West (DS3) subregions. This difference is explained by the limited number of observations within depth range in the new product compared to the observations used in the climatology in these subregions.

Referring to Manca et al.,(2004), the IW core salinity values are relatively more pronounced in Sicily Channel (DI3), Sardinia channel (DI1) and in the Tyrrhenian South (DT3), North (DT1) subregions, where nutrients were lower than the Western subregions (DS3,DS4, DS1 , DF1, DS2, DF4, DF3, DF2). The averages of nutrients within the IW core ties well with the Medatlas climatology averages (Table 2.10), except in subregions with important vertical mixing.

We have verified also average biochemical properties in the deep layer (below 1500db). The new product is slightly higher in nitrate averages (7.74 -8.37 μmol kg^{-1}) than the Medatlas climatology (7.12 - 8.06 μmol kg^{-1}) (Table 2.10). The largest difference is found in Tyrrhenian South (DT3) and North (DT1) subregions. This difference could be due to the fact that, we are comparing two different time periods (2004-2017 and 1908-2001). As for the deep layer

phosphate, average concentrations vary between 0.35 and 0.37 μmol kg^{-1} and are within the climatology limits (0.31 - 0.40 μmol kg^{-1}). In all subregions, there are not large differences. Overall, phosphate is in accordance with the Medatlas climatology. Similar to nitrate, deep average silicate in the new product (8.64 -9.21 μmol kg^{-1}) is higher than the climatology (7.51 to 9.04 μmol kg^{-1}). The largest difference in average silicate is observed in Tyrrhenian North (DT1), South (DT3) and Liguro-Provençal (DF3) subregions.

We then used the Root Mean Squared Error (RMSE) as statistical index to quantify the difference between averaged regional profiles from the new products and Medatlas product. The climatology annual profiles were interpolated to the regional average profiles of the new product, and the average RMSE for each layer and subregion was calculated.

Fig. 10 shows the regional evolution of RMSE in the main water masses for the three nutrients. For nitrate (Fig. 10 A), the RMSE vary between 0.12 μmol kg^{-1} in Tyrrhenian North (DT1) and 1.36 μmol kg^{-1} Gulf of Lion (DF2) in the surface layer, between 0.07 μmol kg^{-1} in the Sardinia Channel (DI1) and 2.35 μmol kg^{-1} in Gulf of Lion (DF2) in the intermediate layer, and between 0.11 μmol kg^{-1} Algerian East (DS4) and 0.79 μmol kg^{-1} Gulf of Lion (DF2). The RMSE decreases in the Algerian East (DS4), Tyrrhenian North (DT1), Tyrrhenian South (DT3), Sardinia Channel (DI1) and Sicily Channel (DI3). This illustrates the low difference between the two products.

For phosphate (Fig. 2.12 B), the RMSE ranges between 0.0022 μmol kg^{-1} in the Tyrrhenian South (DT3) and 0.12 μmol kg^{-1} in the Ligurian East (DF4) in the surface layer, and between 0.003 μmol kg^{-1} in the Liguro-Provençal subregion (DF3) and 0.048 μmol kg^{-1} in the Alboran Sea (DS1), while in the deep layer RMSE varied between 0.0087 in the Gulf of Lion (DF2) and 0.057 μmol kg^{-1} in the Tyrrhenian North (DT1).

Silicate RMSE (Fig. 2.12 C) is between 0.13 μmol kg^{-1} in the Algero-Provençal subregion (DF1) and 3.5 μmol kg^{-1} in the Ligurian East subregion (DF4) in the surface layer, between 0.10 μmol kg^{-1} in the Sardinia Channel (DI1) and 2.54 μmol kg^{-1} in the Gulf of Lion (DF2) in the intermediate layer, and in deep layer, RMSE ranges between 0.33 μmol kg^{-1} in the Algerian East (DS4) and 1.43 μmol kg^{-1} in the Liguro-Provençal subregion (DF3).

The best agreement between the two products was observed in the intermediate and deep layer. The lowest RMSE was confined to the deep layer in most of the subregions while the highest difference was found in the surface layer since it is subjected to intense vertical mixing mainly in the northern WMED. Comparing averages in subregions, showed similar differences in nutrient between the two products particularly in the Gulf of Lion (DF2), the Liguro-Provençal (DF3), Ligurian East (DF4) and Algerian East (DS4), due to the relative high variability in nutrient concentrations in these subregions. These differences are not significant as there is discrepancy on the number of observations used in the two products.

Overall, inorganic nutrients of the new product agree very well with the MEDAR/Medatlas climatology. The main features of the spatial distribution in the inorganic nutrients were in accordance with the findings of Manca et al., (2004), where the relative high content in

nutrient was found in the intermediate layer of the Algerian subregions (DF1, DS3, DS4) than in other subregions (Table 2.10). Besides, the highest concentrations in deep layer silicate were reported in the Algerian subregions (9.21 μmol kg^{-1} (DS3) in the new product; 9.04 μmol kg^{-1} (DS4) in the climatology) in the two products, which is indicative of the poor regional ventilation and of the longer residence time of deep water especially in these subregions.

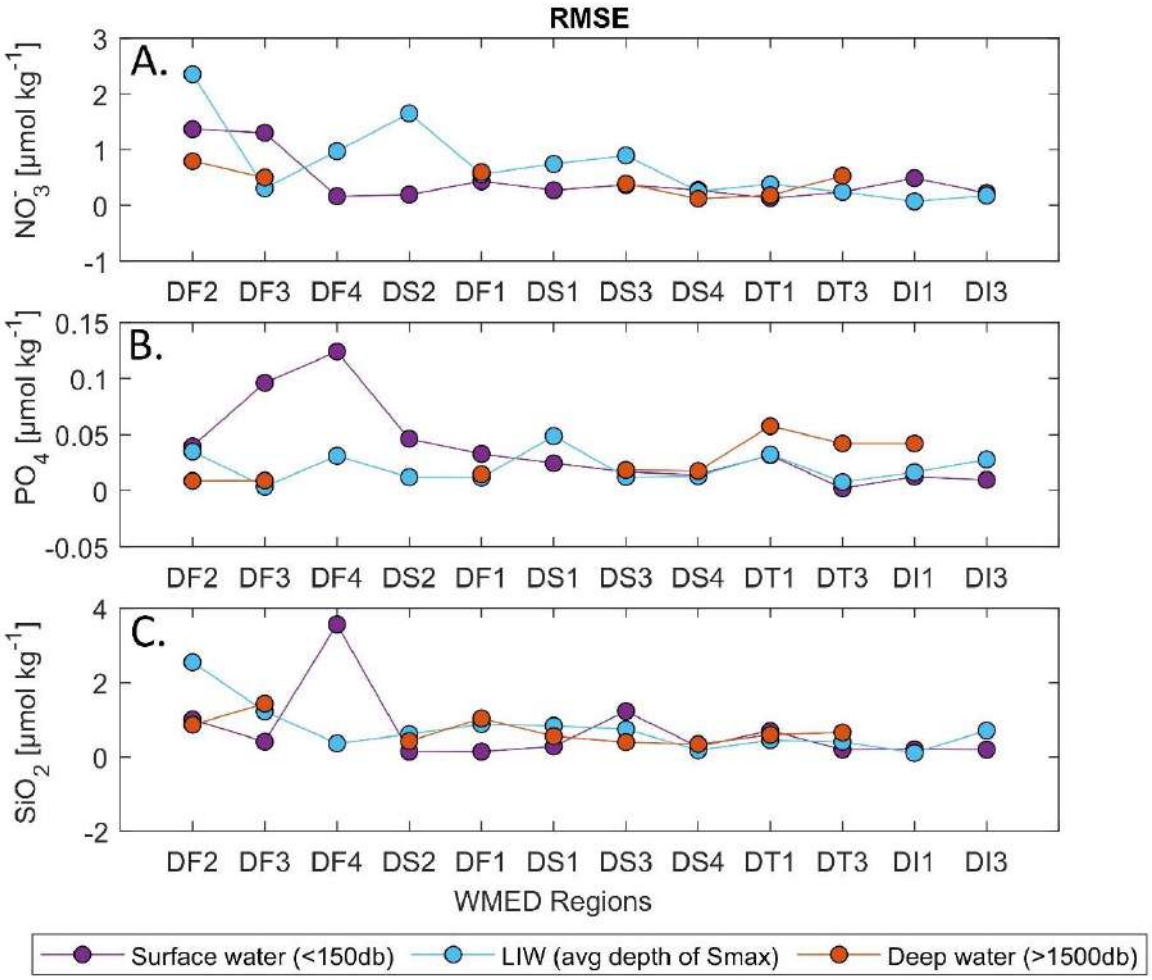

Figure 2.12: RMSE regional averages of water mass properties computed between the new adjusted product and MEDAR/Medatlas climatology for nitrate (A.), phosphate (B.) and silicate (C.).

2.5 Data availability

The final product is available as a .csv merged file from PANGAEA, and can be accessed at https://doi.org/10.1594/PANGAEA.904172 (Belgacem et al. 2019).

Ancillary information is in the supplementary materials with the list of variables included in original and final product. Table 2.1 summarizes all cruises included in the dataset. The dataset include frequently measured stations and key transects of the WMED with in situ physical and

chemical oceanographic observations. As mentioned, two files are accessible, both include oceanographic variables observed at the standard depths (Appendix A).

- *Original dataset: CNR_DIN_WMED_20042017_original.csv:* This is the original dataset with flag variable for each of the following parameter: CTD salinity, nitrate, phosphate, and silicate from the primary quality control (detailed in section 2.3.1).
- *Adjusted dataset: CNR_DIN_WMED_20042017_adjusted.csv*: This is the product after primary quality control and after applying the adjustment factors from the secondary quality control. Recommendations of section 2.4.4 are included, as well as quality flags.

2.6 Final remarks

An internally consistent data set of dissolved inorganic nutrients has been generated for the WMED (2004-2017). The accuracy envelope for nitrate and silicate was set to 2%, a predefined limit used in GLODAP and CARINA data products. Regarding phosphate data, these were almost entirely outside this limit, because of its natural variations and overall, very low concentrations in the WMED, a highly P-limited basin. Using a crossover analysis (2^{nd} QC toolbox) to compare cruises with respect to reliable reference data, improved the accuracy of the measurements by bias-minimizing the individual cruises. The new product was broadly in consistent with the earlier climatology MEDAR/Medatlas.

The publication of a quality-controlled extensive (spatially and temporally) database of inorganic nutrients in the WMED was timely and fills a gap in information that prevented baseline assessments on spatial and temporal variability of biogeochemical tracers in the Mediterranean. In combination with older databases in the same region (e.g. bottle data available in the MEDAR/Medatlas database), this new database will thus constitute a pillar on which the Mediterranean marine scientific community will be able to build on original research topics on biogeochemical fluxes and cycles and their relation to hydrological changes that occurred in the period covered by the dataset.

The dataset is also relevant for the modelling community as it can be used as an independent data product to assess reanalysis products or it can be assimilated in new reanalysis products.

Chapter 3. BIOGEOCHEMICAL FOOTPRINT OF THE WESTERN MEDITERRANEAN WATER MASSES

A detailed analysis of the stoichiometry of the WMED system is presented in this chapter. The remineralization ratio of the different elements is investigated between subregions of the WMED to determine the relative abundance of the different macronutrients.

The variation of the ratios is explored at different depth levels as well and compared to the fixed reference Redfield thresholds. However, the ratio varies in different oceanic zones. Results reveal the vertical gradient in dissolved inorganic nutrients with depth. The decreasing trend of N:P ratio and increase in Si:N ratio at greater depths are well identified. Ratios varied from East to West. Such gradients impact carbon and nutrient availability .

The surface WMED layer stoichiometry is lower than the relative Redfield ratio. This pattern suggests the existence of Nitrate limitation episodes. The use of the reference Redfield does not fit the Mediterranean Sea conditions. The ratio deviates and there is evidence that the ratio varies regionally.

3.1 Introduction

Nutrients are issued from the oxidation of organic matter in a molecular proportion that is described by the Redfield ratios (Redfield et al., 1963). The deviation from stoichiometric ratio in diverse biogeochemical regions is influenced by physical processes such as upwelling in the Alboran Sea, convective mixing in the north WMED and enhanced atmospheric depositions. These processes load nutrient to the surface layer supporting primary production and leading to a deficiency in oxygen at subsurface waters due to the active microbial remineralization of organic matter and respiration (Voss et al., 2013), giving rise to different patterns of denitrification, and nitrogen fixation (Silva et al., 2009).

Elemental ratios of inorganic nutrients (C, Si, N, P, O_2) are fundamental to link biogeochemical cycles. Changes in carbon sequestration have been associated with changes in Redfield ratios. The elemental ratio in plankton is thought to be conserved (Falkowski et al., 1998) following the stoichiometric model (Si: N:P:O2= 15:16:1:138 ;Redfield et al., 1963), representing the average photosynthesis and respiration (Geider and La Roche, 2002). The ratio could vary with the environmental conditions (temperature) or growth rate of phytoplankton. It has been reported that the ratio is subjected to spatial variability and varies with depth depending on the dissolved oxygen levels (Paulmier and Ruiz-Pino, 2009).

Dissolved oxygen is important to include in order to fully understand the biogeochemical properties of the water column, since the biogeochemical cycle of nutrients and carbon are connected to the changes in dissolved oxygen through respiration and primary productivity. Generally, C:N:P composition of primary production affects the nutrient composition of the surface layer. According to Geider and La Roche (2002), the Redfield value is obtained in optimum conditions where no nutrient is limiting. When there is a limiting nutrient, a deviation in ratios is observed.

The Mediterranean Sea functions differently from the global ocean. It has long been known as a nutrient-depleted area and exhibits spatial diverseness. The global stoichiometric ratios of nutrients (N:P and Si:N) found in phytoplankton, when nutrients are not limiting, are 16:1 and 0.94 respectively, while in the Mediterranean Sea this ratio exceeds this reference: in the WMED N:P is about 23:1 (Pujo-Pay et al., 2011) and Si:N is <1, while in the EMED N:P is about 28:1 , and Si:N exceeds 1.3 (Powley et al., 2017). With climate change, the nutrient content of the Mediterranean Sea is predicted to vary, since the region responds rapidly to any change. Even though it is often researched (Kress and Herut, 2001; Krom et al., 2005; Ribera d'Alcalà, 2003), the anomalous nutrient ratios remain an open question for a better understanding of the Mediterranean Sea functioning.

Various factors can potentially alter nutrient contents. In the northern WMED, known to be one of the productive areas of the Mediterranean Sea since it holds the deep convection, the

most important fertilizing process responsible for the enrichment of the surface layer with nutrients. The highest chlorophyll concentrations are found during winter seasons and linked to the uplift of the nutrient-rich water and its mixing with the surface waters (Segura-Noguera et al., 2016). The Alboran Sea is also known as an upwelling region, where there is a permanent input of nutrients to the surface.

As already described in Chapter 1, silicate concentrations increase with depth, due to a low remineralization rate, while nitrate and phosphate increase to a maximum value at intermediate water, associated to a minimum in dissolved oxygen (García-Martínez et al., 2019). Nitrate and phosphate decrease at deeper layers, while oxygen increases at depth, since deep water is ventilated by winter deep convection. It has been evidenced that a decrease in dissolved oxygen concentrations is linked to the reduction in solubility with the warming of water masses and the weakening of the ventilation process (Schmidtko et al., 2017).

In this chapter, regional variations of biogeochemical footprint of different water masses and their Redfield ratios are examined, using 14 years of quality-controlled data from research cruises carried out between 2004 and 2017 (as described in Chapter 2).

The overall objective of this chapter is to describe the basin wide distribution of nutrients in the five regions of the WMED (Sicily Channel (SIC); Tyrrhenian Sea (TYR); North WMED and Ligurian Sea (NWMED & LIG); Algerian Sea (AS); and Alboran Sea (ALB)), as well as to characterize the biogeochemical footprints of regional water masses. Ratios are compared to the reference Redfield ratios.

This chapter addresses the question of nutrient limitation and the variability of ratios found in the various depth layers, and a better understanding of the deviation from the Redfield ratios. A new insight into the link between salinity and inorganic nutrients is studied. This elemental description is a useful reference to understand the WMED biogeochemistry.

The chapter is organized as follows: in section 2, the data distribution per region is recalled; in section 3, the method of investigation is addressed; in section 4 the results are presented; some observations are discussed analyzing the results with emphasis on the properties of the most significant depth layers. The concluding remarks of the present work are summarized in section 5.

3.2 Dataset

The analysis is based on the CNR_DIN_WMED_20042017 biogeochemical dataset (Belgacem et al., 2019) spanning 14 years, which has been extensively described in Chapter 2. During 24 cruises samples for the analysis of nitrate, phosphate and silicate concentrations have been taken and then underwent a careful quality control(Belgacem et al., 2020).

Samples were grouped in five regions, and figure 3.1 shows the stations within each region. Regions have been defined according to the dynamic of the WMED, formation , transport, and the circulation patterns of the three main water masses of the surface, intermediate and deep layer as described in section 3.2 of chapter 1.

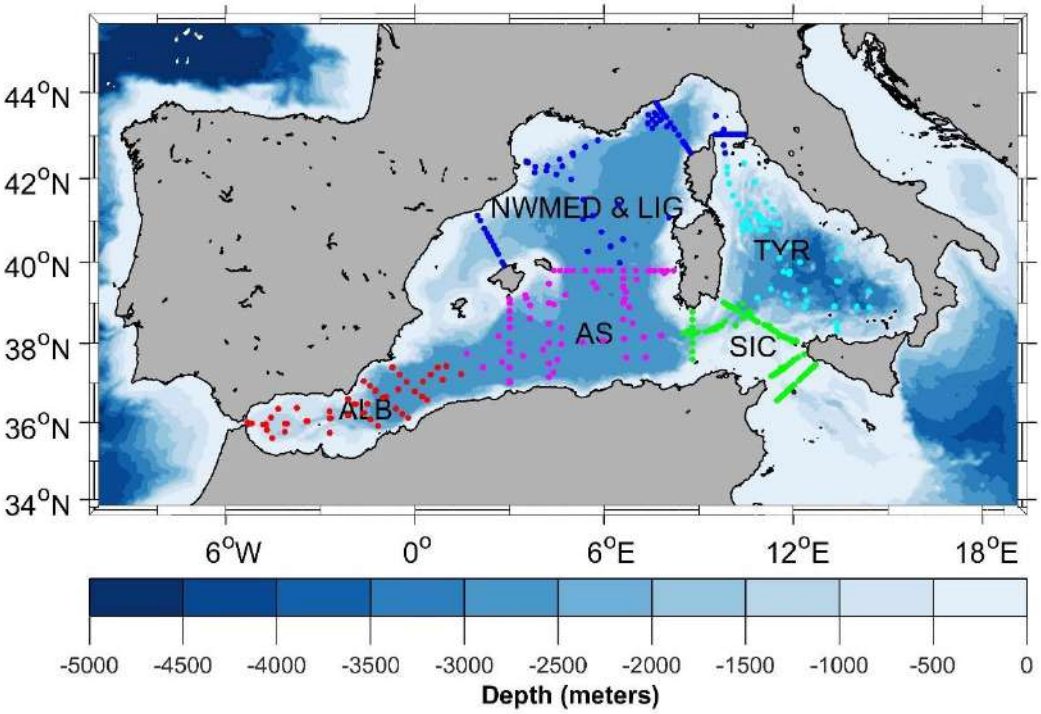

Figure 3.1: Map of the WMED showing station locations and regions: green dots in the Sicily Channel (SIC); cyan dots in the Tyrrhenian Sea (TYR); blue dots in the North WMED and Ligurian Sea (NWMED & LIG); magenta dots in the Algerian Sea (AS); red dots in the Alboran Sea (ALB).

As detailed in chapter 2, at each station, pressure (dbar), salinity, temperature (◦C, SBE-3/F thermistor), and dissolved oxygen concentration (O_2, μmol kg^{-1}, SBE-43 sensor) were measured with a CTD-rosette consisting of SBE 911 plus General Oceanics Rosette System with 24 12-liters Niskin Bottles.

Salinity and potential temperature were derived using Sea-Bird Scientific routine and processed on board. CTD profiles of temperature, salinity and dissolved oxygen were obtained by sampling the signals at 24 Hz, during the downcast at a speed of 1 m s^{-1}.

Dissolved oxygen samples were collected with the same Niskin bottles used to sample nutrients. Then dissolved oxygen is analyzed on board with Winkler titration (Grasshoff et al., 1999). To this, water samples were treated soon after collection with reagents by adding manganese (II) and alkaline iodide with semi-automatic dispensers.

The oxygen bottles were shaken for about one minute, so that each oxygen molecule enters in contact with the reagents then a precipitate is formed. After fixation, samples are stored for a few hours in the dark prior to titration. Then, the precipitated hydroxide was dissolved using the sulfuric acid. The titration is carried out with a standardized thiosulfate using an

automated potentiometric titration system Metrohm 798 MPT Titrino. The titrated samples of dissolved oxygen were used to calibrate CTD profiles of oxygen, and any aberrant or unusual value was removed

Dissolved oxygen was used then to calculate the apparent oxygen utilization (AOU), that was computed from the difference between dissolved oxygen saturation concentration (estimated from in situ temperature and salinity) and the measured in situ dissolved oxygen, following (Owens and Millard, 1985).
The monthly data distribution is shown in Figure 3.2. Most observations were collected between May and October. Therefore, the study is more representative for warm and mild seasons.

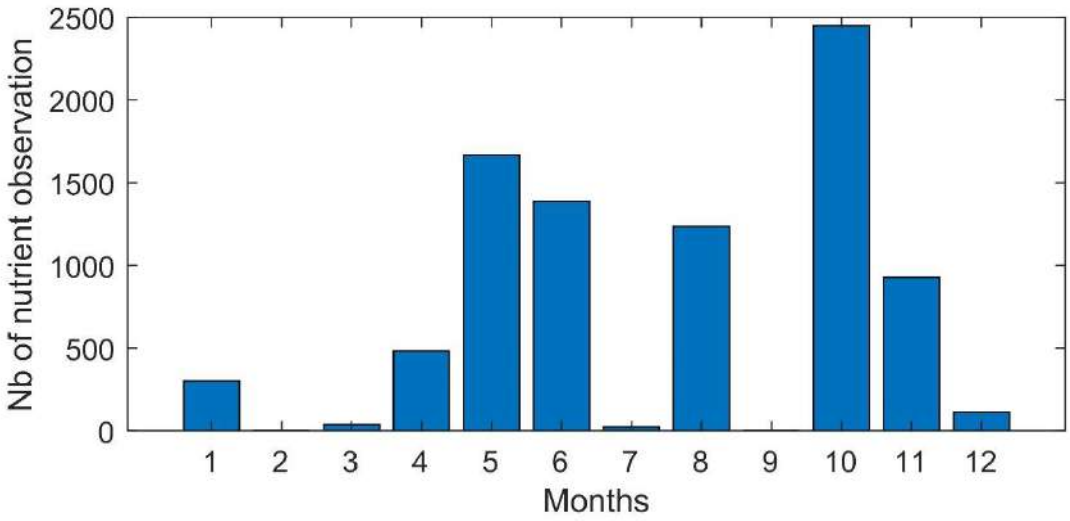

Figure 3.2: Monthly distribution of nutrient observations used in this chapter.

3.3 Methods

The approach applied is based on the estimation of spatial averages over the entire time period (2004-2017) of physical and biogeochemical parameters (i.e. salinity, temperature, nitrate, phosphate, silicate and oxygen concentrations). The WMED is divided in five subregions considering the physical and hydrological characteristics (Fig. 3.1).

- Region 1: the Sicily Channel region (SIC) in direct contact with the EMED.
- Region 2: the Tyrrhenian Sea (TYR), the most isolated sub basin of the WMED.
- Region 3: the northern WMED and Ligurian Sea (NWMED & LIG), where deep water formation occurs within a permanent cyclonic circulation.
- Region 4: the Algerian Sea (AS), under the influence of the AW and the mesoscale anticyclonic features.

- Region 5: the Alboran Sea (ALB), under the direct influence of the AW input, and permanent upwellings.

Samples were grouped by depth range in the five regions. For each variable, statistical average and standard deviation, are computed. Generally, water masses tend to follow specific depth layers. Averages were computed according to a surface, intermediate and deep layers and by subregion.

Considering the local temperature-salinity diagrams (Fig. 3.3), three layers are defined (Table 3.1): 0-150 m, representative of the surface water (AW); 150-400 m (Sicily region) or 150-600 m, representative of the intermediate water (IW); 600-1500 m, the transitional layer that includes the transitional water masses, and the deep layer from 1500 m to the bottom, including WMDW.

Since salinity is a conservative tracer, the relationship between nutrients and salinity was analyzed since the use of salinity helps separate water masses. Following Pujo-Pay et al. (2011) and Ribera d'Alcalà (2003), molar stoichiometry was used to describe processes that regulated WMED biogeochemistry.
Redfield developed the relationship between elements (carbon, nitrate, phosphate)(as detailed in section 1.3.4). Similarly, the relationship with the apparent oxygen utilization was deduced with the various nutrients.
These ratios are expected to be similar to those in the plankton. Hence, any change in concentrations would infer similar changes in the ratio of the phytoplankton (Redfield et al., 1963).
In the present study, ratios were calculated between nutrients, and between dissolved oxygen and nutrients using the two known approaches indicated by Kress and Herut (2001): the first approach considers the ratio as the slope of the regression model fitted to the ratio: N:P, Si:N, AOU:P, AOU:N , AOU:Si (see Fig. 3.7-3.8-3.9-3.10-3.11) according to the equation ($y = ax + b$) of the linear relationship between elements in the property-property plots.
The second approach considers the average ratios for each region over depths (Fig. 3.7-3.11 (f)). Here we applied this method using the median ratios.
These two methods were also used by Redfield because the interpretation of both methods is complementary. When ratios from the two approaches coincide, the regression lines should pass through zero of the origin, this is interpreted as nutrient co-variation (Pujo-Pay et al., 2011) meaning that concentration of nitrate and phosphate for examples are in balance. In the case where the regression line do not pass through the origin, b , the intercept in the linear regression indicates a shortage of an element relative to the other in the case of a negative intercept, however, an excess is noted in the case of a positive intercept (Pujo-Pay et al., 2011).

In this analysis, all nutrient fractions are included, i.e. nutrients that have been regenerated (the oxidative) within the water column and those transported by mixing (performed nutrients).

Properties in the different regions are presented as property-property scatter plots for all observations, both as a function of depth and as a function of each other (Fig.3.7-3.11 (g)).

3.4 Results

3.4.1 Biogeochemical footprints of regional water masses

Water masses share common properties such as temperature, salinity and biogeochemical characteristics that are distinct from surrounding waters. These properties are not uniformly distributed in space, which explains the difference between regions.

The definition of water masses is not limited by physical properties such as temperature-salinity -pressure relationship. Physical and biogeochemical properties, both conservative and non-conservative can be considered in defining a water mass.

Water masses are particularly important when following the changes in biogeochemical applications. In a recent work, Schroeder et al. (2020) considered the intermediate water in the WMED as a proxy to identify thermohaline, biogeochemical and carbonate system transformations.

Figure 3.3 shows temperature-salinity diagrams for the five regions. During the period 2004-2017, changes in the physical properties of the deep water in the WMED have been reported (Schroeder et al., 2016). Here, only a regional climatological average at different layers of the WMED is shown. Within the three main layers of the WMED, water masses are defined based on their salinity (Table 3.1).

The nutrient depleted surface layer (below 150 m) show the lowest average salinity of about 37.13±0.63 in the Alboran Sea, 37.61±0.42 in the Algerian Sea, 38.19 ±0.21 in the NWMED & Ligurian Sea, 38.13±0.22 in the Tyrrhenian Sea and 37.9±0.3 in the Sicily channel. These salinities refer to the characteristics of the Atlantic surface water. As it flows eastward, it progressively loses its initial properties, through the mixing with the resident Mediterranean water masses.

In the Alboran Sea, the surface layer (<150 m) shows the highest content in nitrate (2.71±2.6 μmol kg^{-1}), phosphate (0.16±0.1 μmol kg^{-1}), and also silicate (2.05±1.57 μmol kg^{-1}) with the lowest dissolved oxygen (214.41±23.37 μmol kg^{-1}) while in the Northern WMED & Ligurian Sea, salinity was about 38.19 ±0.21. To the East, the surface Tyrrhenian layer showed very low concentrations in nutrients (0.99±1.4 μmol kg^{-1}, nitrate; 0.05±0.05 μmol kg^{-1} ,phosphate and 1.5±0.86 μmol kg-^{1} ,silicate) followed by a high dissolved oxygen (230.4± 20.3 μmol kg^{-1}).

The surface layer in the Tyrrhenian Sea (low surface nutrient) and Alboran Sea (relatively high surface nutrient) seems to behave oppositely with respect to nutrient concentration.

Dissolved oxygen on the other hand, was rather constant across the region (Table 3.1) due to the equilibrium with the atmosphere (Kress and Herut, 2001).

At the intermediate layer, generally, there is the IW, one of the most important waters of the Mediterranean. Its depth varies from one region to the other, depending on the local topography. Here, the IW properties are explored within 150-600 m depth. In average, the lowest salinity is found in the Alboran Sea (38.42± 0.13, at 150-600 m) accompanied with large values of nutrients (8.22±1.6 μmol kg^{-1} , nitrate; 0.36±0.09 μmol kg^{-1} ,phosphate and 6.48±1.9 μmol kg^{-1}, silicate) and low content in dissolved oxygen (172.40±13.2 μmol kg^{-1}). The IW water, as it moves from where it formed (Cretan Sea or Levantine basin), becomes richer in nutrients and poorer in dissolved oxygen.

In the Sicily Channel, the IW shows the highest salinity (38.69± 0.09). We also distinguish a relative low concentration in nitrate (5.86 ±1.2 μmol kg^{-1}), phosphate (0.24±0.05 μmol kg^{-1}) and silicate (5.72±1.5 μmol kg^{-1}). These features are found more pronounced in the Tyrrhenian Sea (150-600 m) (Table 3.1). In the Western most regions (Alboran Sea, Algerian Sea and the North WMED & Ligurian Sea), the intermediate layer is characterized by high content in nutrients, with values exceeding 7.4 ±1.3 μmol kg^{-1} for nitrate, 0.33±0.068 μmol kg^{-1} for phosphate and 5.99±1.99 μmol kg^{-1} for silicate.

Similar difference between subregions is also noted in the layer between 600 and 1500m; Very low nutrient concentrations are found in the Sicily region and Tyrrhenian Sea for the three nutrients and the largest values are in the Northern WMED & Ligurian and Algerian Sea.

In the deep layer (> 600 db), large salinity and temperature values (38.64±0.04 , 13.69±0.1 °C at 600-1500 m and 38.52±0.026, 13.45±0.0 °C at > 1500 m) are found in the Tyrrhenian Sea along with low nutrient concentrations (7.73±0.8 μmol kg^{-1} , nitrate; 0.36±0.04 μmol kg^{-1},phosphate; 9.15±0.8 μmol kg^{-1}, silicate) . Similar observations are found also in the Sicily region (7.8±0.9 μmol kg^{-1}, nitrate; 0.35±0.05 μmol kg^{-1}, phosphate; 8.86± 1.0 μmol kg^{-1}, silicate). The deep layer of the Algerian Sea, showed high content in nitrate (8.24±0.7 μmol kg^{-1}), phosphate (0.36±0.04 μmol kg^{-1}) and silicate (9.00±0.94 μmol kg^{-1}), this was also observed in the Northern WMED & Ligurian Sea (nitrate, 8.18±0.7 μmol kg^{-1}), phosphate (0.375±0.03 μmol kg^{-1}) and silicate (8.818±0.9 μmol kg^{-1}).

The relatively low content in nutrient in the easternmost regions (SIC and TYR) at intermediate depths (150-600 m and 600-1500 m) is the result of the significant amount of the EMED intermediate and deep depleted waters, flowing through Sicily Channel to the Tyrrhenian Sea where a vertical mixing occur and the physical and biogeochemical properties are changing the resident WMED waters as indicated also the study of Manca et al. (2004).

Comparing dissolved oxygen concentrations, we noticed that there is an accord with nutrient content at intermediate and deep layers. The highest values tie in with high nutrient concentrations for example in the North WMED and Ligurian Sea. This area of the WMED is well-ventilated, below 1500 m where oxygen concentrations exceed 200 μmol kg^{-1}. This is

mainly due to the vertical mixing and to the winter deep convection responsible for the increased oxygenation of the deep water, related to the high inflow of a new water mass.

Contrarily, the minimum dissolved oxygen concentrations are found with high nutrient contents, with values varying between 172 and 185 μmol kg^{-1} in the easternmost subregions.

The averages presented in Table 3.2 reflect the distribution of the classical water masses in the WMED, as defined by salinity and temperature, and showing the importance of thermohaline circulation in changing the water mass properties. However, there are significant differences between the water mass and nutrient distributions. Nutrient concentrations show strong contrast along the water column and between regions as well (Williams and Follows, 2003). In the next section, the relationship between nutrients and salinity is examined.

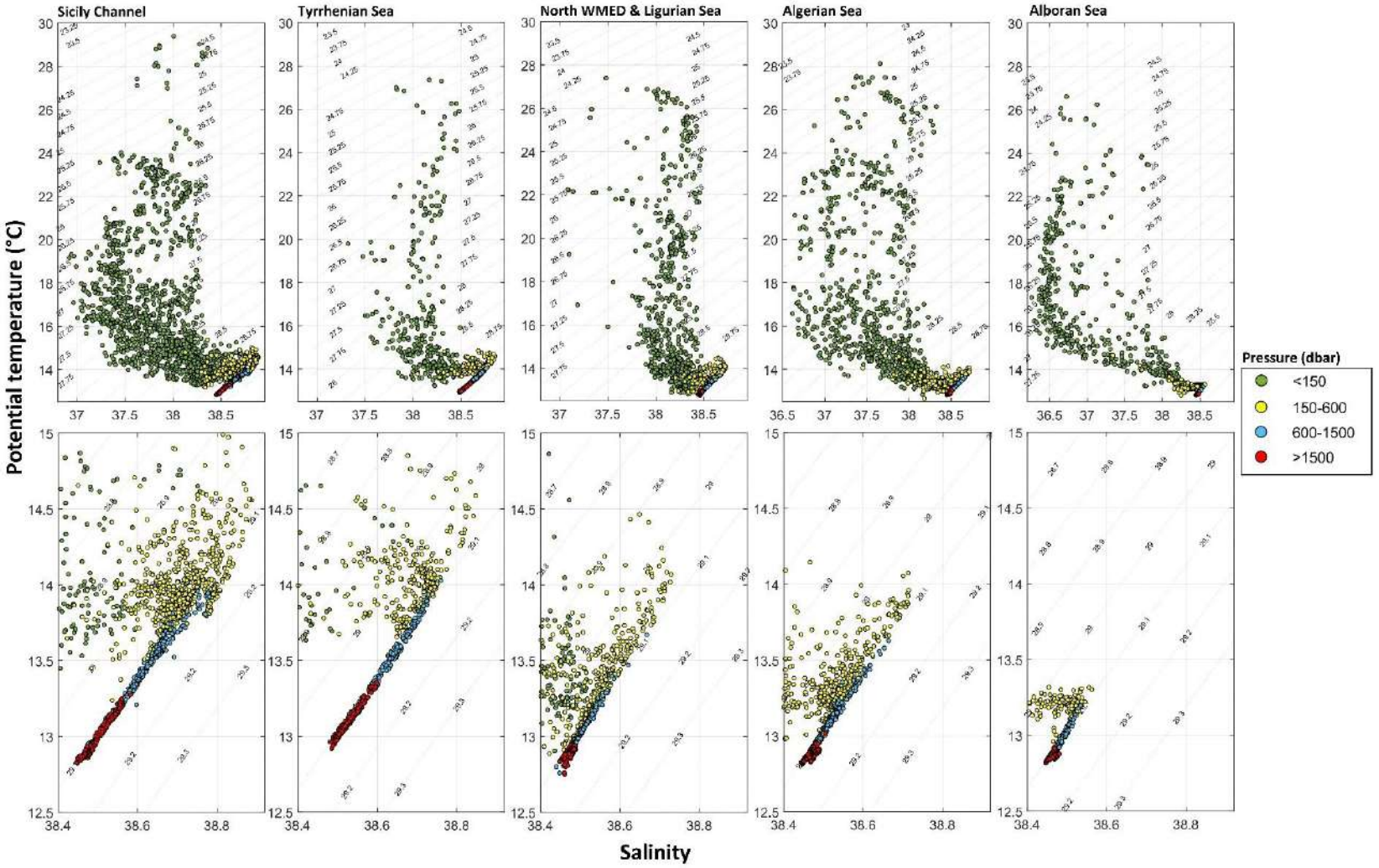

Figure 3.3: Temperature- salinity diagram versus pressure in the five subregions. Top panel represents the entire water column; bottom panels are a zoom on the intermediate and deep layer. Potential density isolines are superimposed.

Table 3.1: Physical and biogeochemical properties of depth-averaged surface, intermediate and deep layer (average ± standard deviation) in Sicily Channel, Tyrrhenian Sea, North WMED & Ligurian Sea, the Algerian Sea and the Alboran Sea.

REGION/ depth range	Sample number	Mean salinity and std	Mean potential temperature and std (°C)	Mean Nitrate and std (μmol kg^{-1})	Mean phosphate and std (μmol kg^{-1})	Mean silicate and std (μmol kg^{-1})	Mean oxygen and std (μmol kg^{-1})
Sicily channel (SIC)							
<150m	1504	37.9±0.3	16.69±3.1	1.24±1.5	0.067±0.05	1.64± 1.1	226.2 ±19.3
150-600	793	38.69± 0.09	14.01±0.2	5. 86 ±1.2	0.24±0.05	5.72±1.5	181.4±9.7
600 -1500 m	410	38.61±0.06	13.65±0.1	7.02±0.9	0.31±0.05	8.28±1.2	183.17±7.7
>1500 m	249	38.49± 0.03	13.27±0.1	7.8±0.9	0.35±0.05	8.86± 1.0	192.53± 9.2
Tyrrhenian Sea (TYR)							
<150m	367	38.13±0.22	16.5±3.3	0.99±1.4	0.05±0.05	1.5±0.86	230.4± 20.3
150-600	286	38.67±0.09	14.10±0.2	5.71±0.9	0.244±0.05	4.99±1.3	183.87±9.0
600 -1500 m	191	38.64±0.04	13.69±0.1	6.71±0.8	0.31±0.04	7.73± 1.1	182.83± 6.8
>1500 m	330	38.52±0.026	13.45±0.0	7.73±0.8	0.36±0.04	9.15±0.8	189.08±8.3
North WMED & Ligurian Sea (NWMED&LIG)							
<150m	731	38.19 ±0.21	16.59±3.7	1.69±2.1	0.08±0.082	1.96±1.36	226.80± 20.5
150-600	450	38.53±0.07	13.44± 0.2	7.48±1.3	0.33±0.068	6.51±1.895	185.08± 12.7
600 -1500 m	259	38.49±0.02	13.14±0.1	8.36±0.9	0.38±0.038	8.82±1.04	191.53±11.06
>1500 m	281	38.475±0.01	13.18±0.06	8.18±0.7	0.375±0.03	8.818±0.9	202.9±10.9
Algerian Sea (AS)							
<150m	827	37.61±0.42	17.34±3.8	1.17±1.5	0.068±0.062	1.507±1.121	226.38±20.6
150-600	526	38.47±0.16	13.45±0.25	7.74±1.7	0.33±0.08	5.99±1.99	178.90±15.4
600 -1500 m	373	38.50±0.03	13.18±0.11	8.39±0.8	0.38±0.04	8.825±1.0	183.6±9.9
>1500 m	649	38.46±0.01	13.2±0.07	8.24±0.7	0.36±0.04	9.00±0.94	196.25±10.89
Alboran Sea (ALB)							
<150m	472	37.13±0.63	16.87±3.08	2.71±2.6	0.16±0.1	2.05±1.57	214.41±23.37
150-600	255	38.42± 0.13	13.25±0.15	8.22±1.6	0.36±0.09	6.48±1.9	172.40±13.2
600 -1500 m	168	38.48±0.01	13.1±0.05	8.14±1.2	0.37±0.06	8.819±1.21	181.31±5.43
>1500 m	158	38.46±0.01	13.160±0.06	8.03±1.1	0.34±0.05	8.92±1.12	190.9± 6.1

Blue : lowest values ; red : highest values with respect to other regions.

3.4.2 Property-property plots

To understand the relationship between inorganic nutrients and the water column structure, the distribution of salinity with inorganic nutrients is studied here. The distribution of dissolved inorganic nutrients in the WMED follows several patterns. Nutrients can be used as water mass tracers to define the limits of a water mass if compared with conservative tracers such as salinity and temperature.

Nutrient-salinity plots are used to identify water masses in the predefined regions and their depth distribution (Fig.3.4-Fig.3.9).

The region with the highest variability is the Alboran Sea (ALB), where boxplots in Fig.3.4f suggest that nitrate concentrations values are much more scattered than other regions.

Between 150-600 m, the Alboran Sea shows large nutrient concentration compared to the other subregions. The medians, which generally are close to the average, are all at different levels. The high variability in nutrient values of the surface layer (Figure 3.3) reflect mixing processes and an important phytoplankton consumption.
Between 150-600 m, boxplots of nitrate (Fig. 3.4f) and phosphate (Fig. 3.6f) show that from SIC-TYR to the other westernmost regions, there is an increase in concentrations. This is the well-known decreased oligotrophy gradient from the Eastern to Western regions.
Figure 3.5, Figure 3.7 and Figure 3.9 show respectively nitrate, phosphate and silicate distribution, over an expanded salinity scale, displaying patterns associated to the intermediate and deep layers.

Property plots revealed that nitrate decreases with the increase in salinity (Fig. 3.4). The eastern subregions (SIC-TYR) showed a clear distinction between depth layers, where nitrate content was lower with salinity between 36.6 and 38.9 (at 600-1500 m), while larger concentrations or 'nitrate rich waters' are found with salinity between 38.45 and 38.6 (at depths greater than 1500 m) in NWMED & LIG (Fig. 3.5c), AS (Fig. 3.5d) and ALB (Fig. 3.5e) subregions. This salinity range corresponds to the WMDW (Beuvier et al., 2012).

Figure 3.7 shows the relationship between phosphate and salinity. The low values are found in the Eastern subregions (SIC, Fig. 3.7a; TYR, Fig. 3.7b) at salinity greater than 38.6 mainly between 150 and 1500 m, while Large values of phosphate or 'Phosphate-rich waters' are found with salinity between 38.45 and 38.6 (> 1500 m) in NWMED & LIG (Fig. 3.7c), AS (Fig. 3.9d) and ALB (Fig. 3.9e) subregions similar to nitrate.

For silicate on the other hand, maximum concentrations (Fig. 3.9) are found below 1500 m within salinity values ranging between 38.45 and 38.6 in SIC (Fig. 3.9a), and TYR (Fig. 3.9b) subregions. Lower salinity range is noted between 38.45 and 38.55 in NWMED & LIG (Fig. 3.9c), AS (Fig. 3.9d),and ALB (Fig. 3.9e) subregions.

Silicate behavior was different compared to nitrate and phosphate. It showed a clear distinction between the different layers especially in SIC and TYR subregions. Indeed, Figure 3.8 and Figure 3.9 show a well-defined mixing line between the intermediate water (found at 150 – 600 m) and the waters below (600-1500 m).

Vertical distribution of nutrients in Fig.3.4f and Fig.3.6f and Fig. 3.8f at depths between 150 and 600 m suggests that nitrate and phosphate in the western subregions are variable. These subregions show higher content in nitrate than in the Eastern subregions. Similar observation is found between below 600 m to the bottom, with less variability.

Silicate showed large boxplots (Fig. 3.8f) in the western subregions and smaller ones in the eastern subregions. Below 600 m, silicate was invariable and maintained the same values,

except in SIC and TYR subregions where values between 600-1500 m were lower than the other regions (Fig. 3.8f).

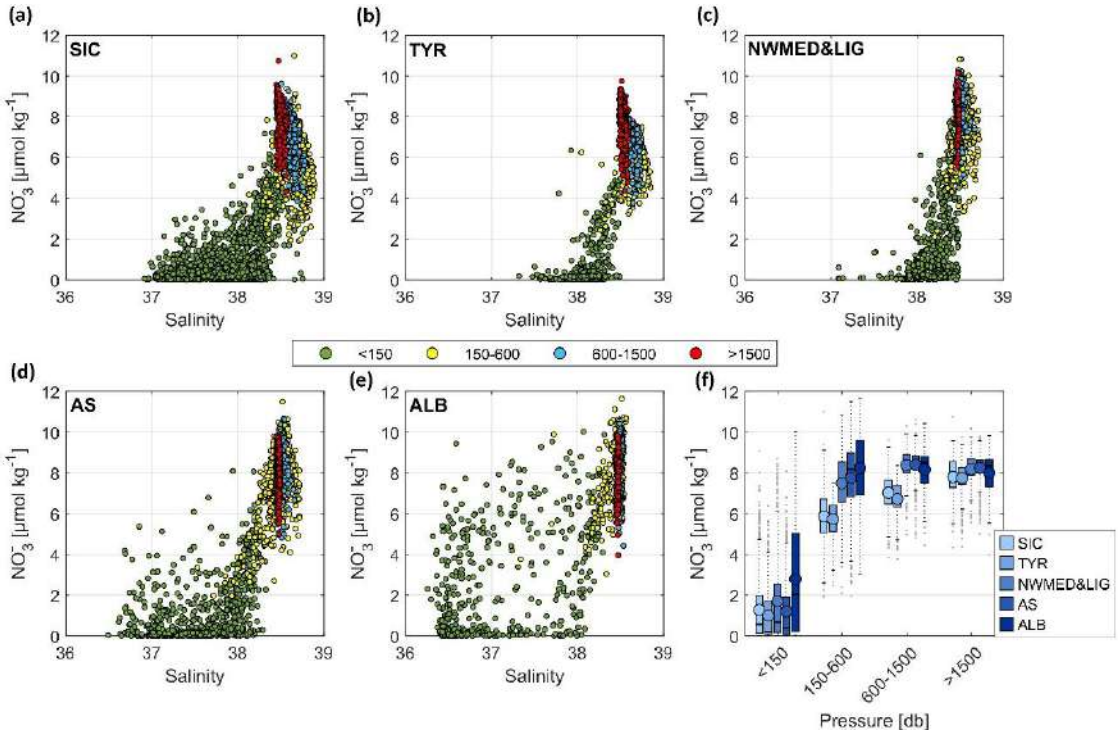

Figure 3.4: Relationships between nitrate concentration against salinity during 2004 -2017 for all observations of the WMED. (a) Sicily region, (b) Tyrrhenian Sea, (c) North WMED and Ligurian Sea, (d) Algerian Sea, (e) Alboran Sea, colors indicates depth range: green, >150 m; yellow, 150-600 m; blue, 600-1500 m and red, below 1500 m. (f) boxplots of regional trend of nitrate against pressure.

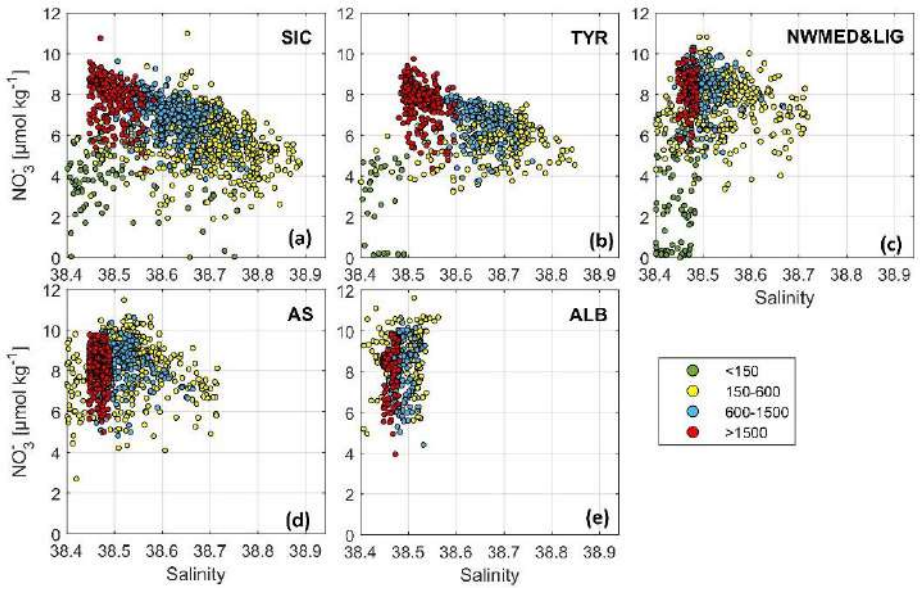

Figure 3.5: Nitrate-salinity relationship over an enlarged salinity scale between 38.4 and 38.9. (a) Sicily region, (b) Tyrrhenian Sea, (c) North WMED and Ligurian Sea, (d) Algerian Sea, (e) Alboran Sea.

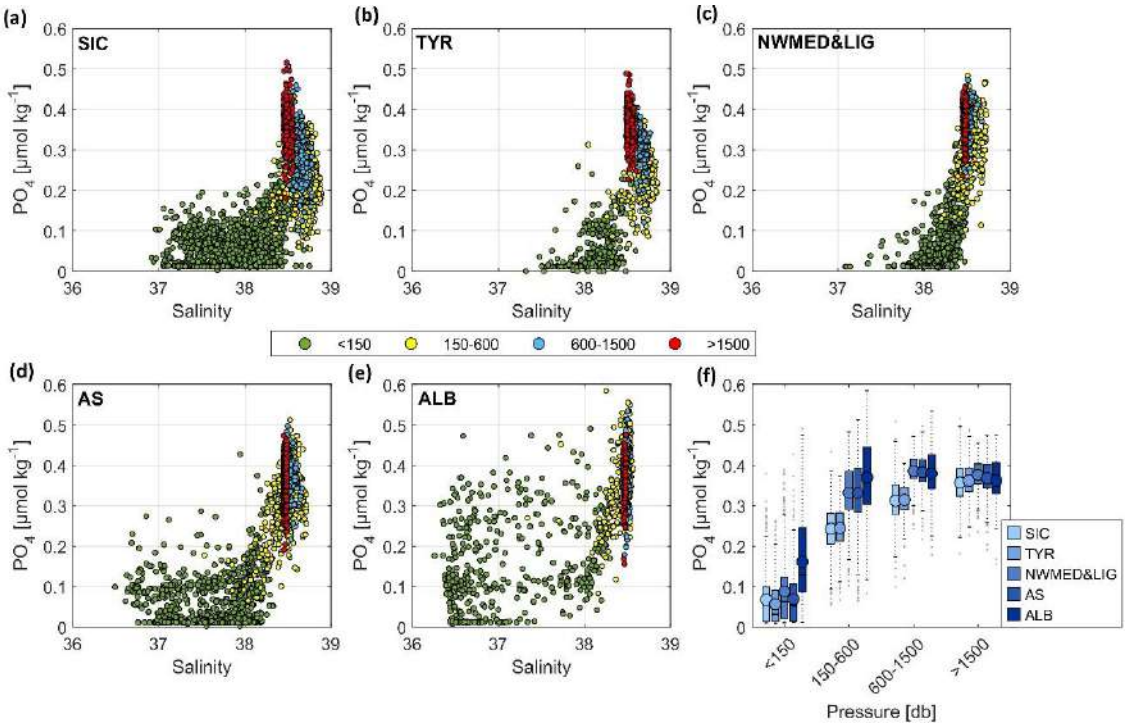

Figure 3.6: The same as Fig. 3.4 but for phosphate.

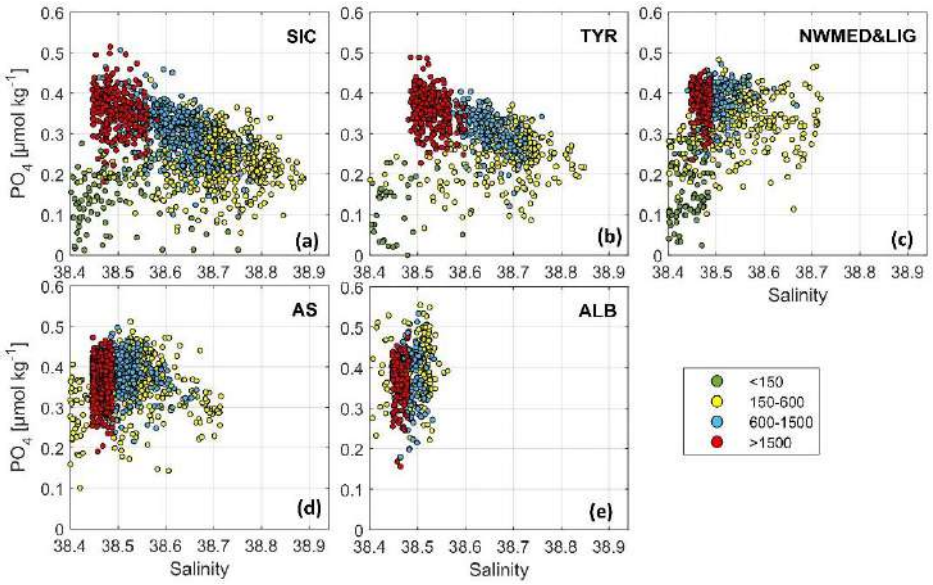

Figure 3.7: The same as Fig. 3.5 but for phosphate.

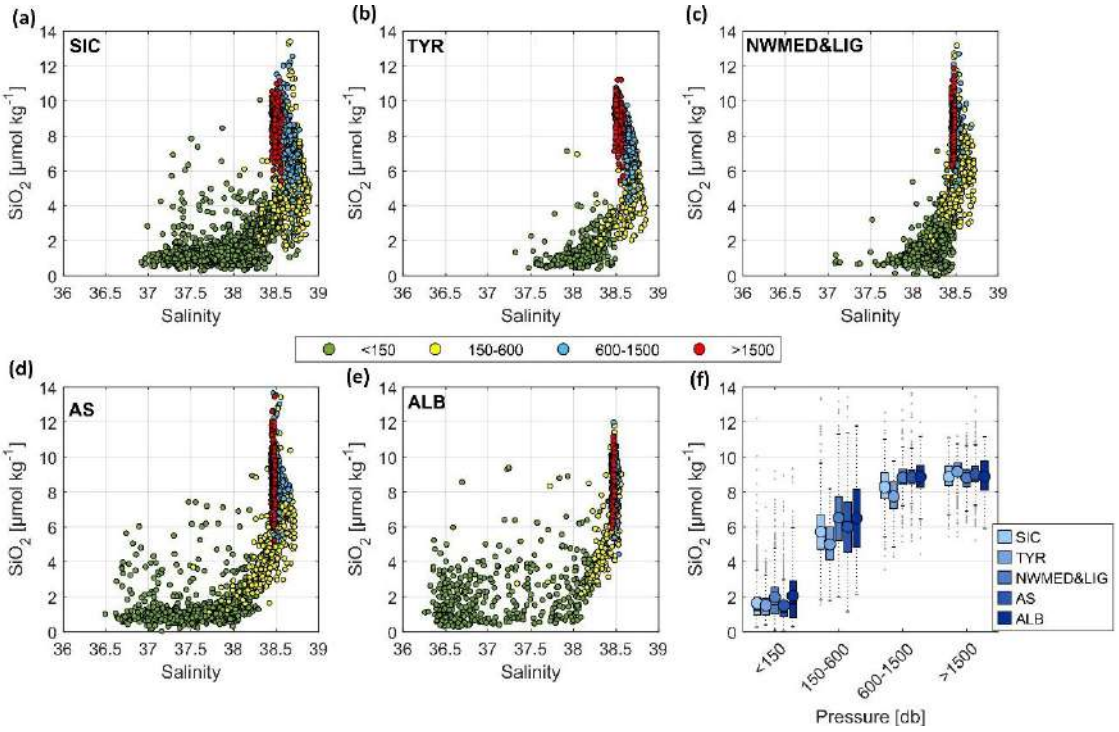

Figure 3.8: The same as Fig. 3.4 but for silicate.

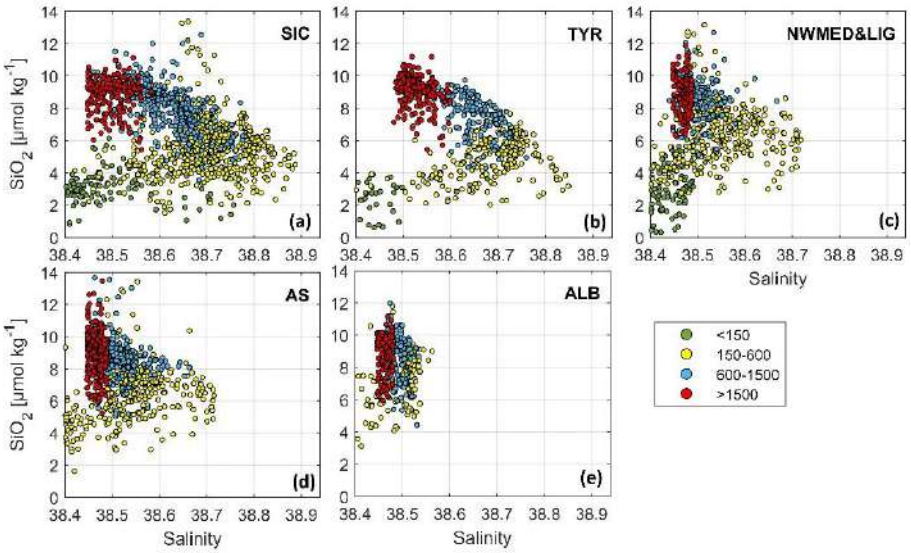

Figure 3.9: The same as Fig. 3.5 but for silicate.

3.4.3 Variability of nutrients ratios

To show regional changes in remineralization ratio clearly and to trace the impact of remineralization process on the distribution of nutrients, we show property-property relationships in Figure 3.10 for five regions, with the linear fit between elements, median ratios over the water column are calculated as well as by depth range (Figure 3.10g). I used a simple approach to compare ratios to the reference threshold value of the world's ocean in order to investigate this deviation and understand the ecosystem dynamics.

3.4.3.1 N:P ratio

Regional N:P ratios is shown in Table 3.2 and Figure 3.10. Ratio was computed as the slope of the regression relationship between the two elements and as the median values along the water column.

The two techniques are complementary as stated by Ribera d'Alcalà (2003). If both ratios are equal then there is balance between the N and P and the regression line passes through the origin, this is the case of the N:P=16:1, Redfield ideal ratio (as shown by the red line in Fig.3.10).

Though, here we observe linear relationship with r^2 >0.87 (in all subregions) and negative (case of SIC, -0.01 μmol kg^{-1} ; NWME & LIG, -0.17 μmol kg^{-1}; AS, -0.09 μmol kg^{-1} and ALB, -0.56 μmol kg^{-1}) and positive intercept (case of TYR regions, 0.19 μmol kg^{-1}). The positive intercept means an excess and the negative intercept reveals a shortage or a lack of an element relative to the other.

Values of slopes showed high values of ratio in all regions (In SIC, 22.33; TYR, 20.84; NWMED & LIG, 22.25; AS 22.39; ALB, 22.74), though, we notice a difference between the ratio computed using the linear regression and the median ratio (Fig.3.10g).

According to Pujo-Pay et al. (2011), the ratios are unequal because of the intercept that is different from zero. Intercept values were negative in all subregions except TYR, meaning that in this subregion there is a preferential utilization of nitrate compared to phosphate. The negative intercepts found in the other regions reveal a preferential utilization of phosphate compared to nitrate.

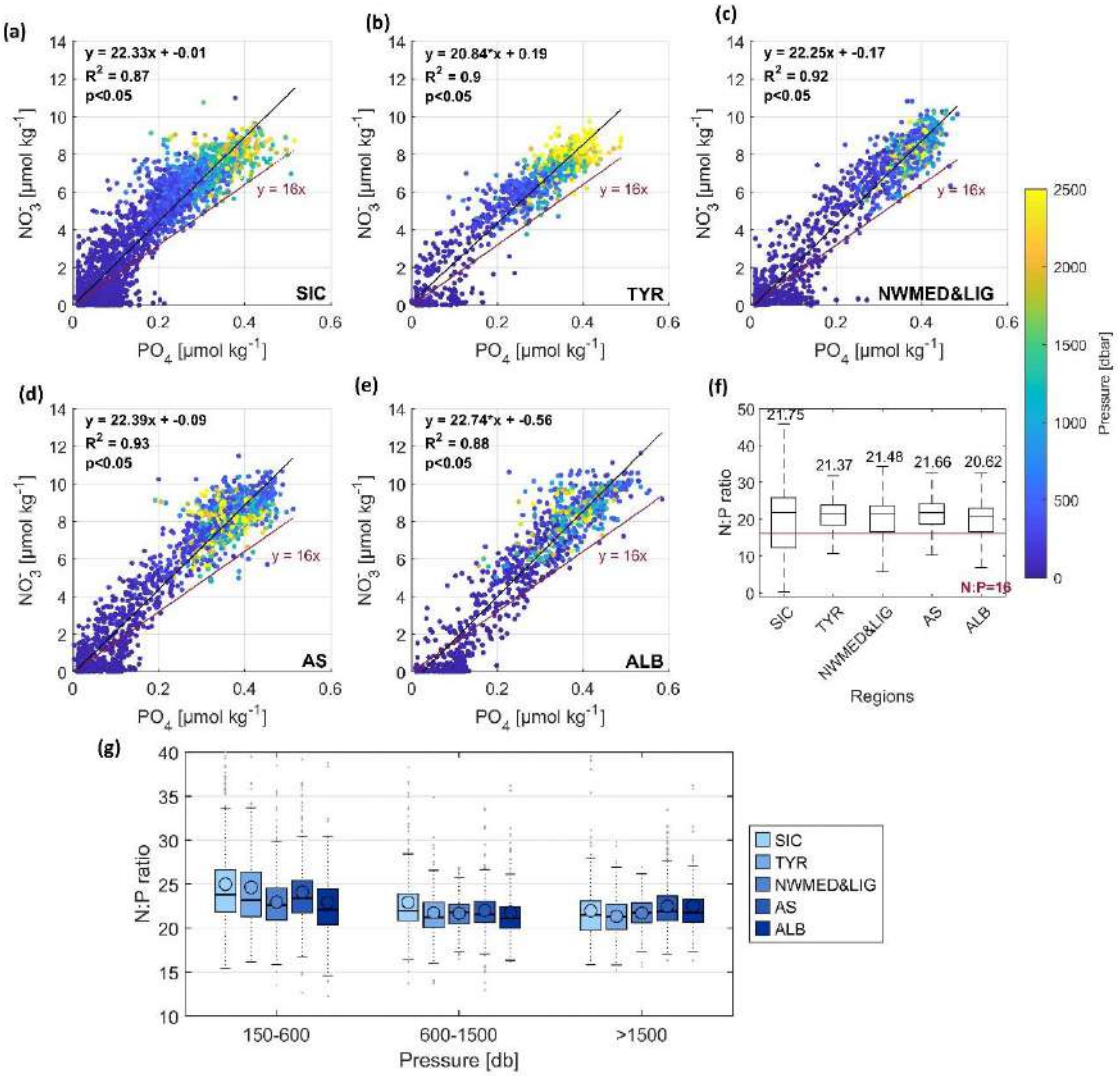

Figure 3.10: Relationship between nitrate and phosphate concentrations (μmol kg^{-1}) in five subregions of the WMED, with pressure colour-coded (dbar); (a) Sicily region, (b) Tyrrhenian Sea, (c) North WMED and Ligurian Sea, (d) Algerian Sea, (e) Alboran Sea, (f) boxplots of median N:P ratio against regions; As point of reference, the red line is the typical oceanic Redfield molar ratio of N :P =16; black line is region regressed ratio. (g) boxplots of regional trends of N:P against pressure with median ratio.

Fig.3.10g and Table 3.2 show the distribution of N:P ratio within various depth/pressure layers. It is evident that N:P ratio varies with depth.

Table 3.2: Molar ratios in different layers and in different subregions of the WMED. Ratio is shown as median ± median absolute deviation.

Ratio/Sub-region	Sicily Channel (SIC)	Tyrrhenian Sea (TYR)	NWMED & Ligurian Sea (NWMED & LIG)	Algerian Sea (AS)	Alboran Sea (ALB)
N:P	21.75±10.4*	21.37±7.3	21.48±7.7	21.66±6.7	20.62±6.2
<150	13.51 ±16.6	8.64±16.6	13.5±14.3	9.63±12.6	15.70±8.86
150-600	23.82±3.7	23.2±3.89	22.60±2.6	23.3±2.70	22.10±2.9
600-1500	21.96±2.7	21.21±2.16	21.79±1.46	21.58±1.80	21.10±2.19
>1500	21.49±2.5	21.33±1.72	21.73±1.33	21.94±1.90	21.7±2.24
Si: N	1..15±6.4	1.16±5.8	1.05±3.7	1.06±5.7	1.0±4.0
<150	2.54± 10.4	4.39±13.14	2.00±6.75	2.87±12.16	0.92±7.73
150-600	0.97±0.12	0.87±0.10	0.86±0.11	0.76± 0.12	0.78± 0.13
600-1500	1.16±0.08	1.15±0.06	1.04±0.05	1.05±0.05	1.07±0.06
>1500	1.13±0.06	1.18±0.04	1.07±0.05	1.08±0.05	1.11±0.05
AOU: N	9.49±72.3	9.18±55.6	7.16±25.6	7.78±46.09	8.72±45.2
<150	6.79±125.45	9.71 ±28.89	9.51±50.76	9.92±115.21	10.44±92.51
150-600	10.77±2.03	9.49±1.453	9.37± 1.55	9.09±1.42	9.18±1.11
600-1500	9.38±1.52	9.56±1.22	6.94±1.24	7.94± 1.05	8.64±0.99
>1500	7.35±1.46	8.01±1.08	5.63±1.141	6.68±1.05	7.83±0.94
AOU:P	214.11±281.9	198.26±203.4	150.82±179.07	170.33±201.6	182.83±121.8
<150	95.34±436.1	42.47±474.7	97.56± 339.9	60.45± 425.0	131.20± 205
150-600	265.36±54.5	247.52±52.1	189.06± 36.5	212.70±41.8	212.92±28.8
600-1500	214.10± 42.0	207.00±30.9	152.00± 23.1	174.70±25.61	184.30±24.4
>1500	165.31±33.59	171.59±23.93	124.04±20.72	150.86±28.39	169.91±21.19
AOU: Si	8.41±7.6	7.86±6.2	6.76±7.2	7.31±6.5	8.94±7.05
<150	3.24±10.7	0.89±11.4	3.49±12.8	1.80±12.5	10.00± 12.4
150-600	11.4±2.5	12.3±2.5	10.11±2.4	12.08±2.9	12.50±2.6
600-1500	7.85±1.2	8.2±1.2	6.60±1.2	7.50±1.03	7.80± 0.9
>1500	6.54±1.0	6.81±0.8	5.23±1.05	6.15±1.0	6.97±0.77

*Median ratio for the whole depth

Median ratios in the surface layer (< 150m) are low in all subregions. The lowest ratio is found in TYR (8.64) while the highest in ALB (15.7). Ratio in the Alboran Sea, seems to be the closest value to Redfield ratio as already reported in previous work (García-Martínez et al., 2019). In this region (Fig.3.10e), the surface water seems to be nitrate limited while in the other regions, there is a shift to phosphate limitation.

Study of Lazzari et al. (2016) reported this character of phosphate limitation in the entire basin with the exception of the Alboran Sea.

In fact, the variability of the ratio in the surface layer is dependent on seasons and the loads of nutrients from external sources .

Between 150 m and 600 m, the ratio is always higher than the Redfieldian ratio 16. The intermediate layer shows the highest ratio of the water column. Yet, there is a slight difference between regions where the lowest ratio is noted in ALB (22.1) and the highest in SIC (23.82) which is explained by the influence of the EMED waters.

Below 600 m, N:P ratio did not vary, values were between 21.10 and 21.96 with similar values in all regions. These values are usually found in the WMED in deep and intermediate layers (Pujo-Pay et al., 2011; Ribera d'Alcalà, 2003).

The observed nitrate to phosphate ratio on all subregions was higher than the expected Redfield ratio. The deviation from the reference is the intense phosphate utilization within the microbial loop by bacteria, and the only source of phosphate is external meaning that phosphate deficiency in the water column is due to the short supply and the unbalanced loads inducing phosphate shortage.

3.4.3.2 Si:N ratio

This section focuses on silicate to nitrate ratio, targeting the regional difference , in order, to assess the utilization of silicate and nitrate at the intermediate and deep layers..

To quantify regional differences, median values, and the slope of silicate with nitrate and intercepts was computed assuming the linear relationship between the two elements. Figure 3.11 summarizes the relationship between silicate and nitrate concentrations. In all regions, the r^2 for the regression is higher than 0.8.

We examined the values of slopes. They showed the silicate consumption to that of nitrate in SIC, TYR and AP subregions (0.97, 1.04 and 0.91, respectively) where it was higher than those found in NWMED & LIG and ALB subregions (0.89, in both). Similar differences were also noted when ratio is computed as the median values (Fig.3.11g).

Slopes, from the regression model used to estimate ratios, are in accordance with Ribera d'Alcalà (2003) who found an Si:N less than 1 in the WMED, but they were not when computing ratio as median values.

The intercepts show significant differences between subregions. The highest intercept is noted in the NWMED& LIG (0.6 μmol kg^{-1}) and the lowest in the ALB (0.15 μmol kg^{-1}). In all subregions, silicate seemed to be in excess compared to nitrate. The intercept is positive, indicating a preferential utilization of nitrate compared to silicate.

Silicate increases with depth, while nitrate tends to be constant when it reaches 6 μmol kg^{-1} in all regions. The gradual increase of silicate is explained by the slow dissolution in silicate (Williams and Follows, 2003).

The low concentrations of nitrate and silicate in the surface layer reflects the result of the consumption of nutrients by phytoplankton.

In all subregions, Si:N ratios were slightly higher than the Redfield ratio Si: N= 15: 16 (0.94), except for ALB (Fig.3.11e) where the regression slope was slightly lower (0.89).

The scatterplots show that the relationship between the two elements is significant, but there is a slight deviation from linearity (Fig.3.11), because silicate continues to increase with depth while nitrate remains constant at greater depths.

In the surface layer (Table 3.2), the ratio Si: N concentrations above 150 in TYR was about 4.39±13.14 and lower values in ALB about 0.92±7.73. The high Si: N values indicate the higher silicate consumption compared to nitrate in the Tyrrhenian Sea surface compared to other regions.

Below 150 m, the ratio tends to increase in all regions (Fig. 3.11g, Table 3.2). At intermediate levels (150-600 m), the ratio decreases from East to West . From 0.97±0.12 to 0.87±0.10 in SCI and TYR regions to 0.86±0.11, 0.76± 0.12 and 0.78± 0.134 in NWMED & LIG, AP and ALB, respectively. This could indicate that there is a decrease in silicate consumption from East to West.

At deep layer (below 600m), Si:N ratio is less variable and exceeding 1 (Si:N=1.04-1.18). Béthoux et al. (2002) related the increased Si:N ratio to the dominance of diatoms. Indeed, diatoms contribute to the organic carbon export due to their siliceous cell composition and rapid mass sinking (Rigual-Hernández et al., 2013).

We found a clear difference between Si:N of Eastern region (SIC ,TYR) and most western regions (NWMED& LIG, AP, ALB) (Fig. 3.11g).

There is a decrease of Si:N from east to west at the different depth layers. According to Ribera d'Alcalà (2003), there is an active vertical transport of silicate responsible for the high Si:N in intermediate and deep layers, adding to that the increased temperature in the intermediate layer, enhancing the dissolution of biogenic silicate increasing the sinking of silicate in deep layers.

In fact the difference in ratio between subregions at these depth levels, reside in the impact of the intermediate and deep waters coming from the EMED where Si:N can exceed 1.3 (Powley, 2017; Ribera d'Alcalà, 2003), which explain the high ratio in SCI and TYR regions.

The northernmost region hydrodynamic is influenced by the atmospheric conditions of the area (cold and dry winters) and Rhone river discharge that occur mainly during spring and autumn (Ulses et al., 2008).

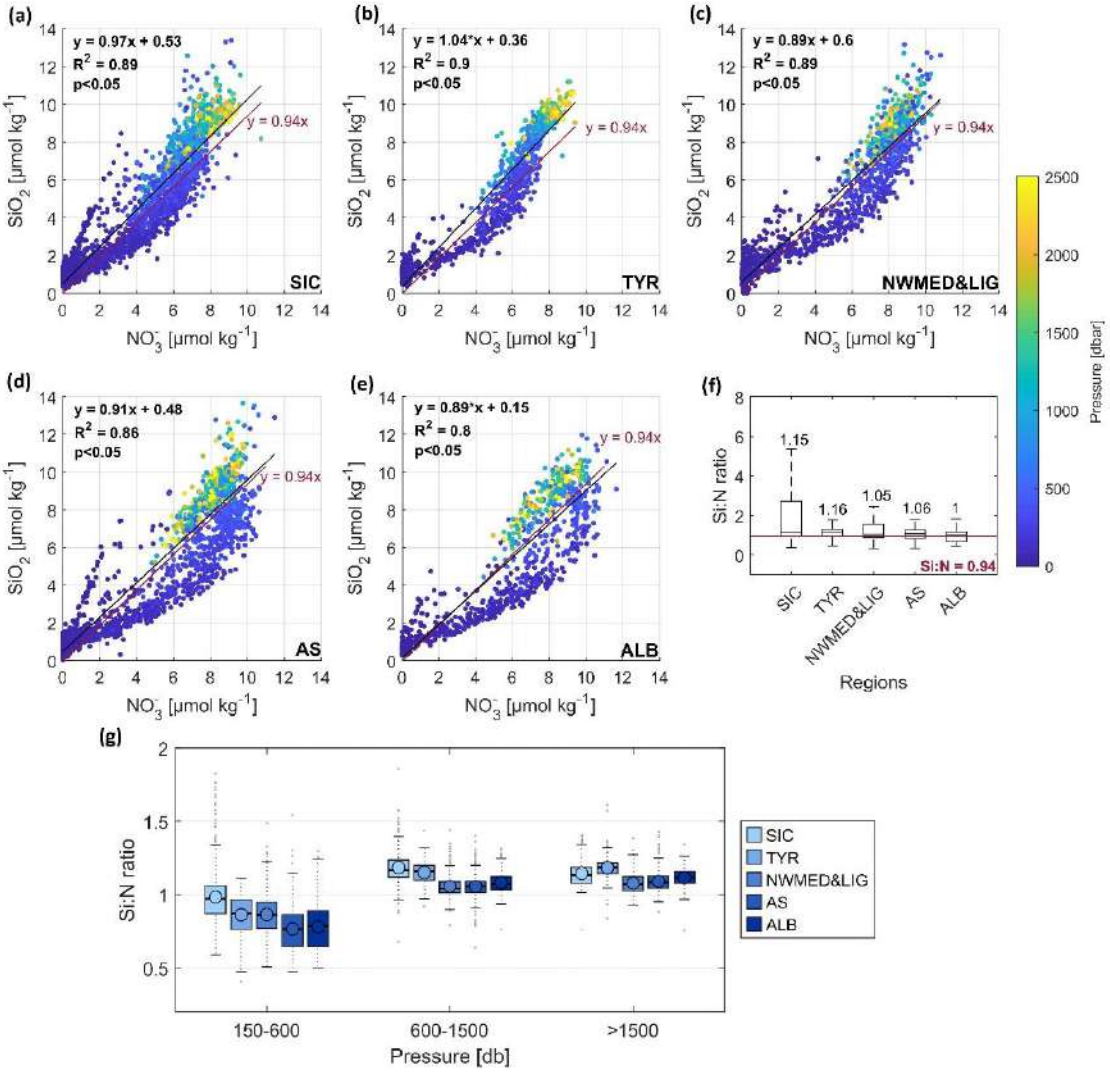

Figure 3.11: Relationship between silicate and nitrate concentrations (μmol kg^{-1}) in five subregions of the WMED , with pressure colour-coded (dbar); (a) Sicily channel, (b) Tyrrhenian Sea, (c) North WMED and Ligurian Sea, (d) Algerian Sea, (e) Alboran Sea, (f) boxplots of median Si:N ratio against regions; As point of reference, the red line is the typical oceanic Redfield molar ratio of Si:N =15:16, Redfield ratio); black line is region regressed ratio, (g) boxplots of regional trend of Si:N against pressure with median ratio.

3.4.3.3 AOU/nutrients ratios

Dissolved oxygen is a tracer for the respiration process. In the surface euphotic layer, oxygen is in excess where there is the biological production. Oxygen production by primary producers exceeds the consumption by respiration. Below the surface layer, microorganisms only consume oxygen by respiration in some areas, respiration proceeds through the use of nitrate to transform organic matter (Sarmiento and Gruber, 2006).

The Apparent Oxygen Utilization (AOU) calculated the extent of respiration process and provides an insight about remineralization in intermediate and deep waters, a process that impacts stoichiometry and nutrient regeneration. In this section, we study the AOU relation

with nutrients in the upper, intermediate and deep-water column, based on the regional difference. The AOU-nutrient scatterplots are similar to the temperature-salinity diagram. They show the mixing between water masses with contrasting nutrients and AOU/O_2. According to Alvarez-Borrego et al. (1972), changes in the water mass biogeochemical property show a linear relationship between elements and the direction of line defined by the ratio would tell about the consumption or production of dissolved oxygen and the nutrient (Nitrate, phosphate or silicate).

The difference between regions is explored based on a regression model as previously described. Scatterplots show the distribution of AOU against nitrate, phosphate, and silicate (Fig.3.12, 3.13, 3.14, respectively).

The regression slope of AOU:N in the different regions are 9.76 (r^2=0.8), 9.07(r^2=0.81), 7.58 (r^2=0.73), 8.08 (r^2=0.79), 8.86 (r^2=0.84), in SIC, TYR, NWMED & Ligurian Sea, AS and ALB regions, respectively. The relationship between AOU and nitrate is not perfectly linear in all regions, plots show curvature when nitrate concentrations exceed 6 μmol kg^{-1}.

In ALB, AOU:N relationship is linear and very close to the Redfield ratio AOU:N= 9. In the surface layer, AOU:N ratios are highly variable and vary between 6.79 and 10.44. The highest values were found in ALB and the lowest values in the Sicily region. Here, we identify this contrast again between the East and the West.

In all subregions, AOU increases with the increase in nitrate. In SIC and TYR subregions and referring to Figure 3.12g, below 1500 m, nitrate decreases with a decline in the AOU (increased O_2). An old deep-water mass is characterized by a high oxygen value, which explains the decline in AOU. In these regions, the low nitrate values are a result of the depleted surface responsible for the decreased sinking of organic matter.

In the other regions (NWMED & LIG, AS, ALB), nitrate continues to increase with the AOU (decrease in O_2). These regions are highly affected by the deep-water formation which explain the higher AOU. Contrary to N:P and Si:N ratios, Figure 3.12g shows a decrease in AOU:N with depth along with a decrease from the East to West.

Generally, positive values of AOU indicate that the effect of respiration at intermediate levels, during which oxygen consumption exceeds its production.

The largest values of AOU:N are noted in the easternmost subregions (SIC and TYR; 150-600 m, 10.77± 2.03; 9.49 ± 1.45; 600-1500 m, 9.38 ± 1.52, 9.56±1.22; below 1500 m, 7.35±1. 46, 8.01±1.08, respectively). This is due to the important increase of AOU at intermediate levels that was also mentioned by Schroeder et al. (2020). These subregions hold an increased level of AOU as a result of the IW inflow.

The AOU is related to the regeneration of nutrients, the scatter plots show that AOU increase with nitrate increase, the maximum is reached at intermediate levels when AOU > 50 μmol kg^{-1} in SIC (Fig.3.12a), and TYR (Fig.3.12b), and AOU> 75 μmol kg^{-1} in the NWMED & LIG

(Fig.3.12c), AS (Fig.3.12d), and ALB (Fig.3.12e), . In these subregions, the AOU:N is lower than 10 below 150 m (Fig. 3.12g), AOU:N values are the highest between 150- 600 m indicating a strong undersaturation, though the difference with layers below 600 m is small.

Scatter plots of Fig.3.13 show the slope of the regression giving the relationship AOU:P in the different subregions with a correlation coefficient between $0.66<r^2<0.74$. Phosphate continues to increase even after the depth level at which it normally has been completely remineralized as already reported in a study of Segura-Noguera et al. (2016) at intermediate depth.

Figure 3.13g show box-plots of regional trend of AOU:P against pressure, that agreed with AOU:N. The ratio was high at intermediate levels (150-600 m) and constant below 600 m (Table 3.2).The difference between regions at different depth levels is persistent also with phosphate.

There is a decreasing trend toward the westernmost subregions (larger ratio in SIC and TYR, lower ratio in NWMED & LIG, AP and ALB), because SIC and TYR waters are nutrient depleted compared to NWMED & LIG, AP and ALB subregions, consequently a lower remineralization rate at greater depths.

Figure 3.14 shows the relationship between AOU and silicate. The two elements show nonlinearity in all subregions with correlation coefficient of $0.55<r^2<0.65$, and a more exponential curve. Here, the analysis is based on median values rather than values of slope from the regression.

The AOU:Si ratio in all subregions was higher than the Redfield ratio AOU:Si =6. The largest median ratio along the water column is found in SIC (8.41, Fig.3.14f) and ALB (8.94, Fig.3.14f). It could be due the abundant presence of diatoms in these two regions.

Figure 3.14g shows boxplots of regional trend of AOU:Si against pressure. The behavior of AOU:Si was the opposite of AOU:N and AOU:P. The ratio decreases with depth.

Large AOU:Si (between 10.11±2.4 and 12.5±2.6) are found at the intermediate depths where the regional difference was not pronounced because IW holds less silicate than the deep waters. Below 600 m, the AOU:Si ratio was lower and varied between 5.23±1.05 and 12.5±2.6.

Comparing the ratio of AOU with nitrate, phosphate and silicate, the AOU:Si relationships, in all subregions there was non-linearity and the distribution show curvature, because silicate continued to increase at greater depths , where nitrate and phosphate content have been reduced through remineralization, this was previously noted by Segura-Noguera et al. (2016).

The non-linearity of AOU:Si and the variability at different depth levels could be related to the different remineralization rate between nutrients.

Overall, the ratio with the AOU *vs.* nutrient in the WMED deviates from the Redfield ratio. The ratio of AOU *vs.* phosphate and Silicate was higher than the respective reference ratio. As for AOU *vs.* nitrate, values varied between subregions.

The results here do not exclude the mixing component. When mixing and oxidation occur at the same time, a linear and non-linear relationship is expected between elements. Here also we did not remove the air-sea interaction. The plots show the two effects of mixing and oxidation which explain the curvature nature of the distribution of points at some parts.

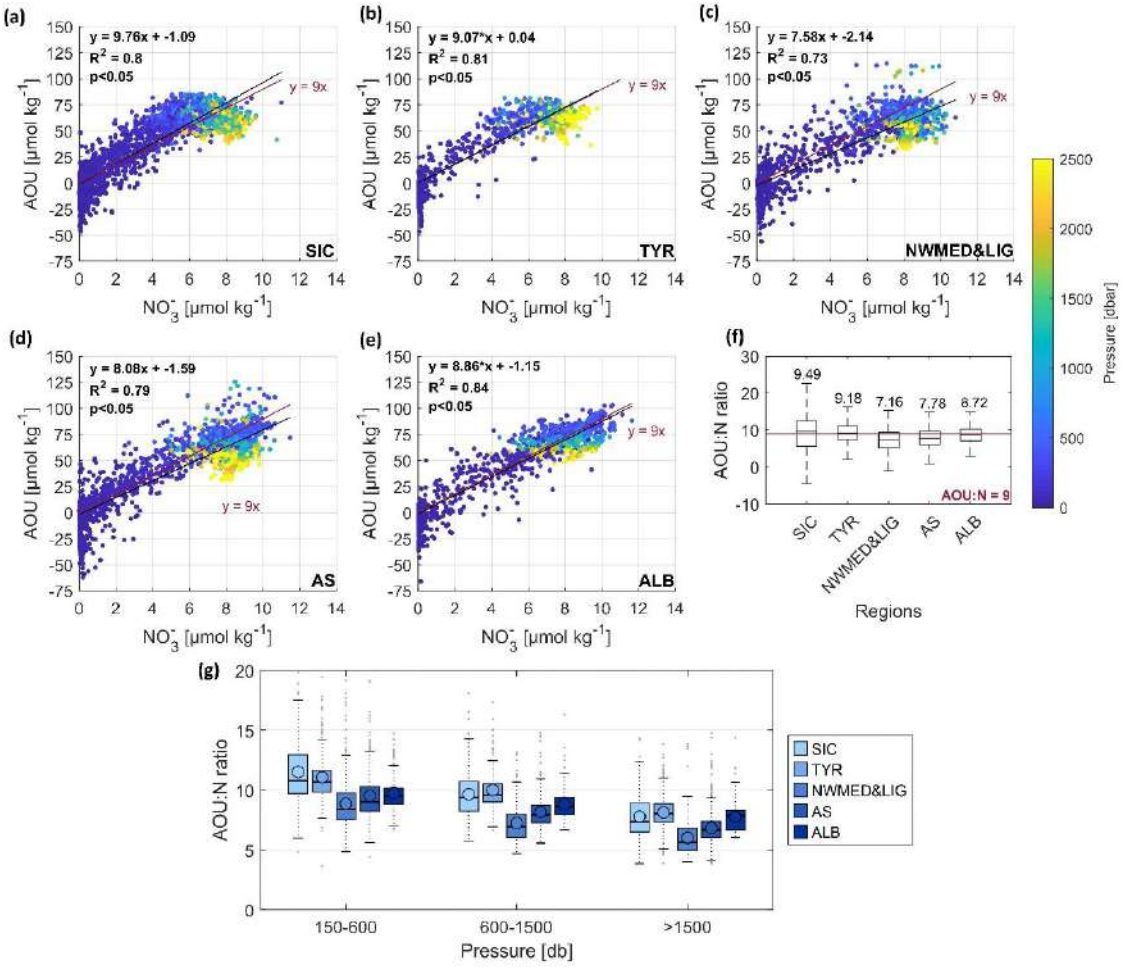

Figure 3.12: Relationship between AOU and nitrate concentrations (μmol kg^{-1}) in five subregions of the WMED, with pressure colour-coded (dbar); (a) Sicily channel, (b) Tyrrhenian Sea, (c) North WMED and Ligurian Sea, (d) Algerian Sea, (e) Alboran Sea, (f) boxplots of median AOU:N ratio against regions; As point of reference, the red line is the typical oceanic Redfield molar ratio of AOU:N = 138:16 (y = 9x); black line is region regressed ratio. (g) boxplots of regional trends of AOU:N against pressure with median ratio.

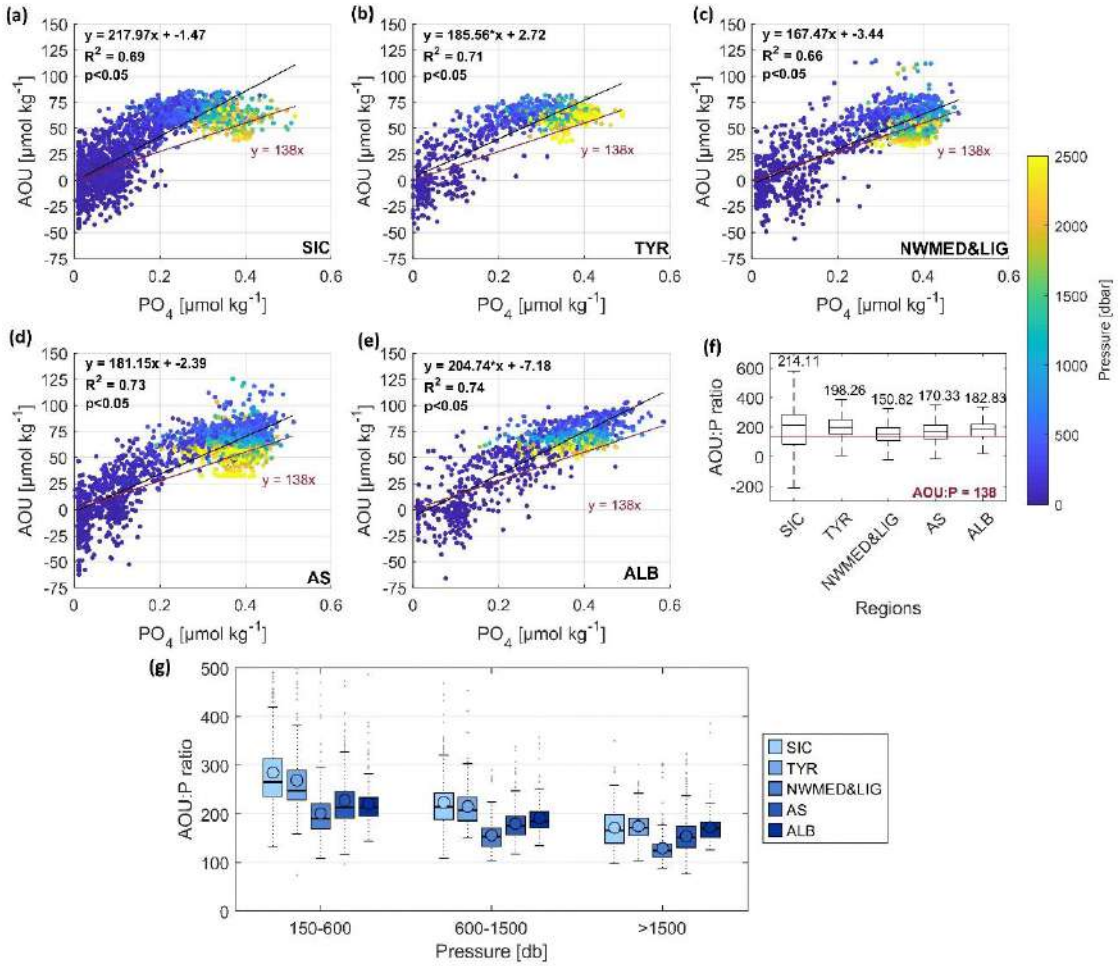

Figure 3.13: Relationship between AOU and phosphate concentrations (μmol kg^{-1}) in five subregions of the WMED, with pressure colour-coded (dbar); (a) Sicily channel, (b) Tyrrhenian Sea, (c) North WMED and Ligurian Sea, (d) Algerian Sea basin, (e) Alboran Sea, (f) boxplots of median AOU:P ratio against regions; As point of reference, the red line is the typical oceanic Redfield molar ratio of AOU:P = 138:1 (y = 138x) black line is region regressed ratio, (g) boxplots of regional trends of AOU:P against pressure with median ratio.

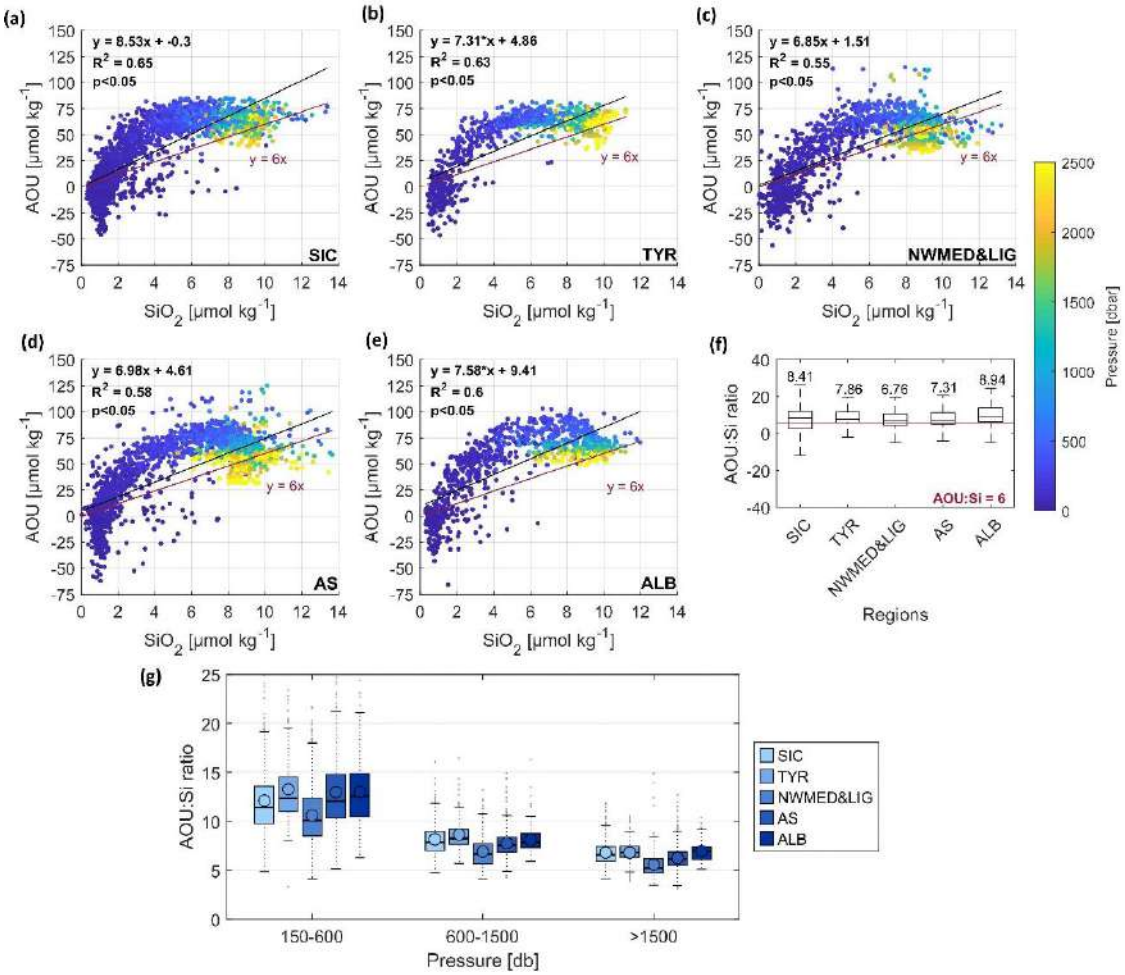

Figure 3.14: Relationship between AOU and silicate concentrations (μmol kg^{-1}) in five subregions of the WMED, with pressure colour-coded (dbar); (a) Sicily channel, (b) Tyrrhenian Sea, (c) North WMED and Ligurian Sea, (d) Algerian Sea, (e) Alboran Sea, (f) boxplots of median AOU:Si ratio against regions; As point of reference, the red line is the typical oceanic Redfield molar ratio of AOU: Si (y = 6x); black line is region regressed ratio. (g) boxplots of regional trends of AOU:Si against pressure with median ratio.

3.5 Discussion and Conclusions

This chapter provides an examination of nitrate, phosphate, silicate and AOU distribution and stoichiometry in the water column along subregions of the WMED during the period 2004-2017, as well as their relationships with salinity. It is worth to mention that the ratios discussed here contain the physical mixing that could contribute to the total variability.

By applying the median ratio and linear equations as described in section 3.3, the ratios N:P, Si:N, AOU:N, AOU:P and AOU:Si gave an extensive picture of the stoichiometry inside the five subregions of the WMED. Here, we give an appropriate estimate of the ratios by subregion and give evidence that the use of the N:P = 16 is not an applicable assumption to define biogeochemistry in the WMED.

The N:P ratio varied between 20.84 and 22.74, the ratio all over the basin is higher than the Redfield ratio. As for Si:N, the ratio varied between 0.89 and 1.04, for the majority of the subregions ,data points were also above the Redfield ratio Si:N = 0.94 except the Alboran Sea that was below.

The maximum nutrients are found in the layer between 600-1500 m (Tab.3.1) in most of the subregions, a feature that was noted also by Moutin and Raimbault (2002), and that was associated to the microbial respiration and its role in the remineralization of organic matter. Since the latter sinks from the upper layer down to deeper layers (Sarmiento and Gruber, 2006).
The accumulation of sinking organic matter at different depth levels has led to the accumulation of inorganic nutrients and to the enrichment of deep layers. This accumulation varies from one region to the other, depending on the sinking rate and the surface layer primary production levels, as well as on local events such as the atmospheric and terrestrial input, inflow of depleted waters from the EMED and deep water convection.

The general averages and ratios can be used as reference values for the biogeochemical studies in the WMED. Redfield values are useful to understand processes that regulate the general biogeochemistry and report tracers that limit primary productivity.

We highlighted the vertical difference and the regional comparison of the biogeochemical variables. We show the anomalous ratio and describe surface, intermediate and deep stoichiometry. The N:P ratio is typically used to identify which of the nutrient elements is limiting.

The deviation of $N:P$ from the Redfield ratio (N:P=16) is used to differentiate between N-limitation ($N:P<16$) and P-limitation ($N:P>16$). In all regions, the median ratio is higher, imposing P-limiting character. However, this ratio varied with depths due to the changes in the dissolved oxygen levels (Paulmier and Ruiz-Pino, 2009).

Various studies has been conducted to explain the high N:P , they associated it to the atmospheric and terrestrial input, the unbalanced river discharge, the increased nitrogen fixation or also to the Saharan dust (responsible for phosphate absorption) (Krom et al., 1991; Ribera d'Alcalà, 2003).

Our data show that above 150 m, N:P ratio is below the reference ratio in all regions and approaches the ratio in the Alboran Sea (Table 3.2), suggesting that Nitrate is the limiting element in the surface layer. Some studies have shown phosphate is limiting phytoplankton growth in the surface layer (Moutin and Raimbault, 2002).

Comparisons of the ratio in the intermediate layer (150-600 m) with the deep layer (below 600 m) and between subregions revealed significant differences. . A relatively high N:P ratio is observed at the intermediate layer in all subregions, while deep layers show constant value. Yet, there is disparity between regions, there is a clear decrease from east to west at the different depths.

In general, nutrients are higher towards the west and are attributed to physical forcing i.e. local currents, deep water convection and elevation of the thermocline to shallower depths.
At 150-600 m, we find phosphate deficits with high N :P ratio, indicating the advection of phosphate-depleted intermediate waters.
Overall, the N:P ratio in the intermediate and deep layer exceeded 20, which was explained by the remineralization of organic matter.

As for AOU *vs.* nutrients, the ratios show a decreasing trend toward deeper layers. High ratios are found at the intermediate layer (Table 3.2). Regionally, AOU:N and AOU:P affirmed large values in the Easternmost regions (the Sicily region and Tyrrhenian Sea) relative to the other subregions. This is due to the lower nitrate and phosphate concentrations at the intermediate and deep water in this part of the WMED, since it is the most affected by the EMED ultra-oligotrophy.

AOU:Si decrease also with depth, higher ratio is also noted at the intermediate layer and did not show regional difference at the selected depth ranges, except in the NWMED & LIG region where the ratio was the lowest, waters of the NWMED & Ligurian Sea seem to be enriched in silicate.

In all subregions, Si:N ratio was generally higher than the estimated Redfield ratio for diatoms of 15:16 (Redfield et al., 1963) except for the Alboran Sea where the ratio was lower (0.89).

Si:N increased with depth below 150 m, and low ratio is noticed at the intermediate layer in all subregions due to the low nitrate concentrations relative to silicate. The Sicily region and Tyrrhenian Sea showed the highest ratio also at different depth ranges. There is an active vertical transport of silicate responsible for the high Si:N at intermediate and deep layers, adding to that the warming of the intermediate layer (Schroeder et al., 2017), in conditions of relatively increased temperature, the dissolution of biogenic silicate is activated consequently increasing the input of silicate in deep layers.

In fact the difference in ratio between regions at these depths reside in the influence of the intermediate and deep waters coming from the EMED where Si:N can exceed 1.3 (Powley, 2017; Ribera d'Alcalà, 2003), which may explain the higher ratio in Sicily region and Tyrrhenian Sea.

In all regions, there is some deviation from linearity, there is one limiting element and another in excess, this is known to be the ideal situation of the WMED waters. This variability in ratios evidence that the WMED is characterized by the coexistence of different biogeochemical regimes as already been reported (D'Ortenzio and Ribera d'Alcalà, 2009; Lazzari et al., 2012; Siokou-Frangou et al., 2010).

Nutrients ratio-ratio plots (Fig. 3.15) summarizes the stoichiometry of the surface layer (Fig. 3.15a) and the deep layer (Fig.3.15b). This revealed the spatial variability in the surface layer and perturbation of the stochiometric ratio that was previously discussed in a study of Fommervault et al. (2015).

The study showed that the ratio is subjected to a seasonal variability. In the winter season, nitrate and phosphate have similar roles, while in summer and spring, ratios are high suggesting that the phytoplankton need more phosphate than nitrate. The distribution of samples is very large on the surface and in deep layers.

The difference between regions is not very well noted (Fig. 3.15), it could be because of the important number of measurements. In figure 3.16, we plot each region apart to understand the local stoichiometry.

The standard stoichiometric ratio is represented with vertical red lines, horizontal blue lines, and diagonal black line according to the formula Si:N:P= 15:16:1.

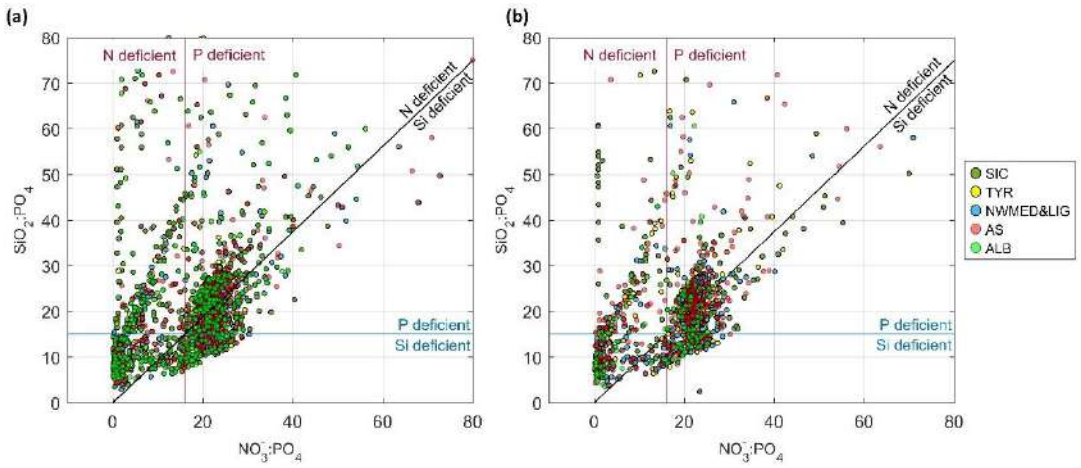

Figure 3.15: Nutrient ratio plots for(a) data above 150 db and (b) below 1500 db. The red line indicates N:P=16:1, the blue line Si:P =15:1 and the black line Si:N =15:16.

Figure 3.16 separates subregions and shows large variability of the surface layer with similar regional patterns.

It seems that the surface layer alternated between various regimes, there is a widespread phosphate deficiency relative to nitrate and also silicate. The upper layer experiences nitrate deficiency relative to silicate. There is an important stoichiometric variability in the surface highly impacted by seasons.

There are some similarities observed between the surface and deep layer ratios. The nutrient ratio: ratio plots for deep layer revealed a reduced variability of the different subregions with N: P >16:1. Compared to the surface layer, observations are clustered showing a less variability in N: P. Regions show a balanced provision of nitrate and silicate.

Similar to the surface, there is phosphate deficiency relative to silicate and a phosphate deficiency relative to nitrate.

Comparing subregions, SIC and AP seems to have the highest variability below 1500 m.

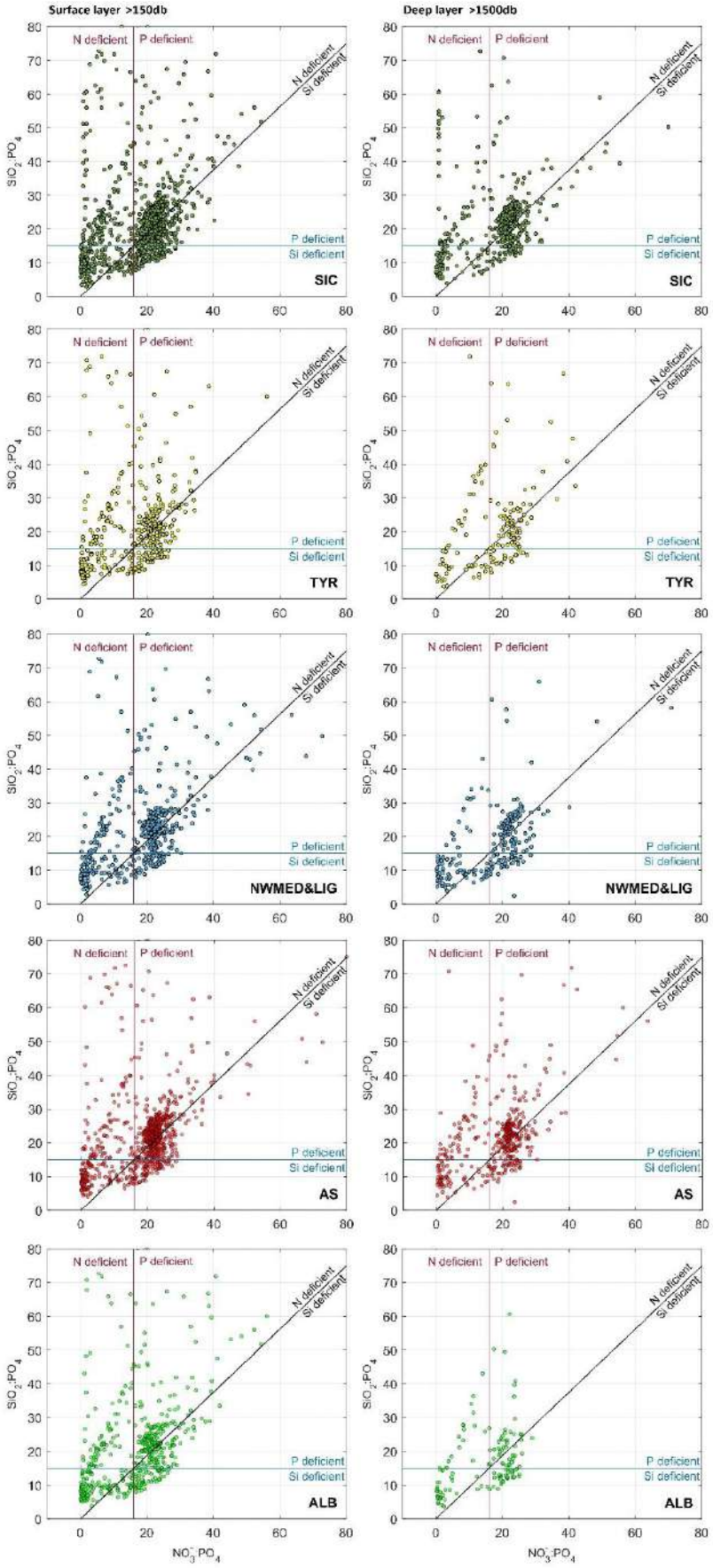

Figure 3.16: Similar as Figure 3.15 but for each region .

Chapter 4. CLIMATOLOGICAL DISTRIBUTION OF DISSOLVED INORGANIC NUTRIENTS IN THE WESTERN MEDITERRANEAN SEA (1981-2017)

The Western MEDiterranean Sea BioGeochemical Climatology (BGC-WMED) presented here is a product derived from in situ observations. Annual mean gridded nutrient fields for the period 1981-2017, and its subperiods 1981-2004 and 2005-2017, on a horizontal 1/4° × 1/4° grid have been produced.

The biogeochemical climatology is built on 19 depth levels and for the dissolved inorganic nutrients nitrate, phosphate and orthosilicate. To generate smooth and homogeneous interpolated fields, the method of the Variational Inverse Model (VIM) was applied.

A sensitivity analysis was carried out to assess the comparability of the data product with the observational data. The BGC-WMED has then been compared to other available data products, i.e. the medBFM biogeochemical reanalysis and the WOA18 (its biogeochemical part). The BGC-WMED product promotes the understanding of inorganic nutrient variability in the western Mediterranean Sea, in space and in time, but can also be used to validate numerical simulations making it a reference data product.

4.1 Introduction

At the global scale, most of the biogeochemical descriptions are based on model simulations and satellite observations (sea surface chlorophyll concentration (Salgado-Hernanz et al., 2019)) but also the increasing use of Biogeochemical Argo floats (D'Ortenzio et al., 2020; Lavigne, 2015; Testor et al., 2018), since nutrient in situ observations are generally infrequent and inhomogeneously distributed in space and time. For this reason, climatological mapping is often applied to sparse in situ data in order to understand the biogeochemical state of the ocean representing monthly, seasonally, or annually averaged fields.

Levitus (1982) was the first to generate objectively analyzed fields of potential temperature, salinity, and dissolved oxygen, and to produce a climatological atlas of the world ocean. The objective interpolation technique was later used to produce the World Ocean Atlas (WOA), the North Sea climatologies and the Global ocean Carbon Climatology resulting from GLODAP data product (Key et al., 2004). In 1994, the first World Ocean Atlas (WOA94, Conkright et al., 1994) was released integrating temperature, salinity, oxygen, phosphate, nitrate, and silicate observations. Every four years there is a renewed release of the WOA with an updated World Ocean database (WOD).

On the regional scale, the first salinity and temperature climatology of the Mediterranean Sea was produced by Hecht et al. (1988) for the Levantine Basin. Picco (1990) was also among the first to describe the climatology of WMED between 1909 and 1987. In 2002, the Medar/Medatlas group (Fichaut et al., 2003) archived a large amount of biogeochemical and hydrographic in-situ observations for the entire region and used the Variational Inverse Model (VIM) (Brasseur, 1991) to build seasonal and interannual gridded fields.

In 2006, the SeadataNet project integrated all existing data, to provide temperature and salinity regional climatology products for the Mediterranean Sea using VIM as well (Simoncelli et al., 2016), and dissolved inorganic nutrients (nitrate, phosphate and silicate) 6-years centered average from 1965 to 2017 are available on the EMODnet chemistry portal (https://www.emodnet-chemistry.eu/).

Within this context, regional climatological fields of in situ nitrate, phosphate and silicate, using the Data Interpolation Variational Analysis (DIVAnd, (Barth et al., 2014)) is presented here, providing a high-resolution field contributing to the existing products (Table 4.1).

The aim of this study is to give a synthetic view of the biogeochemical state of the WMED, evaluate the mean state of inorganic nutrients over 36 years of in-situ observations and demonstrate an observational signal of the effect of the WMT on nutrient distribution.
The chapter is organized as follows, Section 4.2 describes the data sources used and the quality check; Section 4.3 is devoted to the methodology, Section 4.4 analyses the main results, and finally, a discussion, that includes a comparison of the new climatology with other

products and studying the change in biogeochemical characteristics before and after WMT, is presented in Section 4.5.

Table 4.1: Overview of the existing inorganic nutrient climatologies in the Western Mediterranean Sea.

Climatology	**WOA**	**EMODnet**	**Present study**
Reference	(Garcia et al., 2019)	(Míguez et al., 2019)	
Year of release	2018	2018	2020
Parameter	Nitrate/ Phosphate/ Silicate	Nitrate/ Phosphate/ Silicate	Nitrate/ Phosphate/ Silicate
Vertical resolution	Seasonal: 43 levels 0-800m Annual: 102 levels 0-5500m	21 standard depth 0-1100m (Nitrate) 0-1500m (Phosphate) 0-1500m (Silicate)	19 levels 0-1500m
Horizontal resolution	1° latitude longitude grid	1/8°	1/4°
Observation time span	1955-2017	1970 to 2016 (nitrate) 1960 to 2016 (phosphate) 1965 to 2016 (silicate)	1981-2017
Area	Global	Mediterranean Sea	Western Mediterranean Sea
Temporal resolution	Season decadal	Season 6 year running averages	whole observational period, and two sub-intervals (1981-2004, 2005-2017)
Climatology analysis method/ parameter	Objective analysis	DIVA (Data-Interpolating Variational Analysis) tool	DIVAnd (Data-Interpolating Variational Analysis N dimension)
Correlation length	-	optimized and filtered vertically and a seasonally averaged profile was used.	optimized and filtered vertically and horizontally
Signal to noise ratio	-	A constant value =1	A constant value =0.5
Background field	-	the data mean value is subtracted from the data.	the data mean value is subtracted from the data
Detrending	-	No	No
Advection constraint applied	-	No	No

4.2 Data

The climatological analysis depends on the temporal and spatial distribution of the available in situ data, and the reliability of these observations. Due to the scarcity of biogeochemical observations in the WMED, merging and compiling data from different sources was necessary.

4.2.1 Data Sources

In total, 2253 in-situ inorganic nutrient profiles are the base of the biogeochemical climatology of the WMED (Table 4.2) that is described here. These profiles cover the period 1981-2017 and come from four main sources, i.e. the Medar/MEDATLAS (1981-1996, Fichaut et al., 2003), the CNR_DIN_WMED_20042017 biogeochemical dataset presented in chapter 2 (2004-2017, Belgacem et al., 2020), the SeaDataNet data product (2001-2016) and other data collected during the MedSHIP programs (Schroeder et al., 2015), GLODAPv2 and CARIMED data products. All datasets are a selection of oceanographic cruises carried out within European projects or by regional institutions. Data were chosen to ensure high spatial coverage (Fig. 4.1).

Table 4.2: Number of inorganic nutrient profiles and data sources.

Source	N. of profiles	N. of observations	Link
MEDATLAS	940	8839	https://odv.awi.de/data/ocean/medatlasii/
SEADATANET	523	15388	http://seadatanet.maris2.nl/v_rsm/content.asp?screen=0&history=yes
CNR_DIN_WMED_20042017	737	8324	https://doi.org/10.1594/PANGAEA.904172
Other cruises	53	515	MedSHIP programs; GLODAPv2; CARIMED (not yet available online, personal communication by Marta Álvarez)
∑	*2253*	*33066*	-

4.2.2 Data distribution

The distribution per year is shown in Figure 4.1a. Most observations were collected between 1981 and 1995, and between 2004 and 2017, with a marked gap between 1997 and 2003. With the WMT starting in winter 2004/05, the scientific community again started to increase the number of research cruises in the Mediterranean Sea.

Measurement distribution differs from month to month (Fig.4.1b) and tends to be biased towards the warm season. Very few measurements have been done during December-January-February, while June and July are the months with the highest number of available

observations (>7000). Consequently, the climatological product may be considered as being more representative for spring and summer conditions.

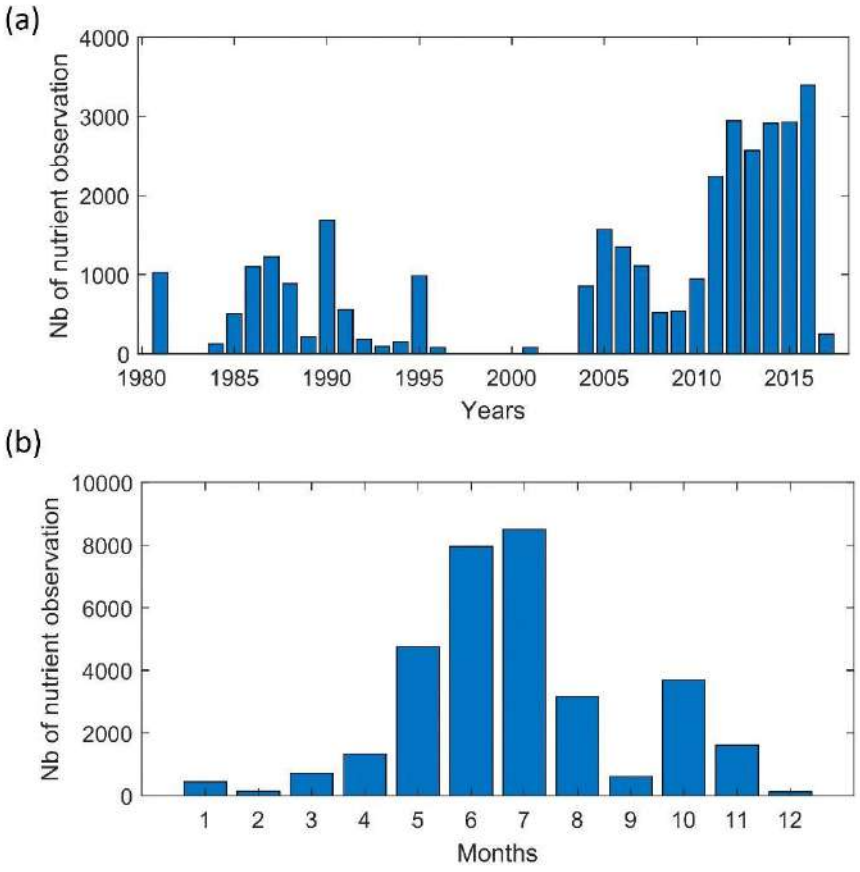

Figure 4.1: Temporal distribution of nutrient observations used for producing the BGC-WMED fields (1981-2017), (a) yearly distribution, and (b) monthly distribution.

Fig. 4.2a shows the regional distribution of nutrient measurements, while Fig. 4.3b indicates the number of observations found in each depth range around the standard levels chosen for the vertical resolution of the climatology.

Hydrological and biochemical measurements have always been repeatedly collected along several repeated transects, known as key regions as the Sicily Channel and the Algero-provençal subbasin ; likewise, the Northern WMED is a well sampled area, as it is an area of deep-water formation. Observation density is still scarce (less than 100 observations) in some areas like the northern Tyrrhenian Sea.

The total number of measurements at each depth range underlines similar remarks, an uneven distribution that needs to be considered in the selection of the vertical resolution to estimate the climatological fields.

Though, the use of 36 year of nutrient measurements to generate the climatological fields significantly reduces the error field.

In our case and taking into account the irregular distribution in seasons and different years. A climatological gridded field was computed by analyzing observations of three time periods regardless of the month: 1981-2004, 2005-2017, 1981-2017.

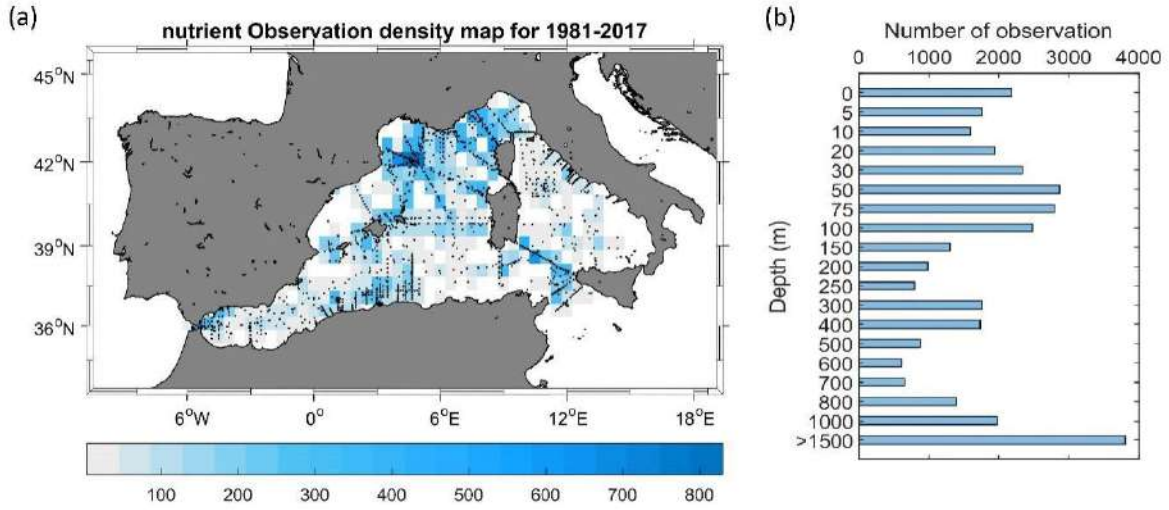

Figure 4.2: (a) Nutrient data density used for climatology analysis. Observations are binned in a regular 1/2° × 1/2° latitude, longitude grid for each year over the period 1981-2017. The total number of years with a profile are shown for all nutrients. Location of the stations included in the analysis are shown as black dots; (b) data distribution per depth range.

4.2.3 Data quality check

Data were gathered from different data sources, thus before merging them, observations were first checked for duplicate (the number of profiles listed in Table 4.2 refers to all data after removing duplicate measurements). Then, data were converted to a common format (similar to the csv CNR_DIN_WMED_20042017 data product, Belgacem et al.,2019). This recently released product contains measurements covering the WMED from 2004 to 2017. The data of the CNR_DIN_WMED_20042017 product have undergone a rigorous quality control process (described in chapter 2), that was focused on a primary quality check of the precision of the data and a secondary quality control targeting the accuracy of the data. Adjustments were applied to measurements when bias is detected.

As detailed in Table 4.2, I combined observations from reliable sources (covering the time period 1981-2017), that were quality controlled according to international recommendations before being published (Maillard et al., 2007; SeaDataNet Group, 2010). Though, these historical data collections coming from sources different from the CNR_DIN_WMED_20042017 have been subjected to a quality check before merging them, to eliminate the effect of any aberrant observation. The check was carried out by computing median absolute deviations in 19 pressure classes (referring to the selected vertical resolution of section 3.2.1) (0-10, 10-30, 30-60, 60-80, 80-160, 160-260, 260-360, 360-460, 460-560, 560-

900, 900-1200, 1200-1400, 1400-1600, 1600-1800, 1800-2000, 2000-2200, 2200-2400, 2400-2600, >2600 db). Any value that is more than three median absolute deviation from the median value is considered a suspected measurement.

In total, 2.35% of nitrate observations, 2.44% of phosphate observations and 2.14% of silicate observations were discarded.

4.3 Methods

4.3.1 Variational analysis mapping tool

Here, the data-interpolating variational analysis (DIVA) method (Beckers et al., 2014; Troupin et al., 2010, 2012) was used to generate the gridded fields. DIVA has been widely applied to oceanographic climatologies, such as the SeaDataNet climatological products (Simoncelli et al.,2014,2016; Iona et al., 2018), EMODnet chemistry regional climatologies (Míguez et al., 2019), or the Adriatic Sea climatologies by Lipizer et al. (2014) and it was also applied to generate the global interior climatology GLODAPv2.2016b (Lauvset et al., 2016). It is an efficient mapping tool used to build a continuous spatial field from discrete, scattered, irregular in-situ data points with an error estimate at each level.

The Western MEDiterranean Sea BioGeochemical Climatology (BGC-WMED) gridded fields have been computed with the more advanced N-dimensional version of DIVA, DIVAnd v2.5.1 (Barth et al., 2014) using Julia as a programming language (https://julialang.org/) under the Jupyter environment (https://jupyter.org/). The code is freely available at https://github.com/gher-ulg/DIVAnd.jl (last access: January, 2020).

DIVA is based on the variational inverse method (VIM) (Brasseur et al., 1996). It takes into account the errors associated with the measurements and takes account of the topography/bathymetry of the study area. The method is designed to estimate an approximated field φ close to the observations and find the field that minimizes the cost function $J[\varphi]$. The cost function is defined as the misfit between the original data d_i, an array of N_d observations, and analysis (observation constraint term) and a smoothness term that measures the uniformity (Troupin et al., 2010):

$$J[\varphi] = \sum_{i=1}^{Nd} \mu_i L^2 \left(d_i - \varphi(x_i, y_i)\right)^2 + \int_D \left(\alpha_2 \nabla\nabla_\varphi : \nabla\nabla_\varphi + \alpha_1 L^2 \nabla_\varphi . \nabla_\varphi + \alpha_0 L^4 \varphi^2\right) dD$$

$$(1)\ Observation\ constraint, \qquad (2)\ Smoothness\ term$$

$$\text{Eq. } (1)$$

where L is the correlation length, ∇ is he gradient operator, $\nabla\nabla_\varphi$: $\nabla\nabla_\varphi$ is the squared Laplacian of φ, D is the domain of interest, α_0 minimize the anomalies of the field itself, α_1 minimize the spatial gradients, α_2 penalizes field variability (regularization), μ_i penalizes the analysis misfits relative to the observations.

The reconstructed fields are determined at the elements of the mesh grid on each isobath using the cost function Eq. (1). The mesh grid is dependent on the correlation length and the topographic contours of the specified grid in the considered region, so there is no need to divide the region before interpolating.

The method computes two-, three- to four-multi-dimensional analyses (longitude, latitude, depth, time). For climatological studies, the four-dimensional extension was used on successive horizontal layers at different depths for the whole time period.

Along with the gridded fields, DIVA yields error fields dependent on the data coverage and the noise in the measurements (Brankart and Brasseur, 1998; Rixen et al., 2000). Full details about the approach is provided extensively by Barth et al. (2014) and Troupin et al. (2018) in the Diva User Guide.

4.3.2 Interpolation parameters

DIVAnd is conditioned by topography, by the spatial correlation length (Lc) and by the signal-to-noise ratio (SNR, λ) of the measurements, which are essential parameters to obtain meaningful results. They are considered more in detail in the following sections.

4.3.2.1 Land-sea mask

A 3D dimension land-sea mask is created using the coastline and bathymetry of the General Bathymetric Chart of the Oceans (GEBCO) 30 sec topography (Weatherall et al., 2015). The WMED is a relatively small area which necessitates a high-resolution bathymetry to generate a mask at different depth layers. The vertical resolution is set to 19 standard depth levels from the surface to 1500 m: 0, 5, 10, 20, 30, 50, 75, 100, 150, 200, 250, 300, 400, 500, 600, 700, 800, 1000, 1500 m, corresponding to the most commonly used predefined levels for the sampling of seawater for nutrient analyses. The resulting fields at each depth level are the interpolation on the specified grid. These depth surfaces are the domain on which the interpolation is performed.

4.3.2.2 The spatial correlation length scale (Lc)

Lc indicates the distance over which an observation affects its neighbors. The correlation length can be set by the user or computed using the data distribution.

For the BGC-WMED biogeochemical climatology, this parameter was optimized for the whole-time span, and at each depth layer. The correlation length has been evaluated by fitting the empirical kernel function to the correlation between data isotropy and homogeneity in correlations. The quality of the fit is dependent on the number of observations (Troupin et al., 2018). The covariance is calculated using the correlation function of the infinite domain.

To assess the quality of the fit, the data covariance and the fitted covariance are plotted against the distance between data points (Fig. 4.3). At 10 m, the correlation length was obtained with a high number of data points, indicating that the empirical covariance used to estimate the covariance and the fitted covariance are in good agreement.

At some depth layers there are irregularities due to an insufficient amount of data points, making it necessary to apply a smoothing filter/fit to minimize/remove the effect of these irregularities. It has been tested whether a randomly selected field analysis (nitrate data from 2006 and 2015) obtained with the fitted-vertical correlation profile is better than the analysis with zero-vertical correlation. A skill score relative to analysis non-fitted-vertical correlation has been computed following Murphy (1988) and Barth et al.(2014):

$$skill\ score = 1 - \frac{RMS^2_{no\ fit}}{RMS^2} \quad \text{Eq. (2)}$$

A large difference in the global RMS between the analysis with the fitted-vertical correlation and the analysis with non-fitted-vertical correlation used for validation was found. The test shows whether the use of the fit in the correlation profile is improving the overall analysis or not. We found that the RMS error was reduced from 0.696 μmol kg^{-1} (analysis without fit) to 0.571 μmol kg^{-1} (analysis with fit), which means using the fitted vertical correlation profile in the analysis improves the skill by 32 %, and the fit is improving the analysis fields.

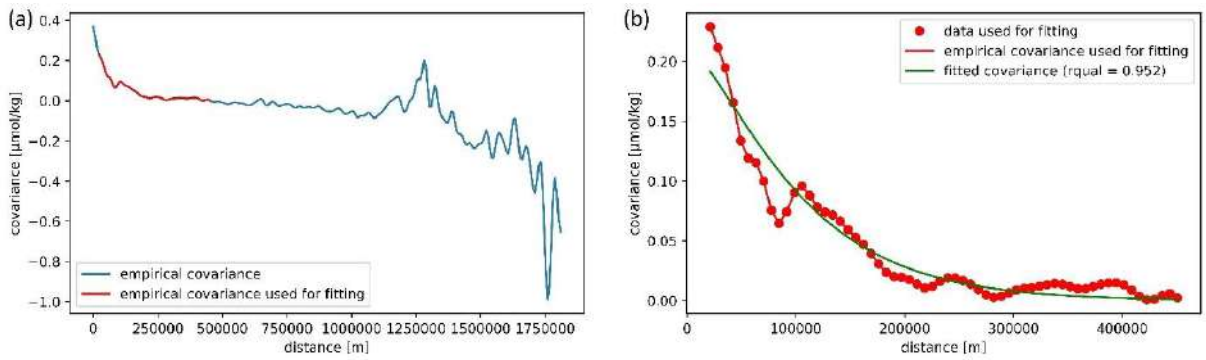

Figure 4.3: Example of the nitrate covariance. (a) The empirical data covariance function is given in red, curve comes from the analysis of observations within depth = 10 m, while (b) the fitted covariance curve (theoretical kernel) is given in green.

Based on the data, DIVA performs a least-square fit of the data covariance function with a theoretical function. Then, a vertical filter is applied and an average profile over the whole period is used (Fig. 4.4). This proceeding is analogous to what has been used for the EMODnet climatology and the North Atlantic climatology, except that in EMODnet climatology, seasonally averaged profiles were used (Buga et al., 2019) and a monthly averaged profiles were used in North Atlantic climatology (Troupin et al., 2010). The filter is applied to discard aberration caused by outliers or scarce observations in some layers, as described above.

Because of the horizontal and vertical inhomogeneity of the data coverage, the analysis was based on a correlation length that varies both horizontally (Fig. 4.4a) and vertically (Fig. 4.4b).

As expected, Lc increases with depth (Fig. 4.4), extending the influence area of the observation, a consequence of the fact that variability at depth is lower and that observations in the deep layer are scarcer (which on the other hand makes the Lc estimate more uncertain).

From the surface to 150-200 m, Lc is rather constant, from 200 to 600 m, the horizontal Lc increases for all nutrients. The vertical Lc behaves similarly, for nitrate and phosphate, due to the homogeneity of the intermediate water mass, as explained also by Troupin et al. (2010). For silicate, the vertical Lc decreases in the intermediate depth, reaching a minimum at 500 m depth. The different behavior of silicate could be explained by the progressive increase in concentrations from the surface to the deep layer, compared to nitrate and phosphate vertical distribution (strong gradient between surface depleted layer and intermediate layer). Silicate is less utilized, and the dissolution of the biogenic silica is slower than the other nutrients (DeMaster, 2003) which explain this progressive increase towards deeper layers (Krom et al., 2014).

Below 600 m, the horizontal Lc for silicate decreases down to 1000 m, and then increases again at 1500 m. For nitrate and phosphate, a similar, but less marked, behavior is observed. The vertical Lc for all nutrients increases progressively from 400 m to 1500 m.

Troupin et al. (2010) and Iona et al. (2018) attributed similar changes observed in Lc for temperature and salinity to the variability of the water masses in each layer. This might also explain the changes found in Lc for nutrients. Indeed, the concentration of nutrients in the WMED increases with depth and is very low at the surface, which explains the constant low values of Lc in this layer.

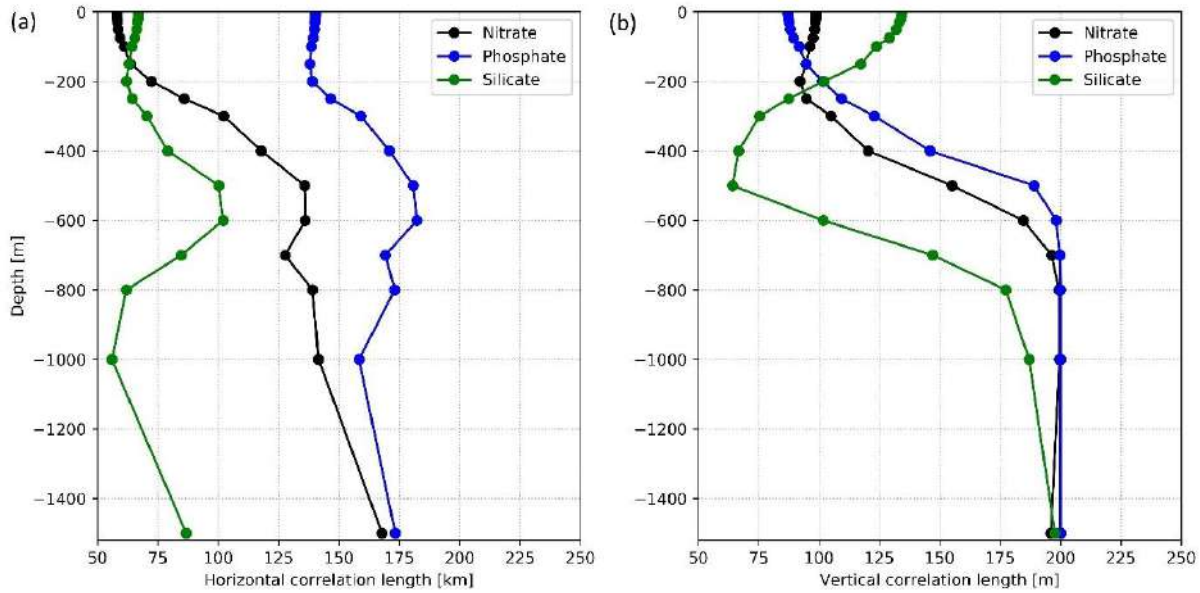

Figure 4.4: (a) Horizontal and (b) vertical optimized correlation lengths, for each nutrient (1981-2017), as a function of depth.

4.3.2.3 Signal-to-Noise Ratio

The signal-to-noise ratio (SNR) indicates the confidence in the measurements. It is the ratio between the variance of the signal and the variance of the measurement noise/error. The SNR defines the representativeness of the measurements relative to the climatological fields, in other words it is the confidence in the data. It not only depends on the instrumental error but also on the fact that observations are instantaneous measurements, and since a climatology is a long-term mean, such observations do not represent exactly the same.

Generally, small SNR values, favor large deviations from the real measurements to give a smoother climatological field. On the other hand, with a high SNR, DIVAnd keeps the existing observations and interpolates between data points.

The need is to find an approximation that does not deviate much from the real observations (further details in Lauvset et al., 2016, and Troupin et al., 2010).

Following the same approach of many climatologies that used the DIVAnd method adopted, i.e. EMODnet climatologies (available on the EMODnet chemistry portal), the Atlantic regional climatologies (Troupin et al., 2010), the Adriatic Sea climatology (Lipizer et al., 2014) and the SeadataNet regional climatology (Simoncelli et al., 2017), the SNR is set to a constant value (Table 4.1).

The analysis is performed with a predefined uniform default error variance of 0.5 for all parameters at all depths. Three iterations are done inside DIVAnd to estimate the optimal scale factor of error variance of the observation (following Desroziers et al., 2005). More details can be found in https://gher-ulg.github.io/DIVAnd.jl/latest/#DIVAnd.diva3d.

Values of SNR provided by means of a generalized cross-validation (GCV) technique (Brankart and Brasseur, 1998) gave a large estimate of the SNR (of the order of 22) showing a discontinuous analysis field and patterns around the cruise transects and do not represent properly the climatological fields.

High SNR means less confidence in the observation, while we presume that the data sources used to generate BGC-WMED climatology are consistent products.

As detailed in Troupin et al. (2010), the GCV calculate SNR that reduces the overall error variance (the generalized cross validator), defined by Wahba and Wendelberger (1980) as:

$$error\ variance = \frac{1}{N}\sum_{i=1}^{N}\left(\frac{(d_i-\tilde{d}_i)^2}{(1\ \ -A_{ii})^2}\right)^2 \quad \text{Eq. (3)}$$

Where *N* is the number of observation, d_i is the observation at location $x = x_i$, $\tilde{d}_i$ is the analysis field at x_i location when observation I is removed, A_{ii} is matrix that connect the analysis fields and observation based on this relationship: $\tilde{d}$=$A_{ii}d$.

This technique was mainly suitable for meteorological fields, and not for oceanographic observations, since observations are collected within short time period during cruise which explain the high value of SNR.

4.3.3 Post-processing of the analysis fields

For post-processing, an integrated assessment of the analysis is performed consisting of outlier detection, in order to remove observations that generate irregular interpolated fields and suspect observations that were not detected in the data quality check of section 4.2.3.

The automatic control measures how consistent the gridded field is with the nearby observations. It is the difference between a measurement and its analysis scaled by the expected error and, based on that, it assigns quality scores to observations. Data points with high quality check scores were considered as suspect and were removed from the analysis. Overall, 0.031%, 0.014%, 0.004% data points, for nitrate, phosphate, and silicate, respectively, were considered inconsistent. An application is shown in Figure 4.5.

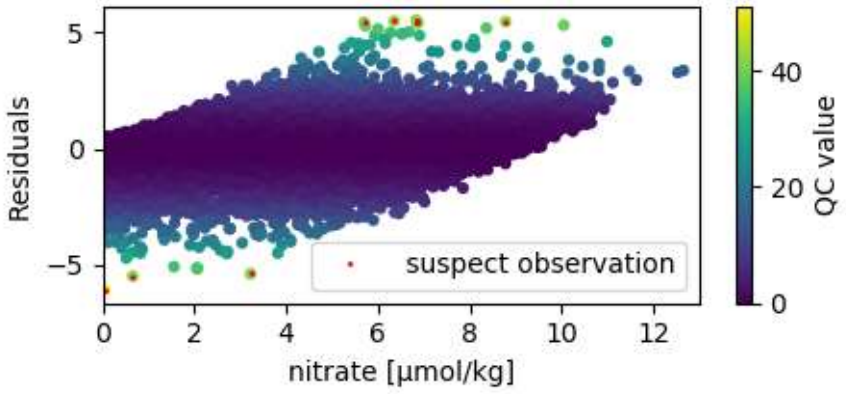

Figure 4.5: Residuals as a function of nitrate observation colored by the quality scores (QC value), in red are the suspect observations.

The quality check values that were used are available in the netCDF files of the product. Selecting the suspect observation can be subjective depending on the expertise of the person checking the quality scores.

4.3.4 Quality check of the analysis fields

We estimated the quality of the climatology for nitrate, phosphate, and silicate by inferring the consistency of the climatological fields with the observations. The quality validation indices are the mean residual and RMS of the difference between the climatology and the observations. Averages over the entire basin were calculated between depth levels (see section 4.2.3).

Residuals are the difference between the observations and the analysis (interpolated linearly to the location of the observations). The residuals are NaN when the observations are not within the domain as defined by the mask and the coordinates of the observations

The result of Fig. 4.6a shows nitrate residuals. From the 0 to 30 m depth, the observations and the analysis have a high level of agreement. Between 30 and 200 m, boxplots are taller, suggesting a larger difference. From surface to the deep layer, the mean residual varied between -0.075 and 0.0765 μmol kg^{-1}. The RMS for nitrate varied between 0.47 and 1.1 μmol kg^{-1}.

As for phosphate residuals (Fig. 4.6b), low level of agreement was found between 75 and 200 m and a lower difference in the surface and below 250 m. The average residual varied between -0.0027 and 0.0026 μmol kg^{-1}. The RMS for phosphate varied between 0.037 and 0.063 μmol kg^{-1} .

Silicate residuals (Fig. 4.6c), on the other hand, seemed more homogeneous at all depth levels. The highest level of agreement was found below 20 m and at 600 m. Overall residuals varied between -0.057 and 0.063 μmol kg^{-1}, while the RMS ranged between 0.567 and 0.963 μmol kg^{-1} .

Over the entire water column, the mean residual was around zero (0.004 μmol kg^{-1} for nitrate, 0.0002 μmol kg^{-1} for phosphate and 0.003 μmol kg^{-1} for silicate) (Fig.4.6), meaning that in general, the difference between the observations and the analysis is small.

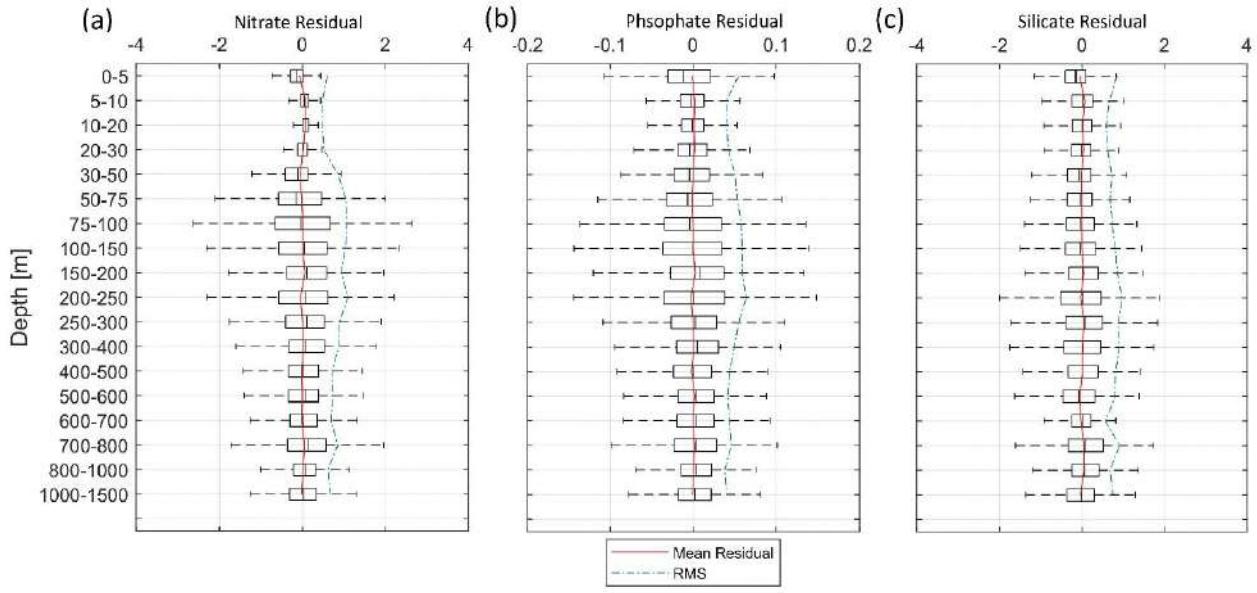

Figure 4.6: Mean residual (difference between the observations and the analysis) of (a) nitrate, (b) phosphate, (c) silicate with mean residual (in red) and mean RMS (dashed blue).

4.4 Results

The final result consists of gridded fields of mapped climatological means of inorganic nutrients for the periods 1981-2004, 2005-2017, and the whole period 1981-2017, produced with VIM described in section 4.3, using data of section 4.2. Together with the gridded fields, error maps have been generated to check the degree of reliability of the analysis.

The particularity of this product is its main focus on the WMED and the higher spatial resolution, compared to the existing climatological products (see Table 4.1). In other products, we have better seasonal and annual resolution, though this product present an average independently from years and seasons that will help improve the general picture of the biogeochemical state of the WMED through integrating the most recent available consistent datasets (see section 4.2).

The resulting climatologies (Tab 4.3.) are aggregated in a 4D netCDF for each nutrient and each time period that contains the interpolated field of the variable and related information: associated relative error, variable fields masked using two relative error thresholds (L1 and L2).

Here is an example of the analysis output found in the netCDF. Figure 4.7 shows the unmasked climatological field of the mean spatial variation of nitrate, relative error field distribution, climatological field masked using relative error with two threshold values (0.3 and 0.5) to assess the quality of the resulting fields.

Table 4.3: Available analyzed fields and available information in the netCDF files.

Variable name	Field name	Description
Lon	longitude	Longitude in degrees east, extent: -7 – 17.25 °E
Lat	Latitude	Latitude in degrees north, extent: 33.5 – 45.85°N
depth	Depth	Depth in meters, 19 levels, range: 0 – 1500 m
nitrate/phosphate/silicate	DIVAnd analyzed climatology	Mapped climatological fields
nitrate_L1/phosphate_L1/ silicate_L1	Nitrate/phosphate/ silicate masked field level 1	Mapped climatological fields masked using relative error threshold 0.3.
nitrate_L2/ phosphate_L2/ silicate_L2	Nitrate/phosphate/ silicate masked masked field level 2	Mapped climatological fields masked using relative error threshold 0.5.
nitrate_relerr/ phosphate_relerr/ silicate _relerr	Nitrate/phosphate/ silicate masked relative error	Mapped relative error filed associated to the climatological field

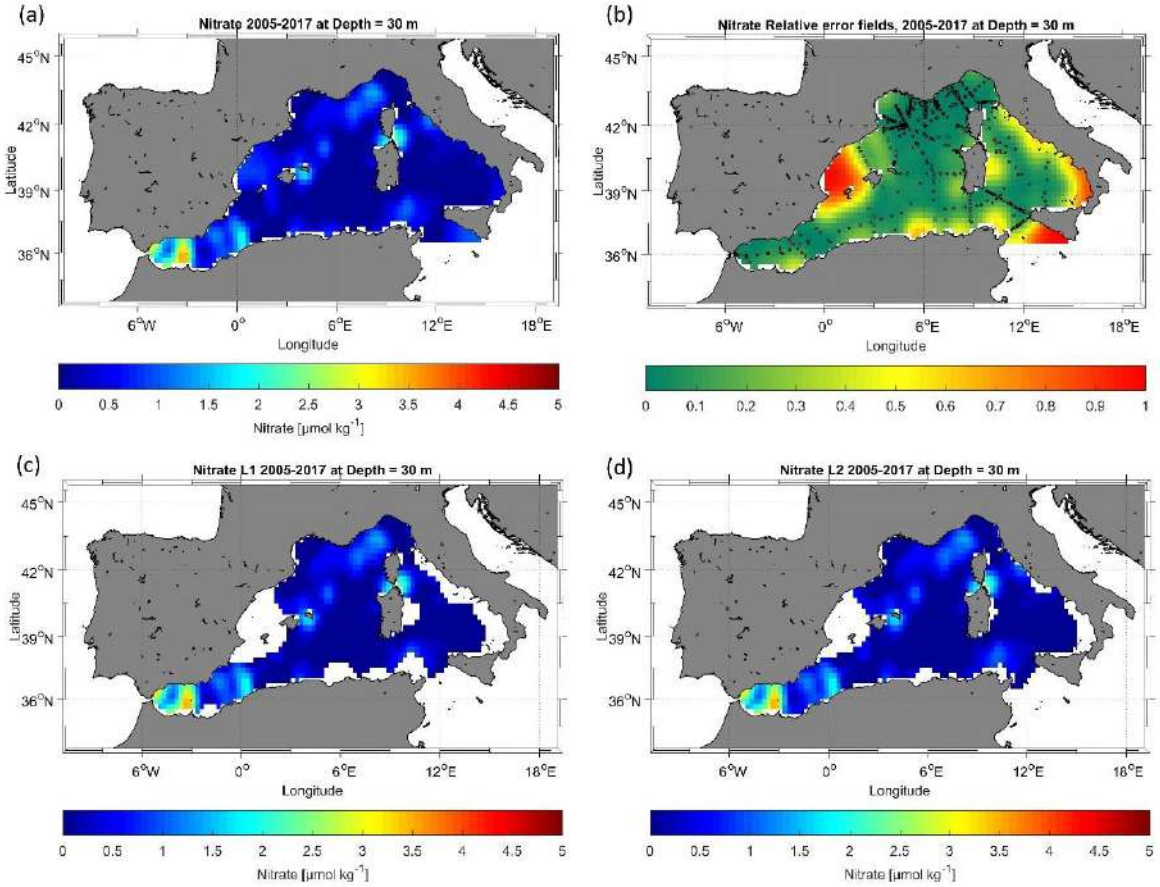

Figure 4.7: Example of nitrate analysis for the period 2005-2017 (a) unmasked analysis field, (b) relative error field distribution with the observation in black circles, (c) masked analysis fields masked using relative error threshold = 0.3, and (d) masked analysis fields masked using relative error threshold = 0.5.

In the following section, a general description of the spatial features of nutrients based on the new climatology horizontal maps is given.

4.4.1 Nutrient climatological distribution

A description of the spatial patterns of the dissolved inorganic nutrients across the domain and over the entire period (1981-2017) is given. The gridded fields for nitrate, phosphate, and silicate are discussed at three depth levels, representative of the surface (at 100m), intermediate (at 300m), and deep layer (at 1500 m). The horizontal maps at the selected depths are shown in Fig. 4.8, while the average vertical profiles of nutrients over the whole area are shown in Fig. 4.9.

4.4.1.1 Surface layer

The nitrate, phosphate and silicate mean climatological field over 1981-2017 is presented in Fig. 4.8 (a, b, c) respectively.

The mean surface nitrate concentration at 100 m is about 3.58 ± 1.16 μmol kg^{-1}. Highest surface values of nitrate concentrations are found in regions where strong upwelling or vertical mixing occurs, such as the Liguro-Provençal basin and the Alboran Sea (see Fig. 4.8a). The convection region (Gulf of Lion and Ligurian Sea) is characterized by an eutrophic regime and a spring bloom (Lavigne et al., 2015), unlike the rest of the basin that shows low nitrate concentrations in the surface layer (< 4 μmol kg^{-1}).
Nutrient patterns in the Alboran Sea have been associated with the distinct vertical mixing that supplies the surface layer with nutrients (Lazzari et al., 2012; Reale et al., 2020).
Indeed, the northern Alboran Sea is known as an upwelling area, where permanent strong winds enhance the regional biological productivity (Reul et al., 2005). Nitrate concentrations distribution at 100 m present a clear distinction between the enriched surface regions in the WMED, under the influence of deep convection processes, and the easternmost depleted region.
The distribution of phosphate concentration has striking similarities with that of nitrate (Fig. 4.8b). The mean surface phosphate concentrations, at 100 m, is 0.16 ± 0.06 μmol kg^{-1}. As for nitrate, the highest surface values are found in the Alboran Sea, Balearic Sea, Gulf of Lion and Liguro-provençal Basin (0.2-0.3 μmol kg^{-1}), while the Tyrrhenian Sea and the Algerian Sea revealed phosphate concentration that were <0.2 μmol kg^{-1}.
Similar patterns were observed by Lazzari et al. (2016), who argued that the variations in phosphate are regulated by atmospheric and terrestrial inputs. It should be noted that the maximum in the surface is found near river discharges of freshwater, like Ebro and Rhone, i.e. the largest rivers of the WMED (Ludwig et al., 2009).
Concerning the distribution of silicate concentration, the surface layer at 100 m (Fig. 4.8c) followed the same pattern as nitrate and phosphate. Over this layer the mean silicate concentration was about 2.7 ± 0.7 μmol kg^{-1}.

As for nitrate and phosphate, the highest values (3-4 μmol kg^{-1}), were recorded in the Alboran Sea, Balearic Sea, Gulf of Lion and Liguro-provençal Basin and in the southern entrance of Tyrrhenian Sea. This surface distribution is in good agreement with the findings of Crombet et al. (2011), relating this local silicate surface maximum to the continental input, river discharge and atmospheric deposition (Frings et al., 2016; Sospedra et al., 2018). The spatial minima were reported in the Tyrrhenian Sea and Algerian Sea (<3 μmol kg^{-1}).

4.4.1.2 Deep and Intermediate layer

At the basin scale, nitrate concentrations increase with depth (Fig. 4.9a), with the highest concentration found at intermediate levels (250-500 m), ranging between 8.8 and 9.0 μmol kg^{-1}. In this 300 m (Fig. 4.8d), nitrate concentrations average is 7.2 ± 1.06 μmol kg^{-1}. High values (> 6.5 μmol kg^{-1}) are found in the westernmost regions (Alboran Sea, Algerian Sea, Gulf of Lion, Balearic Sea and the Liguro-Provençal Basin), while the easternmost regions (Tyrrhenian Sea, Sicily Channel), exhibit much lower concentrations (between 4.5 and 6.5 μmol kg^{-1}).

Similar features are observed in the deep layer, at 1500 m (Fig. 4.8a), with nitrate concentrations increasing all over the basin, reaching on average 7.8 - 7.9 μmol kg^{-1} between 1000 and d 1500 m depth (Fig. 4.9a).
In both layers (300 m and 1500 m), the difference between the eastern opening of the basin (Sicily Channel) and the western side (Alboran Sea) is noticeable: the Sicily Channel and the Tyrrhenian Sea are under the direct influence of the water masses coming from the oligotrophic EMED, which then gradually become enriched with nutrients along its path, as found by Schroeder et al. (2020).
Phosphate concentrations at intermediate depth (see 300 m, Fig. 4.8e), varied between 0.12 and 0.44 μmol kg^{-1}, and the horizontal map shows the same gradual decrease towards east, with the highest concentrations in the westernmost regions and minimum values in the eastern regions (< 0.25 μmol kg^{-1}) .
The average vertical profile over the entire region (Fig. 4.9b), reveals a maximum in phosphate concentrations between 300 and 800 m depth, related to an increased remineralization process.
In the deep layer (see 1500 m, Fig. 4.8h), phosphate concentration on average is about 0.36 ± 0.02 μmol kg^{-1}. And generally, the deep layer is homogeneous (Fig. 4.9b). The difference observed between westernmost regions and the Tyrrhenian Sea remains, though the latter demonstrate higher phosphate concentrations (~0.3 μmol kg^{-1}). This variation could be due to the difference in the water masses. The intermediate water inflow from the EMED brings relatively young waters that are depleted in nutrients, while in the higher concentrations in the deep layer are signatures of the older resident deep water of the Tyrrhenian.
Silicate concentration distribution at intermediate (300 m, Fig. 4.8f) and deep layers (1500m, Fig. 4.8i), were as expected, showing a notable increase, compared to the surface. Here the silicate average concentration is 5.83 ± 0.66 μmol kg^{-1}. The maximum values were observed below 800 m, > 8.034 μmol kg^{-1} (Fig. 4.9c). At 1500 m, silicate distribution is homogeneous all over the basin (on average 8.35 ± 0.39).
Generally, primary producers do not require silicate for their growth as their need for nitrate and phosphate which explain the disparity between nutrients. Though, silicate has an important role in diatoms proliferation, since the latter play a significant role in exporting biogenic matter to deep layers (Dugdale et al., 1995), that explains the progressive silicate accumulation.

Furthermore, at intermediate levels, the water is warmer than the deep waters, enhancing the dissolution rate and the progressive increase in silicate (DeMaster, 2002).
The biogenic silicate is exported to greater depths and continues to dissolve generating inorganic silicate as it sinks to the bottom. The recycling of silicate within the deep-sea sediments is later on redistributed by the deep currents which explain the homogenous horizontal distribution over the entire basin.
Comparing the three nutrients at the same depth levels, at the surface (100 m), it appears that they all show local surface maximum, depending on local events such as strong winds, local river discharge and, vertical mixing (Ludwig et al., 2010).
In other areas, the surface layer depletion in nutrients is due to the primary production and export of organic matter to intermediate and deep layers leading to the accumulation of nutrients in these depth ranges.

The Tyrrhenian Sea is not directly connected to convection regions. Here, the EMED water inflow plays a major role. Li and Tanhua (2020) found an increased ventilation of the intermediate and deep layers during 2001 to 2018 in the Sicily channel and a constant AOU between 2001-2016, suggesting a constant ventilation that explain the peculiar nutrient distribution in that area. In the western side of the WMED, intermediate and deep layers exhibit an increase in nutrients.
Schroeder et al. (2020) explained this increase in nitrate and phosphate at the intermediate layer with the increase of the remineralization rate at these depths along the path of IW.

The deficiency of inorganic nutrients is explained by the effect of the anti-estuarine circulation, with the IW coming from the EMED, which is known to be poor in nutrients (Krom et al., 2014; Schroeder et al., 2020), accumulates nutrient along its path. Thus, this relative nutrient-rich Mediterranean outflow is lost to the Atlantic Ocean.
Overall, in surface layer, circulation, physical processes, and vertical mixing increase nutrient input while the biological pump controls the decrease.
In the deep layer, the variability is lower (standard deviation is reduced toward the bottom (Fig. 4.9) for all three nutrients), the physical processes decrease nutrients and the biological pump through remineralization of the sinking organic matter, increase them. In the WMED, the deep layer constitutes a stock of nutrients.

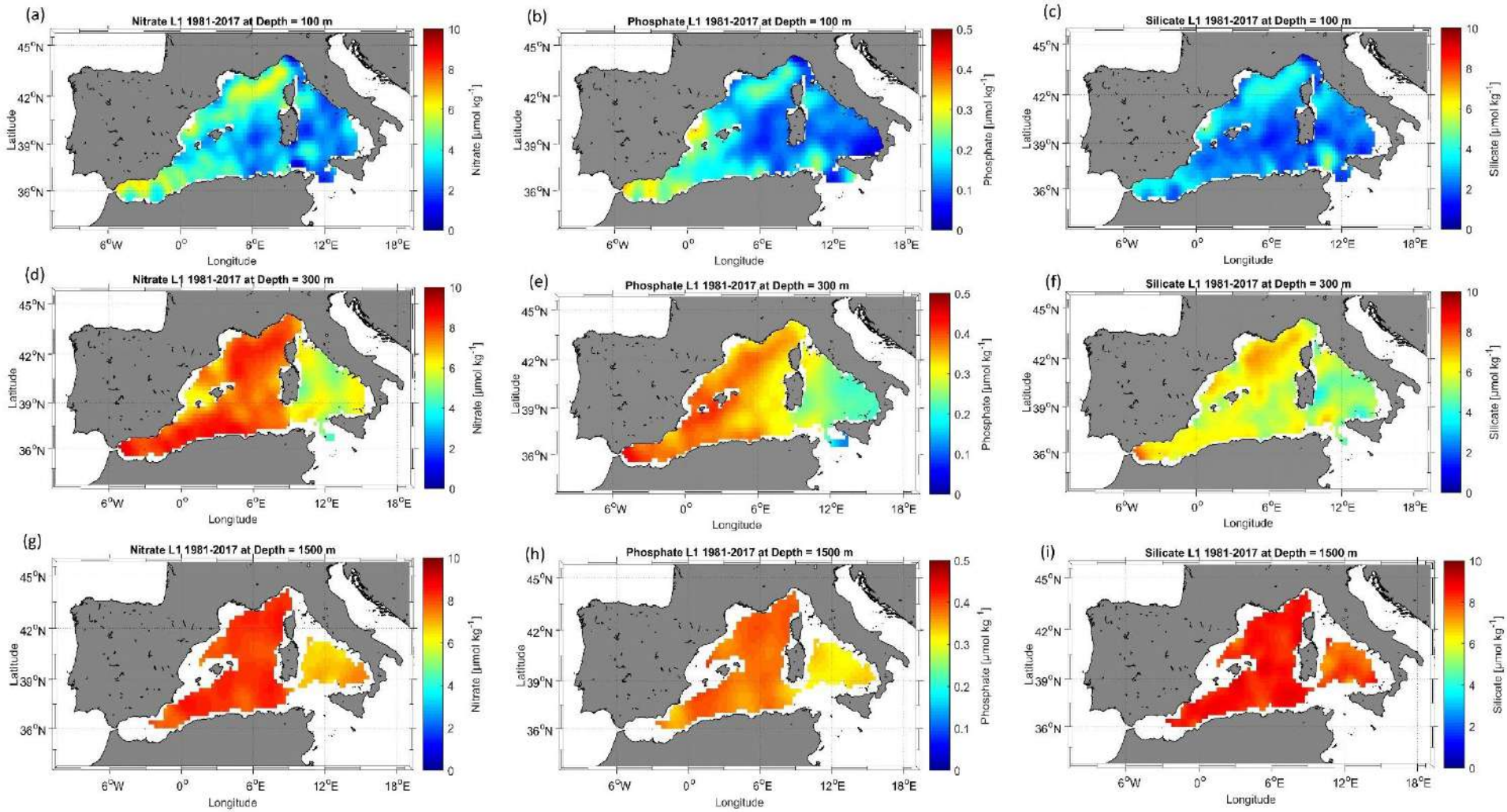

Figure 4.8: Climatological map distribution of nitrate ((a) at 100 m, (d) at 300 m, (g) at 1500 m), phosphate ((b) at 100 m, (e) at 300 m, (h) at 1500 m) and silicate ((c) at 100 m, (f) at 300 m, (i) at 1500 m) for the period from 1981 to 2017.

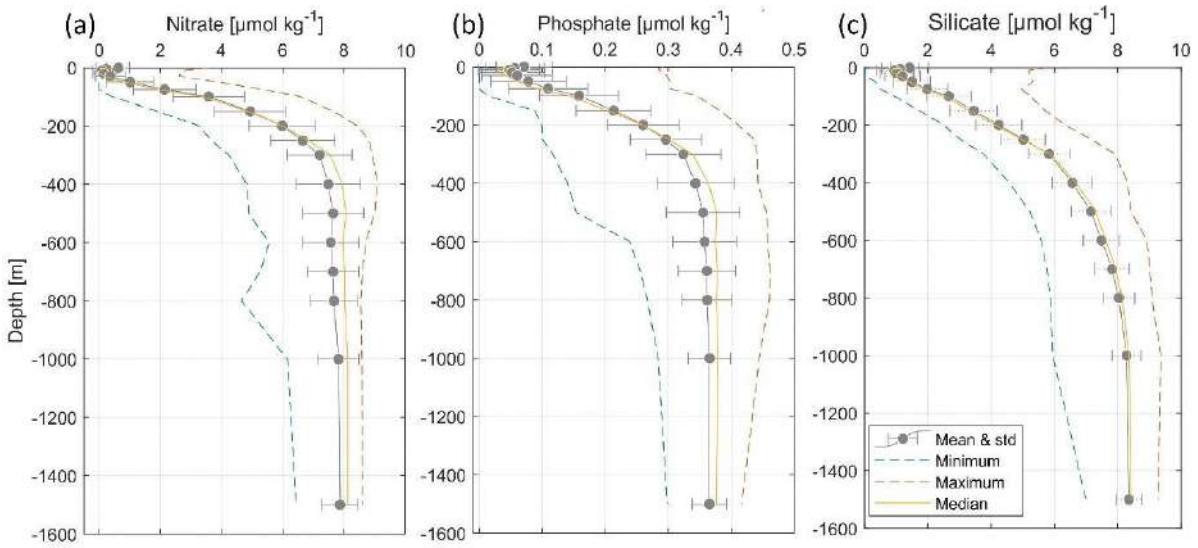

Figure 4.9: Climatological mean vertical profiles of (a) nitrate, (b) phosphate and (c) silicate in the WMED (1981-2017). Dashed blue line indicates the minimum, dashed orange line indicates the maximum, continuous yellow line indicates median profile, error bars and mean profile are in grey.

4.4.2 Error fields

The determination of the error field is important to gain insight in the confidence in the climatological results. Mostly, the error estimate depends on the spatial distribution of the observations and the measurement noise. In DIVAnd there are different methods available to estimate the relative error associated with the analysis fields.

A climatological field is computed at several depths (19 levels in this case), for different parameters (nitrate, phosphate, and silicate in this case). Given these premises and following the approach of similar climatologies (GLODAPv2.2016b, Lauvset et al., 2016; SeaDataNet aggregated data sets products, Simoncelli et al., 2017), for the BCG-WMED the error fields were estimated using the default DIVAnd method, i.e. the “clever poor man's error approach”, a less time consuming but efficient computational approach. According to Beckers et al. (2014) who also provide details about the mathematical background of the error fields computation, this method appropriately represents the true error and provides a qualitative distribution of the error estimate. This estimate is used to generate a mask over the analysis fields. Two error thresholds were applied (0.3 (L1) and 0.5 (L2)). Fig. 4.7b., show the main error that occurs in region void from measurements. An example of the analysis masked with the error thresholds output is shown in Fig. 4.7c(L1) and Fig. 4.7d (L2). The associated error fields with the analysis fields are integrated in the data product.

4.5 Discussion

4.5.1 Comparison with other biogeochemical data products

In this section a comparison of the BGC-WMED product with the most known global and/or regional climatologies, that are frequently used as reference products for initializing numerical models, is done.

Specifically, the analyzed fields are compared to the reference data products WOA18 (Garcia et al., 2019) and MedBFM (Mediterranean Biogeochemical Flux Model, https://www.cmcc.it/models/biogeochemical-flux-model-bfm, Teruzzi et al., 2019).

Since the products used for inter-comparison were not originated from the same interpolation method, not for the same time period and with different spatial resolution, here the comparison is mostly targeted on the general patterns of nutrients in the region.

Comparisons are carried out between horizontal maps (Fig. 4.10-4.11-4.12), as well as along a vertical longitudinal transect (Fig. 4.14-4.15). In addition, following Reale et al. (2020), the first 150 m have been evaluated (Fig. 4.13), since this is a depth level with a representative amount of in situ observations in all three products. The evaluation is based on the estimation of horizontal average, on BGC-WMED climatology, the medBFM biogeochemical reanalysis and the WOA18 climatology by subregion. i.e. a spatial subdivision made according to Manca et al. (2004).

Products have different grid resolution, thus to compare between them, the BGC-WMED new climatological data product (at 0.25° × 0.25°) for periods 1981-2017 and 2005- 2017 and the MedBFM biogeochemical reanalysis (at 0.063° × 0.063°) (Teruzzi et al. 2019) (https://doi.org/10.25423/MEDSEA_REANALYSIS_BIO_006_008) for the period 2005- 2017, are gridded on the WOA18 (1° × 1°) grid using nearest neighbor interpolation. The re-gridding is computed at all depth levels of the different products. The MedBFM reanalysis climatological mean was computed for the period 2005-2017 prior the interpolation.

4.5.1.1 Comparison with WOA18 at 150 m

Fig. 4.10-4.11-4.12 show the analysis at the 150 m depth surface for the three nutrients. The BGC-WMED (1981-2017) product reveals detailed aspects of the general features of nitrate (Fig. 4.10.a), phosphate (Fig. 4.11a) and silicate (Fig.4.12a). It should be noted that the two products do not have similar spatial and temporal distribution of the observations. The new product has a higher spatial resolution.

For the three nutrients, the new product reproduces patterns similar to the WOA18 all over the region. However, fields in the WOA18 are very smoothed and show low values while in the new product nitrate and phosphate concentrations are higher. The average RMS error at 150 m, all over the region is about 1.14 μmol kg^{-1} nitrate (Fig. 4.10c), 0.055 μmol kg^{-1} for phosphate (Fig. 4.11c) and 0.91 μmol kg^{-1} for silicate (Fig. 4.12c).

The difference field for every grid point reflects discrepancy and areas with limited agreement between the two products, that can have a difference >2 μmol kg^{-1} for nitrate (Fig. 4.10c), >0.1 μmol $kg^{-1}$for phosphate (Fig. 4.11c), >1.5 μmol $kg^{-1}$for silicate (Fig. 4.12c).

The distribution of the surface nitrate concentrations (at 150m) (Fig. 4.10a) of the new product is similar to that shown in WOA18 (Fig. 4.10b). The largest difference between the two products occurs in northwest areas and in the Alboran Sea (Fig. 4.10c), areas of higher concentrations, a more nutrient rich surface water as described in section 4.4.1. The difference is pronounced in these regions likely because the new product holds more in situ observations than the WOA18 in the WMED.

Phosphate surface concentrations (Fig. 4.11a) show similar differences as nitrate. The largest difference with the surface phosphate of the WOA18 is found in the Alboran Sea, Northern WMED and Sicily region.

As for silicate, the surface distribution shows large differences between the two products also in the northwest and southeast areas (Fig. 4.12c). The highest values are observed in the northwest area of the new product, and in the Alboran Sea in the WOA18 climatology, this again accounts for the data coverage difference.

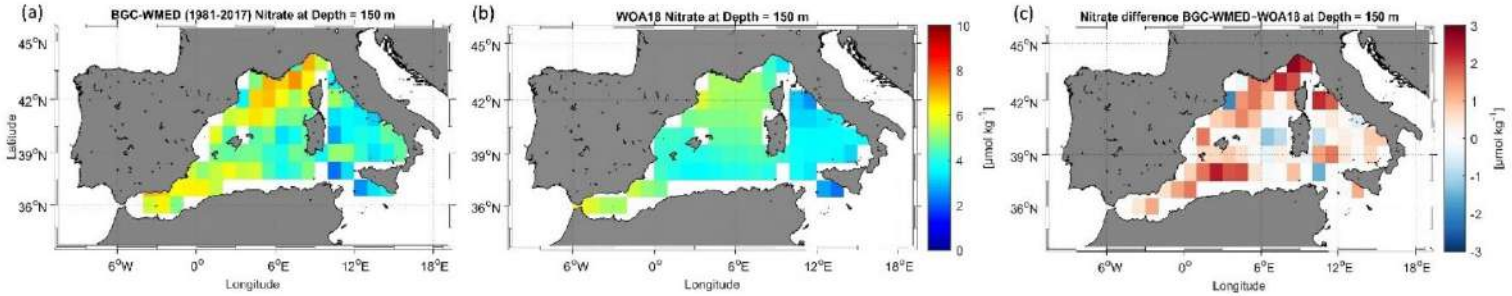

Figure 4.10: (a) BGC-WMED (1981-2017) nitrate climatological field at 150 m depth; (b) WOA18 nitrate climatological field at 150 m depth; (c) difference between BGC-WMED and WOA18 nitrate fields at 150 m .

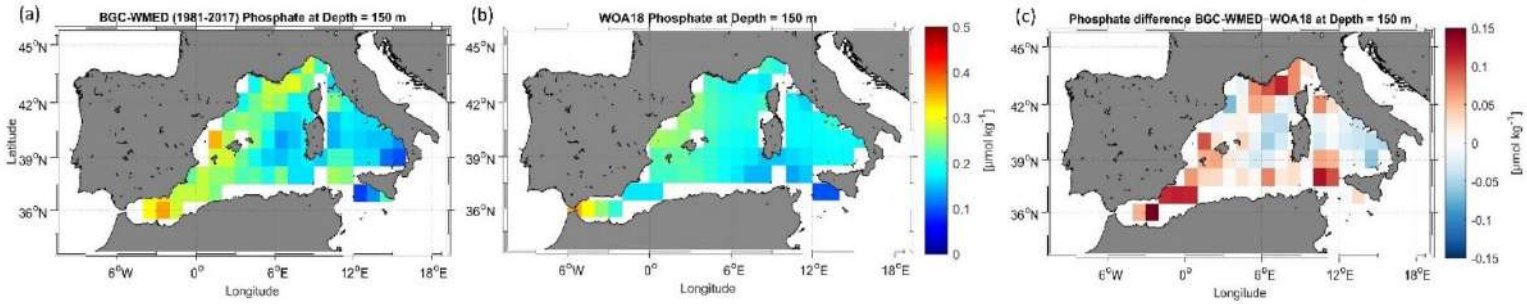

Figure 4.11: The same as Fig. 10 but for phosphate.

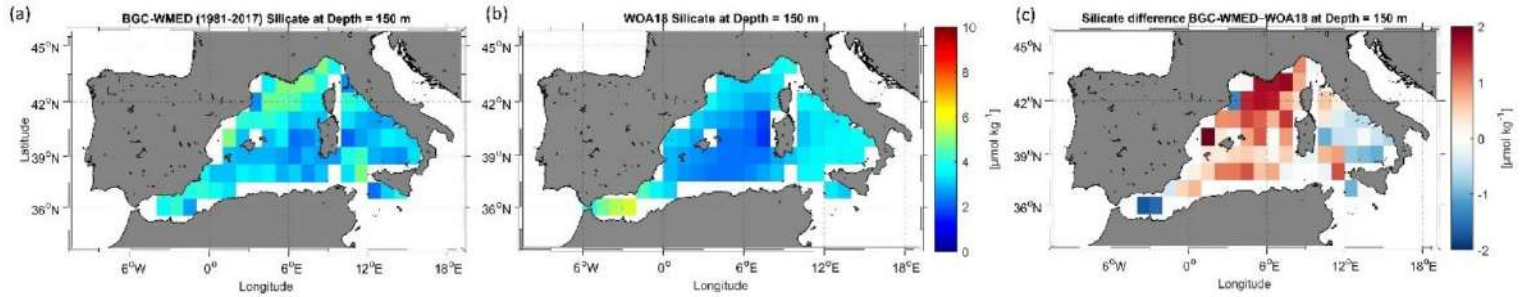

Figure 4.12: The same as Fig. 10 but for silicate.

4.5.1.2 Regional horizontal comparison above 150 m average nutrient concentrations

The inorganic nutrient mean concentrations resulting from the climatology of this work (period 2005-2017), and from both the medBFM reanalysis product and the WOA18 are compared in the upper layer of 12 subregions of the WMED (In Table 4.4 and Fig. 4.13). Results show a general agreement between BGC-WMED and the other two products in some subregions, nonetheless, there are some differences as found in section 4.5.1.1.

Upper layer nitrate average concentrations (Fig. 4.13a) are decreasing eastward, from the Alboran Sea (DS1) to the Algerian basin (DS3, DS4) and the Balearic Sea (DS2). The western part of the basin is an area under the direct influence of the inflowing Atlantic surface waters, where nitrate is known to be present in excess compared to phosphate probably due to atmospheric N_2 input (Lucea et al., 2003). In the DS1, BGC-WMED nitrate levels are lower than the WOA18 nitrate levels while in DS3, DS2 and DS4 the average nitrate concentrations are similar to the WOA18.

From the Algerian basin (DS4, DF1) to Liguro-Provençal (DF3) regions, there is an increase in the average nitrate in all products, this is the south-north gradient. Some difference arises, where the new product is lower than the WOA18.

In the eastern regions, the lowest average concentrations of the WMED are found. Here, the difference is minor between products, medBFM reanalysis is lower than the new product and the WOA18.

As for phosphate (Fig. 4.13b), known to be the limiting nutrient of the WMED, because it is rapidly consumed by phytoplankton (Lucea et al., 2003), its average levels are low in DS1, DS3, DS2 and DS4, in WOA18, medBFM reanalysis and BGC-WMED. The latter did not agree well with the other products in DS2, where it was slightly higher. Phosphate average concentrations slightly increase in DF1, DF2 and DF3 in all three products. The increase is explained by the vertical mixing process occurring in the northern WMED.

Upper surface phosphate concentrations average start to decrease progressively through the Ligurian East (DF4), Tyrrhenian Sea (DT1, DT3), Sardinia Channel (DI1) and Sicily Channel (DI3).The BGC-WMED was in agreement with medBFM reanalysis in those subregions aside from concentrations in DI3, where the new product showed higher levels.

The BGC-WMED climatology shows reasonable agreement in the upper average concentrations of nitrate and phosphate that are similar in order of magnitude to the other products (Fig. 14). The difference with the WOA18 resides in the wider temporal window of the observation (starting from 1955). The new climatology in some subregions has a better

spatial coverage of in-situ observation than the WOA18 (Garcia et al., 2019) and the medBFM reanalysis (Teruzzi et al., 2019).

On the other hand, the average silicate (Fig. 4.13c) of the new product and the WOA18 varied between regions. Significant difference is found between the two products in DS2, DS4, DF1, DF2, DT1, DT3, DI1 and DI3, while in DS1, DS3 and DF4 mean silicate is consistent between the two products.

Overall, the three products show strongly similar features between regions (similar curve shape).

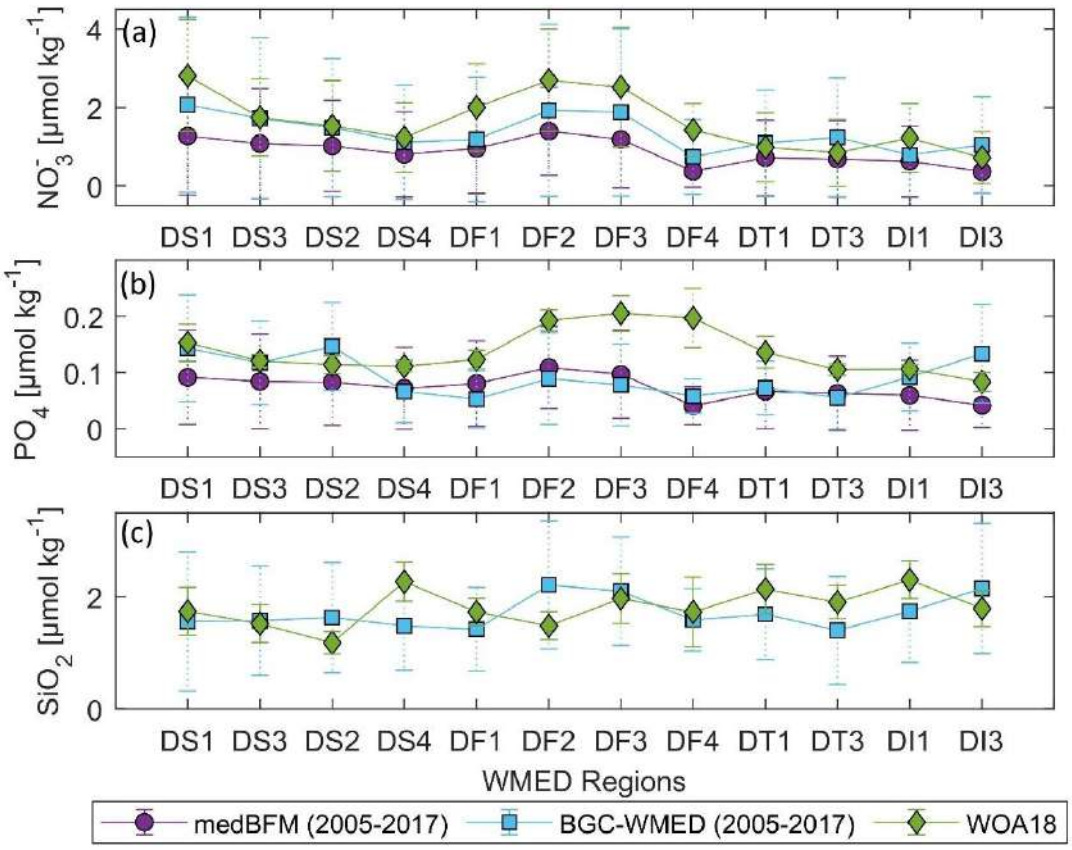

Figure 4.13: Nutrient average concentrations and standard deviation comparison in the upper 150 m (values in Table 4.4).

Table 4.4: Nutrient average concentrations and standard deviation in the upper 150 m. All products were interpolated on 1° grid resolution (see Figure 2.5 of Chapter 2).

Subregion/ Coverage	Data product	Nitrate	Phosphate	Silicate
DS1- Alboran Sea (35°N– 37.3°N, -6°E– -1°E)	medBFM	1.27(±1.4)	0.09(±0.08)	-
	BGC-WMED	2.06(±2.2)	0.14(±0.09)	1.56(±1.2)
	WOA18	2.81(±1.4)	0.15(±0.03)	1.74(±0.4)
DS3- Algerian West (35.36°N– 38.3°N, -1°E– 4.3°E)	medBFM	1.07(±1.4)	0.08(±0.08)	-
	BGC-WMED	1.72(±2.05)	0.11(±0.07)	1.57(±0.9)
	WOA18	1.74(±0.9)	0.12(±0.01)	1.52(±0.3)
DS2- Balearic Sea (38.3°N– 42°N, -1°E–4.3 °E)	medBFM	1.02(±1.1)	0.08(±0.07)	-
	BGC-WMED	1.48(±1.7)	0.14(±0.07)	1.63(±0.9)
	WOA18	1.53(±1.1)	0.11(±0.01)	1.18(±0.2)
DS4- Algerian East (36.3°N– 39.18°N, 4.3°E– 8.24°E)	medBFM	0.80(±1.08)	0.07(±0.07)	-
	BGC-WMED	1.11(±1.4)	0.06(±0.05)	1.48(±0.7)
	WOA18	1.23(±0.8)	0.11(±0.009)	2.27(±0.3)
DF1- Algero-Provençal (39.18°N– 41°N, 4.3°E– 9.18°E)	medBFM	0.96(±1.15)	0.08(±0.07)	-
	BGC-WMED	1.18(±1.5)	0.05(±0.05)	1.42(±0.7)
	WOA18	2.00(±1.1)	0.12(±0.01)	1.73(±0.2)
DF2- Gulf of Lion (42°N–43.36°N, 1°E–6.18°E)	medBFM	1.39(±1.19)	0.10(±0.07)	-
	BGC-WMED	1.92(±2.1)	0.08(±0.08)	2.21(±1.1)
	WOA18	2.68(±1.3)	0.19(±0.01)	1.48(±0.2)
DF3- Liguro-Provençal (41°N– 45°N, 6.18°E– 9.18°E)	medBFM	1.18(±1.2)	0.09(±0.07)	-
	BGC-WMED	1.88(±2.1)	0.07(±0.07)	2.10(±0.9)
	WOA18	2.52(±1.5)	0.20(±0.03)	1.97(±0.4)
DF4- Ligurian East (42.48°N–45°N, 9.18°E– 11°E)	medBFM	0.37(±0.4)	0.04(±0.03)	-
	BGC-WMED	0.74(±0.9)	0.05(±0.03)	1.59(±0.5)
	WOA18	1.42(±0.6)	0.19(±0.05)	1.73(±0.6)
DT1- Tyrrhenian North (39.18°N–42.48°N, 9.18°E– 16.16°E)	medBFM	0.71(±0.9)	0.06(±0.06)	-
	BGC-WMED	1.09(±1.3)	0.07(±0.04)	1.69(±0.8)
	WOA18	0.98(±0.8)	0.13(±0.02)	2.13(±0.4)
DT3- Tyrrhenian South (38°N– 39.18°N, 10°E– 16.16°E)	medBFM	0.68(±0.96)	0.06(±0.06)	-
	BGC-WMED	1.23(±1.5)	0.05(±0.05)	1.40(±0.9)
	WOA18	0.84(±0.8)	0.10(±0.01)	1.90(±0.2)
DI1- Sardinia Channel (36°N– 39.18°N, 8.24°E– 10°E)	medBFM	0.62(±0.9)	0.05(±0.06)	-
	BGC-WMED	0.78(±1.3)	0.09(±0.06)	1.74(±0.9)
	WOA18	1.22(±0.8)	0.10(±0.007)	2.3(±0.30)
DI3- Sicily Channel (35°N– 38°N, 10°E–15°E)	medBFM	0.36(±0.5)	0.04(±0.03)	-
	BGC-WMED	1.04(±1.2)	0.13(±0.08)	2.15(±1.1)
	WOA18	0.72(±0.6)	0.08(±0.01)	1.79(±0.3)

4.5.1.3 Regional vertical comparison of nitrate and phosphate concentrations

As the last step in the comparison between different products, here it is investigated how the new climatology represents the vertical distribution by comparing the new climatological values for the period 2005-2017 with the reanalysis and the WOA18.

We extracted data values along a longitudinal transect across the Algerian basin in the west-east direction (Fig. 4.14). The transect was used and described in previous studies (D'Ortenzio and Ribera d'Alcalà, 2009; Lazzari et al., 2012; Reale et al., 2020) and since the Eastern basin is showing different features, a transect across the Tyrrhenian Sea is extracted (Fig. 4.14). Silicate is not included as it was not represented in the medBFM model.

Vertical sections of nitrate and phosphate in the Algerian Sea show a common agreement between products about the main patterns found along the water column, i.e. the nutrient depleted surface layer and the gradual increase toward intermediate depths, we note as well the west to east decreasing gradient in the three products, yet, there are some inequalities.

Below 100 m, there is a significant difference between products and a poor quantitative agreement. nitrate distribution is dominated by the nutrient enriched water, with high values (>7 μmol kg^{-1}) increasing from east to west (Fig. 4.14). Phosphate shows similar patterns in the surface layer, exhibiting very low concentration in the surface layer and a progressive increase down to 300 m (> 0.35 μmol kg^{-1}) noted also in the WOA18. The reanalysis showed a more smoothed field, below 100-300 m, with phosphate concentration between 0.20 and 0.30 μmol kg^{-1}. The highest values for phosphate were found below 250 m from 0°E to 3°E in the new product. The BCG-WMED transect define very well the different depth layers, the upper intermediate layer is rich with nutrient concentration with > 8 μmol kg^{-1} for nitrate (BGC-WMED) and >0.35 μmol kg^{-1} for phosphate (BGC-WMED and WOA18).

The vertical section along the Tyrrhenian Sea (Fig. 4.14) also shows a decrease from west to east in nitrate concentrations. The same gradient is found also in phosphate in agreement with nutrient distribution shown from the WOA18. From the section of the medBFM reanalysis, it is not easy to identify the west-east gradient that we mentioned before. It could be suggested that the model under-estimate the vertical features in the Eastern (Tyrrhenian Sea: 100-300 m, nitrate vary between 1.4 and 4.2 μmol kg^{-1}, phosphate between 0.13 and 0.20 μmol kg^{-1}) and western part (Algerian basin: 100-300 m, nitrate vary between 2.1 and 5.4 μmol kg^{-1}, phosphate between 0.15 and 0.255 μmol kg^{-1}). These values are lower than the ones found in the BGC-WMED (Tyrrhenian Sea: 100-300 m, nitrate range between 3 to 6 μmol kg^{-1}, as for phosphate values oscillate between 0.10-0.27 μmol kg^{-1};Algerian basin: 100-300 m, nitrate range between 3.6 to 8 μmol kg^{-1}, as for phosphate values oscillate between 0.18-0.36 μmol kg^{-1}).

While the WOA18 reproduce similar patterns as the new climatology (Tyrrhenian Sea: 100-300 m, nitrate vary between 1.8 and 5.7 μmol kg^{-1}, phosphate between 0.33 and 0.20 μmol kg^{-1}) and western part (Algerian basin: 100-300 m, nitrate vary between 2.8 and 6.8 μmol kg^{-1}, phosphate between 0.16 and 0.34 μmol kg^{-1}). The products illustrate the nutrient-poor water in the Eastern side (Tyrrhenian Sea) and the relatively nutrient-rich water found in the Western side (Algerian basin).

The BGC-WMED product captures details in Fig. 4.14 about the longitudinal gradient in nitrate and phosphate, along the water column where nutrient sink deeper from west to east as previously seen in Pujo-Pay et al. (2011) and Krom et al. (2014), an increased oligotrophy from west to east with higher concentrations in the two nutrients in the western side of the section and a more oligotrophic character toward east.

The inequality between products could be explained by the difference in the data coverage, time span and the difference in methods used to construct the climatological fields.

The variability in nitrate and phosphate fields along the transect extracted from the BGC-WMED reflects the high resolution of the product allowing the screening of vertical structure controlling nutrient contents. Based on a visual comparison, the new product is able to reproduce similar patterns as to the WOA18 and to a lesser extent the MedBFM reanalysis. .

Fig. 4.15 examine the vertical difference of nitrate and phosphate concentration for the BGC-WMED with the medBFM reanalysis along the Algerian basin (Fig.4.15a, nitrate; Fig.4.15b, phosphate) and WOA18 (Fig.4.15c, nitrate; Fig.4.15d, phosphate).

The vertical section shows a strong agreement at the surface for nitrate between the BGC-WMED and the medBFM reanalysis (Fig. 4.15a), while the vertical difference with WOA18 demonstrates that nitrate values in the new product are lower than the WOA18 at 50- 75 m (Fig. 4.15c).

The difference increases with depth, below 100 m, the BGC-WMED nitrate climatology is higher than the medBFM with a difference ranging between 0.6 and 2.4 μmol kg^{-1}, similar observation is noted in the WOA18 (Fig. 4.15c). In Fig.4.15a and Fig.4.15c, we identify patterns in the vertical structure of nitrate in the eastern portion of the transect.

Regarding phosphate, differences between the new climatology and the medBFM reanalysis are noted (Fig. 4.15b) where the BGC-WMED show high concentrations in the first 100 m and between 150 m and 300 m (differences of 0.02 - 0.08 μmol kg^{-1}), this difference decreases at 100-150 m. At the eastern portion of the transect (6°E to 7.5°E), we find an agreement between the two products.

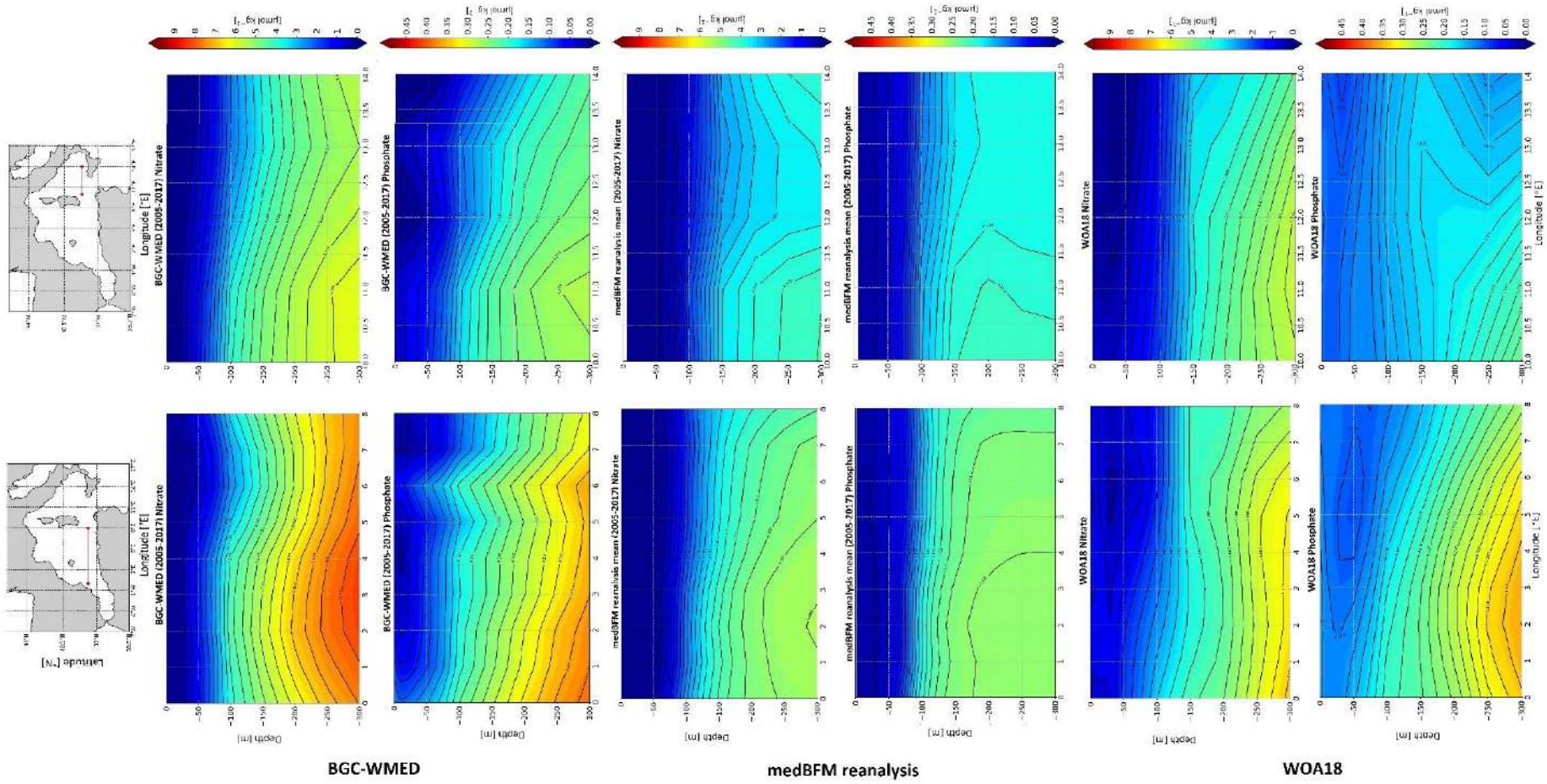

Figure 4.14: Vertical distribution of nitrate and phosphate (in μmol kg^{-1}): from the Algerian basin (bottom panel) and Tyrrhenian Sea (top panel). Colors show the gridded values from the three different products: BGC-WMED; medBFM reanalysis (Teruzzi et al.,2019); and the WOA18 (Garcia et al.,2018).

Conversely, the vertical sections of the differences between BGC-WMED and WOA18 in phosphate (Fig.4.15d) show similarities, with the new product being lower than the WOA18 in the first 50 m. Large difference is found on both sides of the transect below 100 m, while in the center of the transect, the difference in phosphate is reduced to 0-0.02 μmol kg^{-1}.

Fig.4.16 compares the vertical difference of nitrate and phosphate along the Tyrrhenian Sea transect. In general, the difference transect in the Tyrrhenian Sea shows similar features with medBFM reanalysis and the WOA18 as in Algerian basin. Fig.4.16d captures the west to east gradient in phosphate. The WOA18 overestimate phosphate in the surface layer.

Based on the new climatology comparison with the WOA18 and the reanalysis, it is concluded that the new product is consistent with the main features of previous products and show the large-scale patterns and underline well the characteristics of the water mass layers.

The study also provides an examination of the nitrate and phosphate distributions along a longitudinal transect across the Algerian Basin (Western WMED) and across the Tyrrhenian Sea (Eastern WMED). We have shown that the western basin is relatively high in nutrients compared to the Eastern basin.

The increased oligotrophic gradient from west to east could be attributed to the difference in the hydrodynamic patterns related to the water mass specific properties that are affected by the EMED and the Atlantic ocean inflows, and to the local sources of nutrients (Ribera d'Alcalà et al., 2003; Schroeder et al., 2010). Study of Crispi et al. (2001) inferred to the biological activity that is responsible for the oligotrophic gradient.

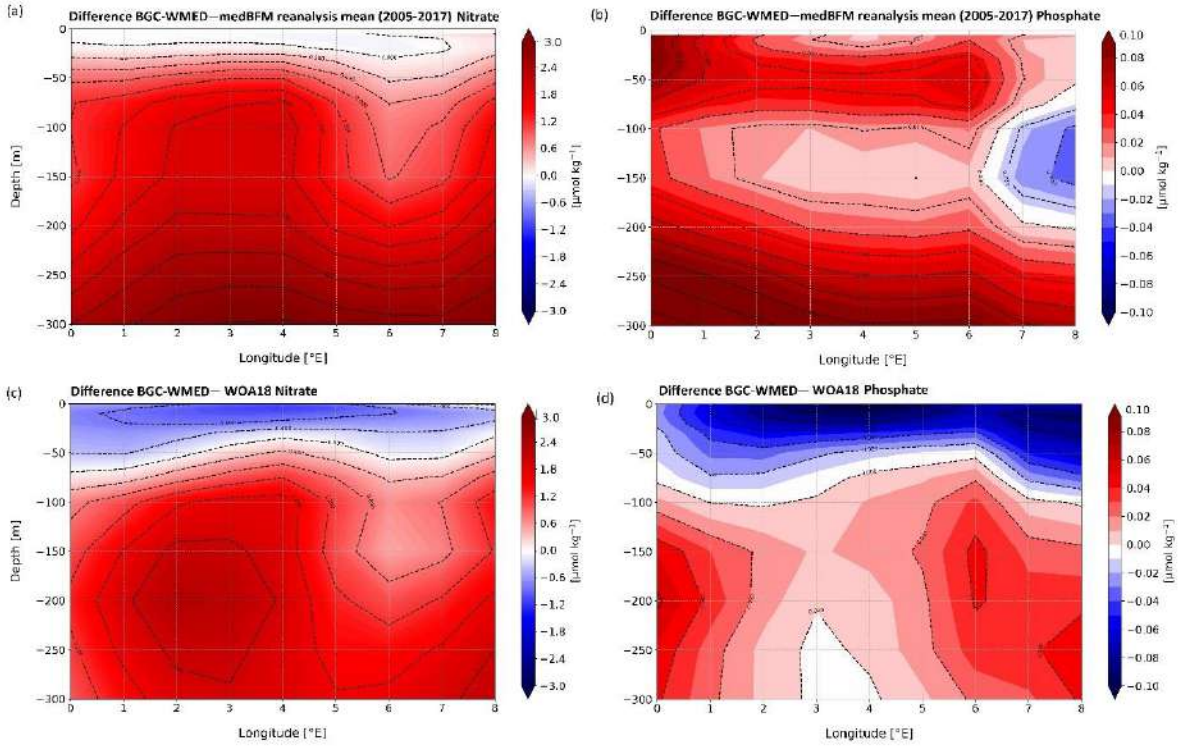

Figure 4.15: Difference of vertical section from Algerian basin between BGC-WMED and medBFM ((a) nitrate, (b) phosphate), BGC-WMED and WOA18 ((c) nitrate, (d) phosphate); with dashed contour lines and labels.

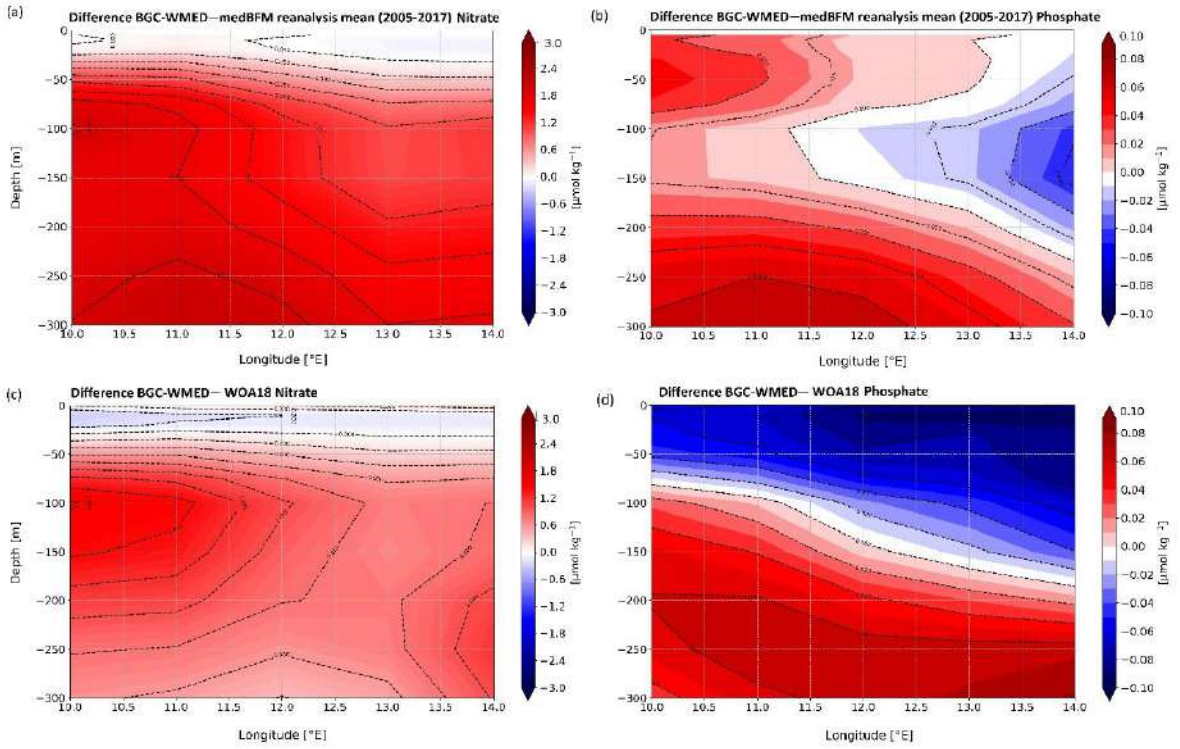

Figure 4.16: Same as Fig.4.15 but for the vertical section from the Tyrrhenian Sea.

4.5.2 Temporal comparison: 1981-2004 vs. 2005-2017

In this section, two climatological periods (1981-2004 vs. 2005-2017) are compared. The distinction between the two periods was based on the termed event of the western Mediterranean transient (WMT) that started in 2004/05 (as detailed in Chapter 1, section 1.3.2.2).

In this section, the possible impact of WMT on biogeochemical characteristics at different depth levels is investigated.

Depth levels that represent the usual three layers in the WMED are considered: the surface (100 m; Fig.4.17a-4.18a-4.19a), intermediate (300 m; Fig.4.17b-4.18b-4.19b) and deep layers (1500 m ; Fig.4.17c-4.18c-4.19c).

The WMED surface layer is dominated by the nutrient-poor AW coming from the Atlantic Ocean through the upwelling area (García-Martínez et al., 2019) in the Alboran Sea, where there is a continuous injection of nitrate, phosphate and silicate to the surface (Fig. 4.17a-4.18a-4.19a), that continued to be high also after WMT (Fig. 4.17d-4.18d-4.19d). Surface nitrate shows an increase of +0.4137 μmol kg^{-1} (Fig. 4.21) between the two periods. The largest increase (>+2 μmol kg^{-1}) is observed in the Sardinia Channel and the Alboran Sea. The increased nitrate in the Alboran sea is consistent with the favorable conditions for nitrogen fixation discussed in Rahav et al. (2013), revealing also that nitrogen fixation rate increases from east-to-west.

In the Algerian Sea and in the Tyrrhenian Sea, the surface layer is depleted in nitrate and phosphate, as also reported also by Lazzari et al. (2016).

The average difference between the two periods in phosphate and silicate show a decrease at 100 m (Fig. 4.18a) of about -0.021 and -0.13 μmol kg^{-1}, respectively. Large changes are noticed in the southern Alboran Sea, Sardinia Channel and Balearic Sea.

As can be seen from Figs.4.17b-4.18b-4.19b, at intermediate depths the Tyrrhenian Sea is poor in nutrients compared to the westernmost parts of the WMED. However, after the WMT (Fig. 4.17e-4.18e-4.19e) an increase in concentrations of the three nutrients can be observed.
On average, the difference between the two periods (pre/post-WMT) for nitrate, phosphate, and silicate, at 300 m depth, are +0.86, +0.007 and +0.21 μmol kg^{-1} (Fig. 4.21b), respectively.
The largest increase (>+2 μmol kg^{-1}) is noticed in the Alboran and Balearic Sea for nitrate.
At 1500 m depth, there is a noticeable increase of nutrients after the WMT, possibly caused by the uplifting of the nutrient rich old WMDW(Fig. 4.17f-4.18f-4.19f). Furthermore, the WMT enhanced the ventilation of the deep layers, which means an increase in the dissolved oxygen,

rendering the deep WMED a region with accelerated mineralization rates (Schroeder et al., 2016; Tanhua et al., 2013b).

Variation at 1500m (Fig. 4.21c) were of the order of +0.75 μmol kg^{-1} in average nitrate, +0.025 μmol kg^{-1} in average in phosphate and + 0.86 μmol kg^{-1} in average silicate.

After WMT, and with the increase of temperature of the water masses, biogenic silicate tends to dissolve faster which explains high concentrations all over the basin even the Tyrrhenian Sea.

The comparison between the climatological periods post-WMT (2005-2017) and pre-WMT (1981-2004) shows a considerable overall increase in the mean nutrient at different depth levels (Fig. 4.20).

After WMT, the Intermediate and deep layers are very well oxygenated, nutrient horizontal distribution shows a significant higher concentration in the three-nutrient compared to the pre-WMT period.

Figure 4.20 gives clearly better overview of the vertical difference. Nitrate displayed a notable difference below 200 m (Fig.4.20a). Phosphate difference between the two-time period was larger below 400 m (Fig. 4.20b).

Silicate concentration demonstrated an enrichment of the deep water compared to the 1981-2004 period. Silicate was different from nitrate and phosphate. It increases progressively with depth (Fig.4.20c). In general, the maximum values are found in the deep layer, which is due to the lower remineralization rate.

This overall change could also be explained by the low rate of denitrification for nitrate and an increase in the remineralization of organic matter, enriching the deep layer in inorganic nutrients, silicate relative depletion before the WMT, could be due to the low diatoms production and the lower sinking rate.

Generally, diatoms exhibit seasonal cyclicity, they are highly affected by the temperature changes, after WMT, the stronger water mixing enhanced the vertical transport of silicate (Ribera d'Alcalà, 2003) contributing to the enrichment of the sediment in diatoms.

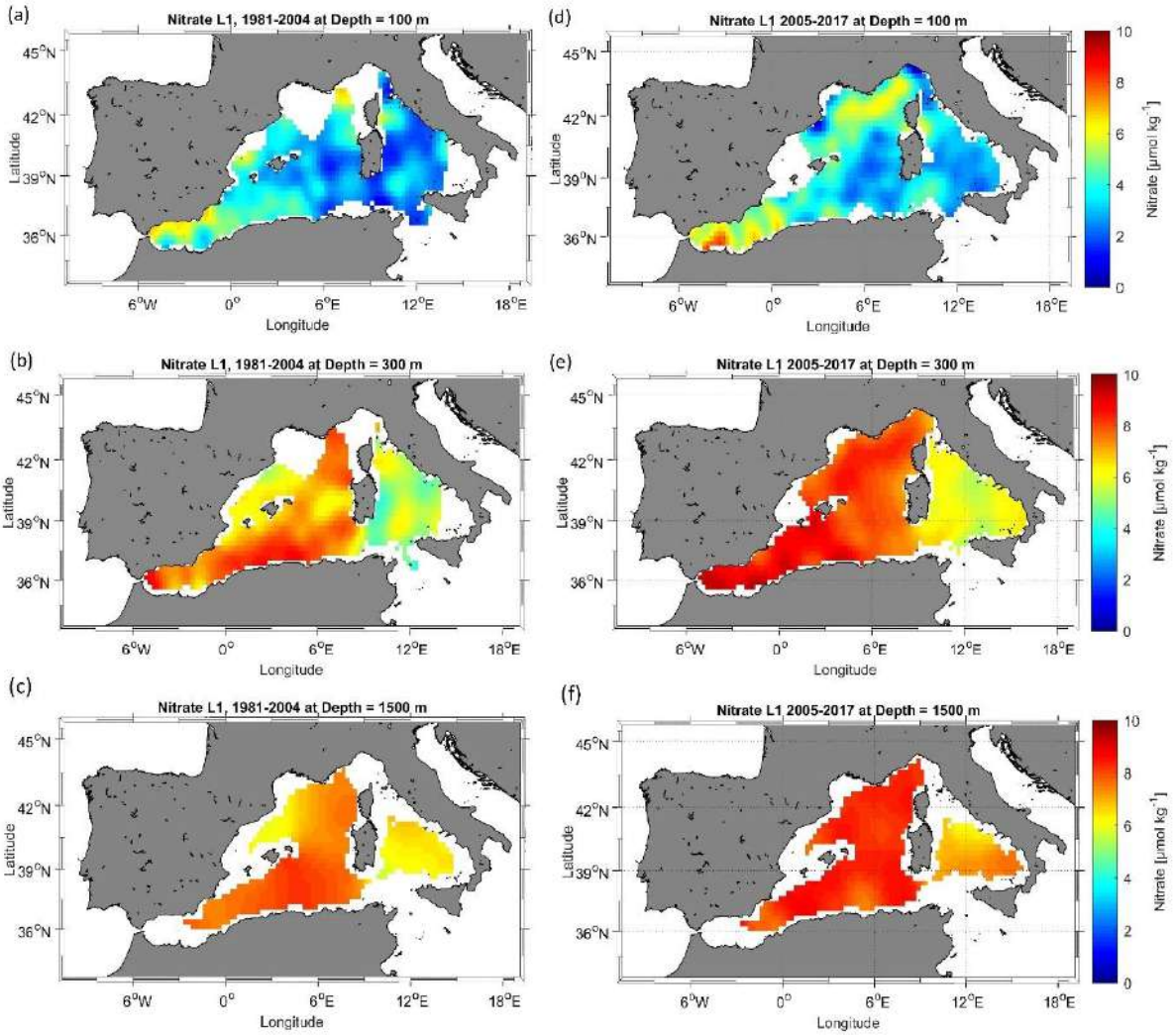

Figure 4.17: Nitrate climatological field (masked analysis fields using relative error threshold = 0.3 (L1)) at 100 m, 300 m and 1500 m, for two periods: 1981-2004 (a, b, c) and 2005-2017 (d, e, f).

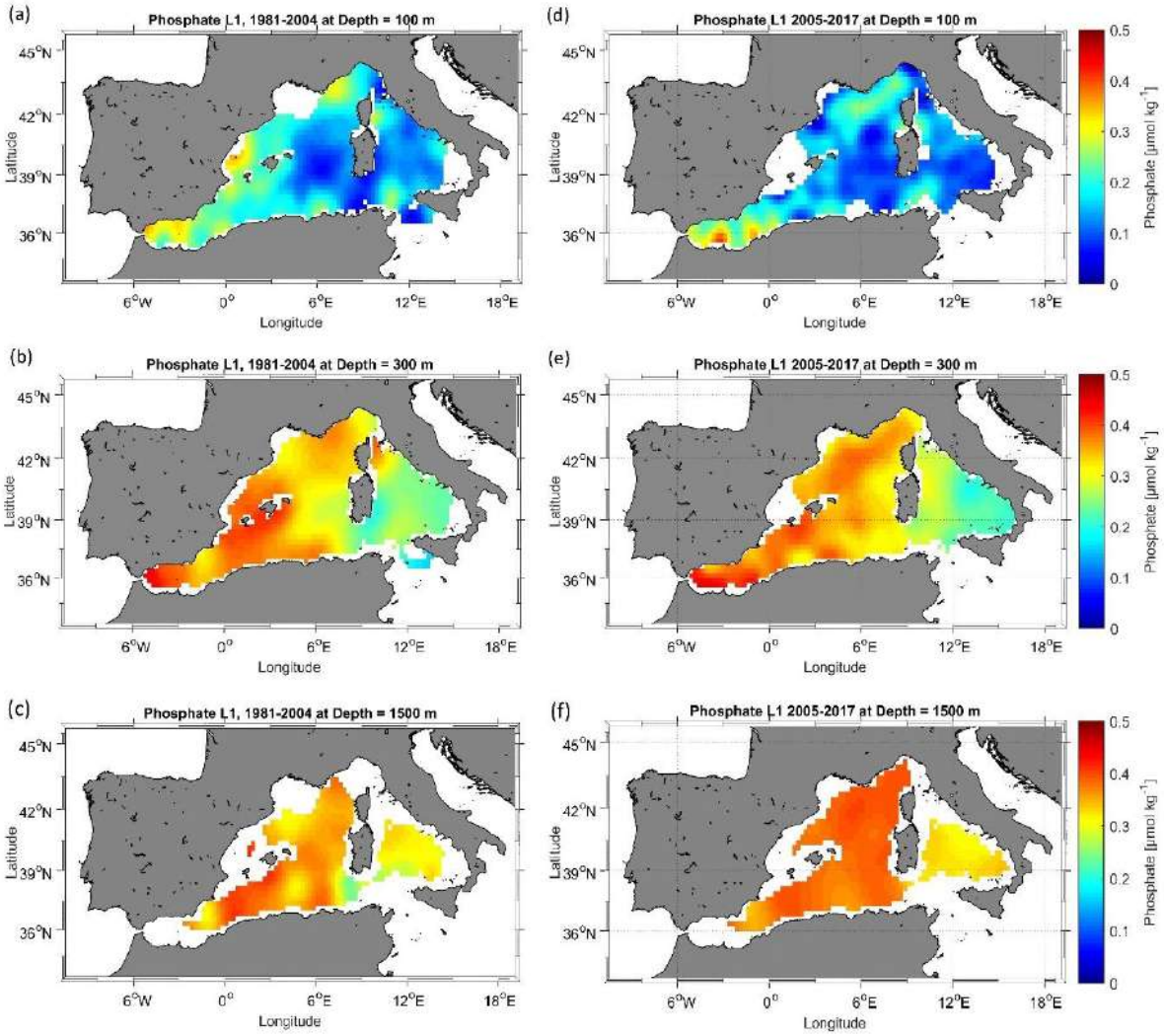

Figure 4.18: The same as Fig. 4.17 but for phosphate.

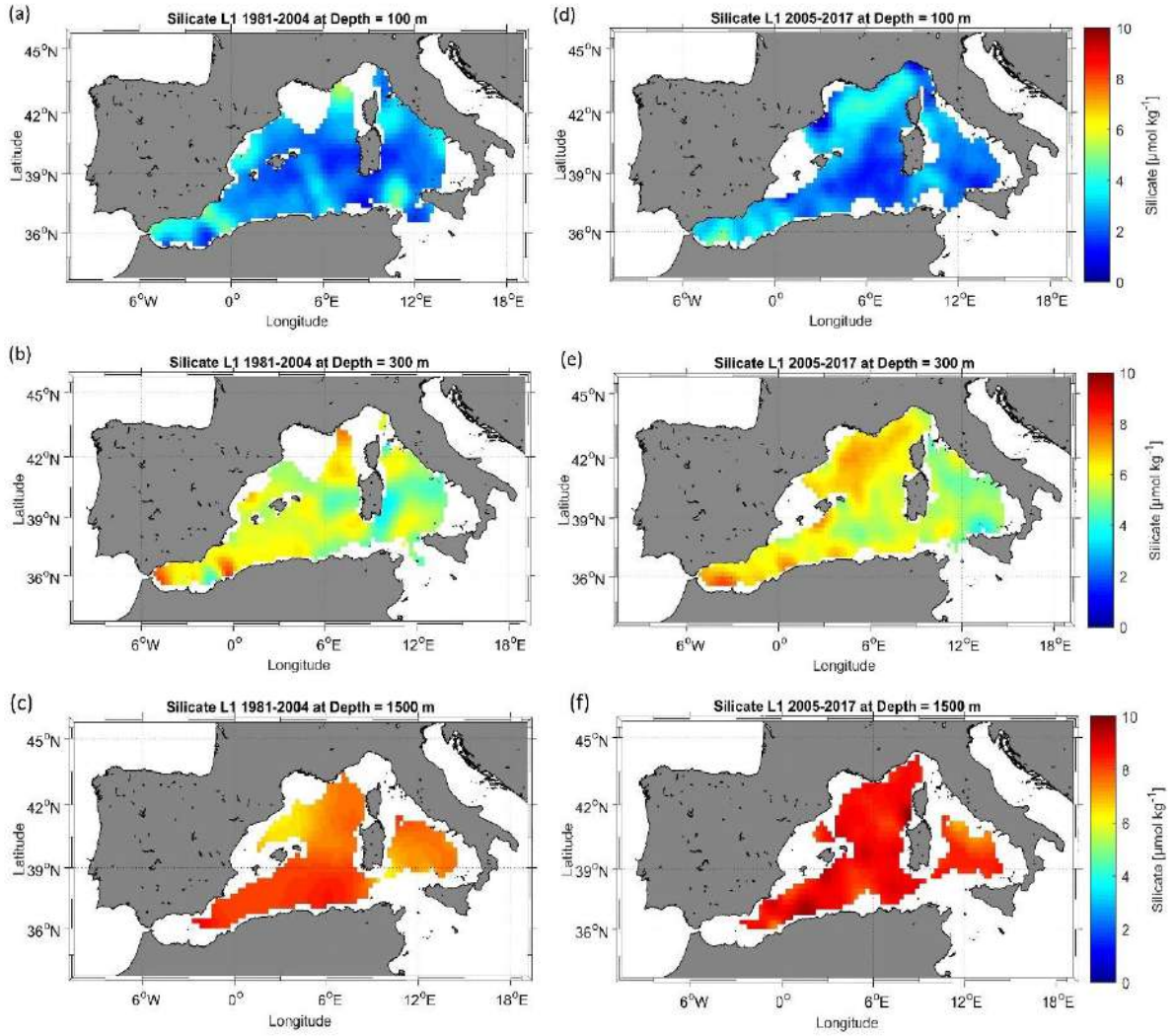

Figure 4.19: The same as Fig. 4.17 but for silicate.

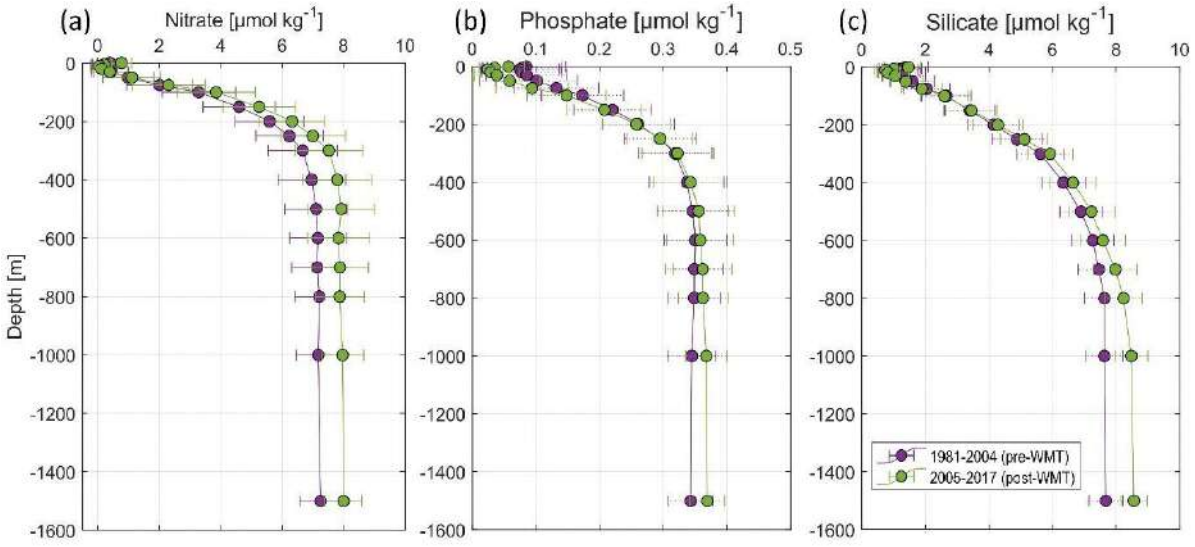

Figure 4.20: Mean vertical profile and standard deviation of (a) nitrate, (b) phosphate and (c) silicate over the WMED before (1981-2004, in violet) and after WMT (2005-2017, in green).

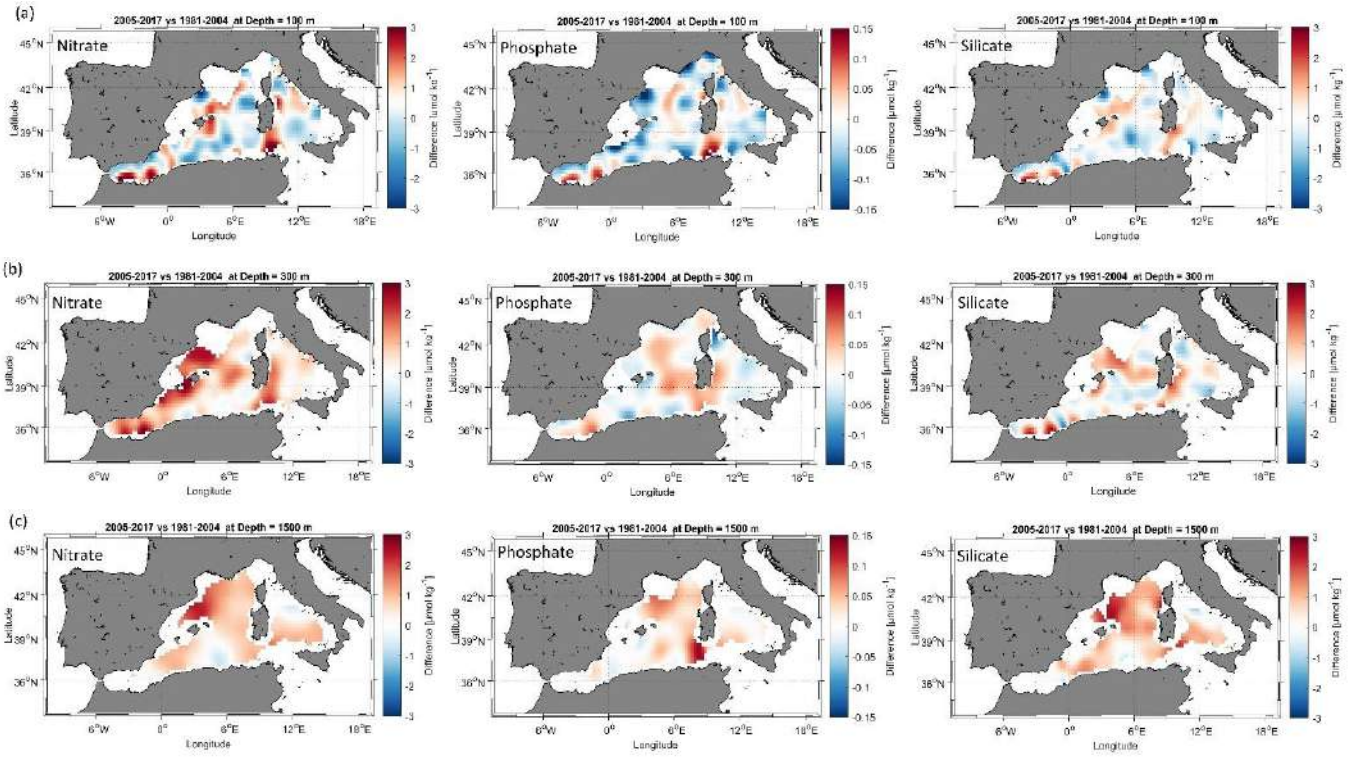

Figure 4.21: (a) Difference field at 100 m between the 1981-2004 and the 2005-2017 climatologies; (b) Difference field at 300 m (c) Difference field at 1500 m.

4.6 Conclusion

This chapter presented reconstructions of climatological fields of nitrate, phosphate, and silicate, using an important dataset collection spanning the period 1981 and 2017. The BGC-WMED product (BGC-WMED, Belgacem et al., in preparation) is generated on 19 vertical levels on 1/4° spatial resolution grid. The new product represents very well spatial patterns about nutrient distribution because of its higher spatial and temporal data coverage, it is contributing to the understanding of the spatial and temporal distribution of nutrients in the WMED.

The novelty of the present work is the use of the variational analysis for the climatological maps production, that takes into consideration physical , geographical boundaries and topography and the resulting estimate of associated error field.

The new product represents very well spatial patterns about nutrient distribution and agrees with previous studies and records. The reference products: WOA18 and medBFM biogeochemical reanalysis tend to underestimate nutrient distribution when compared to the BGC-WMED product. Detail patterns related to the strong east-west gradient of nitrate, phosphate and silicate and vertical features have been presented.

No seasonal or annual analysis fields have been produced because the amount of data and their distribution in time did not allow to do so. However, the aggregated dataset does show improvements in describing the spatial distribution of inorganic nutrients in the WMED with respect to previous studies.

It is acknowledged that computing a climatological mean over a time period is not enough to estimate and detect the 'WMT' driven trend. However, comparing climatologies based on the two time periods: 1981-2004 (pre-WMT) and 2005 -2017 (post-WMT) has already produced important results, since notable changes have been found in nutrient distribution after the WMT at various depths.

The results support the tendency to an increasing load of inorganic nutrients to the WMED and possibly relate to change in general circulation patterns, in deep stratification and warming trends. This, however, remains to be confirmed.

The BGC-WMED is a local, regional climatology, that allows the identification of a substantial enrichment of the waters, except for the Tyrrhenian Sea where the waters are depleted in nutrients with respect to the westernmost area of the WMED. The climatology gives information about the spreading of inorganic nutrients inside the WMED at surface, intermediate and deep layers.

Future work will focus on better understanding of the change in nutrients related to water masses associated with ventilation rate, using climatological fields along isopycnal surfaces instead of depths.

Chapter 5. DISCUSSION AND CONCLUSIONS

5.1 Summary

The thesis is an extensive description of the variability in space and time of inorganic nutrients (nitrate, phosphate, and silicate) within the Western Mediterranean Sea (WMED). Specific discussions and conclusions have been given at the end of each chapter.

After the general introduction to the Biogeochemical processes and the Study area (Mediterranean Sea) in Chapter 1, I worked on quality control and processing of a new database of in-situ measurements in Chapter 2. A new internally consistent data product for the WMED has been released, despite the known scarcity and disparity of the measurements found in the region, enabling biogeochemical insights about the variability of nitrate, phosphate and silicate between subregions with peculiar circulation features for the time period (2004-2017) in Chapter 3. An updated understanding for the WMED biogeochemistry is presented in Chapter 4, using a larger time span dataset for in-situ nutrient through the climatological analysis of two time periods (1981-2004, 2005-2017), highlighting a notable change in the nutrient concentrations at different depth levels. The proposed biogeochemical products are in good agreement with previous datasets and analysis.

The outputs of the Thesis were providing a quality controlled publicly available data product of inorganic nutrient measurement in the WMED, the second output is the climatological analysis that provided an atlas of nitrate, phosphate and silicate with spatial resolution and good data coverage. I compared the new product to the Word Ocean Atlas 2018 and the medBFM model reanalysis. The regional product allowed more detailed analysis with respect to other products with lower resolution. This regional climatology represents a high-resolution baseline dataset to compare with models for validation or for assimilation in model reanalysis.

5.1.1 Research questions

- *Are the CNR-WMED biogeochemical observations consistent with previous measurements in the region?*

The work done to fulfill the consistency analysis using unpublished cruise data, including nitrate, phosphate, silicate, salinity and temperature measurements in the Western Mediterranean Sea, resulted in an accurate, internally consistent and high-quality biogeochemical data product CNR_DIN_WMED_20042017 (Chapter 2).

The assessed data set issued a quality controlled final product from 24 cruises containing 870 nutrient profiles with a total of 9647 nitrate samples, 9666 phosphate samples and 9641 silicate samples spanning the period from 2004 to 2017.

The secondary quality control used the crossover analysis. The secondary quality control routines were developed by Lauvset and Tanhua (2015), and was used to estimate correction in the CARINA (Hoppema et al., 2009) and GLODAPv2.2019 (Olsen et al., 2019) databases.

The method suggests adjustments that reduce biases, increase accuracy, and allow for the inter-comparison between data from various sources. The approach was based on comparing cruise data to high-quality reference data set of the region in order to identify bias and compute adjustments factor that minimizes the offsets between cruise data.

Average adjustment correction factors were 1.06 for nitrate, 1.14 for phosphate and 1.14 for silicate, respectively.

Quality assurance was fundamental for the PhD project to obtain a long-term, quality controlled, and internally consistent data product.

A good quality dataset is a fundamental prerequisite to remove any errors in the observations in order to have accurate results.

- *Is there a regional difference in remineralization ratios in the WMED and is the nutrient variability dependent on physical properties of subregions?*

The resulting data product was used to present a synthesis picture in which we can observe the interaction between chemical and biological processes. These processes are connected with each other so that oxygen, nitrate, phosphate, and silicate concentrations vary following a constant Redfield ratio (Chapter 3). On average, the availability of nutrients is matched to the needs of phytoplankton.

The WMED was divided into five regions based on circulation patterns and topography.

Upwelling regions, and areas of winter convection support primary productivity in the euphotic layer, by fertilizing the surface layer. These processes are one of the main drivers of the higher N:P ratio in the surface layer of Alboran Sea (N:P=15.7) and the Northern WMED (N:P=13.5).

There is a vertical gradient in dissolved inorganic nutrients with depth with a decreasing trend of N:P ratio and increase in Si:N ratio at greater depths. Ratios varied from East to West.

The changes observed in the surface, intermediate and deep layers in nutrient content and ratios gave insight about the changes in the AW, IW and WMDW fingerprints of nutrients along their paths.

The AW crosses the strait of Gibraltar toward the Alboran Sea , where the highest content in nutrient and low dissolved oxygen are noted. N:P ratio was the largest found in the surface layer and the closest to Redfield standards (Si: N:P:O_2= 15:16:1:138, Redfield et al., 1963).

Surface waters evolve along their path, mixing with other resident water masses, interacting with the local atmosphere eventually causing the loss or gain in nutrients. This can be seen in the change of ratios in the five subregions.

In the intermediate layer, ratios change from one region to the other as well.

An intense chemical activity was found below the surface layer, that is made of organic matter remineralization and accumulation of nutrients.

The water masses in the easternmost subregions were low in nutrients and exhibited high ratios: of AOU:N, AOU:P, Si:N, N:P relative to the water masses of the Westernmost subregions.

- *What could cause the vertical gradient in nutrients?*

Sinking organic matter at different depth levels leads to accumulation of inorganic nutrients in the deep layers. This process may vary regionally to another, depending on the initial values found in the surface layer, local events, atmospheric and terrestrial inputs, and inflow of depleted waters from the EMED.

Comparing the three nutrients at the same depth levels, at the surface (100 m), it appears that nitrate , phosphate and silicate show local surface maximums, because of local environmental conditions such as strong winds, river discharge, upwelling and intense vertical mixing (Ludwig et al., 2010); in the Gulf of Lion for example, because of the density gradient, only vertical mixing can load nutrients responsible for fertilizing locally the surface layer.
In other areas, the surface layer depletion in nutrients is due to the export of organic matter to intermediate and deep layers leading.

In the western side of the WMED, intermediate and deep layers show an increase in nutrients. Schroeder et al. (2020) explained this increase in nitrate and phosphate at the intermediate layer with the increase of the remineralization rate at these depths along the path of IW.

The deficiency of inorganic nutrients is explained by the effect of the anti-estuarine circulation, with the IW coming from the EMED, which is known to be poor in nutrients (Krom et al., 2014; Schroeder et al., 2020), accumulating nutrients along its path. Eventually, this relative nutrient-rich Mediterranean outflow is dispersed to the Atlantic Ocean.
Overall, in the surface layer, circulation, physical processes, and vertical mixing increase nutrient input while the biological pump controls the decrease.
In the deep layer, the variability is lower, the physical processes decrease nutrients and the biological pump through remineralization of the sinking organic matter, increase them. In the WMED, the deep layer could represent a source of nutrients.

- *Is climate change impacting the shift in biogeochemical properties and what are the sources of nutrient variability?*

To understand the spatial and the temporal change in nutrients, climatological analysis was conducted (Chapter4). I added data from other sources to have a better spatial and temporal coverage.

I had the opportunity to use the last version of DIVAnd variational analysis for the generation of climatological maps production and a new product that represents with high degree of detail spatial patterns about nutrients distribution. Overall, this product agrees with previous studies and records. The new climatology was compared to WOA18 and medBFM biogeochemical model reanalysis. Detailed patterns related to the strong east-west gradient of nitrate, phosphate and silicate and vertical features have been presented.

The comparison of climatologies based on the two time periods. i.e. 1981-2004 (pre-WMT) and 2005 -2017 (post-WMT), has already produced important results (Chapter 4). Notable changes have been found in nutrient distribution after the WMT at various depths. The analysis was performed on depth layers in order to follow the nitrate, phosphate and silicate change along the water column and investigate nutrients in the depth of the main water masses of the WMED. A collection of a dataset spanning the years 1981 to 2017 was used.

The results support the tendency to an increasing load of inorganic nutrients in the WMED and relate the changes with respect to the general circulation patterns.

It is known that the result of the western Mediterranean transition (WMT, since 2005) is a new deep water that is denser, saltier, and warmer than the old WMDW. Studies have agreed about an overall increase in temperature (Bindoff et al., 2007), salinity and density of intermediate and deep layers after this event (Schroeder et al., 2016; Vargas-yáñez, 2017) and a recent study of Li and Tanhua (2020) demonstrated an enhanced ventilation in deep layer over time in the WMED.

The change in ventilation has impacted the distribution of nutrients thus influenced biogeochemical cycles.

An increased ventilation means an increase in dissolved oxygen in the sea interior, implying an increase in mineralization rate consequently, in dissolved nutrients. However, oxygen is consumed over time by biological activity leading to the decline of the oxygen content, which in turns accelerates the denitrification, a nitrate sink, and promotes the release of phosphate in the case of an increase in temperature (Watson et al., 2017).

The new regional climatology has allowed the identification of a substantial relative increase in nutrients.

In fact, the comparison between the climatological periods post-WMT (2005-2017) and pre-WMT (1981-2004) shows a considerable overall increase in the mean nutrient concentrations

at different depth levels. Changes in the nutrient content of deep-water nutrient pools is a potential source of variability that will impact the supply of nutrients to the euphotic layer.

After the WMT, the Intermediate and deep layers are very well oxygenated, nutrient horizontal distribution shows a significant higher concentration in the three-nutrient compared to the pre-WMT period.
This change could also be explained by the low rate of denitrification for nitrate or also an increased nitrification leading to the increase in the remineralization of organic matter, enriching the deep layer in nitrate. As for the phosphate, the source is likely to come from land-based emissions.
The impact of increased temperature of the sea water triggered longer stratification episodes, inhibiting the diapycnal supply and transport of nutrients, thus nutrients are entrained for longer time.
On average, the difference between the two periods (pre/post-WMT) for nitrate, phosphate, and silicate, at 300 m depth, are +0.86, +0.007 and +0.21 μmol kg^{-1} ,respectively.
Variations at 1500 m were of the order of + 0.75 μmol kg^{-1} on nitrate average, +0.025 μmol kg^{-1} on phosphate average and + 0.86 μmol kg^{-1} on silicate average.

5.1.2 WMED biogeochemical characteristic

In this thesis project, the general biogeochemistry of the WMED has been deeply explored.

The easternmost region of the WMED is under the direct impact of the EMED. IW from the east, is depleted in nutrients responsible for the reduced content in the Sicily Channel and the Tyrrhenian Sea, while in the northern WMED, Ligurian Sea and Alboran Sea, deep convection and upwelling are responsible for the local nutrient enrichment in the surface layer.

The increased oligotrophy toward east is obvious and demonstrates the role of the anti-estuarine circulation where there is a lateral circulation of water masses and inflow of nutrients.

The remineralization ratio showed differences between regions and a clear decrease from east to west at the different depth ranges.

The oxygen utilization vs. nitrate, phosphate, and silicate ratio demonstrates a decreasing trend toward deeper layers. The highest ratios were found in the intermediate layer.

An active vertical transport of silicate is responsible for the high Si:N in the intermediate and deep layers; in addition to that the increased temperature in the intermediate layer accelerates the dissolution of biogenic silicate, eventually increasing the input of silicate in deep layers.

The analysis suggests that the WMED exhibits regional differences depending on the internal dynamics of each region. Variability in ratios evidences that the WMED is characterized by the

coexistence of different biogeochemical regimes as already been reported (D'Ortenzio and Ribera d'Alcalà, 2009; Lazzari et al., 2012; Siokou-Frangou et al., 2010).

The climatological distribution of inorganic nutrient and ratio analysis showed that nutrient enrichment of the WMED waters could be interpreted in relation to the circulation of the water masses.

The WMDW by occupying the deep layer could be considered as a source of nutrients in the WMED. Changes in thermohaline circulation could impact change in the water mass properties thus differences in the nutrient content. The WMT had an impact on nutrient content in the WMED.

5.2 Perspective and future work

The climatology presented in Chapter 4 showed horizontal maps at depth layers. The vertical resolution can be modified using isopycnal surfaces, i.e. surface of constant potential density, instead of depths. It is useful to consider the change in nutrient distribution of deep water masses along such surfaces.

The warming and stratification of the water column would produce a decrease in dissolved oxygen solubility, a reduced ventilation rate and a decrease in marine source nutrient. To have a complete picture about changes in inorganic nutrients, investigating the change in dissolved oxygen is important, through the study of long-term trends of nutrient and apparent oxygen utilization at deep layers.

Following the nutricline depth, i.e. the layer of maximum vertical gradient in nutrient concentrations, the dissolved oxygen minimum, along repeated transects is important to better understand the vertical exchange of nutrients between subregions.

In addition to the water masses circulation and the physical processes occurring in the different regions, the variation in ratio is also impacted by the regional differences in phytoplankton composition. Changes in nutrients should also be related to the composition/size of phytoplankton communities that vary among different regions.

REFERENCES

Alvarez-Borrego, S., Gordon, L. I., Jones, L. B., Park, P. K. and Pytkowicz, R. M.: Oxygen-carbon dioxide-nutrients relationships in the Southeastern Region of the Bering Sea, J. Oceanogr. Soc. Japan, 28(2), 71–93, doi:10.1007/BF02109722, 1972.

Aoyama, M., Woodward, E. Malcolm S. Bakker, K., Becker, S., Björkman, K., Daniel, A., Mahaffey, C., Murata, A., Naik, H., Tanhua, T., Rho, T., Roman, R. and Sloyan, B.: Comparability of oceanic nutrient data., 2016.

Barth, A., Troupin, C., Alvera-Azcárate, A. and Vandenbulcke, L.: Divand-1.0: N-dimensional variational data analysis for ocean observations, Geosci. Model Dev., 7(1), 225–241, doi:10.5194/gmd-7-225-2014, 2014.

Becker, S., Aoyama, M., Woodward, E. M. S., Bakker, K., Coverly, S., Mahaffey, C. and Tanhua, T.: GO-SHIP Repeat Hydrography Nutrient Manual: The precise and accurate determination of dissolved inorganic nutrients in seawater, using Continuous Flow Analysis methods., Go-sh. Progr. SCOR, 49, doi:10.25607/OBP-555, 2019.

Beckers, J. M., Barth, A., Troupin, C. and Alvera-Azcárate, A.: Approximate and efficient methods to assess error fields in spatial gridding with data interpolating variational analysis (DIVA), J. Atmos. Ocean. Technol., 31(2), 515–530, doi:10.1175/JTECH-D-13-00130.1, 2014.

Belgacem, M., Chiggiato, J., Borghini, M., Pavoni, B., Cerrati, G., Acri, F., Cozzi, S., Ribotti, A., Álvarez, M., Lauvset, S. K. and Schroeder, K.: Dissolved inorganic nutrients in the western Mediterranean Sea (2004-2017), Earth Syst. Sci. Data, 12(3), 1985–2011, doi:10.5194/essd-12-1985-2020, 2020.

Bethoux, J. P.: Oxygen consumption, new production, vertical advection and environmental evolution in the Mediterranean Sea, Deep Sea Res. Part A, Oceanogr. Res. Pap., 36(5), 769–781, doi:10.1016/0198-0149(89)90150-7, 1989.

Bethoux, J. P., Morin, P., Madec, C. and Gentili, B.: Phosphorus and nitrogen behaviour in the Mediterranean Sea, Deep Sea Res. Part A, Oceanogr. Res. Pap., 39(9), 1641–1654, doi:10.1016/0198-0149(92)90053-V, 1992.

Bethoux, J. P., Gentili, B., Morin, P., Nicolas, E., Pierre, C. and Ruiz-Pino, D.: The Mediterranean Sea : a miniature ocean for climatic and environmental studies and a key for the climatic funcioning of the North Atlantic, Prog. Oceanogr., 44, 131–146, 1999.

Béthoux, J. P., Morin, P., Chaumery, C., Connan, O., Gentili, B. and Ruiz-Pino, D.: Nutrients in the Mediterranean Sea, mass balance and statistical analysis of concentrations with respect to environmental change, Mar. Chem., 63(1–2), 155–169, doi:10.1016/S0304-4203(98)00059-0, 1998.

Béthoux, J. P., Morin, P. and Ruiz-Pino, D. P.: Temporal trends in nutrient ratios: Chemical evidence of Mediterranean ecosystem changes driven by human activity, Deep. Res. Part II

Top. Stud. Oceanogr., 49(11), 2007–2016, doi:10.1016/S0967-0645(02)00024-3, 2002.

Beuvier, J., Béranger, K., Lebeaupin Brossier, C., Somot, S., Sevault, F., Drillet, Y., Bourdallé-Badie, R., Ferry, N. and Lyard, F.: Spreading of the Western Mediterranean Deep Water after winter 2005: Time scales and deep cyclone transport, J. Geophys. Res. Ocean., 117(C7), n/a-n/a, doi:10.1029/2011jc007679, 2012.

Bianchi, C. N. and Morri, C.: Marine biodiversity of the Mediterranean Sea: Situation, problems and prospects for future research, Mar. Pollut. Bull., 40(5), 367–376, doi:10.1016/S0025-326X(00)00027-8, 2000.

Boyd, P. W.: Beyond ocean acidification, Nat. Geosci., 4(5), 273–274, doi:10.1038/ngeo1150, 2011.

Brankart, J. M. and Brasseur, P.: The general circulation in the Mediterranean Sea: A climatological approach, J. Mar. Syst., 18(1–3), 41–70, doi:10.1016/S0924-7963(98)00005-0, 1998.

Brasseur, P., Beckers, J. M., Brankart, J. M. and Schoenauen, R.: Seasonal temperature and salinity fields in the Mediterranean Sea: Climatological analyses of a historical data set, Deep. Res. Part I Oceanogr. Res. Pap., 43(2), 159–192, doi:10.1016/0967-0637(96)00012-X, 1996.

Brasseur, P. P.: A variational inverse method for the reconstruction of general circulation fields in the northern Bering Sea, J. Geophys. Res., 96(C3), 4891, doi:10.1029/90jc02387, 1991.

Buga, L., Eilola, K., Wesslander, K., Fryberg, L., Gatti, J., Leroy, D., Iona, S., Tsompanou, M. and Lipizer, M.: EMODnet Thematic Lot n ° 4 / SI2 . 749773 Interpolating Variational Analysis (DIVA). Release 2018, , doi:10.6092/A8CFB472-10DB-4225-9737-5A60DA9AF523, 2019.

Crombet, Y., Leblanc, K., Quéuiner, B., Moutin, T., Rimmelin, P., Ras, J., Claustre, H., Leblond, N., Oriol, L. and Pujo-Pay, M.: Deep silicon maxima in the stratified oligotrophic Mediterranean Sea, Biogeosciences, 8(2), 459–475, doi:10.5194/bg-8-459-2011, 2011.

D'Ortenzio, F. and Ribera d'Alcalà, M.: On the trophic regimes of the Mediterranean Sea: a satellite analysis, Biogeosciences Discuss., 5(4), 2959–2983, doi:10.5194/bgd-5-2959-2008, 2009.

D'Ortenzio, F., Taillandier, V., Claustre, H., Prieur, L. M., Leymarie, E., Mignot, A., Poteau, A., Penkerc, C. and Schmechtig, C. M.: Biogeochemical Argo : The Test Case of the NAOS Mediterranean Array, , 7(March), 1–16, doi:10.3389/fmars.2020.00120, 2020.

DeMaster, D. J.: The accumulation and cycling of biogenic silica in the Southern Ocean: Revisiting the marine silica budget, Deep. Res. Part II Top. Stud. Oceanogr., 49(16), 3155–3167, doi:10.1016/S0967-0645(02)00076-0, 2002.

Desroziers, G., Berre, L., Chapnik, B. and Poli, P.: Diagnosis of observation, background and analysis-error statistics in observation space, Q. J. R. Meteorol. Soc., 131(613), 3385–3396, doi:10.1256/qj.05.108, 2005.

Diaz, P., Raimbault, F., Boudjellal, B., Garcia, N. and Moutin, T.: Early spring phosphorus

limitation of primary productivity in a NW Mediterranean coastal zone (Gulf of Lions), Mar. Ecol. Prog. Ser., 211(McGill 1965), 51–62, doi:10.3354/meps211051, 2001.

Dickson, A. G., Afghan, J. D. and Anderson, G. C.: Reference materials for oceanic CO2 analysis: A method for the certification of total alkalinity, Mar. Chem., 80(2–3), 185–197, doi:10.1016/S0304-4203(02)00133-0, 2003.

Dugdale, R. C., Wilkerson, F. P. and Minas, H. J.: The role of a silicate pump in driving new production, Deep. Res. Part I, 42(5), 697–719, doi:10.1016/0967-0637(95)00015-X, 1995.

Falkowski, P. G., Barber, R. T. and Smetacek, V.: Biogeochemical controls and feedbacks on ocean primary production, Science (80-.)., 281(5374), 200–206, doi:10.1126/science.281.5374.200, 1998.

Fichaut, M., Garcia, M. J., Giorgetti, A., Iona, A., Kuznetsov, A., Rixen, M. and Group, M.: MEDAR/MEDATLAS 2002: A Mediterranean and Black Sea database for operational oceanography, Elsevier Oceanogr. Ser., 69(C), 645–648, doi:10.1016/S0422-9894(03)80107-1, 2003.

de Fommervault, O. P., Migon, C., Dufour, A., D'Ortenzio, F., Kessouri, F., Raimbault, P., Garcia, N. and Lagadec, V.: Atmospheric input of inorganic nitrogen and phosphorus to the Ligurian Sea: Data from the Cap Ferrat coastal time-series station, Deep. Res. Part I Oceanogr. Res. Pap., 106, 116–125, doi:10.1016/j.dsr.2015.08.010, 2015a.

de Fommervault, O. P., Migon, C., D'Ortenzio, F., Ribera d'Alcalà, M. and Coppola, L.: Temporal variability of nutrient concentrations in the northwestern Mediterranean sea (DYFAMED time-series station), Deep. Res. Part I Oceanogr. Res. Pap., 100, 1–12, doi:10.1016/j.dsr.2015.02.006, 2015b.

Fommervault, O. P. De, Migon, C., Ortenzio, F. D., Alcala, M. R. D., Coppola, L., Fommervault, O. P. De, Migon, C., Ortenzio, F. D. and Alcala, M. R. D.: Temporal variability of nutrient concentrations in the northwestern Mediterranean sea (DYFAMED time-series station) To cite this version : HAL Id : hal-01130192, Deep. Res. Part I, doi:10.1016/j.dsr.2015.02.006, 2015.

Frings, P. J., Clymans, W., Fontorbe, G., De La Rocha, C. L. and Conley, D. J.: The continental Si cycle and its impact on the ocean Si isotope budget, Chem. Geol., 425, 12–36, doi:10.1016/j.chemgeo.2016.01.020, 2016.

García-Martínez, M. del C., Vargas-Yáñez, M., Moya, F., Santiago, R., Muñoz, M., Reul, A., Ramírez, T. and Balbín, R.: Average nutrient and chlorophyll distributions in the western Mediterranean: RADMED project, Oceanologia, 61(1), 143–169, doi:10.1016/j.oceano.2018.08.003, 2019.

Garcia, H. E., Weathers, K. W., Paver, C. R., Smolyar, I., Boyer, T. P., Locarnini, R. A., Zweng, M. M., Mishonov, A. V., Baranova, O. K., Seidov, D. and Reagan, J. R.: World Ocean Atlas 2018. Vol. 4: Dissolved Inorganic Nutrients (phosphate, nitrate and nitrate+nitrite, silicate)., 2019.

Geider, R. J. and La Roche, J.: Redfield revisited: Variability of C:N:P in marine microalgae and

its biochemical basis, Eur. J. Phycol., 37(1), 1–17, doi:10.1017/S0967026201003456, 2002.

Giorgi, F.: Climate change hot-spots, Geophys. Res. Lett., 33(8), 1–4, doi:10.1029/2006GL025734, 2006.

Gouretski, V. V. and Jancke, K.: Systematic errors as the cause for an apparent deep water property variability: Global analysis of the WOCE and historical hydrographic data, Prog. Oceanogr., 48(4), 337–402, doi:10.1016/S0079-6611(00)00049-5, 2001.

Hecht, A., Pinardi, N. and Robinson, A. R.: Currents, Water Masses, Eddies and Jets in the Mediterreanean Levantine Basin, J. Phys. Oceanogr., 18(10), 1320–1353, 1988.

Hoppema, M., Velo, A., van Heuven, S., Tanhua, T., Key, R. M., Lin, X., Bakker, D. C. E., Perez, F. F., Ríos, A. F., Lo Monaco, C., Sabine, C. L., Álvarez, M. and Bellerby, R. G. J.: Consistency of cruise data of the CARINA database in the Atlantic sector of the Southern Ocean, Earth Syst. Sci. Data, 1(1), 63–75, doi:10.5194/essd-1-63-2009, 2009.

Huertas, I. E., Ríos, A. F., García-Lafuente, J., Navarro, G., Makaoui, A., Snchez-Romn, A., Rodriguez-Galvez, S., Orbi, A., Ruíz, J. and Pérez, F. F.: Atlantic forcing of the Mediterranean oligotrophy, Global Biogeochem. Cycles, 26(2), doi:10.1029/2011GB004167, 2012.

Johnson, G. C., Robbins, P. E. and Hufford, G. E.: Systematic adjustments of hydrographic sections for internal consistency, J. Atmos. Ocean. Technol., 18(7), 1234–1244, doi:10.1175/1520-0426(2001)018<1234:SAOHSF>2.0.CO;2, 2001.

Jutterström, S., Anderson, L. G., Bates, N. R., Bellerby, R., Johannessen, T., Jones, E. P., Key, R. M., Lin, X., Olsen, A. and Omar, A. M.: Arctic Ocean data in CARINA, Earth Syst. Sci. Data, 2, 71–78, doi:10.5194/essd-2-71-2010, 2010.

Key, R. M., Kozyr, A., Sabine, C. L., Lee, K., Wanninkhof, R., Bullister, J. L., Feely, R. A., Millero, F. J., Mordy, C. and Peng, T. H.: A global ocean carbon climatology: Results from Global Data Analysis Project (GLODAP), Global Biogeochem. Cycles, 18(4), 1–23, doi:10.1029/2004GB002247, 2004.

Kress, N. and Herut, B.: Spatial and seasonal evolution of dissolved oxygen and nutrients in the Southern Levantine Basin (Eastern Mediterranean Sea): Chemical characterization of the water masses and inferences on the N : P ratios, Deep. Res. Part I Oceanogr. Res. Pap., 48(11), 2347–2372, doi:10.1016/S0967-0637(01)00022-X, 2001.

Krom, M. D., Kress, N., Brenner, S. and Gordon, L. I.: Phosphorus limitation of primary productivity in the eastern Mediterranean Sea, Limnol. Oceanogr., 36(3), 424–432, doi:10.4319/lo.1991.36.3.0424, 1991.

Krom, M. D., Oceanographic, I. and Shikmona, T.: Nutrient budget for the Eastern Mediterranean : Implications for phosphorus limitation, , 49(5), 1582–1592, 2004.

Krom, M. D., Woodward, E. M. S., Herut, B., Kress, N., Carbo, P., Mantoura, R. F. C., Spyres, G., Thingsted, T. F., Wassmann, P., Wexels-Riser, C., Kitidis, V., Law, C. and Zodiatis, G.: Nutrient cycling in the south east Levantine basin of the eastern Mediterranean: Results from a

phosphorus starved system, Deep. Res. Part II Top. Stud. Oceanogr., 52(22–23), 2879–2896, doi:10.1016/j.dsr2.2005.08.009, 2005.

Krom, M. D., Emeis, K. C. and Van Cappellen, P.: Why is the Eastern Mediterranean phosphorus limited?, Prog. Oceanogr., 85(3–4), 236–244, doi:10.1016/j.pocean.2010.03.003, 2010.

Krom, M. D., Kress, N. and Fanning, K.: Silica cycling in the ultra-oligotrophic eastern Mediterranean Sea, Biogeosciences, 11(15), 4211–4223, doi:10.5194/bg-11-4211-2014, 2014.

Lascaratos, A., Roether, W. and Nittis, K.: Recent changes in deep water formation and spreading in the eastern Mediterranean Sea : a review, , 44, 5–36, 1999.

Lauvset, S. K. and Tanhua, T.: A toolbox for secondary quality control on ocean chemistry and hydrographic data, Limnol. Oceanogr. Methods, 13(11), 601–608, doi:10.1002/lom3.10050, 2015.

Lauvset, S. K., Key, R. M., Olsen, A., Van Heuven, S., Velo, A., Lin, X., Schirnick, C., Kozyr, A., Tanhua, T., Hoppema, M., Jutterström, S., Steinfeldt, R., Jeansson, E., Ishii, M., Perez, F. F., Suzuki, T. and Watelet, S.: A new global interior ocean mapped climatology: The 1° × 1° GLODAP version 2, Earth Syst. Sci. Data, 8(2), 325–340, doi:10.5194/essd-8-325-2016, 2016.

Lavigne, H.: On the vertical distribution of the chlorophyll a concentration in the Mediterranean Sea : a basin scale and seasonal approach, , (March), doi:10.5194/bgd-12-4139-2015, 2015.

Lazzari, P., Solidoro, C., Ibello, V., Salon, S., Teruzzi, A., Béranger, K., Colella, S. and Crise, A.: Seasonal and inter-annual variability of plankton chlorophyll and primary production in the Mediterranean Sea: A modelling approach, Biogeosciences, 9(1), 217–233, doi:10.5194/bg-9-217-2012, 2012.

Lazzari, P., Solidoro, C., Salon, S. and Bolzon, G.: Spatial variability of phosphate and nitrate in the Mediterranean Sea: A modeling approach, Deep. Res. Part I Oceanogr. Res. Pap., 108, 39–52, doi:10.1016/j.dsr.2015.12.006, 2016.

Lejeusne, C., Chevaldonné, P., Pergent-Martini, C., Boudouresque, C. F. and Pérez, T.: Climate change effects on a miniature ocean: the highly diverse, highly impacted Mediterranean Sea, Trends Ecol. Evol., 25(4), 250–260, doi:10.1016/j.tree.2009.10.009, 2010.

Levitus, S.: Climatological Atlas of the World Ocean, Eos, Trans. Am. Geophys. Union, 64(49), 962–963, doi:10.1029/EO064i049p00962-02, 1982.

Li, P. and Tanhua, T.: Recent Changes in Deep Ventilation of the Mediterranean Sea; Evidence From Long-Term Transient Tracer Observations, Front. Mar. Sci., 7(July), 1–23, doi:10.3389/fmars.2020.00594, 2020.

Lipizer, M., Partescano, E., Rabitti, A., Giorgetti, A. and Crise, A.: Qualified temperature, salinity and dissolved oxygen climatologies in a changing Adriatic Sea, Ocean Sci., 10(5), 771–797, doi:10.5194/os-10-771-2014, 2014.

Lucea, A., Duarte, C. M. and Agustı, S.: Nutrient (N , P and Si) and carbon partitioning in the

stratified NW Mediterranean, , 49, 157–170, doi:10.1016/S1385-1101(03)00005-4, 2003.

Ludwig, W., Dumont, E., Meybeck, M. and Heussner, S.: River discharges of water and nutrients to the Mediterranean and Black Sea: Major drivers for ecosystem changes during past and future decades?, Prog. Oceanogr., 80(3–4), 199–217, doi:10.1016/j.pocean.2009.02.001, 2009.

Ludwig, W., Bouwman, A. F., Dumont, E. and Lespinas, F.: Water and nutrient fluxes from major Mediterranean and Black Sea rivers: Past and future trends and their implications for the basin-scale budgets, Global Biogeochem. Cycles, 24(4), 1–14, doi:10.1029/2009GB003594, 2010.

Maillard, C., Lowry, R., Maudire, G. and Schaap, D.: SeaDataNet: Development of a Pan-European infrastructure for ocean and marine data management, in OCEANS 2007 - Europe., 2007.

Manca, B., Burca, M., Giorgetti, A., Coatanoan, C., Garcia, M. J. and Iona, A.: Physical and biochemical averaged vertical profiles in the Mediterranean regions: An important tool to trace the climatology of water masses and to validate incoming data from operational oceanography, J. Mar. Syst., 48(1–4), 83–116, doi:10.1016/j.jmarsys.2003.11.025, 2004.

Migon, C., Nival, P. and Sciandra, A.: The Mediterranean Sea in the Era of Global Change 1., 2020.

Míguez, B. M., Novellino, A., Vinci, M., Claus, S., Calewaert, J. B., Vallius, H., Schmitt, T., Pititto, A., Giorgetti, A., Askew, N., Iona, S., Schaap, D., Pinardi, N., Harpham, Q., Kater, B. J., Populus, J., She, J., Palazov, A. V., McMeel, O., Oset, P., Lear, D., Manzella, G. M. R., Gorringe, P., Simoncelli, S., Larkin, K., Holdsworth, N., Arvanitidis, C. D., Jack, M. E. M., Chaves Montero, M. del M., Herman, P. M. J. and Hernandez, F.: The European Marine Observation and Data Network (EMODnet): Visions and roles of the gateway to marine data in Europe, Front. Mar. Sci., 6(JUL), 1–24, doi:10.3389/fmars.2019.00313, 2019.

Moon, J., Lee, K., Tanhua, T., Kress, N. and Kim, I.: Temporal nutrient dynamics in the Mediterranean Sea in response to anthropogenic inputs, , 5243–5251, doi:10.1002/2016GL068788.Received, 2016.

Moore, C. M., Mills, M. M., Arrigo, K. R., Berman-Frank, I., Bopp, L., Boyd, P. W., Galbraith, E. D., Geider, R. J., Guieu, C., Jaccard, S. L., Jickells, T. D., La Roche, J., Lenton, T. M., Mahowald, N. M., Marañón, E., Marinov, I., Moore, J. K., Nakatsuka, T., Oschlies, A., Saito, M. A., Thingstad, T. F., Tsuda, A. and Ulloa, O.: Processes and patterns of oceanic nutrient limitation, Nat. Geosci., 6(9), 701–710, doi:10.1038/ngeo1765, 2013.

Moutin, T. and Raimbault, P.: Primary production, carbon export and nutrients availability in western and eastern Mediterranean Sea in early summer 1996 (MINOS cruise), J. Mar. Syst., 33–34, 273–288, doi:10.1016/S0924-7963(02)00062-3, 2002.

Muniz, K., Cruzado, A., Ruiz De Villa, C. and Villa, C. R. De: Statistical analysis of nutrient data quality (nitrate and phosphate), applied to useful predictor models in the northwestern Mediterranean Sea, Methodology, 17, 221–231, 2001.

Murphy, A. H.: Skill Scores Based on the Mean Square Error and Their Relationships to the Correlation Coefficient, Mon. Weather Rev., 116(12), 2417–2424, doi:10.1175/1520-0493(1988)116<2417:SSBOTM>2.0.CO;2, 1988.

Olsen, A., Key, R. M., Heuven, S. Van, Lauvset, S. K., Velo, A., Lin, X., Schirnick, C., Kozyr, A., Tanhua, T., Hoppema, M. and Jutterström, S.: The Global Ocean Data Analysis Project version 2 (GLODAPv2) – an internally consistent data product for the world ocean, , 297–323, doi:10.5194/essd-8-297-2016, 2016.

Owens, W. B. and Millard, R. C.: A New Algorithm for CTD Oxygen Calibration, J. Phys. Oceanogr., 15(5), 621–631, doi:10.1175/1520-0485(1985)015<0621:ANAFCO>2.0.CO;2, 1985.

Paulmier, A. and Ruiz-Pino, D.: Oxygen minimum zones (OMZs) in the modern ocean, Prog. Oceanogr., 80(3–4), 113–128, doi:10.1016/j.pocean.2008.08.001, 2009.

Powley, H. R.: Phosphorus and Nitrogen Cycling in the Mediterranean Sea : Circulation , biogeochemistry and anthropogenic forcing, 2017.

Powley, H. R., Cappellen, P. Van and Krom, M. D.: Nutrient Cycling in the Mediterranean Sea: The Key to Understanding How the Unique Marine Ecosystem Functions and Responds to Anthropogenic Pressures, Mediterr. Identities - Environ. Soc. Cult., doi:10.5772/intechopen.70878, 2017.

Powley, H. R., Krom, M. D. and Van Cappellen, P.: Phosphorus and nitrogen trajectories in the Mediterranean Sea (1950–2030): Diagnosing basin-wide anthropogenic nutrient enrichment, Prog. Oceanogr., 162, 257–270, doi:10.1016/j.pocean.2018.03.003, 2018.

Pujo-Pay, M., Conan, P., Oriol, L., Cornet-Barthaux, V., Falco, C., Ghiglione, J. F., Goyet, C., Moutin, T. and Prieur, L.: Integrated survey of elemental stoichiometry (C, N, P) from the western to eastern Mediterranean Sea, Biogeosciences, 8(4), 883–899, doi:10.5194/bg-8-883-2011, 2011.

Rahav, E., Herut, B., Stambler, N., Bar-Zeev, E., Mulholland, M. R. and Berman-Frank, I.: Uncoupling between dinitrogen fixation and primary productivity in the eastern Mediterranean Sea, J. Geophys. Res. Biogeosciences, 118(1), 195–202, doi:10.1002/jgrg.20023, 2013.

Reale, M., Giorgi, F., Solidoro, C., Di Biagio, V., Di Sante, F., Mariotti, L., Farneti, R. and Sannino, G.: The Regional Earth System Model RegCM-ES: Evaluation of the Mediterranean climate and marine biogeochemistry., 2020.

Redfield, a C., Ketchum, B. H. and Richards, F. a: The influence of organisms on the composition of sea water, sea, 2, 26–77, 1963.

Reul, A., Rodríguez, V., Jiménez-Gómez, F., Blanco, J. M., Bautista, B., Sarhan, T., Guerrero, F., Ruíz, J. and García-Lafuente, J.: Variability in the spatio-temporal distribution and size-structure of phytoplankton across an upwelling area in the NW-Alboran Sea, (W-Mediterranean), Cont. Shelf Res., 25(5–6), 589–608, doi:10.1016/j.csr.2004.09.016, 2005.

Ribera d'Alcalà, M.: Nutrient ratios and fluxes hint at overlooked processes in the Mediterranean Sea, J. Geophys. Res., 108(C9), doi:10.1029/2002jc001650, 2003.

Ribera d'Alcalà, M., Civitarese, G., Conversano, F. and Lavezza, R.: Nutrient ratios and fluxes hint at overlooked processes in the Mediterranean Sea, J. Geophys. Res. Ocean., 108(9), doi:10.1029/2002jc001650, 2003.

Rigual-Hernández, A. S., Bárcena, M. A., Jordan, R. W., Sierro, F. J., Flores, J. A., Meier, K. J. S., Beaufort, L. and Heussner, S.: Diatom fluxes in the NW Mediterranean: Evidence from a 12-year sediment trap record and surficial sediments, J. Plankton Res., 35(5), 1109–1125, doi:10.1093/plankt/fbt055, 2013.

Rixen, M., Beckers, J. M., Brankart, J. M. and Brasseur, P.: A numerically efficient data analysis method with error map generation, Ocean Model., 2(1–2), 45–60, doi:10.1016/s1463-5003(00)00009-3, 2000.

Roether, W., Manca, Beniamino B. Klein, B., Bregant, D., Georgopoulos, D., Beitzel, V. and KovaEevic, Vedrana Luchetta, A.: Recent Changes in Eastern Mediterranean Deep Waters., 1996.

Roether, W., Klein, B., Bruno, B., Theocharis, A. and Kioroglou, S.: Progress in Oceanography Transient Eastern Mediterranean deep waters in response to the massive dense-water output of the Aegean Sea in the 1990s, , 74, 540–571, doi:10.1016/j.pocean.2007.03.001, 2007.

Sabine, C. L., Hoppema, M., Key, R. M., Tilbrook, B., Van Heuven, S., Lo Monaco, C., Metzl, N., Ishii, M., Murata, A. and Musielewicz, S.: Assessing the internal consistency of the CARINA data base in the Pacific sector of the Southern Ocean, Earth Syst. Sci. Data, 2(2), 195–204, doi:10.5194/essd-2-195-2010, 2010.

Salgado-Hernanz, P. M., Racault, M. F., Font-Muñoz, J. S. and Basterretxea, G.: Trends in phytoplankton phenology in the Mediterranean Sea based on ocean-colour remote sensing, Remote Sens. Environ., 221(October 2018), 50–64, doi:10.1016/j.rse.2018.10.036, 2019.

Sarmiento, J. L. and Gruber, N.: Ocean Biogeochemical Dynamics., 2006.

Sarmiento, J. L. and Toggweiler, J. R.: A new model for the role of the oceans in determining atmospheric PCO 2, Nature, 308(5960), 621–624, doi:10.1038/308621a0, 1984.

Schmidtko, S., Stramma, L. and Visbeck, M.: Decline in global oceanic oxygen content during the past five decades, Nature, 542(7641), 335–339, doi:10.1038/nature21399, 2017.

Schroeder, K., Tanhua, T., Bryden, H., Alvarez, M., Chiggiato, J. and Aracri, S.: Mediterranean Sea Ship-based Hydrographic Investigations Program (Med-SHIP), Oceanography, 28(3), 12–15, doi:10.5670/oceanog.2015.71, 2015.

Schroeder, K., Chiggiato, J., Bryden, H. L., Borghini, M. and Ismail, S. Ben: Abrupt climate shift in the Western Mediterranean Sea, Nat. Publ. Gr., 1–7, doi:10.1038/srep23009, 2016.

Schroeder, K., Chiggiato, J., Josey, S. A., Borghini, M., Aracri, S. and Sparnocchia, S.: Rapid response to climate change in a marginal sea, , (May), 1–7, doi:10.1038/s41598-017-04455-5,

2017.

Schroeder, K., Cozzi, S., Belgacem, M., Borghini, M., Cantoni, C., Durante, S., Petrizzo, A., Poiana, A. and Chiggiato, J.: Along-Path Evolution of Biogeochemical and Carbonate System Properties in the Intermediate Water of the Western Mediterranean, Front. Mar. Sci., 7(May), 1–19, doi:10.3389/fmars.2020.00375, 2020.

Segura-Noguera, M., Cruzado, A. and Blasco, D.: Biogeoquímica de los nutrientes, oxígeno disuelto y clorofila a en el mar Catalán (Mar Mediterráneo noroccidental), Sci. Mar., 80(S1), 39–56, doi:10.3989/scimar.04309.20A, 2016.

Shepherd, J. G., Brewer, P. G., Oschlies, A. and Watson, A. J.: Ocean ventilation and deoxygenation in a warming world: posters, Philos. Trans. R. Soc. A Math. Phys. Eng. Sci., 375(2102), 20170241, doi:10.1098/rsta.2017.0241, 2017.

Silva, N., Rojas, N. and Fedele, A.: Water masses in the Humboldt Current System: Properties, distribution, and the nitrate deficit as a chemical water mass tracer for Equatorial Subsurface Water off Chile, Deep Sea Res. Part II Top. Stud. Oceanogr., 56(16), 1004–1020, doi:10.1016/j.dsr2.2008.12.013, 2009.

Siokou-Frangou, I., Christaki, U., Mazzocchi, M. G., Montresor, M., Ribera D'Alcala, M., Vaque, D. and Zingone, A.: Plankton in the open mediterranean Sea: A review, Biogeosciences, 7(5), 1543–1586, doi:10.5194/bg-7-1543-2010, 2010.

Sospedra, J., Niencheski, L. F. H., Falco, S., Andrade, C. F. F., Attisano, K. K. and Rodilla, M.: ScienceDirect Identifying the main sources of silicate in coastal waters of the Southern Gulf of Valencia (Western Mediterranean Sea), Oceanologia, 60(1), 52–64, doi:10.1016/j.oceano.2017.07.004, 2018.

Tanhua, T.: Matlab Toolbox to Perform Secondary Quality Control (2nd QC) on Hydrographic Data, ORNL CDIAC-158. Carbon Dioxide Inf. Anal. Center, Oak Ridge Natl. Lab. U.S. Dep. Energy, Oak Ridge, Tennessee, 158, doi:10.3334/CDIAC/otg.CDIAC_158, 2010.

Tanhua, T., Brown, P. J. and Key, R. M.: Science Data CARINA : nutrient data in the Atlantic Ocean, Earth, 1, 7–24, doi:10.3334/CDIAC/otg.CARINA.ATL.V1.0, 2009.

Tanhua, T., Heuven, S. van, Key, R. M., Velo, A., Olsen, A. and Schirnick, C.: Quality control procedures and methods of the CARINA database, Earth Syst. Sci. Data, 2, 35–49, 2010.

Tanhua, T., Hainbucher, D., Schroeder, K., Cardin, V., Álvarez, M. and Civitarese, G.: The Mediterranean Sea system: A review and an introduction to the special issue, Ocean Sci., 9(5), 789–803, doi:10.5194/os-9-789-2013, 2013a.

Tanhua, T., Hainbucher, D., Schroeder, K., Cardin, V., Álvarez, M. and Civitarese, G.: The Mediterranean Sea system: A review and an introduction to the special issue, Ocean Sci., 9(5), 789–803, doi:10.5194/os-9-789-2013, 2013b.

Testor, P., Bosse, A., Houpert, L., Margirier, F., Mortier, L., Legoff, H., Dausse, D., Labaste, M., Karstensen, J., Hayes, D., Olita, A., Ribotti, A., Schroeder, K., Chiggiato, J., Onken, R., Heslop,

E., Mourre, B., D'ortenzio, F., Mayot, N., Lavigne, H., de Fommervault, O., Coppola, L., Prieur, L., Taillandier, V., Durrieu de Madron, X., Bourrin, F., Many, G., Damien, P., Estournel, C., Marsaleix, P., Taupier-Letage, I., Raimbault, P., Waldman, R., Bouin, M. N., Giordani, H., Caniaux, G., Somot, S., Ducrocq, V. and Conan, P.: Multiscale Observations of Deep Convection in the Northwestern Mediterranean Sea During Winter 2012–2013 Using Multiple Platforms, J. Geophys. Res. Ocean., 123(3), 1745–1776, doi:10.1002/2016JC012671, 2018.

Troupin, C., MacHín, F., Ouberdous, M., Sirjacobs, D., Barth, A. and Beckers, J. M.: High-resolution climatology of the northeast Atlantic using Data-Interpolating Variational Analysis (Diva), J. Geophys. Res. Ocean., 115(8), 1–20, doi:10.1029/2009JC005512, 2010.

Troupin, C., Barth, A., Sirjacobs, D., Ouberdous, M., Brankart, J. M., Brasseur, P., Rixen, M., Alvera-Azcárate, A., Belounis, M., Capet, A., Lenartz, F., Toussaint, M. E. and Beckers, J. M.: Generation of analysis and consistent error fields using the Data Interpolating Variational Analysis (DIVA), Ocean Model., 52–53, 90–101, doi:10.1016/j.ocemod.2012.05.002, 2012.

Troupin, C., Watelet, S., Ouberdous, M., Sirjacobs, D., Barth, A., Toussaint, M. and Beckers, J.: Data Interpolating Variational Analysis User Guide, , 836723, doi:10.5281/zenodo.836723, 2018.

Ulses, C., Estournel, C., Puig, P., Durrieu de Madron, X. and Marsaleix, P.: Dense shelf water cascading in the northwestern Mediterranean during the cold winter 2005: Quantification of the export through the Gulf of Lion and the Catalan margin, Geophys. Res. Lett., 35(7), 2–7, doi:10.1029/2008GL033257, 2008.

Vargas-yáñez, M.: Updating temperature and salinity mean values and trends in the Western Mediterranean : The RADMED project Progress in Oceanography Updating temperature and salinity mean values and trends in the Western Mediterranean : The RADMED project, Prog. Oceanogr., 157(September), 27–46, doi:10.1016/j.pocean.2017.09.004, 2017.

Voss, M., Bange, H. W., Dippner, J. W., Middelburg, J. J., Montoya, J. P. and Ward, B.: The marine nitrogen cycle: Recent discoveries, uncertaintiesand the potential relevance of climate change, Philos. Trans. R. Soc. B Biol. Sci., 368(1621), doi:10.1098/rstb.2013.0121, 2013.

Wahba, G. and Wendelberger, J.: Some New Mathematical Methods for Variational Objective Analysis Using Splines and Cross Validation, Mon. Weather Rev., 108(8), 1122–1143, 1980.

Watson, A. J., Lenton, T. M. and Mills, B. J. W.: Ocean deoxygenation, the global phosphorus cycle and the possibility of human-caused large-scale ocean anoxia, Philos. Trans. R. Soc. A Math. Phys. Eng. Sci., 375(2102), doi:10.1098/rsta.2016.0318, 2017.

Weatherall, P., Marks, K. M., Jakobsson, M., Schmitt, T., Tani, S., Arndt, J. E., Rovere, M., Chayes, D., Ferrini, V. and Wigley, R.: A new digital bathymetric model of the world's oceans, Earth Sp. Sci., 2, 331–345, doi:doi: 10.1002/ 2015EA000107, 2015.

Williams, R. G. and Follows, M. J.: Physical Transport of Nutrients and the Maintenance of Biological Production, in Ocean Biogeochemistry, pp. 19–51., 2003.

APPENDIX

- **Appendix A**

- Database description

The database includes 870 stations sampled during 24 cruises between 2004 and 2017 in the Western Mediterranean Sea (the reference cruise 29AJ20160818 was included in this dataset as cruise #24 because, it is part of the CNR-ISMAR data collection program), mainly on board of research vessels owned by the Italian National Research Council. It includes bottle data combined with CTD data.

In all stations, measurements were carried out with a CTD-rosette system consisting of a CTD SBE 911 plus and a General Oceanics rosette with 24 12-l Niskin Bottles at the observed depth of the bottle sample. Temperature measurements were performed with an SBE-3/F thermometer with a resolution of 10^{-3} °C and conductivity measurements were performed with an SBE-4 sensor with a resolution of $3 \cdot 10^{-4}$ S m^{-1}. The probes were calibrated before and after the cruise. Except for salinity, no certified reference material (CRM) was used. CTD salinity was calibrated against measurements made with a salinometer.

Samples of nitrate, phosphate and silicate were frozen to -20°C and stored before being analyzed in laboratories onshore.

Measurements were subjected to a rigorous quality control (primary and secondary quality control) and the dataset presented is the product adjusted after the application of quality control approaches.

- Database organization details

Cruise identification: To guarantee the comparability between measurements, an alphanumeric identification code (ID) together with an expedition code (Expocode) are defined a unique identifier.

Appendix.

Parameter	Unit/format	Variable in Dataset	Method/ description	Comment	Original Dataset	Adjusted Product
Expedition code	12 digits	EXPOCODE	*Shipcode_yyyy_mm_dd yyyy_mm_dd: cruise starting day*		✓	✓
Cruise ID		CRUISE	From 1 to 24		✓	✓
Event date	yyyy-mm-dd	DATE			✓	✓
Event time	hhmm	TIME			✓	✓
Day	dd	DAY			✓	✓
Month	mm	MONTH			✓	✓
Year	yyyy	YEAR			✓	✓
Longitude		LATITUDE			✓	✓
Latitude		LONGITUDE			✓	✓
Station number		STNNBR			✓	✓
Niskin bottle number		BTLNBR			✓	✓
Cast number		CASTNO			✓	✓
Pressure	dbar	CTDPRS	CTD pressure		✓	✓
Depth	Meters	DEPTH	Depth from pressure		✓	✓
Salinity		CTDSAL	CTD salinity	PSS-78	✓	✓
Salinity flag		CTDSAL_FLAG_W	WOCE flags		✓	✓
Temperature	°C	CTDTMP	CTD temperature	ITS-90	✓	✓
Potential temperature		THETA	Theta from CTDTMP & CTDSAL		✓	✓
Nitrate	μmol kg^{-1}	NITRAT	standard colorimetric methods*		✓	✓
Nitrate flag		NITRAT_FLAG_W	WOCE flags After 1st quality control		✓	
Recommended nitrate flag		NITRAT_FLAG_re	Flags after 2nd QC Flag 2: adjusted and acceptable Flag 3: adjusted and recommended questionable	Details in Section 4.4		✓
Phosphate	μmol kg^{-1}	PHSPHT	standard colorimetric methods*		✓	✓
Phosphate flag		PHSPHT_FLAG_W	WOCE flags After 1st quality control		✓	
Recommended phosphate flag		PHSPHT_FLAG_re	Flags after 2nd QC Flag 2: adjusted and acceptable Flag 3: adjusted and recommended questionable	Details in Section 4.4		✓
Silicate	μmol kg^{-1}	SILCAT	standard colorimetric methods*		✓	✓
Silicate flag		SILCAT_FLAG_W	WOCE flags After 1st quality control		✓	
Recommended silicate flag		SILCAT_FLAG_re	Flags after 2nd QC Flag 2: adjusted and acceptable Flag 3: adjusted and recommended questionable	Details in Section 4.4		✓

*Standard colorimetric methods of seawater analysis (Grasshoff et al. (1999)).

- Data format

Original dataset: CNR_DIN_WMED_20042017_original.csv: This is the original dataset with 24 fields including flag variables of 24 cruises for nitrate, phosphate, silicate and CTD salinity from the primary quality control.

Adjusted dataset: CNR_DIN_WMED_20042017_adjusted.csv: This is the adjusted product with 24 fields, after removing outlier data (issued from primary quality control) and after applying adjustment.

Appendix B

Figure S1. Weighted mean offset for nitrate, before (grey) and after adjustment (blue). Error bars indicate the standard deviation of the absolute weighted offset. The dashed lines indicate the accuracy limit 2% for an adjustment to be recommended.

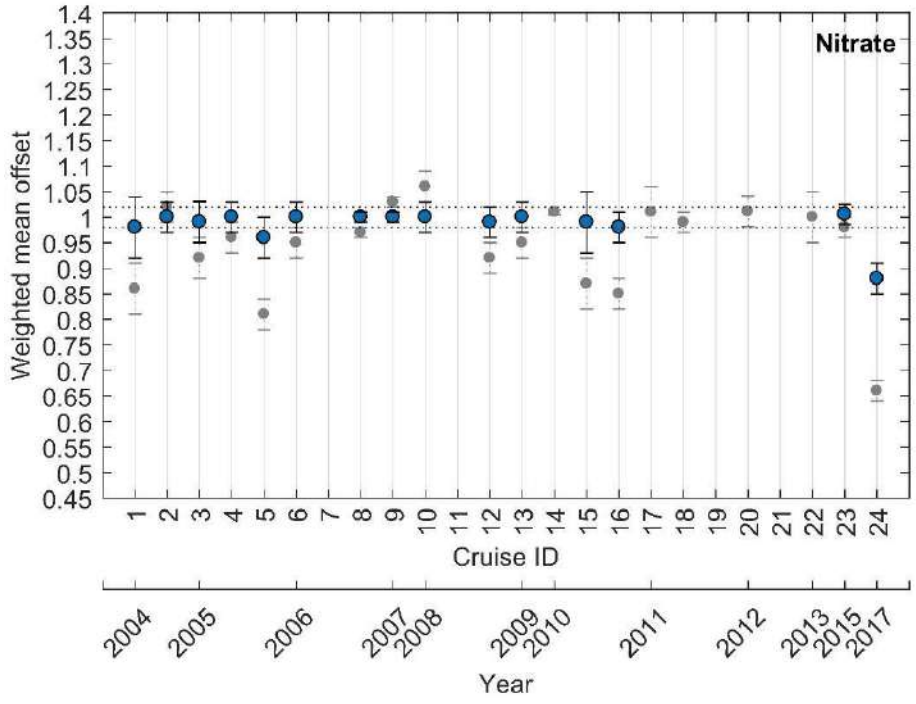

Figure S2. Same as Fig. 2S but for phosphate.

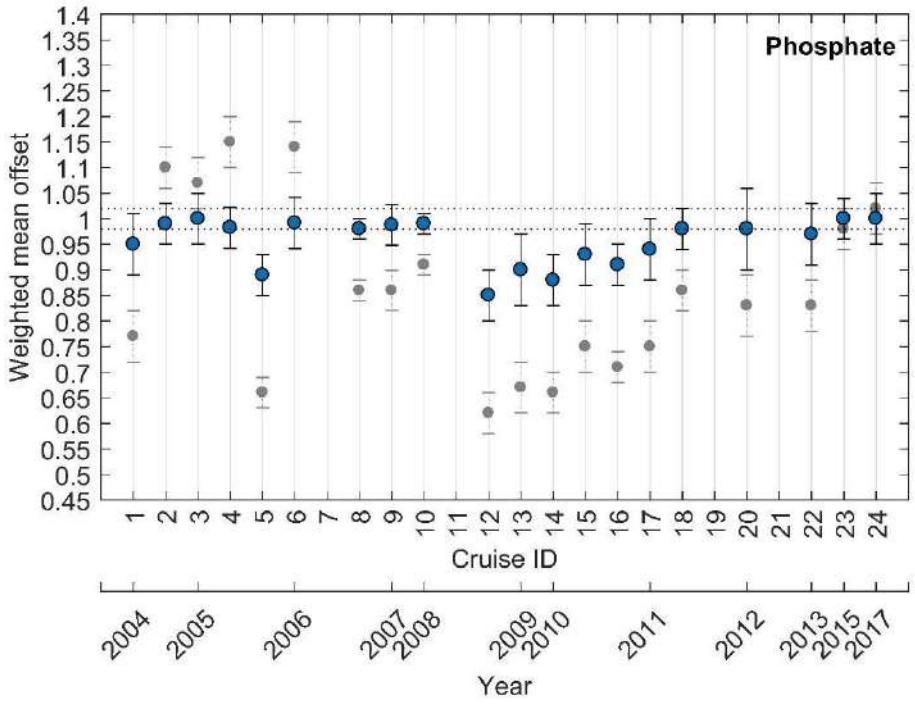

Figure S3. Same as Fig. 2S but for silicate.